Heavy oil recovery by forward in-situ combustion

Adewusi, Victor Adesegun

Award date:
1986

Awarding institution:
University of Bath

HEAVY OIL RECOVERY

BY FORWARD IN-SITU COMBUSTION

Submitted by Victor Adesegun Adewusi
for the degree of Ph.D.
of the University of Bath
1986

ProQuest LLC
789 East Eisenhower Parkway
P.O. Box 1346
Ann Arbor, MI 48106-1346

"Seest thou a man diligent in his business?
he shall stand before kings; he shall not
stand before mean men."

PROVERBS 22.29

To my sister, Temilade.

ACKNOWLEDGMENTS

This study was carried out under the supervision of Dr. M. Greaves. I am sincerely thankful for his invaluable assistance throughout the course of the study. Gratitude is also extended to Dr. R. Field who participated in the approval of the first year project report and for his keen interest in the progress of the work.

The financial support of BP (Petroleum Engineering Branch) at Sunbury-on-Thames in addition to providing the crude oil samples used in this study is gratefully acknowledged.

Many individuals provided technical aids and services at various times. In this regard, I am grateful to the technicians in the School of Chemical Engineering and Mr. T. Walton, the indispensable store man whose co-operation has proved to be priceless. Special thanks are due to Geoffrey Venn, Alan Shave, Leslie Steel, Michael Lock and John Bishop for their greatly beneficial assistance, especially during the construction stage of the experimental apparatus. I also wish to acknowledge the relentless assistance of the staff members of the University Computer Unit. In particular, Dr. R.N. Yardley and David Cunningham provided useful information on the use of Graphic packages. John Gardiner, Alison Giles and other computer operators on their part gave a great deal of attention to the Graphic plotter which was used in producing most of the figures. Other individuals whose assistance is highly appreciated included Mike Moon and Gordon Waddington, who gave up their precious time to prepare some of the drawings in a form that enabled their direct production.

More than a formal acknowledgment is due to Shelley Clark for her skilful processing of the manuscript on to magnetic disks for direct production of the thesis by electronic means. The zeal with which she worked is commended.

Finally, my grateful appreciation is expressed to close friends for their continued support and encouragement. Not enough can be said to express my gratitude and deep thanks for their concern and significant contribution to the success of this project.

ABSTRACT

Enhanced oil recovery by forward in-situ combustion has been studied experimentally in a vertical combustion tube. The tube, which was 63.5mm I.D and 876.3mm long, was designed for a working pressure of 1725kPa. A total of 12 combustion tube experiments were conducted at maximum pressure of 1020kPa and oxygen concentration levels up to 35%. The process of wet combustion was investigated using water-gas injection ratios up to $6.3m^3/Msm^3$. The experiments utilized a 22.8° API Maya crude in a sand matrix consisting of washed silica sand and 8.4% kaolin. The initial oil saturation was less than 30% with a water saturation of approximately 20%.

Very significant increases in the combustion front velocity were achieved under wet combustion conditions and with oxygen enrichment. There was also a substantial reduction in the injected gas required for combustion but this increased with increasing pressure. The molar CO/CO_2 ratio increased with oxygen enrichment but showed a marked decrease as the pressure and water injection rate were increased.

The reaction rate during dry combustion was kinetically controlled as demonstrated by the significant increase in the activation energy with oxygen enrichment and average combustion peak temperature. The sharp reduction in the activation energy during wet combustion revealed the increased role of oxygen diffusion.

Oil production started earlier during wet combustion. This was also observed with oxygen enrichment at low pressures. Both the rate of oil production and the overall recovery increased significantly with increasing water injection rate but

decreased with increasing pressure. The oil produced by in-situ combustion showed a 20% increase in API gravity and viscosity reduction up to 70%.

CONTENTS

Chapter 1

INTRODUCTION

1.1 Heavy Oil Recovery

A petroleum reservoir consists of porous rock or unconsolidated sand media in which varying proportions of oil, water (brine) and gas are trapped. The ease with which the oil can be displaced from the pore space of the reservoir matrix is dependent on many factors, not least the viscosity of the oil. During production, the reduction in pressure in the reservoir causes lighter components to be liberated from the crude oil. One effect of this is to make the remaining oil heavier, with resultant increase in its viscosity. Generally, therefore, the residual oil in a depleted reservoir is heavier than the oil which was initially in place.

Considerable amounts of heavy oil and tar sands have been discovered. The estimated reserves of these heavy hydrocarbon deposits amount to some 1,800 billion barrels, of which 610 billion barrels are predicted to be recoverable (Meyer et al., 1984). The primary and secondary recovery of heavy oils is low, mainly due to their low mobility. In the case of a 25° API crude, for example, primary recovery may only be 5 to 10 percent, increasing to 15 percent with water flooding techniques (Farouq Ali, 1974). Waterflooding is usually not a very efficient process for recovery of heavy oil. Typically, the recovery is only about 300 to 350 bbl/ac-ft for a 65cp oil, and following breakthrough, the watercut increases rapidly to undesirably high values (>90%). In spite of this, it may still be economic to waterflood heavy oil reservoirs (Farouq Ali, 1974).

The high viscosities of heavy crude oils is the predominant factor limiting economic recovery. Any reduction in the viscosity will give rise to an increase in the oil mobility and hence increase in production. The most effective method of lowering the viscosity is by the application of heat to the reservoir. Since the relation between oil viscosity and temperature is an exponential one, the higher the oil viscosity, the greater is the rate of viscosity reduction at any given temperature. Heat may be introduced into the reservoir in the form of hot water, hot gases or steam. It may also be generated in situ by burning part of the oil in the reservoir. This process is known as 'in-situ combustion' (Kuhn et al., 1953; Grant et al., 1954; Szasz, 1961).

The process of in-situ combustion involves injecting air or oxygen into the oil reservoir via an injection well. An air permeability path through the reservoir is first established and ignition of the crude oil is achieved either spontaneously or by other indirect means. This may occur in the vicinity of the injection well (forward combustion) or at the producing well (reverse combustion). With continued air injection, a combustion front propagates through the reservoir, essentially at a steady rate. The heat wave which is generated is sustained by the chemical reactions taking place at the combustion front. The fuel for the combustion process in forward combustion is a residual material in the form of coke. The coke deposits on the sand grains during distillation and cracking of the oil ahead of the combustion front. This process is very complex, involving simultaneous heat and mass transfer with chemical reactions in a multi-phase saturated porous medium (Cooperman, 1959; Tadema, 1959; Gottfried, 1965).

The economy of dry forward combustion can be improved by heat recuperation from the swept or burned formation at the rear of the combustion front through water injection. This may be achieved simultaneously, or alternatively with air injection, and the process is termed 'wet combustion'. It is most advantageous if this is carried out at the earliest opportunity, before excessive heat loss to the cap and base rock occurs. At low water rates, the heat recovered from the burned zone is transported through the combustion front as superheated steam, which then serves to preheat the reservoir formation. At higher water rates, this heat recovered may be insufficient to vaporize all of the injected water, giving rise to partially quenched combustion. This will tend to reduce the combustion-front peak temperature, with heat transport through the combustion zone by saturated steam. Wet combustion process provides a more efficient heat distribution and less oil is consumed as fuel, thereby increasing the velocity of the combustion front. This results in a lower air requirement per barrel of oil recovered and increased efficiency of the displacement process (Buxton, 1972).

1.2 Product Gas Characteristics

The development of in-situ combustion process is primarily directed towards enhanced oil recovery, but the conditions which are established in the reservoir are such that it can be considered to operate as partial oxidation reactor. The wide range of the gaseous reaction products generated, especially in wet combustion, has therefore aroused some interest as to their possible application.

Firstly, gas-combustion turbines can be used to recover the energy of compression, the sensible heat and the heat of

combustion of a low-heat value (62,8Btu/SCF) combustion gases (Stinson et al., 1975; Kaye et al., 1982). Pollution problems can then be solved while combustion gases are used to supplement the liquid fuel usually used to operate the turbine. This would obviously offer significant savings. It is also possible to inject a mixture of recycle gas containing combustible components such that the mixture with air lies outside the explosion limit. In this way, a combustion front can be propagated without there being a need for residual fuel (coke) to be present (Szasz, 1960). This approach may therefore alleviate a major problem encountered with some light oil reservoirs, in which insufficient residual fuel is available to maintain combustion.

Large quantities of CO_2 are required for injection into oil reservoir for enhanced oil recovery. The miscibility of CO_2 at sufficiently high pressures with reservoir oil promotes swelling of the oil, and reduces oil viscosity. These effects often result in higher ultimate recovery (Hvizdos et al., 1983). The effluent gases from in-situ combustion processes are an abundant potential source of CO_2. Also, it is feasible that synthesis gases may be recovered from the in-situ combustion gases. Figure 1.0 shows the chemicals and fuels using synthesis gas as a feedstock.

The main objectives of the project were:
(1) to design and construct an experimental combustion tube apparatus to simulate the conditions for in-situ combustion of heavy crude oil, and (2) to investigate the effect of air injection pressure, water-air injection ratio and oxygen enrichment on the performance of forward combustion process. The investigation is particularly concerned with the effect of operating parameters on the combustion characteristics, combustion reaction kinetics and the recovery and properties of the produced oil.

The thesis is arranged so that the relevant literature on in-situ combustion is reviewed first. Following this, a separate chapter was devoted to equipment description and operations. Chapters five through to seven contained different aspects of results' presentation, discussion and conclusion. The recommendations for future work were given in the final chapter.

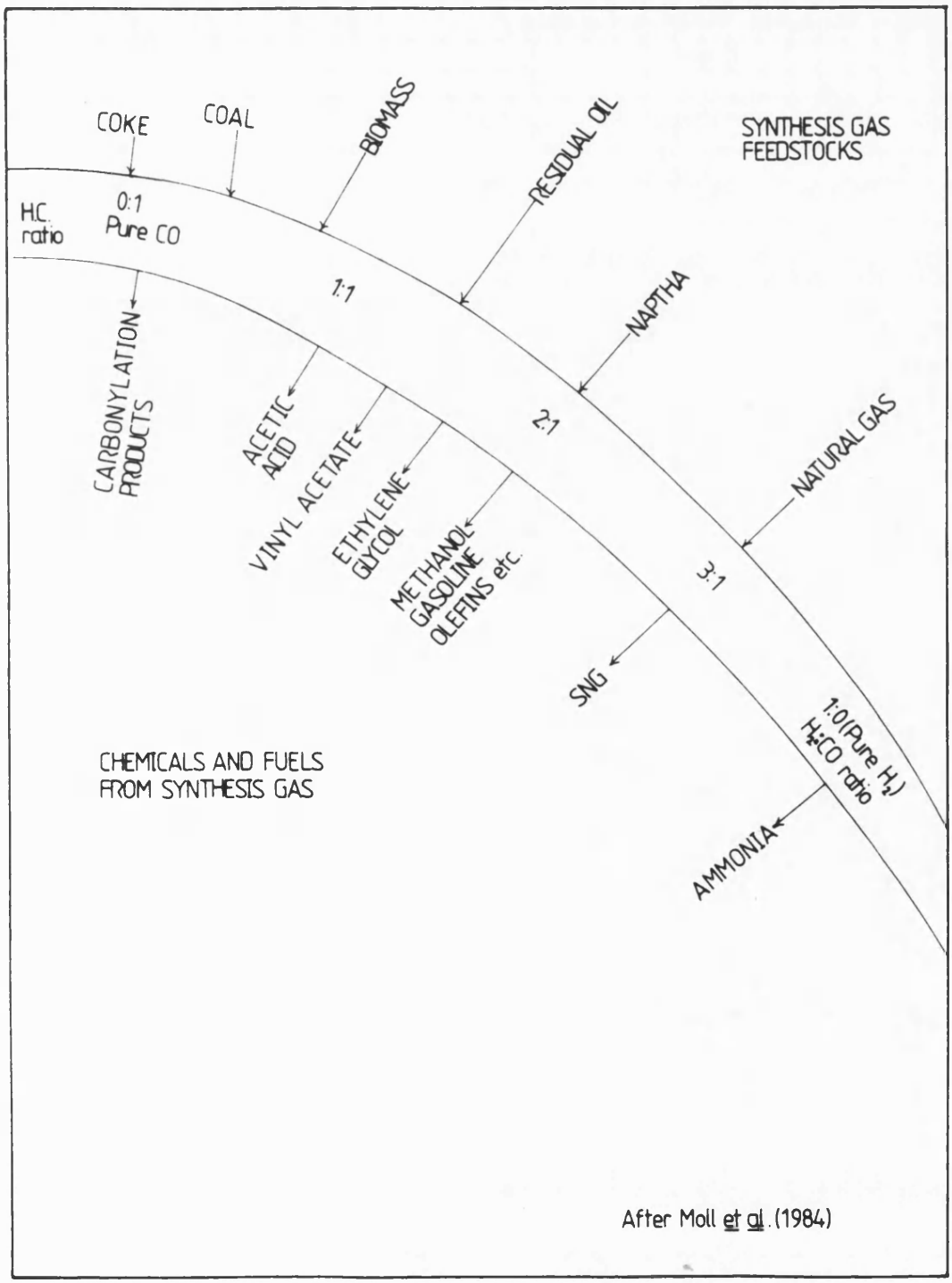

Figure 1.0 SYNTHESIS GAS FEEDS AND PRODUCTS

Chapter 2

IN-SITU COMBUSTION DEVELOPMENT AND MECHANISM

2.1 Development of In-Situ Combustion Process

The idea of simulating oil production by the application of thermal energy dates back to the Russian Scientist Mendeleev, who in 1888, proposed the underground gasification of coal for producing combustible gases. Lewis, in 1917, stated that "of the oil retained in the sand after a well has reached economic exhaustion under customary production methods, part is retained so tightly by capillary forces in the finest pores as well as by adhesion to the surface of the sand grains that its removal seems possible only by using heat or solution" (Lewis, 1917). In 1920, steam was applied in the United States for the purpose of melting paraffin accumulations in the vicinity of the well bore. An increase in the rate of oil production was noticed in this instance (Hester et al., 1954).

Howard, in 1923, received a patent for the underground distillation of oil (Howard, 1923). It was proposed that an air-gas mixture could be ignited electrically and the heat generated would vaporize the oil so that the vapours could be produced with the flue gases from the production wells. The first field test of underground combustion, however, is credited to the USSR (Sheinman et al., 1938). In this test, experiments were conducted in a shallow, pressure depleted reservoir during the period from 1933 to 1935 to improve oil recovery by a process called

crude oil gasification. The experiment indicated that combustion in an oil bearing sand could be initiated and maintained and significant quantities of oil recovered. This work actually became the forerunner of an oil recovery mechanism known today as "In-situ combustion". However, it was not until the early 1950's that several investigators started both theoretical and laboratory studies of the process concurrent with field tests.

Benham and Poettmann (1958) derived an equation for the stoichiometry of underground combustion process. The equation which takes the form:

$$V_b = \frac{1.875 \times 10^{-2}(12 + p)YUa}{((2q + 1)/(q + 1) + p/2)Z} \qquad 2.1$$

gives the combustion-front velocity (V_b) as a function of air flux (Ua), fuel consumption (Z), efficiency of oxygen utilization (Y), atomic ratio of hydrogen to carbon (p) of the fuel burned and ratio of moles of carbon dioxide to carbon monoxide (q) produced. They also showed how the amount of injected air required to displace the oil in one cubic metre of reservoir space could be calculated. This equation represented as

$$Ua/V_b = \frac{((2q + 1)/(q + 1) + p/2)Z}{1.875 \times 10^{-2}(12 + p)Y} \qquad 2.2$$

has a direct bearing on the evaluation of compression cost for the process. There was a good agreement between the values calculated from these equations and the experimentally observed values from laboratory tube runs. In a later publication, Poettmann (1964) presented these calculations in graphical form.

Martin et al. (1958) conducted laboratory experiments involving propagation of burning zone through unconsolidated sands in a linear tube. The data presented include

and fuel requirements, rates of advance, combustion temperatures, coke and fluid distributions. Their results were found to be predictable on the basis of the stoichiometric considerations by Benham et al. (1958). In their later paper, Martin et al. (1962) described an experiment conducted using a flood-pot technique to determine the fuel availability and the corresponding theoretical air requirements. Both consolidated and unconsolidated porous media were employed. For the former, burning proceeded radially from the perimeter of the sample towards a "well" in the centre, while for the unconsolidated sand pack, flow was linear, as in a conventional tube run experiment. The technique is relatively quick and easy owing to the small sample sizes that can be used. The authors concluded that the amount of fuel available for in-situ combustion is not a constant, but varies with crude oil characteristics, type of porous media, oil saturation, air flux and time-temperature relationships. Thus, the fuel availability for specified field applications should be determined using actual reservoir crude and core material at the process condition expected during in-situ combustion in the reservoir.

Showalter (1963) performed combustion-drive tests in a test cell using a sand bed 0.25m in diameter by 3.05m long. He established that the air required for forward combustion was a function of the API gravity of the oil. With other factors constant, the fuel concentration and hence the air requirement for combustion increased as the API gravity of the oil decreased. This conclusion was in agreement with the result of laboratory and field experiments published earlier on by Kuhn et al. (1953). The latter also showed that the amount of fuel burned had an important effect on the combustion-front velocity and that the minimum rate of advance was controlled by heat loss between the burning front and the

surrounding strata. Showalter also pointed out that an increase in pressure resulted in a slight increase in fuel concentration.

Fuel availability, air requirements and the amount of heat released were computed by Dew et al. (1965). In addition, a number of graphs were presented to demonstrate how combustion efficiency, temperature rise, porosity, hydrogen to carbon ratio of fuel and the crude oil gravity affected these parameters.

Wilson et al. (1958) described the fluid dynamics of forward combustion process. A technique was developed which predicted the behaviour of fluids ahead of the burning front. Also, a practical scheme for predicting the production history was presented. The pressure effects on forward combustion were demonstrated in a later work published by Wilson et al. (1963). In this instance, experiments were performed in a linear near-adiabatic system with pressure variation from atmospheric to 1,000psig. They concluded that forward combustion appears to be a fuel dominated process where peak temperature and combustion-front velocity are not very sensitive to changes in pressure. The slight increase in peak temperature and combustion-front velocity with increase in pressure which existed at low fluxes virtually disappeared at high fluxes provided all the oxygen was consumed.

A description of a high pressure laboratory combustion tube system designed to operate with oxygen enrichment was presented by Hansel et al. (1982). Initial tests with the system utilised a light crude with a low value of OIP and simulated reservoir conditions. The injected gas composition was varied from 21% O_2 [air] to 95% O_2 at a constant total gas flux. Their results showed that runs at 40% O_2 and above produced satisfactory combustion while others did not. The combustion-front velocity increased with

oxygen enrichment and time required for initial oil production and the total injected gas required per barrel of oil both decreased.

There has been a growing interest in the area of reaction kinetics in porous media as applied to in-situ combustion. This is because of the crucial role it plays in low-temperature oxidation, cracking and combustion reactions. Tadema (1959) who used Differential thermal analyses, found that there were two different combustion reactions for a crude oil, which occurred at about 270°C and 400°C. Analysis of exhaust gas showed that near the 270°C peak, oxygen was taken up and coke-like residue was formed. Only a small fraction of oxygen was found as carbon oxides while the majority went into water formation. At the high-temperature peak of 400°C, the oxygen reacted to form mainly carbon oxides with little water produced. No hydrocarbon residue was left in the bed. Tadema also found that the atomic hydrogen to carbon ratio of the fuel burned decreased with increasing peak temperature in accordance with other findings (Martin et al., 1962). Reed et al. (1963) used a similar Differential thermal analysis technique to study the reaction kinetics associated with the oxidation of hydrocarbon in porous media.

Gottfried (1966) in his work on theoretical aspects of underground combustion in segregated oil reservoirs, related the reaction rate term to three principal variables, namely, fuel concentration, oxygen concentration and temperature. The reaction order with respect to both fuel and oxygen concentrations was assumed to be unity. Also, the magnitude of the Arrhenius constant was varied by trial since no experimental data were available. He reported an activation energy of 22,000Btu per lbmole for the system considered.

Bousaid (1967) studied the oxidation of crude oil in an unconsolidated porous media. He obtained an expression for the burning rate of carbon as a function of carbon concentration, oxygen partial pressure and combustion temperature. The carbon burning rate for the two types of crude oil used indicated a first order reaction with respect to both carbon concentration and oxygen partial pressure. The effect of combustion temperature on the reaction rate constant matched the Arrhenius equation, while the activation energy was similar for the two crudes examined. The presence of clay however decreased the activation energy. In addition, Bousaid indicated that low-temperature oxidation at reservoir temperature was significant.

The kinetics of both low-temperature oxidation (LTO) of crude oils (occurring below 250°C) and high-temperature combustion reaction of the coke left behind after thermal cracking of the crude was studied by Dabbous (1971). Isothermal integral reactor analysis was used to obtain rate equations for the overall rate of LTO reaction. The reaction order with respect to oxygen was found to be between 0.5 and 1.0. The order of the reaction was dependent upon the crude but independent of the properties of the porous media. The activation energy of the reaction was insensitive to the type of crude or porous medium and is in the neighbourhood of 31,000 Btu per lbmole. The LTO reaction was found to be in the kinetics-influenced region. Also light crudes appeared to be more susceptible to partial oxidation at low temperatures because of their relatively high hydrogen content. Most of the reacted oxygen was consumed by hydrogen and hydrocarbon oxidation reactions rather than by carbon oxidation, which is in accordance with Tadema's result (Tadema, 1959). Dabbous used Differential reactor analysis for the combustion cell

kinetic data. The carbon combustion reaction rate was found to be first order with respect to the average oxygen partial pressure and second order with respect to the average carbon concentration. The activation energy for the carbon burning reaction was 25,320Btu per lbmole.

Burger et al. (1972) estimated the heat of combustion in high-temperature zone during in-situ combustion, from the real hydrogen to carbon ratio of the fuel and the carbon monoxide to carbon dioxide molar ratio in the exhaust gases. In this way, they showed the influence of additives (in the oil or on the matrix) on crude oil oxidation and coke availability in porous media. Other in-situ combustion reaction kinetics studies can be found in literature (Fassihi et al., 1980; Vossoughi et al., 1982; Lin et al., 1984).

Wet combustion process has attracted much attention as a technique for improving the heat transport efficiency of dry-forward combustion. Among the early studies in this area was that of Dietz and Weijdema (1967). In describing the basic principles of wet combustion, they classified the process into "Normal wet" and "Partially quenched", corresponding to increasing amounts of water injected. They showed that the air requirement per unit of formation swept during partially quenched was much less than in dry or normal wet combustion. In a later publication, Dietz (1970) developed guidelines for designing and evaluating large-scale projects. These include a method for estimating the required water and air injection rates, for a given oil production rate.

The combination of forward combustion and waterflooding has been termed COFCAW by Parrish et al. (1969). They identified the major benefit of the process to be a marked reduction in the air to oil ratio because less oil was burned as fuel.

Consequently more oil is potentially recoverable. Similar results were obtained by Alderman et al. (1971) and Garon et al. (1974).

Beckers et al. (1970) gave a theoretical description of various semi-steady states that may develop in a linear adiabatic wet combustion process. Formulas were presented that give the combustion-front velocity as a function of water to air ratio injected for each of the possible states. They concluded that, depending on the water and air injection rates and the fuel available for combustion, there are, in principle, intermediate semi-steady states occurring between the normal wet and partially quenched regions which were identified by Dietz et al. (1967).

Smith and Perkins (1973) developed a numerical simulation model for laboratory wet combustion experiments in order to study the end-effects associated with short combustion tubes. In contrast to dry forward combustion, the process of wet combustion is transient in nature. Therefore, stable combustion may not occur until the heat wave has travelled a distance which may be considerably greater than the length of most laboratory combustion tubes. In addition, they concluded that the water to air injection ratio also has an important effect on stability.

Burger and Sahuquet (1973) found that the combustion-front velocity was higher in wet combustion than in dry, the velocity increasing with this ratio. As long as a high-temperature zone existed, they also found that no coke remained behind the combustion front. This appears to contradict the partially quenched combustion results of Dietz et al. (1967). Alternatively, Burger and Sahuquet's results did not extend into the partially quenched region.

The reaction kinetics associated with wet combustion have been studied by Pusch (1976). Above 300°C he observed that the rate of reaction was almost independent of temperature and a decrease in the activation energy occurred from 86.3 to 12.5 x 10^3 joules per mole as soon as steam entered the combustion zone. The explanation was that the reaction was controlled by the diffusion of oxygen at higher temperatures, but at lower temperatures, it was determined by the chemical reaction rate. He attributed the phenomenon to the influence of steam. The presence of steam made relatively large proportions of the fuel surface to be inaccessible to oxygen. Only the oxygen molecules arriving at the free active sites of the fuel surface are able to react with the fuel. The reaction is therefore limited by the mass flow rate of oxygen. Other wet combustion studies include those of Thomas (1983) and Hughes (1985).

The trend in the development of numerical model to simulate the process of in-situ combustion has been towards more rigorous treatment of the fluid flow and interphase mass transfer, inclusion of more components, more comprehensive description of reaction kinetics and stoichiometry, and fully implicit treatment of the finite difference model equation.

Initial attempts at simulation were concerned primarily with the heat transfer aspect of combustion (Bailey et al., 1959; Ramey, 1959; Bailey et al., 1960; Thomas, 1963; Chu, 1963). These models considered convective and conductive heat transports for linear and radial flow geometry. A more sophisticated heat-transfer model was developed by Chu (1964), which accounts for the effects of vaporization and condensation as a function of the temperature distribution, but neglects the accompanying phase changes by assuming constant fluid distributions.

The two-dimensional treatment by Smith and Farouq Ali (1971) accounts for heat generation in the combustion zone, heat transfer by conduction and convection (single phase flow) in the reservoir, heat losses by conduction to adjacent formations, and different permeability to gas (air) flow on either side of the combustion zone.

Gottfried (1966) and Khelil (1969) investigated special case when combustion is initiated in a reservoir containing a gas cap, that is, when the oil bearing layer has an overlying "clean" porous zone containing only gas. The models considered the various transport mechanisms taking place in such reservoir.

The reviewed models above are useful in some aspects of heat transfer in combustion process as a first approximation. They are far from being satisfactory as a general purpose simulator, partly because of the specialized geometry to which they apply and partly because of the many stringent assumptions employed. The most important of these is the neglect of multi-phase fluid flow and reaction kinetics. Further, no realistic representation of vaporization and condensation of the reservoir fluids and their hydrodynamic effects on the process were included. Also, fluid flow, normally restricted to gas (air) was usually one-dimensional and both rock and fluid properties were assumed to be uniform and constant.

In 1965, Gottfried presented a more generalized mathematical model of the in-situ combustion process (Gottfried, 1965). This simulator includes such features as (1) flow of three fluid phases, (2) heat generation from reaction kinetics considerations, (3) vaporization and condensation of water and, (4) conduction and convection of heat in the reservoir. The simulator successfully exhibited all the major thermal and hydrodynamic

characteristics of the in-situ combustion process, including the propagation of the combustion zone, the formation of a steam plateau and water and oil banks. However, the model has several limitations due principally to its one-dimensional nature and the requirement for a large amount of computer time.

The most comprehensive and sophisticated combustion models described to date appear to be those of Crookston et al. (1979), Grabowski et al. (1979), Youngren (1980), and Coats (1980). These models describe non-isothermal, multi-phase flow of fluid in porous media which takes into account phase changes and chemical reactions involved. They are three dimensional, including four phases namely, oil, water, gas and solid phase usually referred to as coke. These models are general in nature except for the welbore-reservoir coupling which was accounted for in the recent work of Rubbin et al. (1985).

A few reports describe the field application of in-situ combustion. Gates and Ramey (1958) reported the results of a 2.5 acre five-spot pattern involving a 12.9° API crude in the south Belridge field in California. During these tests water cuts increased and emulsion problems were encountered as the burning front approached the producing wells, but significant production was obtained. Coke-bearing formation samples recovered after the completion of the test, contained from 15.89 to 86.52 kg of coke per cubic metre of bulk volume.

The results of a five-well field experiment in Oklahoma were reported by Moss et al. (1959). In this test, the API gravity of the produced oil increased by as much as 2° and the viscosity decreased from 5000cps to 800cps. The minimum rate of the burning front was estimated to be approximately 0.037 metre per

day. The largest factor controlling the direction of the burning front appeared to be the characteristic of the reservoir itself.

Clark et al. (1965) reported the performance of a successful in-situ combustion test conducted by the Marathon Oil Company on August 22, 1961, at the Fry Unit, Crawford County, Illinois. The test was carried out in a 3.3 acre inverted five spot. During the test, the average air injection rate was 43042sm^3 per day. The cumulative air-oil ratio was 326sm^3 per barrel of oil and the oxygen utilization efficiency was 87 percent.

The full-scale COFCAW project at Sloss field, Nebraska by Amoco Production Company was reported by Parrish, Pollock and Craig (1974). In this 960 acre project, more than a million barrels of oil were displaced from a previously waterflooded reservoir. Production rates were as high as 550 BOPD and injected air-water ratios were low, about 11.335sm^3 per barrel in a high pressure light oil reservoir. Corrosion problems associated with COFCAW were controlled using inhibitors and critical equipment was made of corrosion-resistant material. More comprehensive reviews of fire-flood field project have been given by Farouq Ali (1972) and Chu (1977, 1982). The topics covered include screening guides for selection of in-situ combustion projects, reservoir performance prediction, project design, well completions for injectors and producers, ignition methods and operational problems.

2.2 The Physical Mechanisms of In-Situ Combustion Process

In-situ combustion is probably the most complex enhanced oil recovery process. The basic process involves several iteractive stages, including heat transfer, phase change and chemical reaction. All these phenomena are coupled through the

hydrodynamics of multi-phase flow in porous media. There are two fundamentally different processes of in-situ combustion : forward combustion (also known as dry-forward combustion) and reverse combustion. Wet combustion is a modified form of forward combustion. The mode of operation and the major physical and chemical phenomena occurring in each of these processes are described below.

2.2.1 Forward Combustion Process

The process is initiated by injecting air for a short period to establish a continuous gas permeability between the injection and producing wells. Once this is accomplished, the formation oil, in the vicinity of the well bore is ignited. Depending on the crude composition, ignition may be spontaneous. If not, it can be induced by using dowhnole heaters, preheating the injection air or preceding air injection with an addition of oxidizable chemical such as linseed oil (Herbeck et al., 1977). As air injection continues, the combustion zone moves into the formation as a narrow band away from the injection towards the producing well.

A distinct variation of in-situ combustion is reverse combustion. In this case, unlike forward combustion, the direction of the combustion zone movement is opposite to that of the air flow. Thus, the formation is ignited in the vicinity of a producing well, whereas air is injected into the injection well. In such a case, the combustion zone will move away from the producing well, towards the injection well, in the direction of increasing oxygen concentration. Meanwhile, the fluids displaced pass through the hot combustion zone, and are thus produced. Unlike forward combustion, the combustion zone does not need to consume all the fuel

ahead of it. The amount of hydrocarbons consumed would depend on the air injection rate. Furthermore, the produced fluids are subjected to very high temperatures occurring within the combustion zone, and as a result, cracking of the heavier fractions takes place, and thus, the produced hydrocarbons have a vastly different character (much lighter, less viscous) from that of the in-place hydrocarbons. This allows the production of oil which is too viscous to flow under reservoir conditions (Pollen, H. K. Van and assoc., 1980). In spite of this benefit, reverse combustion is expected to have limited application in future, if any, and probably to crudes having relatively low reactivity with oxygen. This is because a valuable fraction of the crude is burned as fuel, leaving the undesirable fraction in the region behind the combustion front. More importantly, however, spontaneous ignition may occur near the injection well, initiating a forward combustion drive, thereby cutting off the oxygen supply to the reverse combustion front (Schumacher, 1980; Chu, 1982). Figure 2.21 illustrates the basic concepts behind forward and reverse combustion.

Insight into the mechanism of forward combustion process can be gained by inspection of typical temperature and saturation profiles illustrated in Fig. 2.22. As the combustion front progresses under stabilized conditions through the formation, it gives rise to a number of distinct temperature zones which are characteristic of the fluid saturations developed in the reservoir. The temperature profile is usually characterized by a peak temperature in the combustion zone, a steep front followed by a steam plateau downstream and a gradual decline upstream. The series of fluid saturated zones consist of burned zone, combustion zone, multi-phase (or evaporation) zone, a three-phase (or condensation) zone, an oil bank zone and the virgin oil zone. These zones contain

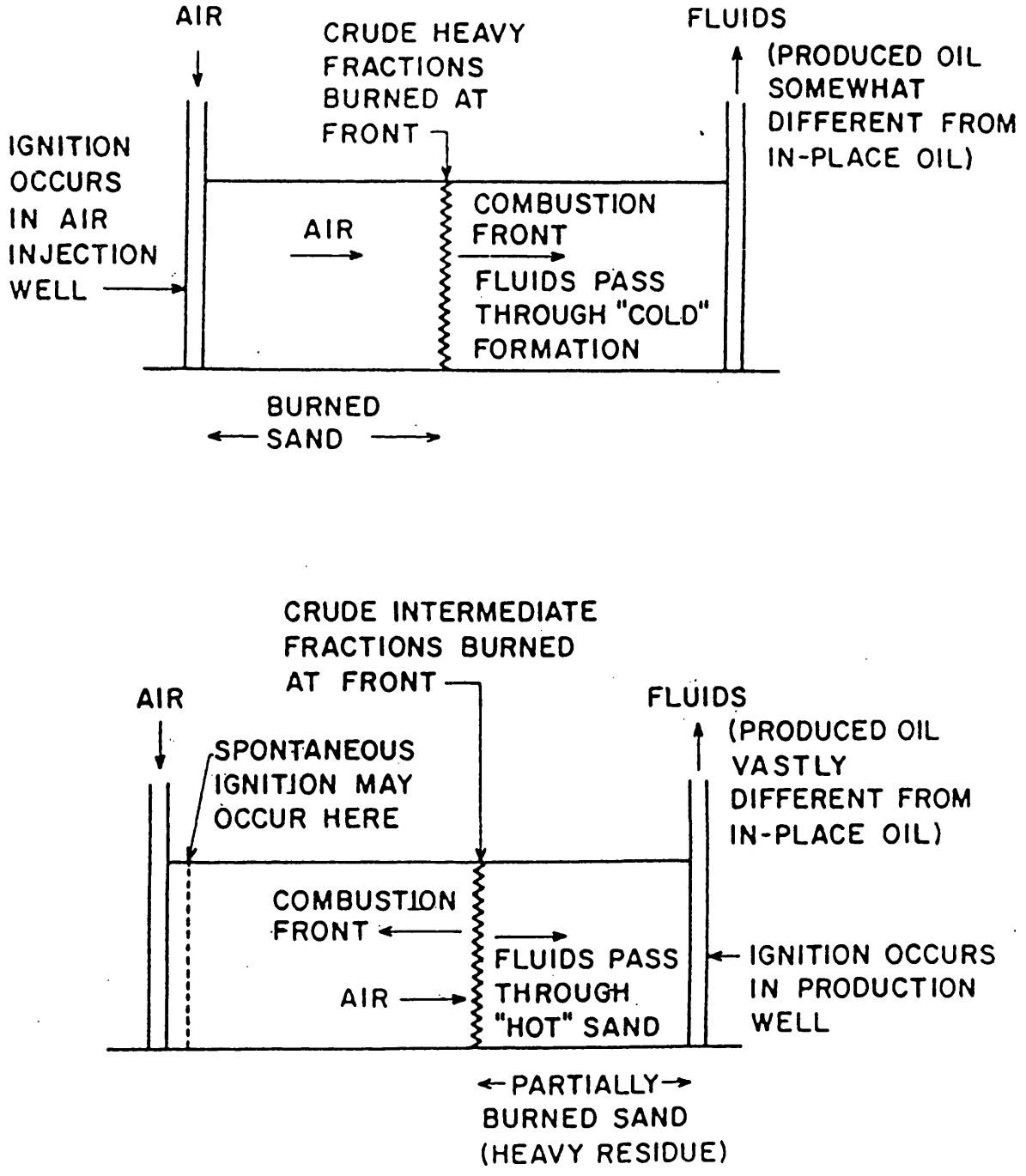

Figure 2.21 SCHEMATIC OF FORWARD AND REVERSE IN-SITU COMBUSTION PROCESSES

air, coke, (steam, gases, hot water and light hydrocarbons), (gases, oil and water), (oil and gas) and virgin oil respectively.

Burned zone: In this zone, combustion has already taken place and the formation is completely clean, only air is flowing and being heated by the hot matrix and part of the combustion energy is recovered in this way.

Combustion zone: In the multi-phase zone, crude oil is vaporized and cracked or carbonized to produce a coke deposit on the sand surface. This deposit serves as the fuel in the combustion zone. The chemical reactions occurring between the injected oxygen and the deposited fuel provide the heat source for the process. It is visualized that a combustion front moves through the sand matrix, in much the same way that the burning front moves through a cigarette (Showalter, 1963). The front moves only as fast as it depletes its fuel supply and the heat generated is carried away by conduction through solid matrix and also by convection by combustion water, vaporized formation water, hot combustion gases and other combustion products.

Multi-phase or Vaporization zone: The heat transported from the combustion zone causes water and oil ahead of combustion zone to be vaporized and displaced downstream of the formation. At the leading edge of the combustion zone, where the temperature is in excess of 700°F, fractionation of the oil takes place. As these fluids move downstream to cooler regions of the formation, they are condensed. According to Wilson et al. (1958), the fluids will redistribute themselves downstream in such a manner that the relative permeability characteristics of the formation are satisfied. Thus the oil flows ahead to form the oil bank, combustion reaction water and connate water end up as steam, which later condenses to form a water bank.

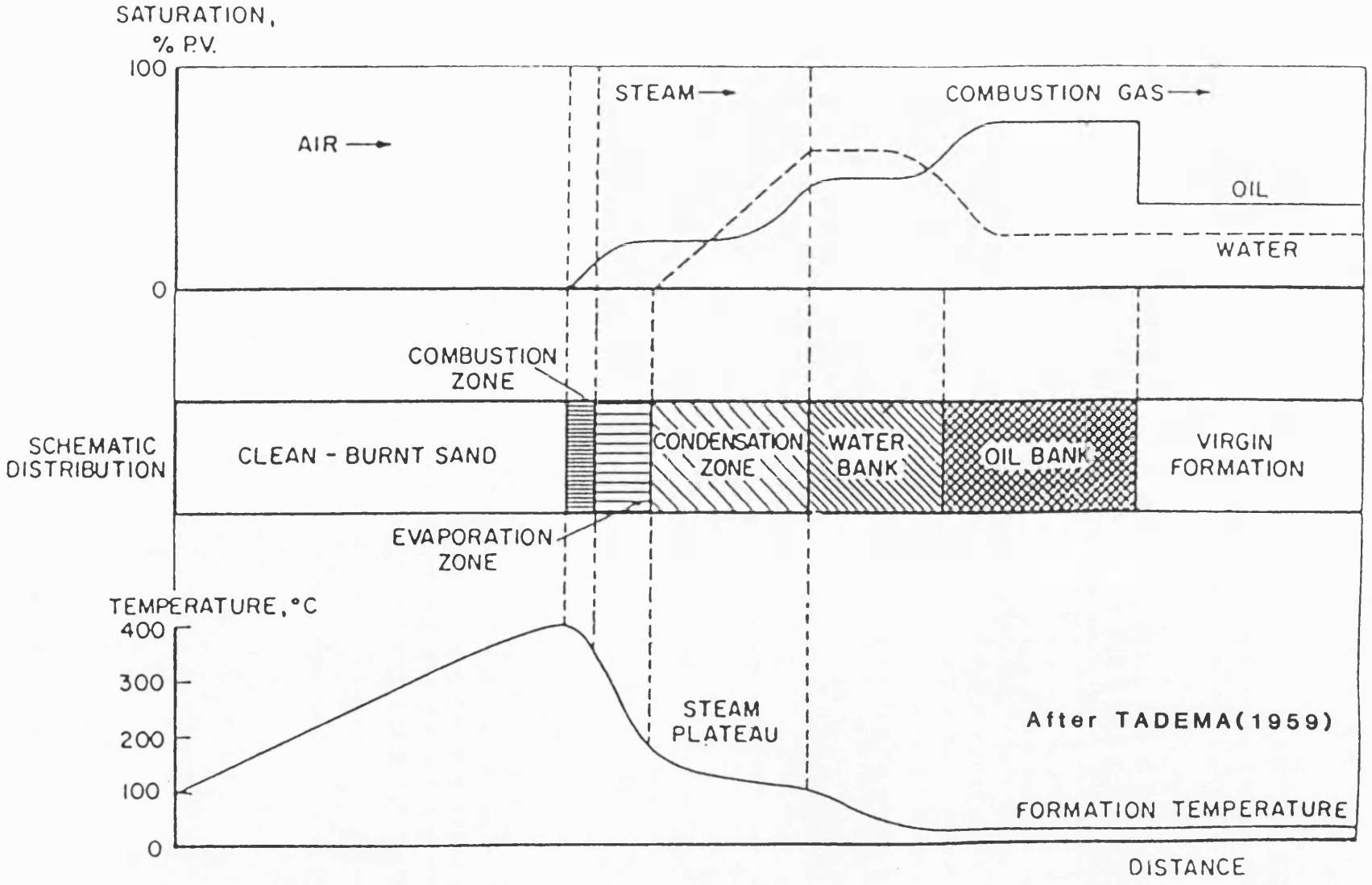

Figure 2.22 SCHEMATIC SATURATION AND TEMPERATURE DISTRIBUTION

The heavy fractions which have neither been displaced nor vaporized undergo pyrolysis to produce the coke which then serves as fuel for the combustion reaction.

Three-phase or Condensation zone: This zone consists of a steam plateau region (upstream) followed by water bank. In the steam plateau region, the temperature profile and zone length remains stabilized and relatively constant throughout the process at the condensation point of steam under the prevailing conditions. Both steam- and water-drive mechanisms are very active in this zone, causing the displacement of the oil bank ahead as they stabilize in size and migrate through the reservoir. The residual oil left behind after a steam drive is usually of the same order of magnitude as the fuel used during combustion (Flock et al., 1971). Steam drive has therefore been considered to play an important role in fuel deposition.

Oil bank: In the oil bank, the light hydrocarbons previously distilled condense, mixing with original oil to produce a miscible displacement effect. In addition, the combustion gases act as a partial gas drive. The oil saturation is high while the water saturation is equal to that of virgin formation.

Overall, the displacement mechanisms which produce high recoveries in forward combustion process can be summarized as: gas drive mechanism, thermal drive including viscosity reduction, thermal expansion and fractional distillation, steam, hot and cold water-drive mechanisms and miscible displacement processes. Thus forward combustion process combines the advantages of many of the known secondary recovery methods.

2.2.2 Wet Combustion Process

Heat utilization in dry-forward combustion is very inefficient. The low heat capacity of air means that the heat recovery rate is low and only about 20% of the generated heat is carried forward of the flame front (Herbeck et al., 1977). The remaining heat in the sand matrix is left behind and is eventually lost to the overlying and underlying rock strata. In order to increase heat recovery, it was proposed that water be injected with air, the wet combustion process (as opposed to dry combustion). Water has a heat capacity approximately 100 times that of air on a volumetric basis (at 500psia), and is thus capable of transporting that much more heat compared with air (Farouq Ali, 1974). The water injected with the air modifies the combustion front mechanism and hence the characteristics of the prevailing temperature and saturation profiles (Dietz et al., 1967; Dietz, 1970; Parrish et al., 1969; Beckers et al., 1970; Burger et al., 1973). It has been recognised that there are three distinct temperature and saturation profiles which could be established during wet combustion process. Burger and Sahuquet (1973) classified the processes under which these occur into "normal wet", "incomplete" and "superwet" combustion, corresponding to decreasing values of the air-water ratio. This is illustrated in Fig. 2.23.

In normal wet combustion, water evaporates behind the combustion front and all the coke is burned. Part of the burned-out reservoir is cooled so that some of the injected water establishes a water saturation there. The cooling effect of the injected water can give rise to incomplete combustion, leaving some fuel unburnt. This is because the residence time of the oxygen in the high-temperature zones is insufficient to achieve complete

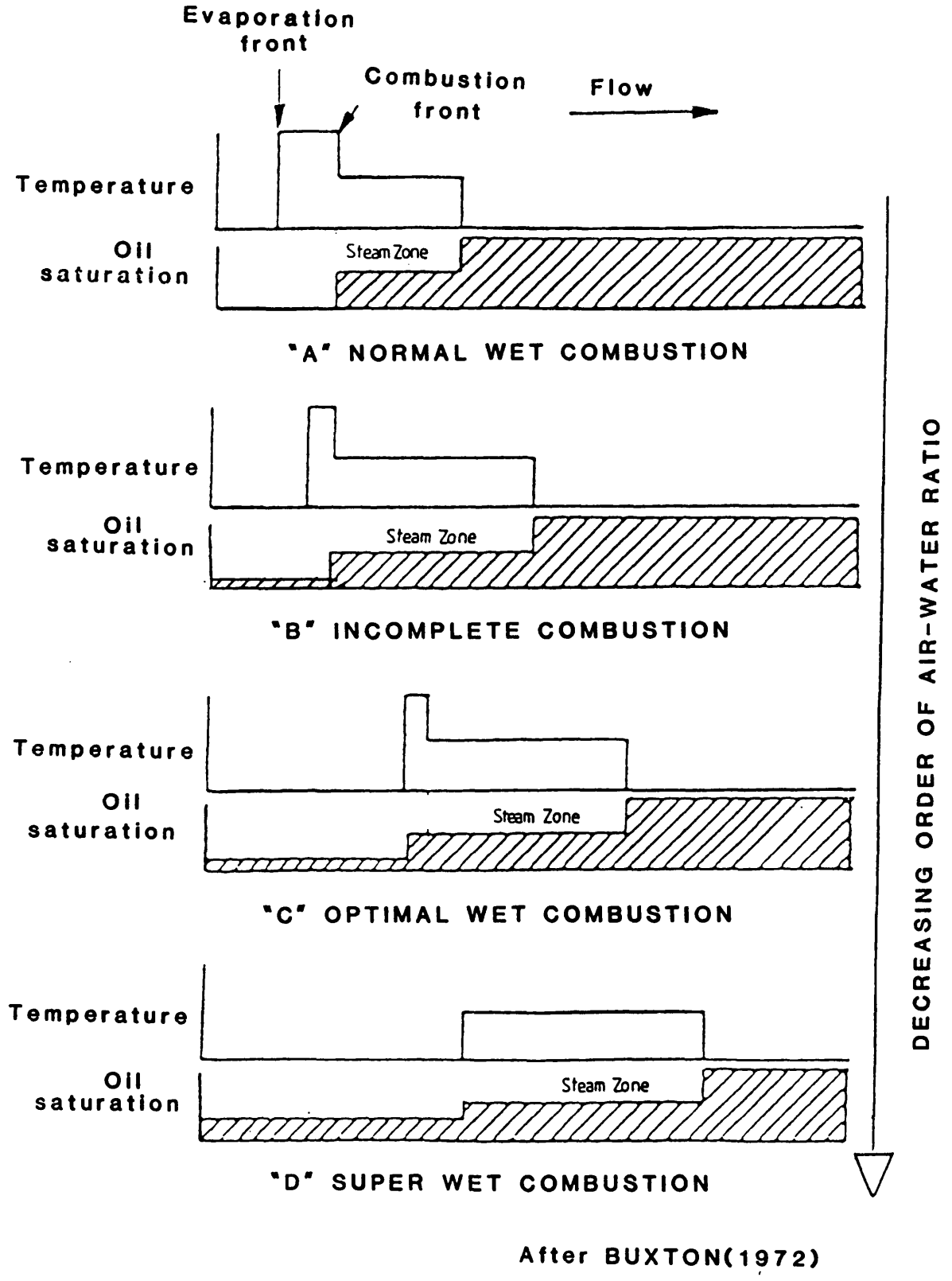

Figure 2.23 EFFECT OF INJECTED AIR-WATER RATIO

combustion (Dietz et al., 1967). In both normal wet and incomplete combustion, superheated steam passes through the burning front and the peak temperature is therefore higher than the vaporization temperature of water at the prevailing pressure. According to Pusch (1976), the higher the operating pressure, the broader the range of normal wet combustion. Also, normal wet combustion range is broader under adiabatic than in non-adiabatic conditions.

On the other hand, superwet combustion is obtained when the amount of heat available in the burned-out rock is too low to vaporize the water reaching the combustion front. The peak temperature then disappears and a vaporization-condensation plateau is likely to move through the porous media (Dietz et al., 1967). In this case, more coke will be left behind. However, it is possible to operate under this condition and still achieve 100 percent oxygen utilization (Buxton, 1972). The term "partially quenched" combustion refers to either the incomplete combustion (Dietz, 1970; Beckers et al., 1970) or the superwet (Dietz et al., 1967).

While the advantages of water injection are recognised, there is the possibility that too low in air-water ratio could cause the vaporization front to overrun the combustion front, thereby causing the combustion to be extinguished. Conversely, if the air-water ratio is too high, all the injected water will be trapped upstream of the combustion zone and will not assist in transporting energy downstream (Buxton, 1972). Certainly, there exists an "optimal wet" combustion mode. According to Buxton (1972), this will correspond to the case when the evaporation-front velocity is equal to the combustion-front velocity, as shown in Fig. 2.23. At this ratio, the maximum steam zone exists which has a sufficiently high temperature capable of further reducing the oil saturation by

cracking and vaporization. The saturation and temperature profiles that exist under these optimum conditions are shown in Fig. 2.24.

Several factors do affect the optimum air-water ratio injected. These factors include the reservoir pressure, porosity, relative permeability characteristics of the reservoir rock, and the extent of heat losses during operation (Parrish et al., 1965).

The injected air-water ratio and the manner in which this ratio changes with changing reservoir pressures depend primarily on the latent heat of steam. As the reservoir pressure increases, a lower air-water ratio is needed to support combustion. This is because at higher pressures, the latent heat or the enthalpy of vaporization of steam decreases thereby reducing its cooling effect on the combustion front. However, the maximum pressure employed for any given case will depend on the depth of the formation to be burned, and to that extent will it determine or limit the variation in air-water ratios applicable for such a case. Shallow formations, obviously, cannot be subjected to extreme fluid pressures because of the likelihood of fracturing.

A portion of the injected air and water is normally required to fill the reservoir pore space between the injection well and the advancing combustion zone. The injected air-water ratio is therefore not always the same as that reaching the combustion front. The volume of the injected air and water trapped in the reservoir pore space varies with the reservoir pressure and relative permeability characteristics of the formation.

Heat losses to the surrounding strata depend primarily upon the thickness of the formation being burned and the velocity with which the combustion front moves through the

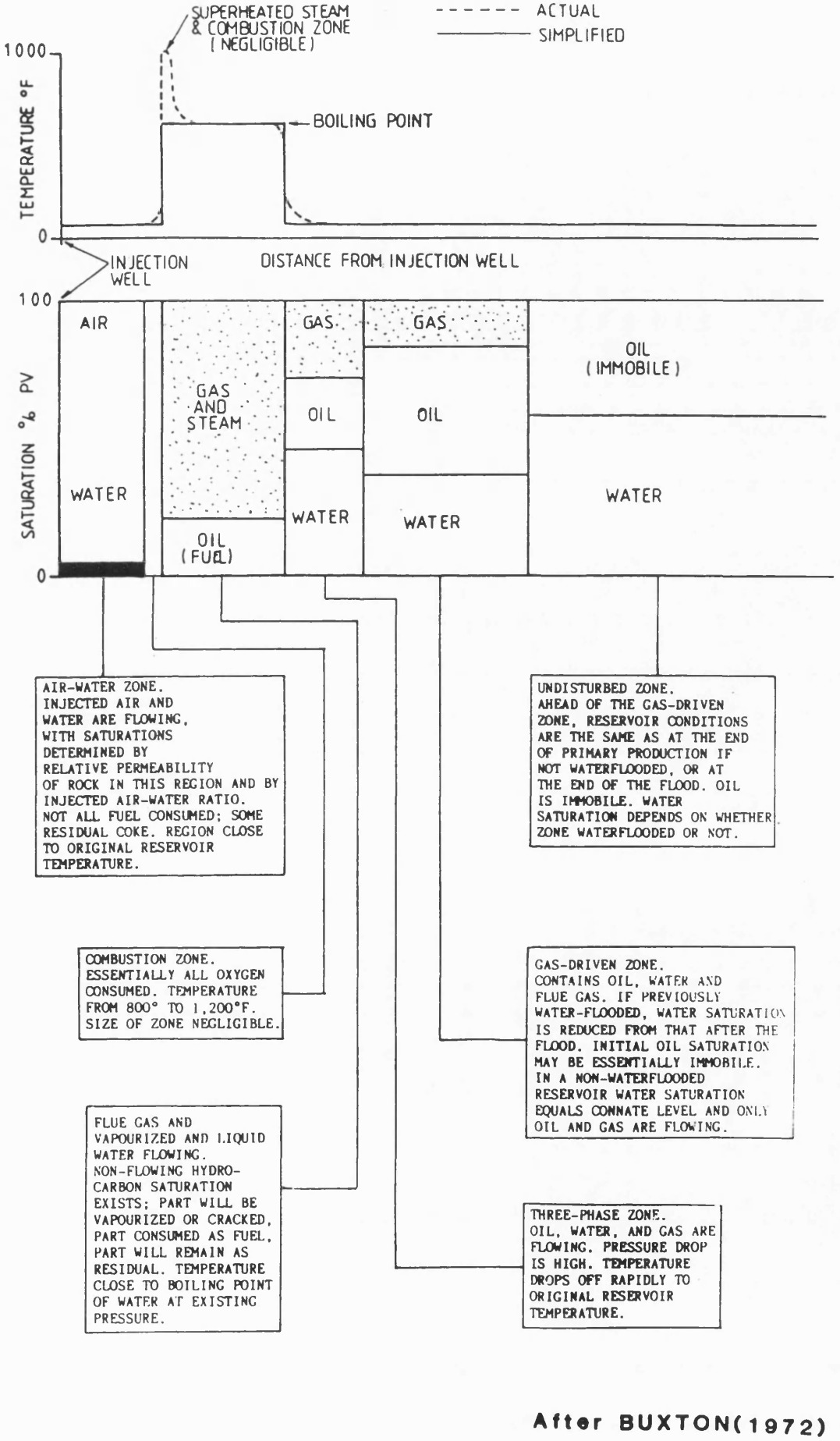

Figure 2.24 OPTIMIZED WET COMBUSTION PROCESS

formation. Heat losses decrease as formation thickness and the combustion-front velocity increase. If heat loss becomes excessive and it is not to result in extinguishing of combustion, some additional air should be used to compensate for heat losses (Parrish et al., 1965).

Chapter 3

CHEMICAL REACTION KINETICS AND HEAT TRANSFER

The most critical region in the in-situ combustion process is the combustion front, where the temperature reaches its maximum value. The ability to sustain a stable combustion front depends on the extent of the exothermic combustion reactions involved (Burger et al., 1972). Specifically, the velocity of the combustion front and hence the air requirement depends on the rate of fuel deposition and rate of combustion, that is the reaction kinetics. Although extensive work had been done on the modelling of in-situ combustion, the understanding of the complex physico-chemical processes taking place within the combustion zone is far from complete. An analysis of the reaction kinetics is developed relating the effect of fuel concentration, oxygen partial pressure and combustion temperature. This enables a quantitative assessment of the important kinetic parameters affecting the process, to be determined.

3.1 Reaction Kinetics of In-Situ Combustion

Overall, the in-situ combustion process can be characterized by a simple two-step reaction path (Burger et al., 1972). These steps are fuel deposition and fuel combustion. However, another type of reaction is also important, low-temperature oxidation of crude oil (LTO reaction). Low-temperature oxidation is initiated upon air injection prior to ignition, or after ignition when oxygen is available downstream of the combustion front. This may result from (1) incomplete oxygen consumption in the

high-temperature combustion zone (2) air channelling around the front, or (3) a tilted combustion front surface (Burger et al., 1972; Dabbous et al., 1974; Bousaid et al., 1968; Thomas et al., 1979).

3.1.1 Low-Temperature Oxidation

Reactions between oxygen and petroleum hydrocarbons at temperature below 650°F (343°C) are termed low-temperature oxidation reactions (LTO). Combustion reactions, on the other hand, occur in the temperature range of 650°F (343°C) to 1200°F (650°C). LTO reactions are characterized either by the absence of carbon oxides or else low levels of carbon oxides in the effluent stream. In other words, more oxygen reacts with the in-place hydrocarbons than can be accounted for in the produced gases. Some of the LTO products are alcohols, aldehydes, ketones, carbonoxylic acids and peroxides (Burger et al., 1972). It has been reported that aldehydes promote the LTO reaction (Crawford, 1968). LTO has an adverse effect on the viscosity and distillation characteristics of crude oil. Martin et al. (1962) emphasized that LTO increases the oil viscosity and alters the distillation characteristics of crude oil. Okandan et al. (1982) also pointed out that LTO causes a decrease in the API gravity of oil. It significantly increases the amount of fuel available for combustion (Burger et al., 1972; Dabbous et al., 1974). LTO also influences the properties of the porous media. A great deal of consolidation and increased surface roughness of the porous media are the consequence of LTO (Dabbous, 1971). Since the displacement of oil, in the reservoir by in-situ combustion mechanism is primarily controlled by the physical properties and distillation characteristics of the crude,

LTO can seriously affect the movement of oil and water and ultimately, the performance of an in-situ combustion process.

3.1.2 Fuel Deposition and Combustion

Under the effect of heat, crude oil vaporizes and cracks to leave behind a bituminous-type residue called fuel or coke. The mechanism of fuel deposition is thus controlled by the two processes of evaporation of crude oil components and the kinetics of the cracking reaction. These two processes determine how much fuel eventually will be available in the form of coke, for combustion reaction (Lin et al., 1984). Factors which have an important influence on these processes and hence the fuel availability include the rock properties (permeability, porosity and mineral content like clay), the fluid properties (oil viscosity, specific gravity, distillation characteristics, oil, water and gas saturations), as well as the air flux, oxygen concentration and the prevailing temperature and pressure (Farouq Ali, 1974). It has been reported that low-temperature oxidation also has a significant effect on the fuel availability and fuel characteristics (Fassihi et al., 1984). However, if oxygen is completely used in the combustion zone, low-temperature oxidation should not play an important role in fuel deposition mechanism.

For a system with a sufficiently high cracking rate, the coke deposited serves as the main fuel for sustaining the propagation of the combustion front. If the cracking rate is, however, too low, then some residual crude oil will also be burned (Lin et al., 1984). Another combustion reaction which has been

recognised is the burning of oil vapor, but according to Verma (1978), this makes only relatively small contribution.

When coke is the sole source of fuel, the fuel (coke) deposition and combustion reactions become essentially competitive (Fassihi et al., 1980; Thomas, 1963). Predominance of one or the other controls to a large extent the behaviour of the combustion process. Since combustion reaction is slower than fuel deposition (Fassihi, 1981), the fuel combustion step should have a greater influence on the behaviour of the combustion process. The role of fuel deposition may however, become very important in "segregated" forward combustion (Gottfried, 1966; Khelil, 1969). A segregated forward combustion arises either when an oil zone is overlain by a clean porous zone, containing only gas, or as a result of vertical permeability variations and gas channelling. In either of these cases, both horizontal and vertical combustion interfaces develop. Gottfried (1966) and Khelil (1969) in their studies of segregated forward combustion, concluded that "fuel deposition and migration" mechanism described the process accurately.

3.1.3 Reaction Kinetic Model

The reaction between fuel and oxygen in forward combustion is a heterogeneous type flow reaction. As reacting fuel is consumed, combustion zone moves forward through the sand pack. A number of transport processes are involved in this reaction path (Dabbous, 1971). Firstly, it is necessary for oxygen to move from the bulk gas stream to the fuel interface and then be adsorbed on to the reaction surface. This is followed by chemical reaction between oxygen and the fuel. Combustion products must desorb and finally transfer into the bulk gas stream. Since these steps occur

successively, they can be considered to offer resistances in series with the slowest step controlling the overall rate of the reaction. Dabbous et al. (1974) found that the role of diffusion in dry foward combustion is not significant since changes in air flux have very little effect on oxygen consumption. Therefore, in the absence of diffusion limiting effect, it can be assumed that chemical reaction is the limiting step. This assumption has been found to be adequate for dry forward combustion (Fassihi et al., 1980).

The chemical reaction rate for the combustion of crude oil in a porous medium can be expressed by (Bousaid, 1967; Fassihi et al., 1980):

$$-Rc = -\frac{dCc}{dt} = kC_c^m Po_2^n \qquad 3.1$$

where C_c = carbon concentration on sand grains.

Po_2 = partial pressure of oxygen

t = reaction time

k = reaction rate constant

and m, n = reaction order

The reaction rate constant, k, is related to temperature by the Arrhenius equation:

$$k = A_r \exp(-E/RT) \qquad 3.2$$

where E is the activation energy and A_r is the Arrhenius constant or frequency factor. The constant, A_r may also be a function of surface area of the rock (Fassihi et al., 1980).

The carbon concentration C_c remaining within the reacting bed can be computed from the carbon oxides produced as function of time. The carbon burning rate ($-dC_c/dt$) can be

determined by differentiation of the carbon concentration versus combustion time curve. Equation (3.1) can then be utilized to compute the reaction orders m and n with respect to carbon concentration and oxygen partial pressure respectively, and the heterogeneous reaction rate constant k at any particular temperature. The equation can be rearranged in a variety of ways to allow the estimation of these parameters. For instance, if the change in oxygen partial pressure is small during isothermal combustion, it follows from Equation (3.1) that

$$\log(-dC_c/dt) = \log k_1 + m\log C_c \qquad 3.3$$

$$\text{where } k_1 = kP_{O_2}^n \qquad 3.4$$

Thus, m can be computed from the slope of a linear correlation of $\log(-dC_c/dt)$ and $\log C_c$. The reaction order with respect to oxygen partial pressure may be found in exactly the same manner. From Equation (3.1)

$$\log\left\{\frac{-dCc/dt}{Cc^m}\right\} = \log k + n\log Po_2 \qquad 3.5$$

Thus n and the heterogeneous rate constant k can be obtained from a linear correlation of $\log\left\{\frac{-dCc/dt}{Cc^m}\right\}$ and $\log Po_2$.

The value of n obtained could be verified by arranging Equation (3.1) in the form:

$$\log\left\{\frac{-dCc/dt}{P_{O_2}^n}\right\} = \log k + m\log Cc \qquad 3.6$$

The correct value of n is obtained if a linear graph of $\log\left\{\frac{-dCc/dt}{P_{O_2}^n}\right\}$ versus log Cc gives a slope 'm' numerically equal to that obtained by Equation (3.3).

It is essential to point out that in the above analysis, the combustion tube data has been treated as differential reactor data. But strictly speaking, a combustion tube is an integral reactor since both carbon concentration and oxygen partial pressure are functions of time and reaction path, hence the kinetic data obtained should be integral data (Bousaid et al., 1968). A more appropriate and rigorous analysis would require combining material balances and reaction rate expressions to provide an expression relating the dependent and independent variables. However, the resulting expressions cannot be integrated analytically to provide useful interpretative expressions because of their complexity (Dabbous, 1971). Several authors, including Smith (1956) and Bousaid et al. (1968) have discussed this problem. The treatment of the in-situ combustion tube data as differential reactor data has been found to be a reasonable basis for analysis (Bousaid et al., 1968).

3.2 Heat Generation and Transfer

3.2.1 Heat of Combustion

The high-temperature partial oxidation reactions taking place in the combustion zone can be represented, according to Benham and Poettman (1958), by the stoichiometric equation:

$$CH_p + \left(\frac{2q + 1}{2(1 + q)} + \frac{p}{4}\right)O_2 \rightarrow \frac{q}{1 + q} CO_2 + \frac{1}{1 + q} CO + \frac{p}{2} H_2O \qquad 3.7$$

where p is the atomic hydrogen to carbon ratio of the hydrocarbon fuel and q is the molar CO_2/CO ratio in the combustion products.

The heat (H) released by this reaction is given, after Burger and Sahuquet (1972) by:

$$H = \frac{265{,}700 + 197{,}850(1/q)}{(1 + 1/q)(12 + p)} + \frac{31{,}175p - 171{,}700}{12 + p} \qquad 3.8$$

in calories per gram of fuel burned, when the water of combustion condenses.

In field operation, transmission of part of the heat released from the combustion zone to the surrounding strata is inevitable. Such heat transmission may be considered to be lost for all practical purposes. Therefore, the combustion zone heat generation rate should be such that, in spite of the heat loss, the temperature remains above the minimum ignition temperature of the crude oil involved. Otherwise, extinction may occur. This implies that at any given time, there is a critical fractional heat loss, based on total heat released, above which, steady propagation of the combustion front may be impeded. A simplified heat transfer model is proposed (Section 3.2.2) to study heat flow in the vicinity of the combustion zone.

3.2.2 Heat Transfer Model

The model accounts for heat generation due to combustion and transport arising from conduction and convection. Vaporization and condensation are regarded as heat consumption and generation processes, respectively. In practice, the condensation of

steam does not need to be accounted for because the temperature existing in the vicinity of the combustion front is much higher than the saturated steam temperature at the prevailing pressure. A heat loss term is included to account for any non-adiabatic condition. The model is further subject to the following simplifying assumptions.

(1) The burning front moves axially at constant velocity in a cylindrical system.

(2) Temperature is constant in the radial direction within the combustion tube, but heat may be lost at the circumference of the tube through an annular insulation to the surroundings.

(3) Thermal and physical properties are invariant with temperature and pressure.

(4) The temperatures of the porous media and the process fluids are equal at any point and time

(5) Heat flow by convection is assumed to be in the direction of fluid flow only. Heat transfer by radiation is negligible.

Restricting the analysis to the flow of gas and steam, and employing the above assumptions, a heat balance can be written for a differential element ahead of the combustion front (Figure 3.1). A moving coordinate system such that the combustion front is always at the origin of the x-coordinate is used. Thus the x-coordinate represents distance from the combustion front. The position of the combustion front at any time is the product of the

constant front-velocity and the time. The heat balance is written as follows:

Net rate of heat accumulation	=	Net rate of heat transfer by conduction	+	Net rate of heat transfer by convection +
Rate of heat generated by combustion	+	Rate of heat loss to adjacent formations	+	Rate of heat consumption by vaporization.

Writing each component of the balance in terms of physical properties of the reservoir results in the following equations:

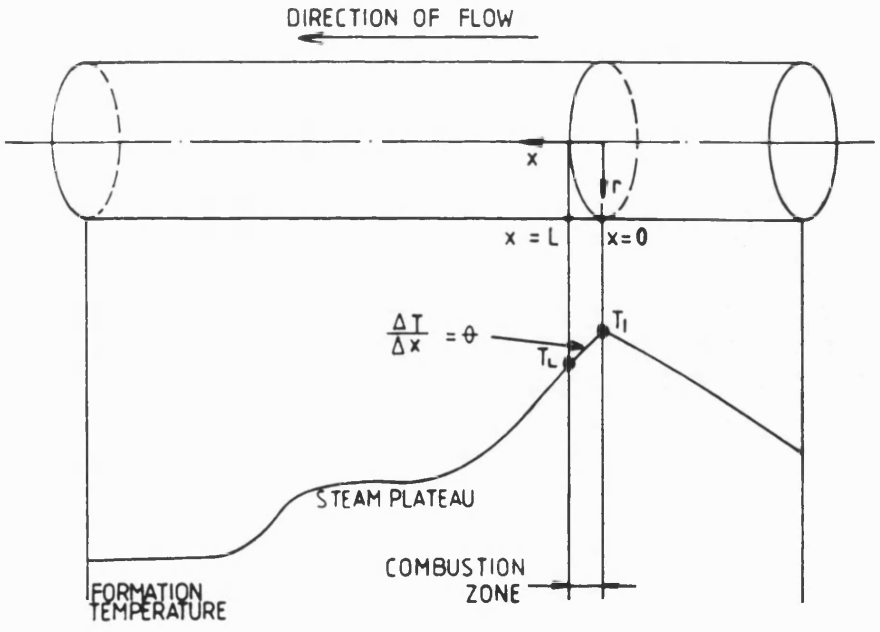

Figure 3.1 ANNULAR RING OVER WHICH ENERGY BALANCE IS MADE

Net rate of heat transfer by conduction $= -K(2\pi r\Delta r)\left\{\left(\frac{\delta T}{\delta x}\right)_x - \left(\frac{\delta T}{\delta x}\right)_{x+\Delta x}\right\}$

Net rate of heat transfer by convection $= U_g\rho_g F_g C_g(2\pi r\Delta r)\{Tx - Tx+\Delta x\} + U_g\rho_s F_s C_{sh}(2\pi r\Delta r)\{Tx - Tx+\Delta x\}$,

Rate of heat generated by combustion $= (2\pi r\Delta r\Delta x)R_f L_c$,

Rate of heat loss to adjacent formations $= -(2\pi r\Delta r\Delta x)Q$,

Rate of heat consumption by vaporization of steam $= (2\pi r\Delta r\Delta x)(\Phi S_w\rho_w C_w \frac{\delta T}{\delta t} + S)$

Net rate of heat accumulation $= (2\pi r\Delta r\Delta x)C_r \frac{\delta T}{\delta t}$

Substituting these expressions into the total heat balance yields the partial differential equation for the region ahead of the burning front:

$$(\Phi S_w\rho_w C_w + C_r)\frac{\delta T}{\delta t} = K\frac{\delta^2 T}{\delta x^2} - U_g(\rho_g F_g C_g + \rho_s F_s C_{sh})\frac{\delta T}{\delta x} + R_f L_c - Q - S \qquad 3.9$$

The left hand side term of Equation (3.9) can be expanded as,

$$(\Phi S_w\rho_w C_w + C_r)\frac{\delta T}{\delta t} = -(\Phi S_w\rho_w C_w + C_r)\frac{\delta T}{\delta x}\cdot\frac{\delta x}{\delta t} \qquad 3.10$$

$$= -(\Phi S_w\rho_w C_w + C_r)V_b\frac{\delta T}{\delta x} \qquad 3.11$$

Also, the steam heat term, S can be expanded as,

$$S = WR_f h_s \qquad 3.12$$

Substituting these expressions into Equation (3.9), we obtain, after simplification:

$$K\frac{\delta^2 T}{\delta x^2} + \left((\Phi S_w \rho_w C_w + C_r)V_b - U_g(\rho_g F_g C_g + \rho_s F_s C_{sh})\right)\frac{\delta T}{\delta x} + R_f(L_c - Wh_s) - Q = 0 \qquad 3.13$$

The constants Cr and K in Equation (3.13) are the heat capacity and thermal conductivity of the reservoir at initial saturations and are defined by the following equations (Smith, 1971; Archer, 1985):

$$C_r = \Phi S_w C_w \rho_w + \Phi S_o C_o \rho_o + \Phi S_g C_g \rho_g + (1 - \Phi) C_m \rho_m \qquad 3.14$$

$$K = \Phi K_f + (1 - \Phi) K_m \qquad 3.15$$

$$\text{Also, } S_o + S_w + S_g = 1.0 \qquad 3.16$$

To facilitate the discussion of Equation (3.13) new terms are defined as follows

$$\alpha = -\left(\frac{(\Phi S_w \rho_w C_w + C_r)V_b - U_g(\rho_g F_g C_g + \rho_s F_s C_{sh})}{K}\right) \qquad 3.17$$

$$\beta = -\left(\frac{R_f(L_c - Wh_s) - Q}{K}\right) \qquad 3.18$$

Introducing these terms, Equation (3.13) becomes an ordinary differential equation of second degree in x.

$$\frac{d^2T}{dx^2} - \alpha\frac{dT}{dx} - \beta = 0 \qquad 3.19$$

Initial and Boundary Conditions: To complete the mathematical formulation of the model, the initial and boundary conditions must be defined. It is stipulated that there is no influx of heat by conduction at the inlet of the boundary where the temperature

attains its maximum value. Within the combustion zone itself, a constant temperature gradient is assumed to prevail over its entire thickness L. The initial and boundary conditions become,

$$T(0) = T_1 \qquad 3.20$$

$$T(x) = T_x \qquad 3.21$$

$$\frac{dT}{dx}(x) = \theta \ , \ 0<x\leq L \qquad 3.22$$

With the assumptions as stated previously, Equation (3.19) and its governing initial and boundary conditions, constitute a simplified heat transfer model for the combustion zone.

Solution Procedure: Fortunately the form of Equation (3.19) makes it possible to be solved analytically and a detailed discussion of the various steps involved is provided in Appendix A. The solution relates the radial heat loss Q to the combustion-front location x and takes the form,

$$Q = K\alpha\left(\frac{(T_x - T_1)e^{\alpha L} - \theta(e^{\alpha x} - 1)}{e^{\alpha x} - 1 - xe^{\alpha L}}\right) + R_f(L_c - Wh_s) \qquad 3.23$$

The percent radial heat loss P_h from the combustion zone is thus given by,

$$P_h = \frac{100Q}{R_f L_c} \qquad 3.24$$

A computer program written in Fortran IV was employed to evaluate the quantities Q and P_h for the stabilized periods of a series of laboratory in-situ combustion runs (See Appendix D).

Chapter 4

EXPERIMENTAL APPARATUS AND PROCEDURE

4.1. Design Consideration

It is important that the laboratory in-situ combustion experiments simulate the conditions which actually exist in underground reservoirs. Thus the sequence of events in the laboratory combustion tube must be similar to that experienced by a reservoir element during the approach of the combustion front. The factors, therefore, which must be considered in designing in-situ combustion equipment include, combustion tube orientation and dimensions, ignition mode, heat loss control and choice of process variables.

Firstly, the laboratory combustion tube is often designed to operate in a vertical position in order to avoid gravity segregation effects such as a tilted combustion front surface. For the same reason, horizontal combustion tube is usually supported on steel rollers to permit rotation around its axis (Burger, et al., 1973). Also, a small diameter combustion tube is required in order to achieve a uniform temperature in the porous medium, otherwise hot sports might be generated (Wilson et al., 1963). Similarly, homogeneous distribution of fluids can be achieved by using a small diameter tube, so that segregation is largely compensated by gravity (Smith et al., 1973). Small diameters also favour displacement stability at an early period of operation (Wilson et al., 1963).

As regards the length of laboratory combustion tube, Smith and Perkins (1973) showed that end-effects due to short

combustion tube may significantly distort experimental results especially in wet combustion tests. In their numerical simulation study of wet combustion performance for a long adiabatic system, Smith and Perkins concluded that, because of the apparently highly transient nature of wet combustion, stabilization may not occur until the heat wave has travelled a distance considerably greater than the length of most laboratory combustion tube. The system length used to arrive at the above conclusion was 30.5 metres. However, several investigators including Alderman et al. (1971), Garon et al. (1974) and Ejiogu et al. (1979) have succussfully used a considerably shorter length of tube for their laboratory investigation. For instance, Garon and Wygal (1974) used a 0.813 metre long, 54.0mm i.d. tube with 0.635mm walls for their wet combustion test at pressure up to 13,790kPa and water-air injection ratio from 0 to $13m^3/Msm^3$. Tube length is therefore not the only important stabilization factor - Smith and Perkins have also reported water-air injection rato to be important.

The various ignition methods have been described in section 2.2.1. Briefly, these include the use of wall heaters (downhole heaters, in the field), preheating injection air or preceding air injection with addition of an oxidizable chemical such as linseed oil and spontaneous ignition of the crude oil in place depending on its composition. The heat loss to the over- and under-budden in the field application of in-situ combustion is lower than the heat loss by thermal conduction in laboratory combustion tube experiments (Martin et al., 1958). Excessive heat loss, as mentioned in section 2.2.2, could cause extinction of combustion front. Also, operational instability could be aided by excessive heat loss. When laboratory combustion tube experiments are conducted adiabatically, both the burning front and steam plateau move at

nearly constant velocities, giving rise to nearly constant peak temperature.

A minimum air flux is required to support combustion. Martin et al. (1958) calculated this air flux to be $1.22 sm^3/m^2hr$ and thus suggested a value between 1.22 and $3.05 sm^3/m^2hr$ to be satisfactory even for heavy crude oils in unconsolidated reservoir. There is also a critical injected water-air ratio above which water injection has effect on dry combustion. According to Burger and Sahuquet (1973), this value lies between 0.5 and $0.8 m^3/Msm^3$.

4.2 Combustion Tube Equipment

The experimental apparatus consists of four principal components; namely, the combustion tube assembly, flow control system, temperature control system and fluid analysis system. A schematic flow diagram of the apparatus is shown in Fig. 4.1. The principal components are described separately below.

4.2.1 Combustion Tube Assembly

The combustion tube assembly is shown in Fig. 4.2, with Table 4.1 showing details of its major parts. The assembly consists of a 152.4mm i.d. mild steel pressure jacket and a 63.5mm i.d. stainless steel combustion tube. A 76.2mm i.d. mild steel tube is also positioned concentrically round the combustion tube to support the band heaters and the thermocouples' connections. The combustion tube and the middle tube have the same overall length of 876.3mm and equal wall-thicknesses of 12.7mm. The pressure jacket is also 876.3mm long with a wall thickness of 19.1mm.

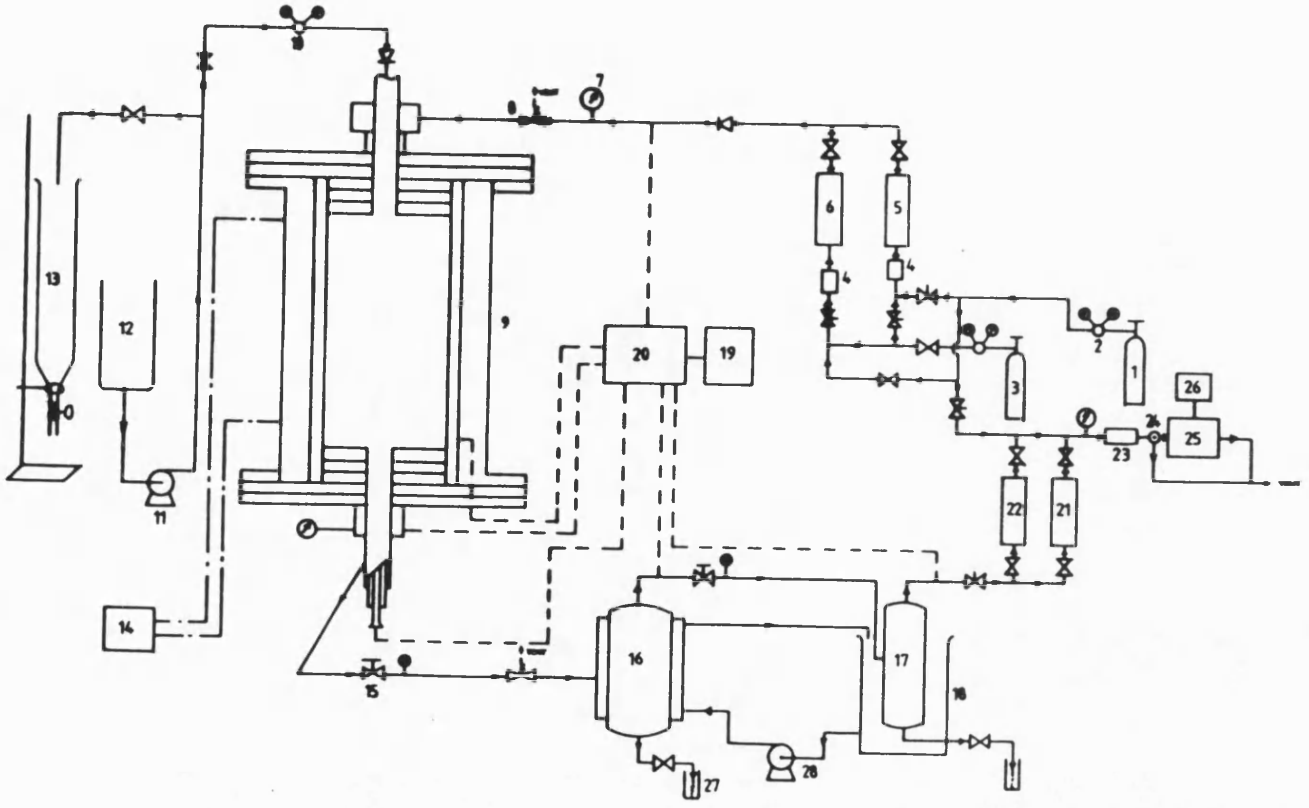

Figure 4.1 SCHEMATIC FLOW DIAGRAM OF IN-SITU COMBUSTION APPARATUS

KEY TO FIGURE 4.1

1. High Pressure Air/Enriched Air Cylinder
2. Two-stage Pressure Regulator
3. High Pressure Nitrogen Cylinder
4. Flow Controller
5. Gas Feed Rotameter (low range)
6. Gas Feed Rotameter (high range)
7. Pressure Gauge
8. Relief Valve
9. Combustion Cell
10. Pressure Regulator
11. Water Pump
12. Water Tank
13. 250ml Burette
14. Temperature Controller
15. Back-Pressure Regulator
16. Low-Pressure Separator
17. Ice Condenser
18. Ice Bath
19. Digital Temperature Display
20. Electrical Selector Switch
21. Produced Gas Rotameter (low range)
22. Produced Gas Rotameter (high range)
23. Oxygen Analyser
24. Switching Valve
25. Gas Chromatograph
26. Electronic Integrator
27. Mini-vials
28. Water Circulating Pump

On/Off valve
Check valve
Needle valve
Wall Heaters' Termination Cable
Thermocouples' Lead Wire
Flow Lines

Figure 4.2 COMBUSTION TUBE ASSEMBLY

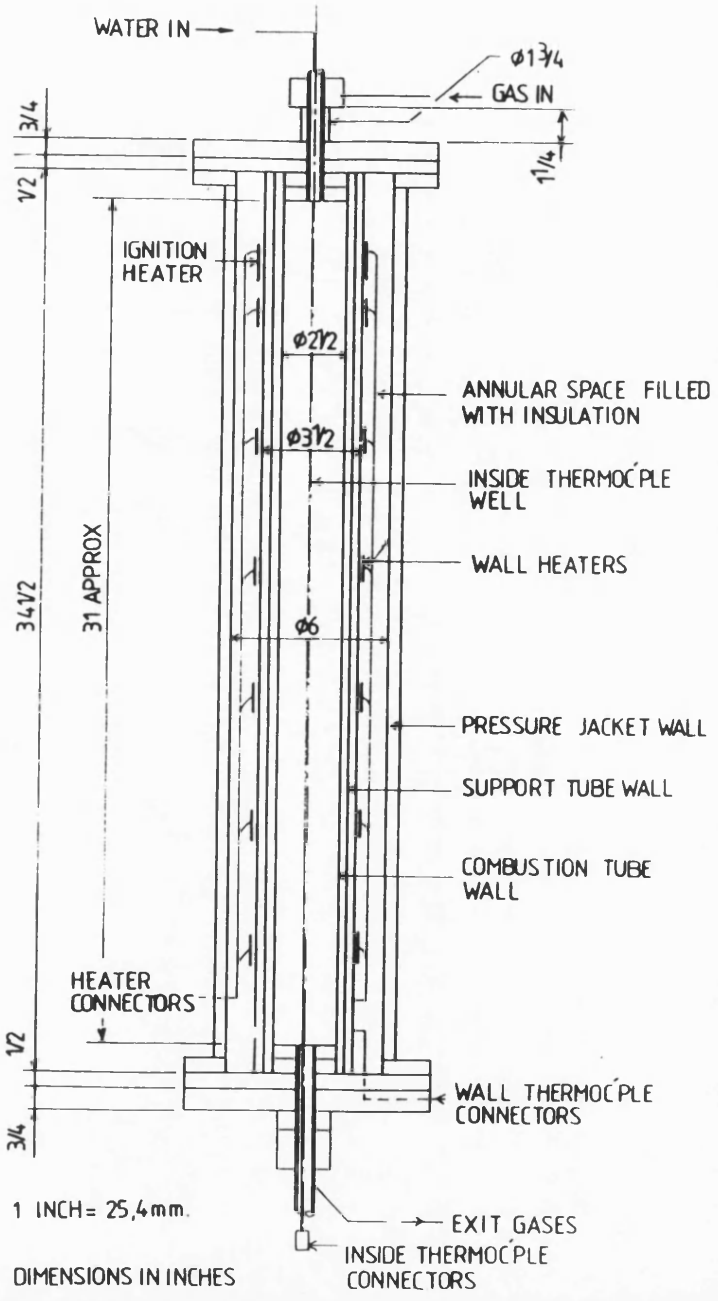

Table 4.1 COMBUSTION TUBE ASSEMBLY

Combustion Tube	Type 321 st. steel, 63.5mm I.D. x 12.7mm wall, 876.3mm length
Support Tube	Mild steel, 76.2mm I.D. x 12.7 mm wall, 876.3mm length
Pressure Jacket	Mild steel, 152.4mm I.D. x 19.1mm wall, 876.3mm length
Band Heaters	"Watlow St. Louis" 2-piece band heaters, 88.9mm I.D. x 38.1mm width, 500 watts.
Thermowel	Inconel tube, 9.5mm I.D. x 3.2mm wall
Thermocouple	Type K chromel-alumel, 0.315mm O.D x 1270mm length
Flanges	Type 304 st. steel, 235mm diameter x 19.1mm thickness
End packing	"Syndanyo" block, 235mm diameter x 12.7mm thickness
Screen	100 mesh st. steel used at bottom of pack
Annulus insulation	12.7mm thick ceramic fibre blanket. Vermiculite.
Gaskets	"Klingerite" gasket, serviceable to 500°C., 235mm O.D. x 3.2mm thickness.
Sealing compound	Dow corning RTV3145, silicon rubber based

The middle tube contains fifteen equally spaced holes (on 50.8mm pitch) arranged down the tube with consecutive holes at 120 degrees out of phase from each other. The holes were drilled as shown in Fig. 4.3 to suit fifteen 1.6mm chromel-alumel type thermocouples pressure gland connections. These were silver soldered into position. The thermocouples were installed so that the sensing points just touch the wall of the combustion tube. The middle tube is also equipped with seven 88.9mm i.d. electrical band heaters, which are distributed over the length of the tube. The topmost heater is used for ignition purposes while the other six are used to establish a partial adiabatic combustion tube operation. The power output of each heater is 500 watts.

Two 9.5mm BSP threaded holes, each of diameter 30mm and at a distance of 723.9mm apart were drilled on to the sides of the pressure jacket. These holes were to serve as the exit and relief points in the event that the annulus is pressurized through the gas inlet on the top flange. However, they were converted to outlets for the bandheaters' termination cables, while the annulus inlet point on the top flange was sealed off with nitrogen blanket. An external view of the pressure jacket is shown in Fig. 4.4.

Figures 4.5a to 4.5c show the detailed structure of the bottom end of the combustion tube assembly. This consists of a 19.1mm thick stainless steel end plate and a 12.7mm thick end packing ('syndanyo' block), each of 235mm in diameter. Three circular rows of concentric holes were drilled on both the plate and the packing. The first inner row consists of eight 8.5mm diameter equally spaced and threaded holes to suit 6.4mm bolts for securing the support tube in position on the end packing. The middle row comprises fifteen equally spaced and threaded holes for the thermocouples pressure gland connections, which provide the

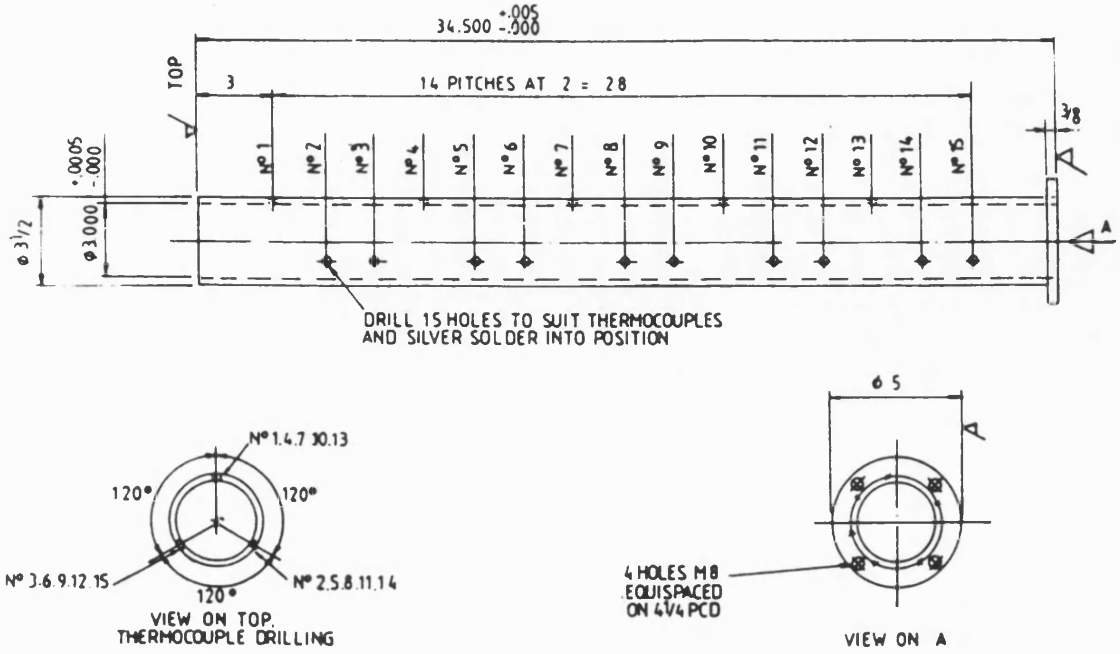

Figure 4.3 SUPPORT TUBE AND THERMOCOUPLE POSITIONS

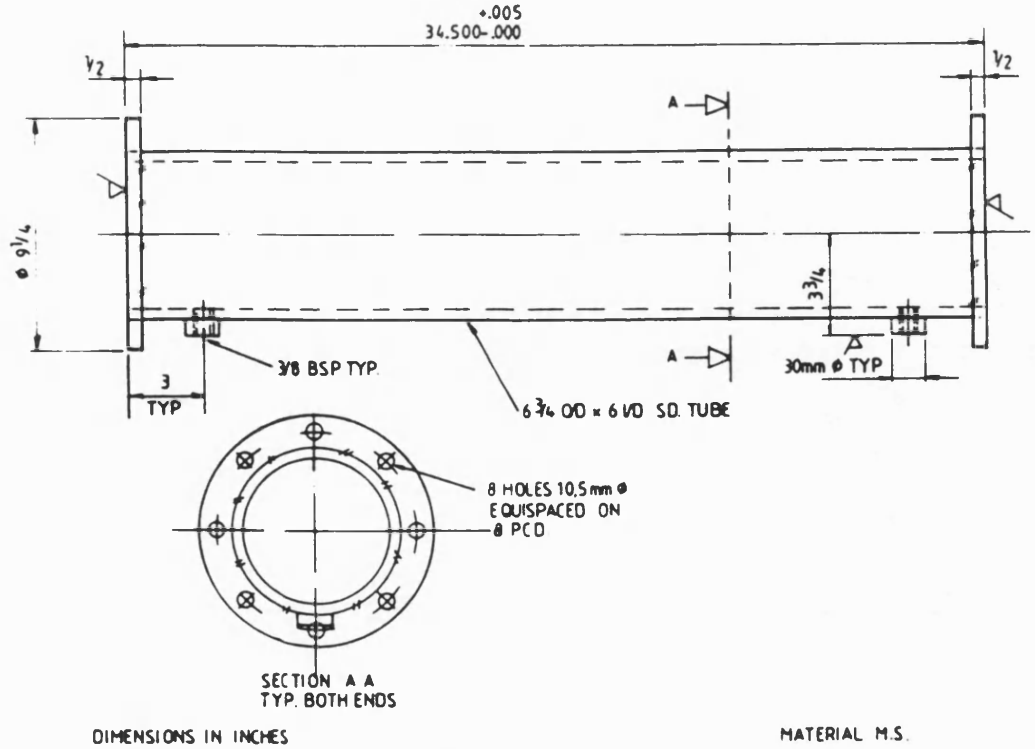

Figure 4.4 PRESSURE JACKET

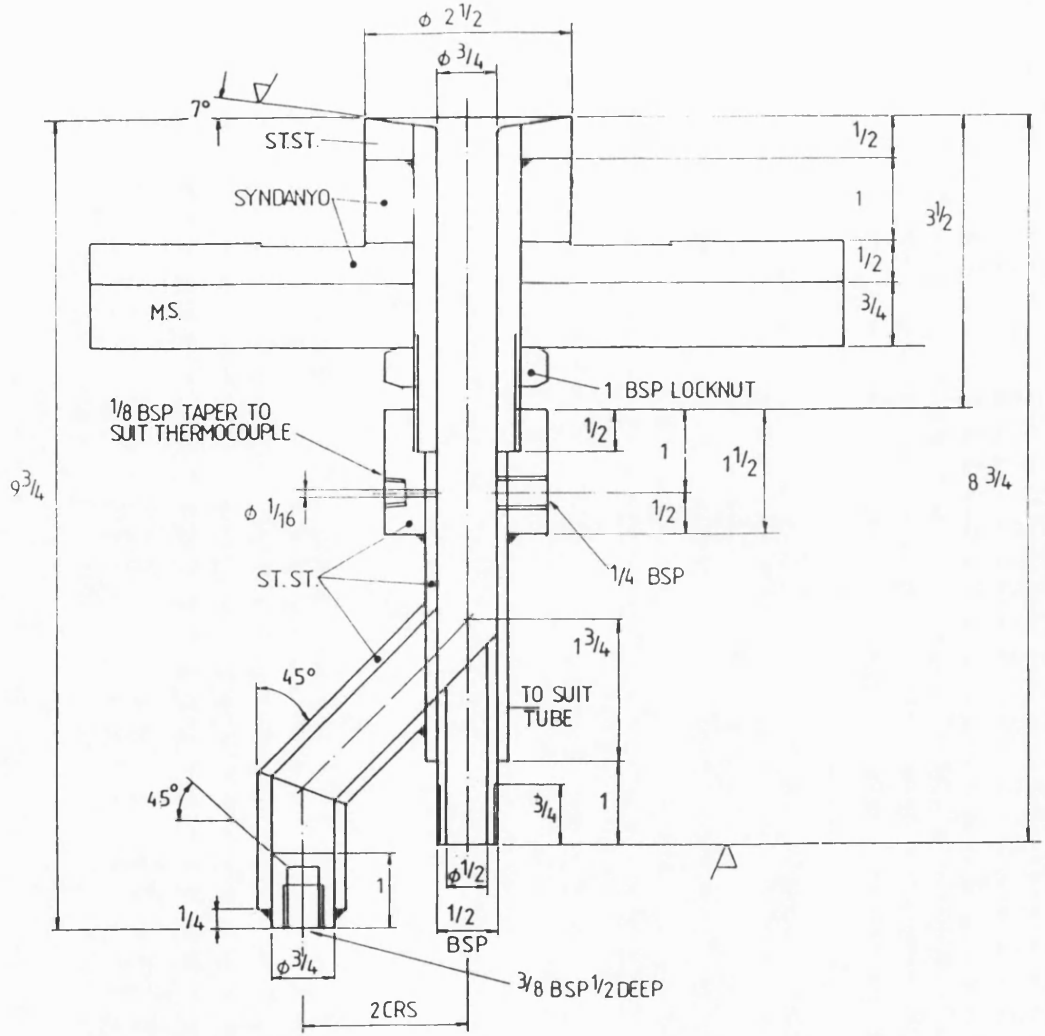

DIMENSIONS IN INCHES

Figure 4.5a BOTTOM FLANGE AND PACKINGS AND CONNECTIONS

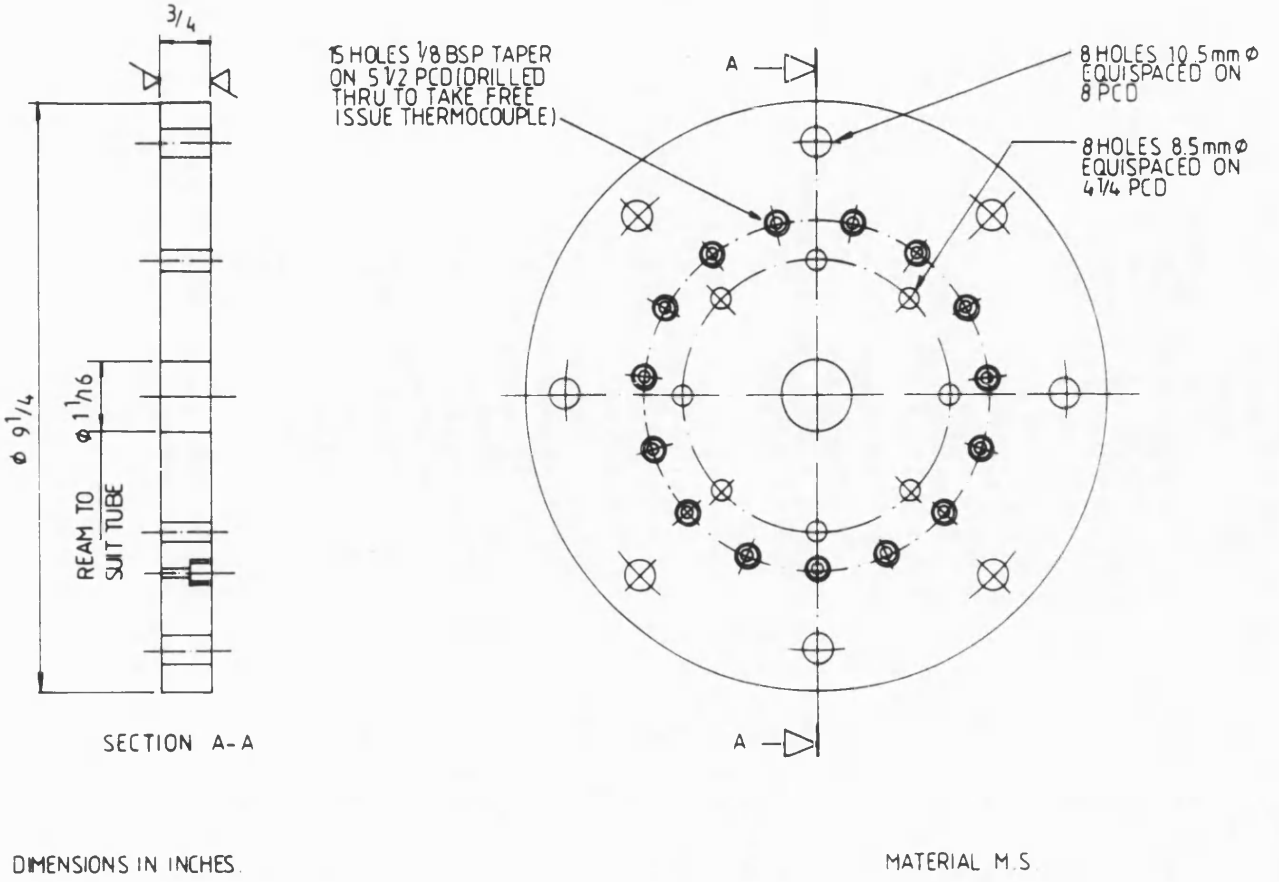

Figure 4.5b BOTTOM END PLATE

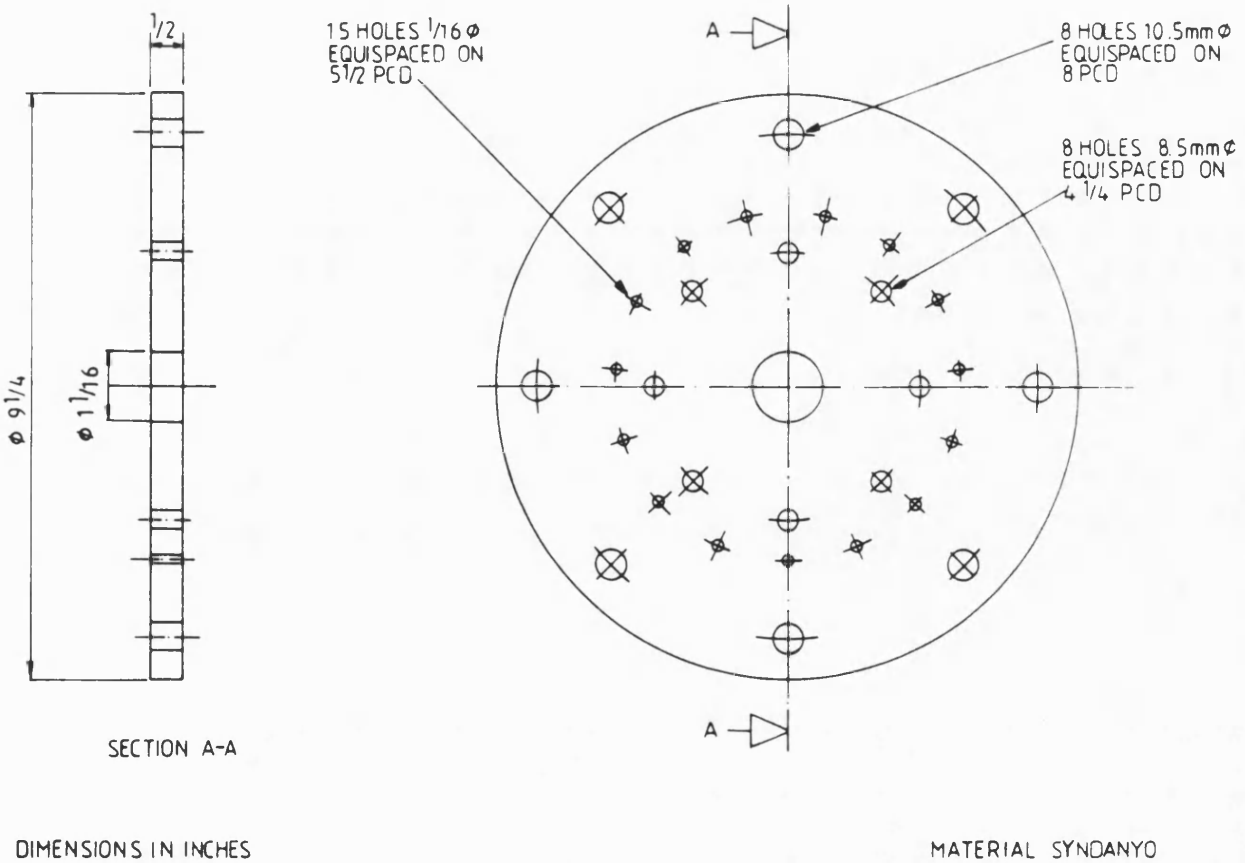

Figure 4.5c BOTTOM END PACKING GASKET

entrances for the wall thermocouples. The last outer row of eight 10.5mm diameter holes were also threaded to suit 8.5mm bolts to secure the pressure jacket in position. A 19.1mm i.d. by 3.4mm thick stainless steel pipe provides the exit for the produced fluid from the combustion tube. This was connected to the bottom of the combustion tube by a 12.7mm thick stainless steel plate and 25.4mm thick 'syndanyo' block, each of 63.5mm diameter and 27mm central holes. A 25.4mm BSP locknut was used to secure the end plate and the packing to the exit pipe in order to achieve tight contact between the end plate and the insulating syndanyo blocks and the inner plate. The exposed surface of the inner plate was slightly shaped into a conical surface, having a sloping angle of 7 degrees to the horizontal. This prevents accumulation of the produced liquids during operation. A 100-mesh screen positioned on the conical surface prevents sand production.

The external portion of the exit pipe was modified as shown in Fig. 4.5a to carry a pressure tap, thermocouple connection and the axial thermocouple well in addition to serving as the flow paths for the produced fluids. The thermowell is a 12.7mm O.D. inconel tube containing a spiral row of fifteen chromel-alumel type thermocouples positioned on a 50.8mm pitch. It runs along the central axis of the combustion tube such that the interior thermocouple junctions are at the same level as the exterior (wall) thermocouple junctions. The thermocouples were connected to the electrical control panel by lead wires. The paired wall and axial thermocouples measure the radial temperature gradient across the combustion tube.

The arrangement of the end plate, the 'syndanyo' insulating blocks and the inner plate for the top end of the

combustion tube assembly is similar to that at the bottom of the tube except that there is only one circular row of concentric holes for securing the pressure jacket at the top. A manifold block made of stainless steel was tightly screwed on to the inlet pipe through a 19.1mm BSP tapped hole to provide separate entrances for injected gas and water into the combustion tube. The top end arrangement is shown in Fig. 4.6a and other auxiliary parts are shown in Figs. 4.6b to 4.6d.

In order to minimize radial heat loss, a 12.7mm thick ceramic fibre blanket was wrapped around the support tube. In addition, the annulus space between the support tube and the pressure jacket was filled with a fine granular insulating material - Vermiculite insulator. The 'syndanyo' insulating blocks at each end of the tube also prevent axial heat loss by conduction through the end plates. The combined effect of the syndanyo blocks, the vermiculite and the insulating blanket serve to reduce external heat loss during combustion tube experiment. 'Klingerite' gaskets, serviceable to 500°C, and a silicon rubber based sealing compound (Dow corning RTV 3145) were used to provide a gas tight seal at the top and bottom ends of the combustion tube. The system was designed to operate in vertical position with a pressure rating of 1725kPa.

4.2.2 Flow Control System

The flow control system comprises several control and relief valves, pressure and flow regulators, flowmeters, pressure taps and gauges, air, nitrogen, helium and enriched air (30 and 35% oxygen) cylinders equipped with two-stage pressure regulators.

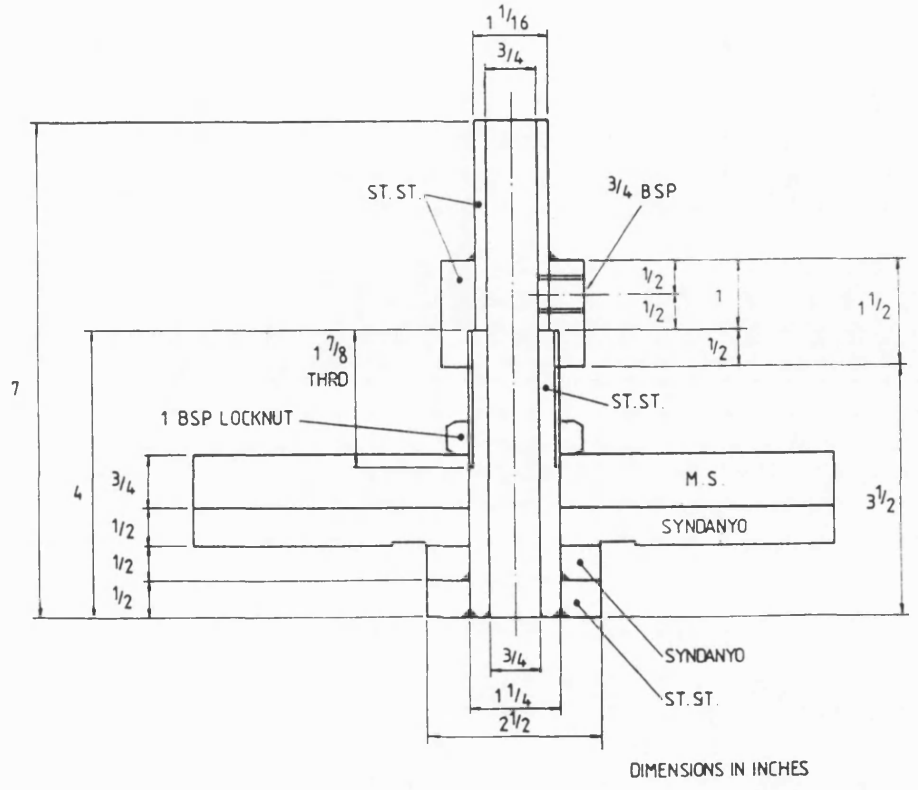

Figure 4.6a TOP FLANGE AND PACKINGS AND CONNECTIONS

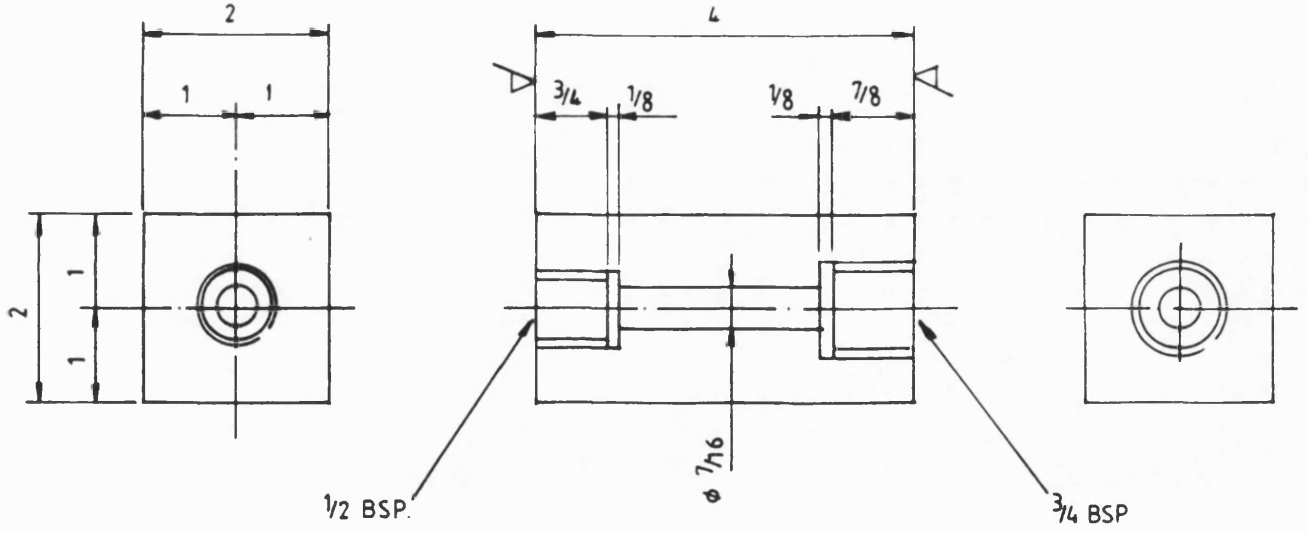

DIMENSIONS IN INCHES

MATERIAL STAINLESS STEEL

Figure 4.6b MANIFOLD BLOCK FOR FEED TUBE

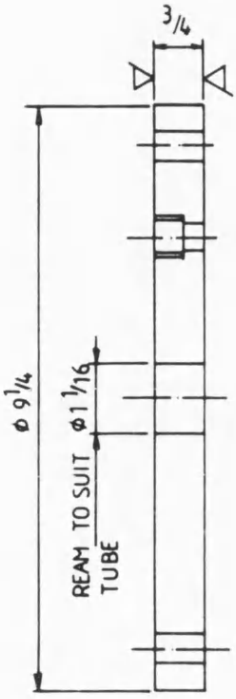

SECTION A-A

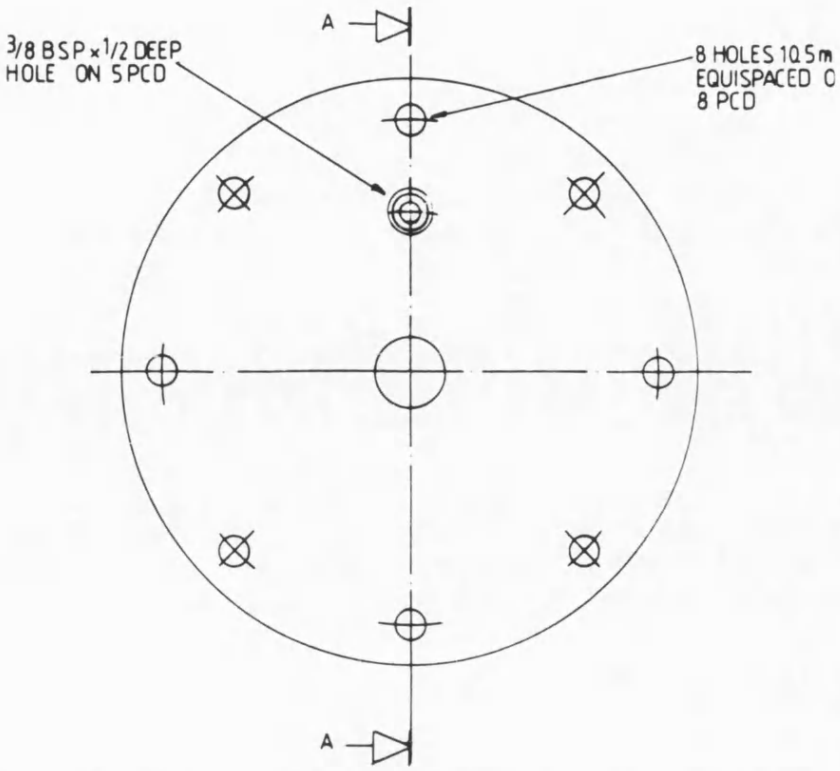

DIMENSIONS IN INCHES

MATERIAL M.S.

Figure 4.6c TOP END PLATE

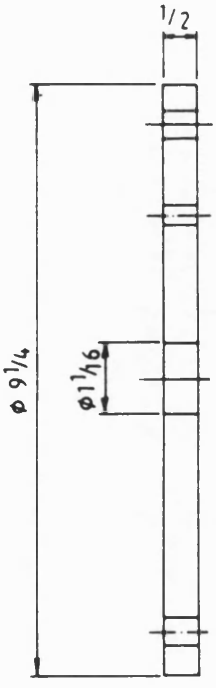

SECTION A-A

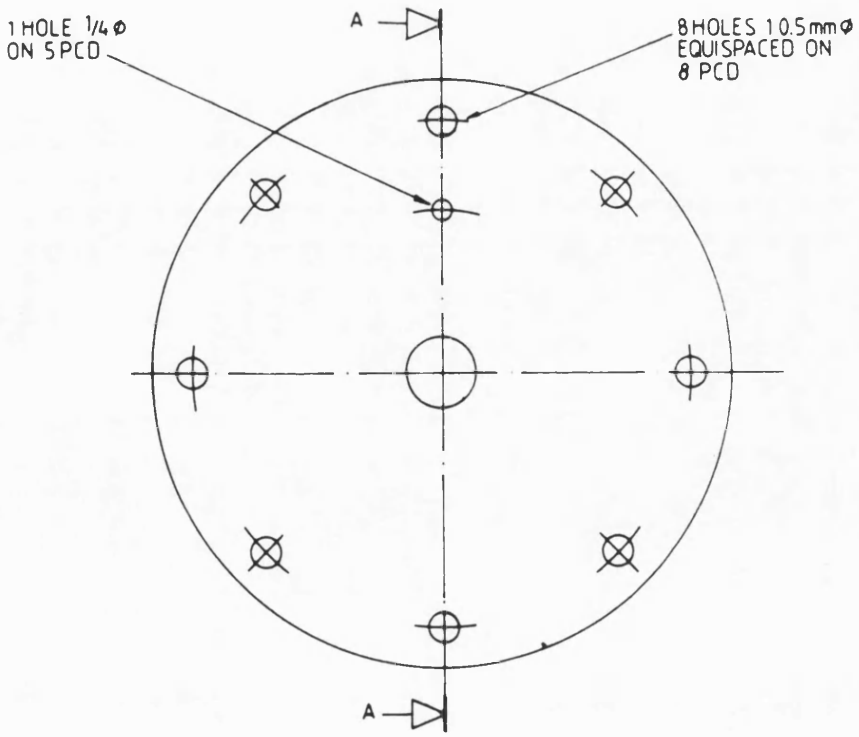

DIMENSIONS IN INCHES

MATERIAL SYNDANYO

Figure 4.6d TOP END PACKING

Also, a 0.22gph capacity metering pump which supplied from a water tank, was used for water injection into the combustion tube. Figure 4.1 shows the fluid flow path in the system. The gas feed to the combustion tube passed through a needle valve, a constant flow controller, a flowmeter and a check valve. A sampling line was created on the gas feedline so that the gas feed composition could be checked periodically with the gas chromatograph. An on-line relief valve was also installed on the gas feedline to prevent excessive pressure build up in the combustion tube. The relief valve discharges into the fume cupboard.

The produced fluid from the combustion tube passed through a back pressure regulator at the exit of the combustion tube and a low pressure glass separator (LPS) further downstream. The needle valve on the gas feedline and the combustion tube back pressure regulator were used to establish the required gas fluxes and operating pressures in the combustion tube. The back pressure regulator also protected the combustion tube against effects of any operation downstream. A relief valve with a cracking pressure of 10psig was installed at the inlet of the LPS to prevent overpressurizing the glass separator. The constant low pressure required inside the separator was however established using the back pressure regulator on its exit line. The gases from the separator passed through an ice condenser to effect separation of volatile light hydrocarbon components from the gas stream. Efficient separation of gases from liquid product was achieved by periodic circulation of cold water between the ice bath and the LPS outer glass jacket using a small centrifugal pump. The produced gas from the condenser was then metered through a flowmeter. A

highly efficient metering valve installed at the inlet of the produced gas flowmeter was used to maintain a constant produced gas flow rate. The metered gas finally discharged into the fume cupboard. A sampling line taken from the discharge line was connected to the gas chromatograph for on-line analysis of the produced gas. On the water injection line, there are shut-off valve, pressure regulator and a check valve. The shut-off valve was used to isolate the pump head while being drained prior to operation. The pressure regulator provided the means for controlling the water injection pressure to the required level. A vent line was installed on the pump delivery line to release any trapped air. The vent line was also used for the pump calibration.

4.2.3 Temperature Control System

Figure 4.7 shows the lay-out of the combustion tube temperature monitor and control system. The system comprises four 12-way selector switches (TSS) connected to a microprocessor based digital temperature display (DTD). This provided a visual observation of the temperatures measured by 30 axial and wall thermocouples and two others installed at the inlet and outlet of the combustion tube for measuring the temperatures of the injected and the produced gases respectively.

In addition, a Pye Ether (on/off) temperature controller (TC1) with analogue read-out regulates the power input to the ignition heater (BH1/2), while other wall heaters are individually controlled by a microprocessor based temperature controller (TC2). The latter is also equipped with an alarm control facility (AD). Panel mounted electrical switches (BHS) were provided for switching on and off the power supply from the mains.

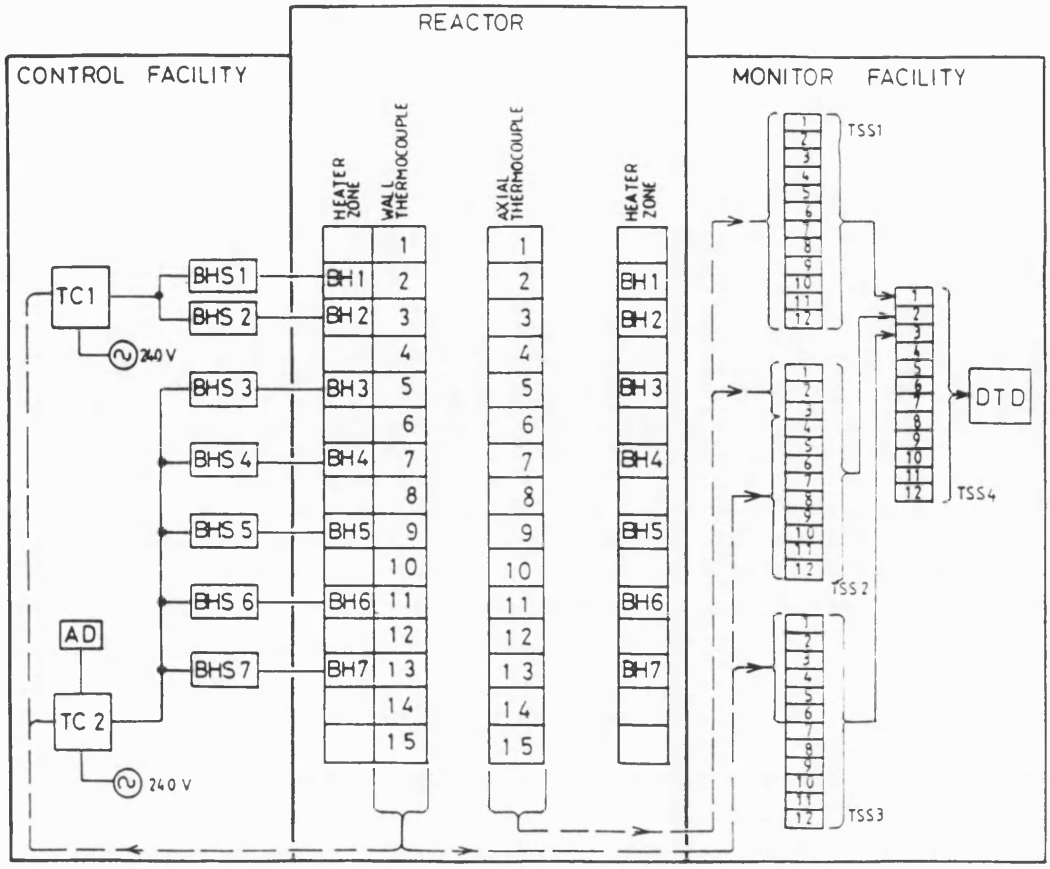

Figure 4.7 COMBUSTION TUBE TEMPERATURE MONITOR AND CONTROL SYSTEM

4.2.4 Fluid Analysis System

A servomex oxygen analyser 570A with a digital output was used to monitor the level of oxygen in the produced gas. The analyser was connected to an alarm control device which signals when the oxygen level of the produced gas exceeds the preset value. Two separate gas chromatographs were used for the detailed analysis of the liquid and gas products. One is equipped with thermal conductivity detector (TCD) and the other with a dual flame ionization detector (FID). Both chromatographs are Pye Unican 104 series.

The dual FID gas chromatograph was equipped with constant gas-flow controllers for carrier and make-up gases.

This makes the instrument suitable for capillary column application. The instrument has programmable controller which enables either a linear temperature change or isotherm operation over the oven temperature range of 35-500°C. A 50 metre glass capillary column (G-SCOT) with OV-101 as the stationary phase was used for analysing the liquid samples. In order to achieve optimum capillary column performance, a splitless injection system (SIS), which was primarily designed for the G-SCOT column, was used. The function of the SIS is to minimize the effective dead volume by reducing the injected sample size to within the capacity of G-SCOT which is considerably less than required for conventional packed column. Samples were introduced into the system using 1 microliter SGE syringe.

The gas chromatograph with TCD was used for the on-line analysis of the produced gas. This was achieved with a 1.524 metre long spherocarb 80/100 packed column. Spherocarb is a spherically shaped, non-friable carbon molecular sieve developed in 1976 by Analab (Field Instrument, England) for separating, in one analysis, complex gas mixtures.

A Hewlett-Packard (HP) 3390 series integrator connected to the two gas chromatographs by a switching mechanism provide the chromatographic data. Other analytical instruments employed are Brookfield synchro-lectric viscometer and PAAR digital density meter DMA 35. They were used for a more detailed analysis of the liquid products. The specification of major instruments used is contained in Table 4.2. Figure 4.8 is a photograph of the complete experimental apparatus.

Table 4.2 INSTRUMENTS IN THE CIRCUIT

Control Valve	1. "Brooks" model 8510 straight pattern needle valve, max. flow rate 0.18sm³/hr, air, pressure limit 6600kPa, temp. limit 120°C material st. steel.
	2. "Porter" Teflon metering valve max. flow rate 0.354sm³/hr, air, pressure limit 700kPa, temp. limit 121°C, material TFE virgin teflon
Flowmeters	1. "Brooks" model 3750/8805 flowmeter with integrally-piped flow controller, flow range 0.16-1.6sm³/hr, air, accuracy ± 10% pressure limit 6900kPa, temp. limit 94°C, scale 0-100 divs. with calibration curve material 316 st. steel.
	2. "Porter" series F150 flowmeter, flow range 0-0.98sm³/hr, air, accuracy ± 5% full scale, pressure limit 1400kPa, temp. limit 94°C scale 0-150mm with calibration curve material Borosilicate glass
	3. "Platon Flowbits" G.A.P. flowmeter with glass tapered tubes, flow range 0.036- 0.36sm³/hr, pressure limit 355kPa 0.060-0.72sm³/hr pressure limit, 10150kPa, accuracy ± 1 % mass flow temp. limit 100°C, scale Direct reading on tube material Borosilicate glass tube, red dural float.
Pressure Indicator	"Budenberg" pressure gauge 114.3mm Dial, pressure range 0-700kPa, 0-7000kPa
Pressure Regulators	1. "Veriflow" CSG880 series pressure regulator, inlet pressure range 0-28000kPa, adjustable outlet pressure range 0-4200kPa, inlet and outlet gauges 50.8mm diameter max. flow 12sm³/hr, air, temp. limit -4°C to +121°C material 316 st. steel
	2. "Veriflow" BPR40 series back pressure regulator, inlet pressure range 0-4900kPa max. flow 15sm³/hr, air, gauge 50.8mm diameter. material 303 st. steel

	3. "Veriflo" BPR30 series Back pressure regulator, inlet pressure range 0-700kPa max. flow 6.0sm^3/hr, air, gauge 50.8mm diameter, material 316 st. steel.
Electrical Selector Switches	"Electroplan" panel mount 12-way selector unit 3750SP for type K- T/C
Temperature Controller and Indicator	"Eurotherm" 810 microprocessor based 3-term controller and indicator, input-type KT/C output - 2A/240V slow cycle relay output scale range 0-300°C, full scale alarm
Gas analysers	1. "Taylor" servomex 570A oxygen analyser, internally mounted sampling pump, sample gas pressure 2.3-70kPa Digital output 0-100% O_2, Accuracy ±0.1%, linearity 0.1 Temperature range 0 to 50°C Intrinsically safe 2. "Pye" heated kathrometer programmed chromatograph, model 44 3. "Hewlett Packard" electronic plotting/reporting integrator, series 3390
Liquid analysers	1. "Pye" heated dual flame ionization detector programmed chromatograph, model 64 2. "PAAR" digital density DMA35, Digital output 0-1000kg/m^3, Temperature range 0-40°C. 3. "Brookfield" synchro-Lectric viscometer. Digital output 0-4000 cp.
Metering pump	"MPL" metering pump, capacity 0-0.22gph, Discharge pressure 7000kPa, stroking speed 100spm, Material 316 st. steel

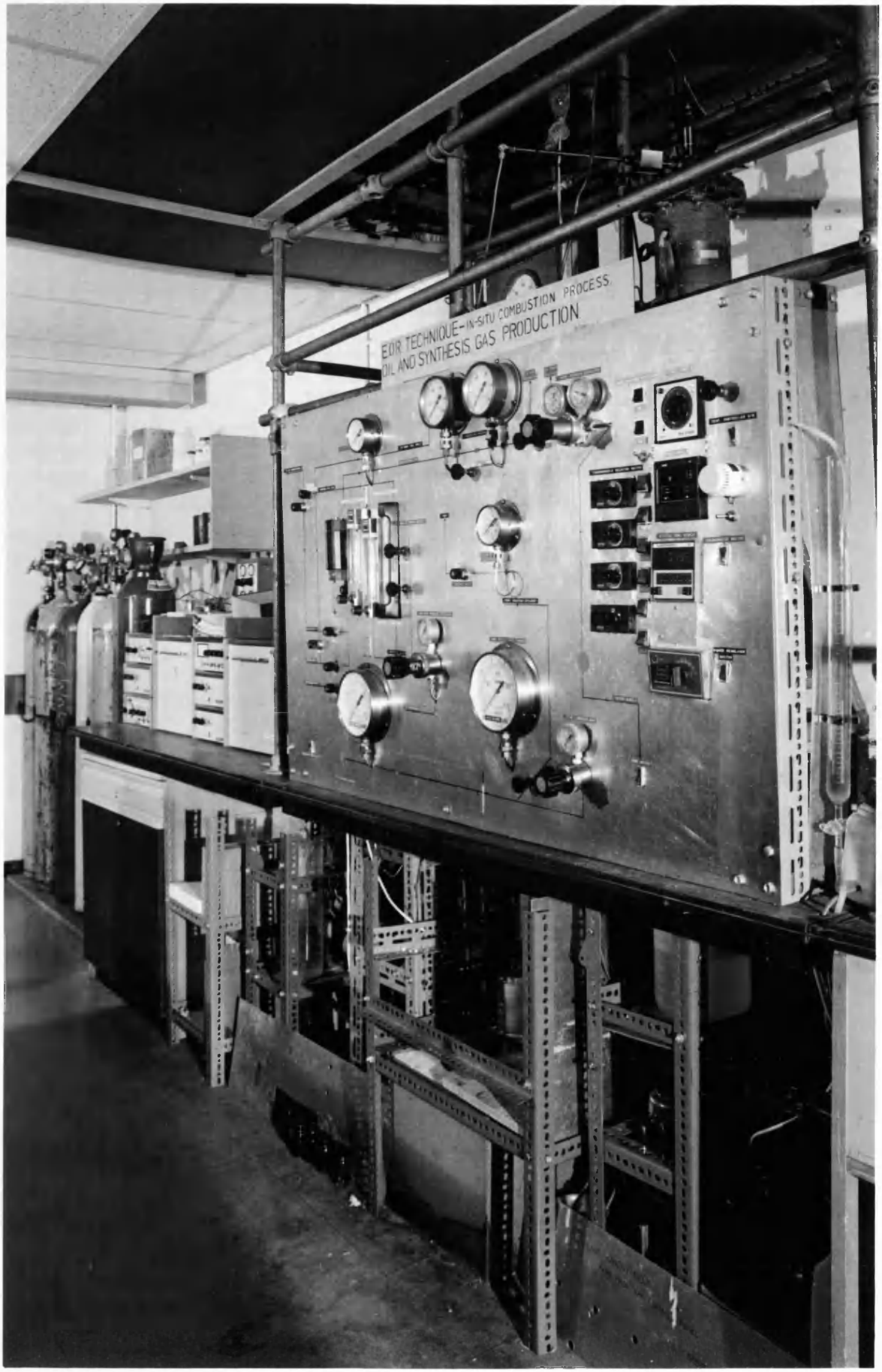

Figure 4.8 PHOTOGRAPH OF EXPERIMENTAL APPARATUS

4.3 Experimental Procedure

The procedure for the experiments is classified into three major parts:

1. Preparation of Combustion Tube,
2. Combustion Tube Run,
3. Post-Operation Procedure.

4.3.1 Combustion Tube Preparation

For each experiment, approximately 2.5kg of pure silica sand, 0.25kg of kaolinite clay, 1.0×10^{-4} cubic metre of water and 1.3×10^{-4} cubic metre of crude oil were mixed in a plastic mixing bowl with a wooden spoon. Care was taken to prevent losses of material and to ensure homogeneity throughout. Packing of the combustion tube was carried out at room temperature via the injection end. In each batch of approximately 0.75kg of mixture introduced, the combustion tube contents were tamped gently with a 1.0 metre length stainless steel rod fitted with a horizontal disc at its tamping end. In this way, the combustion tube was tightly and uniformly packed with the thermowell in position. During the packing process, representative samples were periodically taken. These were later subjected to toluene extraction by the USBM method (Rall et al., 1946) to determine the initial liquid saturation and porosity of the medium. The sand mixture remaining at the end of the packing process was weighed to determine the amount of material packed.

After charging the combustion tube with the sand, oil and water mixture, the combustion tube and the pressure jacket were sealed off at the top end, and the inlet and outlet flow lines were connected. The sealing compound which was applied required

about 24 hours to cure properly. The combustion tube assembly was checked for leaks by pressurizing with nitrogen. Any leaks detected with the aid of soap solution were immediately corrected.

The remaining steps included checking and replacement, if necessary, of the oxygen analyser filter element and the eventual calibration of its meter. Finally, all of the instruments and electrical connections were checked. For wet combustion tests, however, the operation of the metering pump was checked and then set at the required water injection rate.

4.3.2 Combustion Tube Run

Nitrogen injection at 0.015sm^3/hr and 140kPa inlet pressure was used to establish gas permeability through the sand pack. This was continued until all the trapped air was displaced from the tube. When no oxygen was detected in the effluent gases by the oxygen analyser and gas chromatograph, the wall heaters were turned on, and the temperature of the sand pack was raised uniformly to 70°C. While the nitrogen was still flowing through the sand pack, the ignition heater was turned on and the temperature of the top of the bed allowed to reach 300°C. Nitrogen injection was then stopped, and air injection commenced immediately. This procedure ensured that fast ignition of the oil occurred, thus eliminating any low-temperature oxidation reactions effect. An ignited state was identified when a rapid rise in temperature occurred at the sand face. This was also confirmed by the sudden drop in oxygen and an increase in carbon monoxide and carbon dioxide concentrations in the effluent gas. After ignition was achieved, the inlet flow control valve and the back pressure regulator at the combustion tube exit were used to establish the required run conditions; namely, the gas injection pressure and the

gas flux. At this stage, the heat input to the ignition heater was regulated to maintain a constant inlet temperature. The other wall heaters were used separately to provide partial adiabatic condition at different combustion front locations by maintaining the corresponding wall temperatures at 350°C. In all of the tests, data pertaining to combustion tube wall- and axial-temperature profiles, inlet and outlet pressures, the effluent gas flow rate and composition were recorded on the 15 to 30 minute-cycles. In addition, the separator and the condenser were frequently checked for the first sign of liquid production. The produced liquids were collected in mini-vials of known weights, at intervals of 30-45 minutes.

In the case of wet combustion tests, water injection at a preset rate was commenced once the stabilized combustion front had travelled a distance of two or three thermocouple positions.

Close monitoring of the process was maintained throughout the entire period of each combustion test. This was necessary to ensure steady propagation of the combustion front. The run was terminated when the combustion front just passed the last axial thermocouple situated near the bottom of the tube. The wall heaters (and water pump, for wet combustion) were then switched off. Also, gas injection was switched back to nitrogen to quench the combustion front. Extinction of the front was indicated by a sudden drop in carbon oxides concentrations in the produced gas. Continued nitrogen injection was used to cool the combustion tube prior to unpacking. Finally, after the combustion tube assembly had cooled down to ambient condition, the system was depressurized by shutting off the nitrogen supply and gradually reducing the back pressure to zero.

4.3.3 Post-Operation Procedure

At the end of each combustion run, the combustion tube was opened from the injection end. Sand pack samples were removed from the tube in approximately 152mm intervals for visual inspection. Representative samples were then subjected to toluene extraction to determine the fluid distribution along the tube. The produced liquids were separated into oil and water fractions by a high speed MSE centrifuge and each fraction was weighed. In those cases where emulsion had formed, a known quantity of toluene was added before centrifuging. These samples, which were mainly a small fraction of the total recovery, were used only for material balance purposes. The uncontaminated oil fractions were mixed together and analysed to determine the densities, viscosities and simulated distillation data. All of the temperature, meter and produced gas compostion data for the successful runs were stored in files created in the University Multics computer.

Chapter 5

IN-SITU COMBUSTION CHARACTERISTICS

A total of 18 forward in-situ combustion experiments were performed on Maya crude which has an API gravity of 22.8°. The results of 12 successful runs are presented and discussed. The other six runs were judged to be unsatisfactory in the sense that they failed due to operational problems with the equipment or because complete analysis of these results was not possible. Typical equipment problems which were experienced in particular experiments included blockage of the water injection line due to accumulation of sand particles. This caused difficulties in operating the water injection (metering) pump. There were also unexpected small leaks on the tube which led to shutdown of the equipment.

The twelve successful runs comprise six dry and six wet experiments conducted at pressures of 380, 690 and 1020kPa. In addition to using air as the oxidant gas, a number of experiments involved the use of oxygen enrichment to a level of 30 and 35% oxygen. The wet combustion experiments employed water-gas injection ratios (WGR) up to $6.32 m^3/Msm^3$. A summary of the major experimental conditions employed for each combustion run is given in Tables 5.1 and 5.2.

The experimental investigations cover the effect of operating pressure, WGR and oxygen enrichment on primary in-situ combustion characteristics, which is the subject of this chapter. Treatment of combustion reaction kinetics, oil recovery and properties of the produced oil are covered in later chapters.

The combustion characteristics for the various experiments are analysed by comparing such dependent variables as:

TABLE 5.1 SUMMARY OF SAND PACK PROPERTIES

SAND PACK PARAMETERS												
RUN NO	SILICA SAND (30-60 mesh)	CLAY (Kaolin)	OIL	WATER	POROSITY	PACK DENSITY	SATURATIONS % PORE VOL.		LIQUID IN PLACE m^3/Mm^3		INITIAL BED TEMPERATURE	CRUDE OIL PROPERTIES
	%wt	%wt	%wt	%wt	Per cent	$kg/m^3 x10^{-3}$	Oil, So_i	Water Sw_i	OIL	WATER	°C	
01	83.98	8.43	4.11	3.48	28.8	1.14	22.2	17.2	63.71	49.48	70	Crude Oil : Maya
02	83.97	8.43	4.10	3.50	26.7	1.17	24.4	19.1	65.12	50.97	70	Gravity, °API : 22.8
03	83.96	8.43	4.16	3.45	25.7	1.19	25.6	19.5	65.11	50.96	70	Viscosity (Cp)
04	84.02	8.44	4.11	3.11	25.7	1.19	25.6	19.7	65.87	50.54	70	at 100°F : 40.0
05	83.98	8.44	4.11	3.48	26.2	1.18	25.5	19.8	66.83	51.86	70	Density (g/cc)
06	83.98	8.44	4.11	3.48	24.7	1.20	26.7	20.7	65.99	51.23	70	at 100°F : 0.92
07	83.99	8.44	4.11	3.46	24.8	1.20	26.8	20.7	66.39	51.25	70	Avg. Boiling Pt.
08	84.00	8.44	4.11	3.45	25.5	1.19	26.0	20.0	66.20	50.96	70	(°C) : 275.4
09	84.00	8.44	4.11	3.45	28.0	1.15	22.9	17.6	63.98	49.25	70	Mol. Weight : 204
10	83.99	8.44	4.11	3.46	24.7	1.20	27.0	20.9	66.71	51.50	70	C/H Weight Ratio : 7.87
11	83.95	8.43	4.11	3.51	24.2	1.21	27.7	21.7	67.13	52.57	70	UOP Character-
12	83.98	8.44	4.11	3.48	24.8	1.20	27.2	21.1	67.49	52.40	70	isation Factor : 10.88

TABLE 5.2 SUMMARY OF OPERATING PARAMETERS

CONTROL PARAMETERS							
RUN NO	INJECTED GAS ANALYSIS, VOL.%		SYSTEM PRESSURE	AVERAGE GAS INJECTION RATE	TOTAL GAS FLUX	OXYGEN FLUX	WATER-GAS INJECTION RATIO
	O_2	N_2	kPa	sm^3/hr	sm^3/m^2hr	sm^3/m^2hr	m^3/Msm^3
01	21.0	79.0	380	0.0333	10.53	2.21	0.00
02	21.0	79.0	380	0.0516	16.28	3.42	0.00
03	21.0	79.0	690	0.0533	16.84	3.54	0.00
04	21.0	79.0	1020	0.0552	17.44	3.66	0.00
05	30.0	70.0	380	0.0505	15.96	4.79	0.00
06	35.0	65.0	380	0.0527	16.63	5.82	0.00
07	21.0	79.0	690	0.0557	17.59	3.69	2.03
08	21.0	79.0	380	0.0343	10.82	2.27	3.16
09	21.0	79.0	380	0.0347	10.95	2.30	6.32
10	21.0	79.0	1020	0.0538	16.98	3.57	1.47
11	30.0	70.0	380	0.0540	17.05	5.12	1.83
12	35.0	65.0	380	0.0567	17.90	6.27	1.79

Produced gas composition, combustion tube temperature profile, fuel combustion rate, combustion-front velocity, atomic hydrogen-carbon ratio, fuel consumption, air requirement and oxygen utilisation. Most of these variables are averages taken over the stabilized combustion period. A summary of the main results for all of the 12 experiments is given in Table 5.3 and detailed results are presented graphically.

TABLE 5.3 SUMMARY OF COMBUSTION TUBE RUN RESULTS

RUN NO:-	01	02	03	04	05	06	07	08	09	10	11	12
COMBUSTION FRONT VELOCITY (m/hr)	0.068	0.078	0.068	0.063	0.082	0.107	0.115	0.076	0.092	0.094	0.114	0.128
NORMALIZED FRONT VELOCITY (m^3/sm^3)x10^3	6.458	4.790	4.038	3.612	5.138	6.434	6.538	7.024	8.402	5.536	6.690	7.150
AVC COMBUSTION FRONT PEAK TEMPERATURE (°C)	399	410	406	406	416	424	418	383	384	405	400	414
PRODUCED GAS ANALYSIS												
CO, VOL.%	3.388	3.366	3.382	3.201	4.638	5.226	2.492	2.205	2.128	2.113	3.152	3.127
CO_2, VOL.%	13.182	12.986	13.492	13.366	17.019	17.976	14.446	14.588	13.943	14.859	16.532	15.615
CH_4, VOL.%	0.000	0.073	0.000	0.000	0.000	0.074	0.000	0.000	0.000	0.047	0.000	0.527
MOLAR CO/CO_2 RATIO	0.26	0.26	0.25	0.24	0.27	0.29	0.17	0.15	0.15	0.14	0.19	0.20
ATOMIC H/C RATIO	0.56	0.65	0.60	0.76	0.69	0.80	0.49	0.47	0.75	0.45	0.94	2.04
OXYGEN UTILISATION, %	99.94	100.00	100.00	100.00	100.00	100.00	100.00	99.23	99.40	99.90	99.10	98.90
FUEL COMBUSTION RATE												
CARBON (kg/hr)x10^3	3.10	4.80	5.00	4.90	6.20	6.70	5.00	3.00	2.90	4.90	5.60	5.30
COKE (kg/hr)x10^3	3.20	5.00	5.20	5.20	6.60	7.20	5.30	3.10	3.10	5.10	6.10	6.30
FUEL (COKE) CONSUMPTION												
kg Coke/100kg sand	1.32	1.75	2.05	2.20	2.14	1.75	1.19	1.09	0.92	1.42	1.38	1.27
kg Coke/m^3 reservoir vol.	14.99	20.50	24.38	26.12.	25.25	21.09	14.29	12.95	10.58	17.08	16.73	15.30
GAS REQUIREMENT												
Sm^3gas/m^3 reservoir vol.	154.9	208.9	247.7	276.8	194.6	155.4	153.0	142.2	118.9	179.8	149.6	139.9
Sm^3gas/kg of OIP	2.66	3.50	4.10	4.58	3.17	2.57	2.24	2.25	2.04	2.97	2.40	2.11
Sm^3gas/kg of produced oil	4.04	6.04	6.68	7.87	5.90	3.92	2.87	3.07	2.68	4.27	3.39	3.07
Sm^3gas/kg of coke burned	10.80	10.84	10.57	10.92	8.31	7.65	10.67	10.76	11.13	10.65	8.99	9.11
HEAT GENERATION RATE (kJ/hr)	104.0	165.9	171.3	178.4	220.1	244.2	176.6	103.9	110.5	169.8	221.6	274.8
CUMULATIVE (NET) HEAT LOSS %	22.0	25.0	-	-	30.0	6.00	-	-	-	-	-	-

5.1 Produced Gas Composition

Figures 5.1 to 5.6 show the composition profiles (CO and CO_2) of the exit combustion gases at pressures of 380, 690 and 1020 kPa. The trend of molar $CO/(CO + CO_2)$ ratio under these conditions, as a function of combustion time is shown in Figs. 5.7 to 5.12. Both the level of CO and CO_2 and the molar ratio exhibit

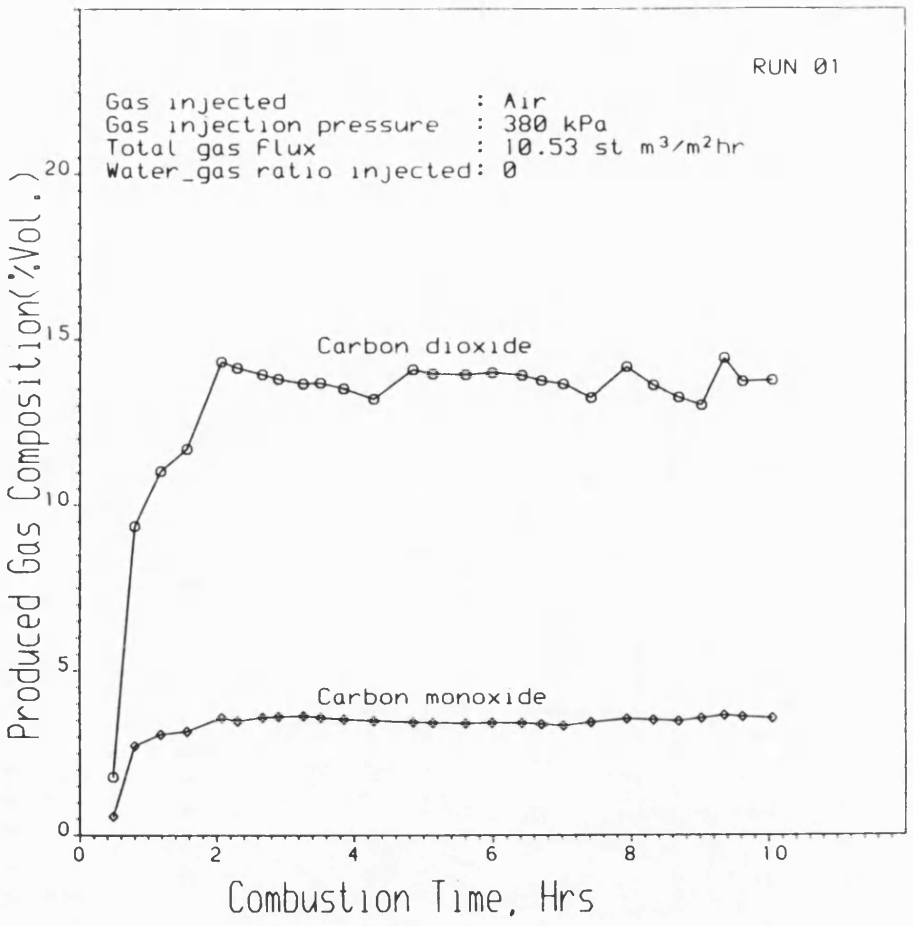

Figure 5.1 PRODUCED GAS COMPOSITION PROFILE

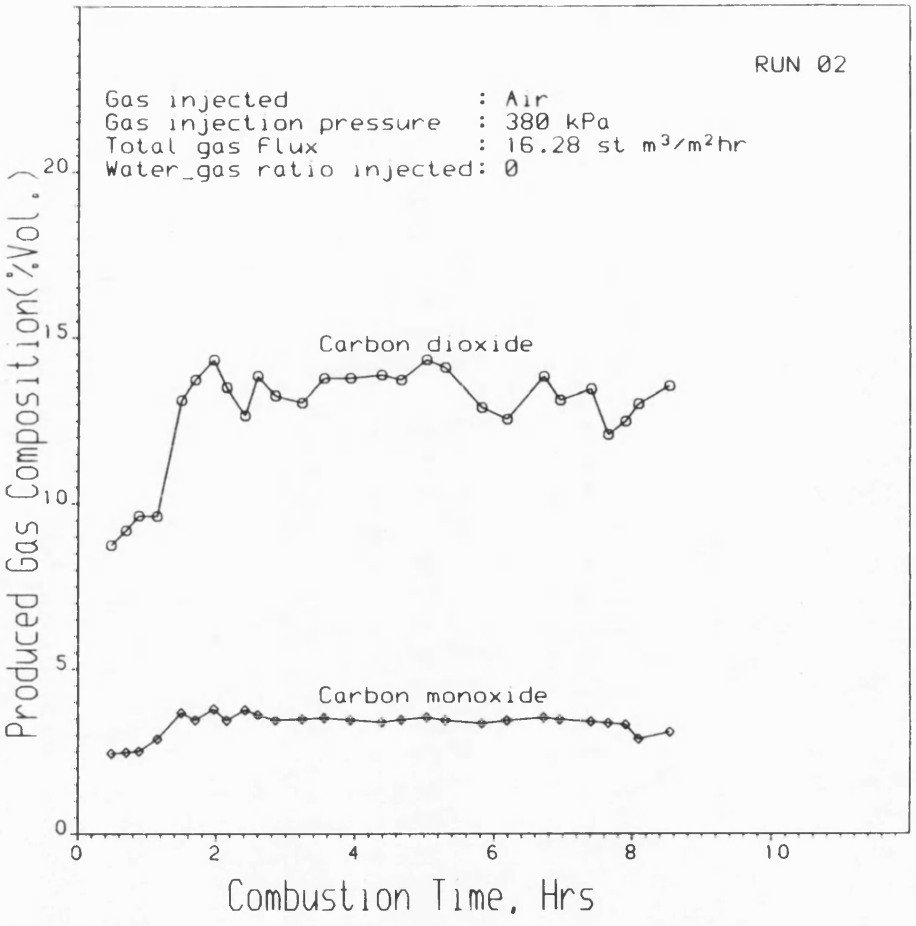

Figure 5.2 PRODUCED GAS COMPOSITION PROFILE

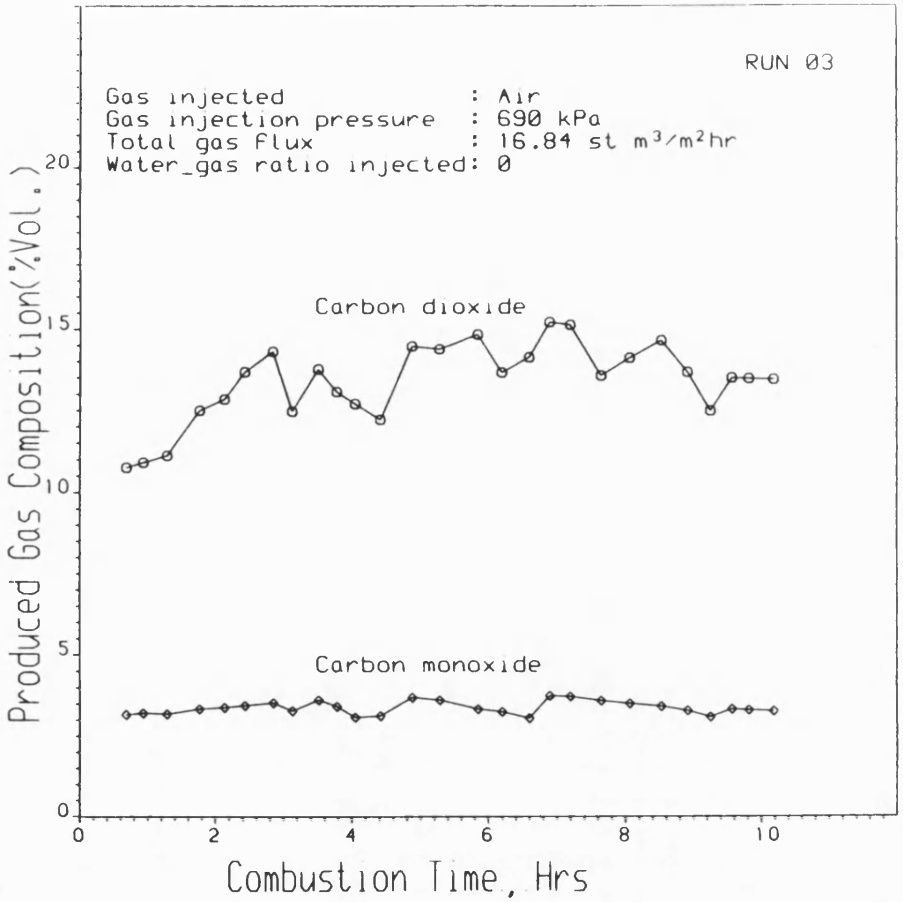

Figure 5.3 PRODUCED GAS COMPOSITION PROFILE

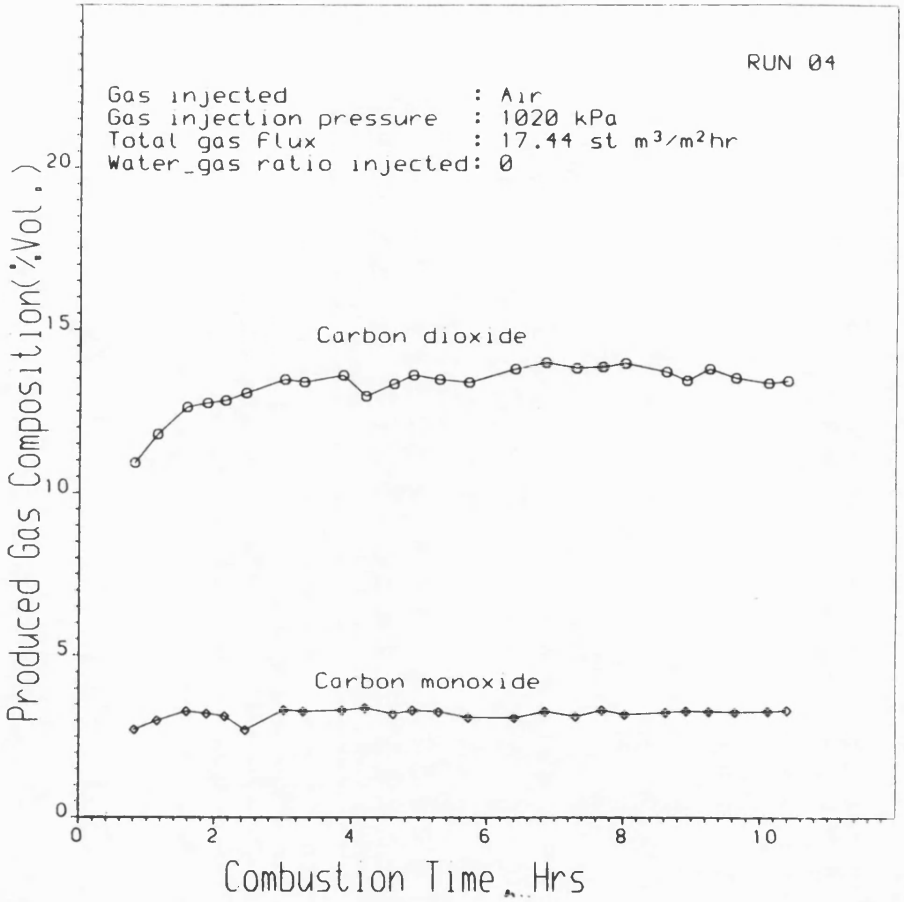

Figure 5.4 PRODUCED GAS COMPOSITION PROFILE

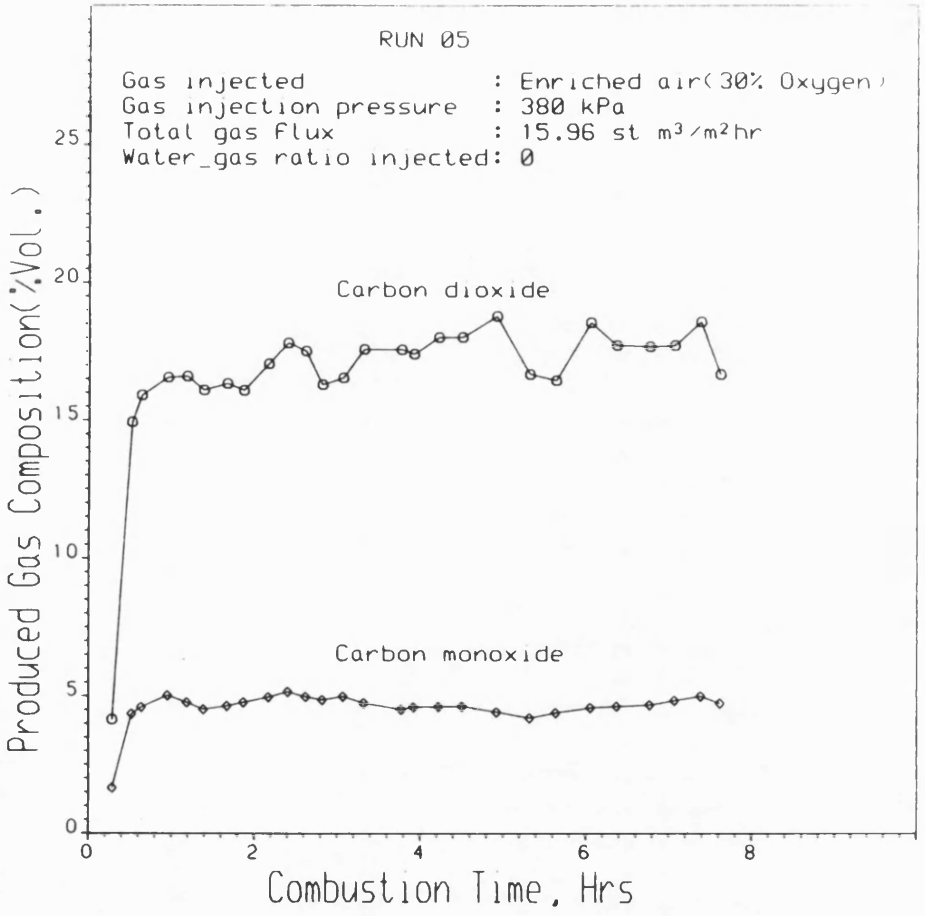

Figure 5.5 PRODUCED GAS COMPOSITION PROFILE

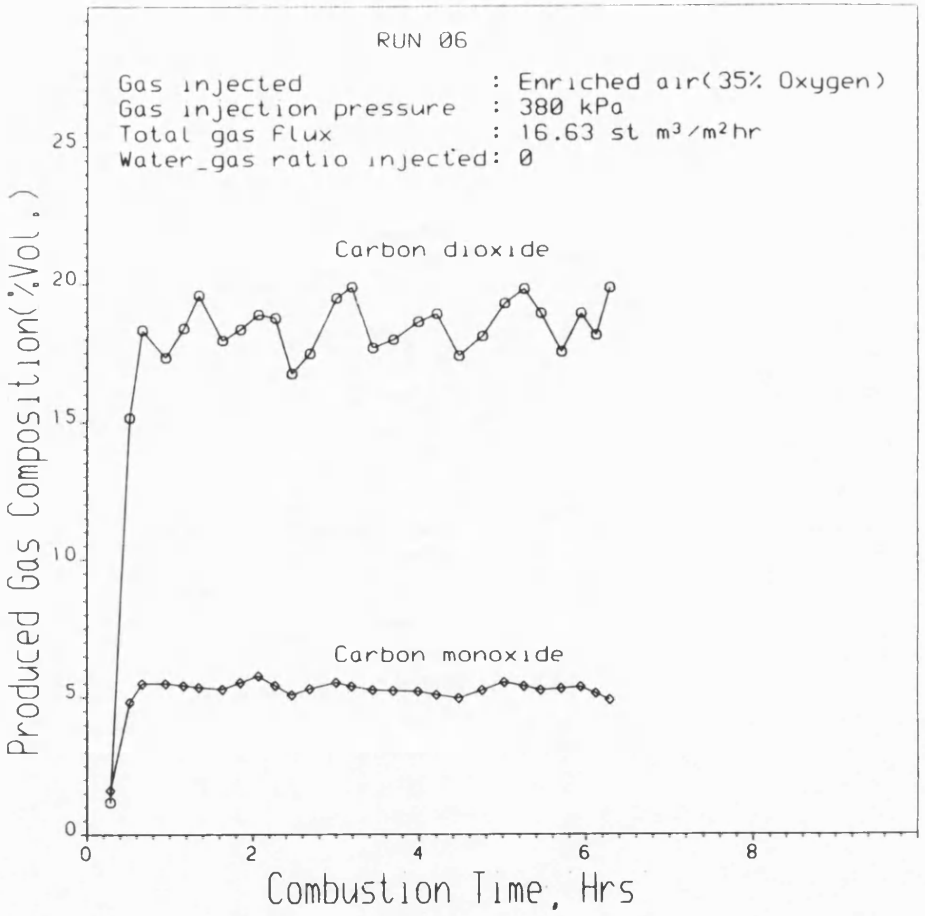

Figure 5.6 PRODUCED GAS COMPOSITION PROFILE

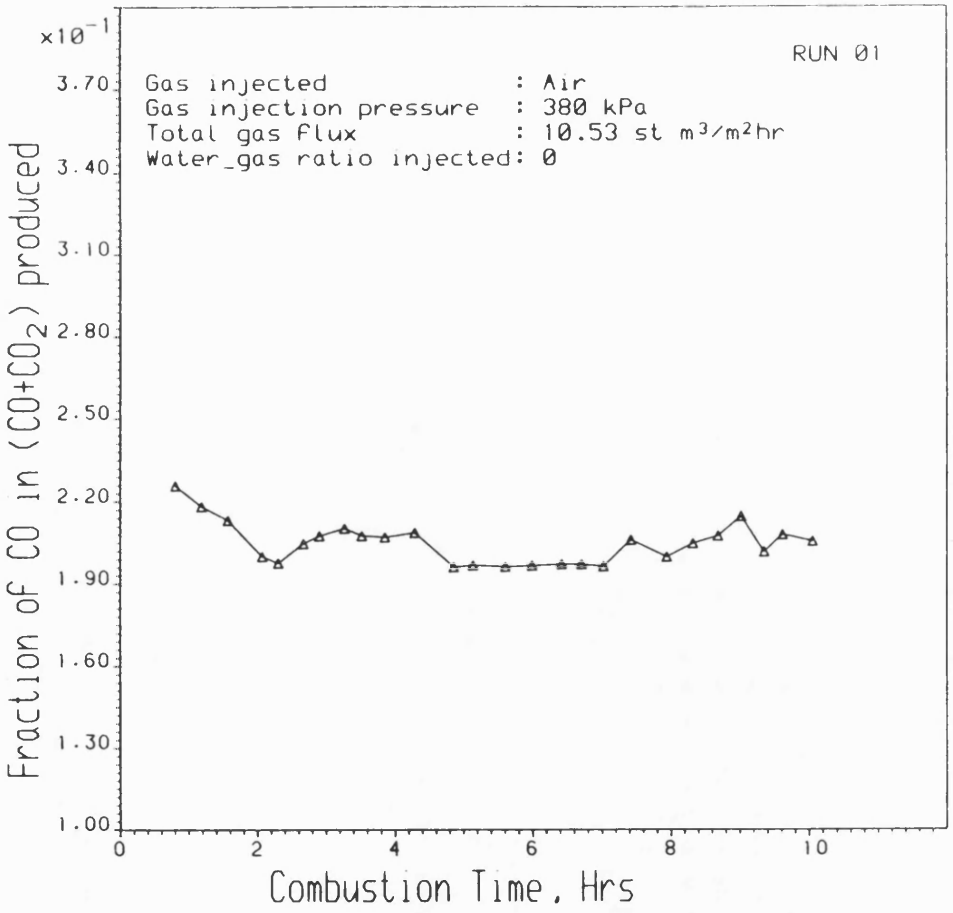

Figure 5.7 FRACTION OF CARBON GASIFIED AS CARBON MONOXIDE

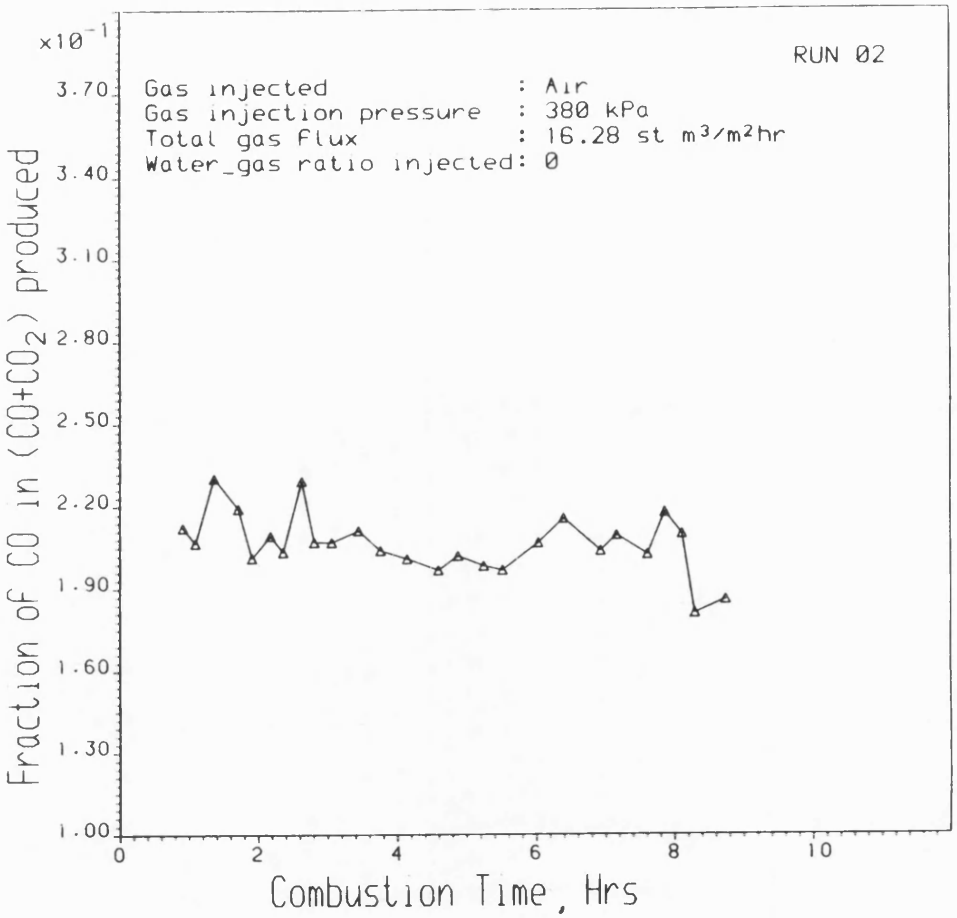

Figure 5.8 FRACTION OF CARBON GASIFIED AS CARBON MONOXIDE

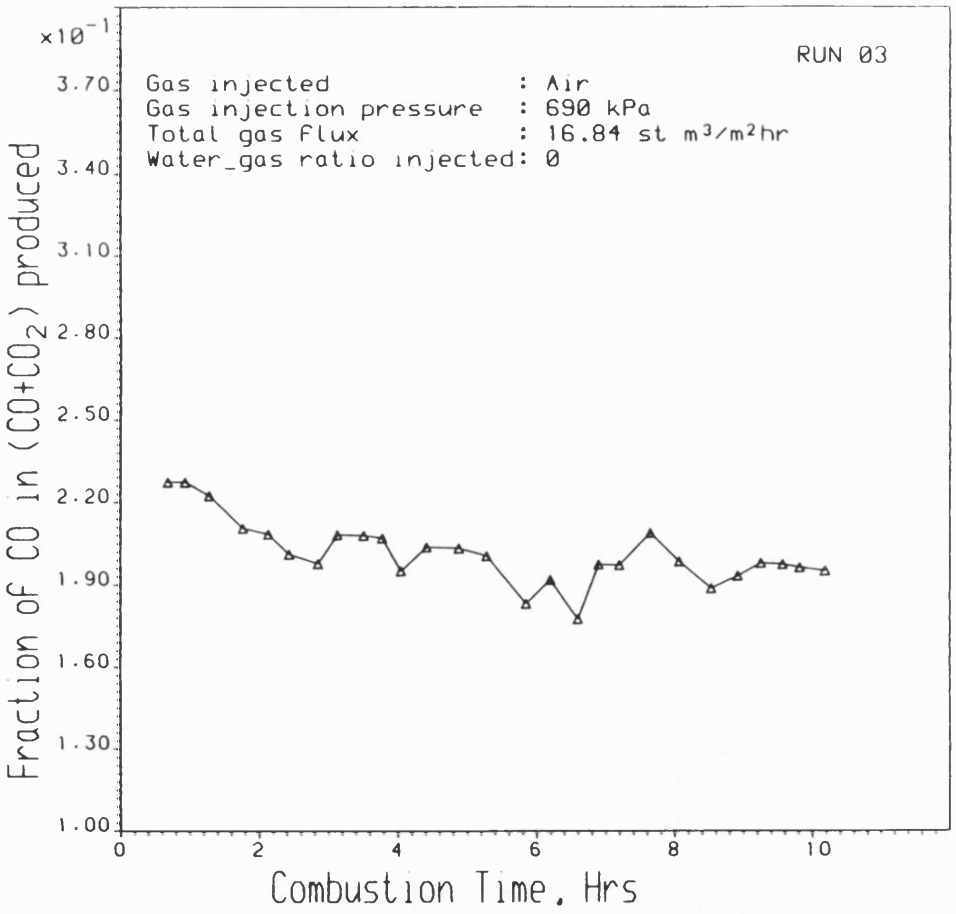

Figure 5.9 FRACTION OF CARBON GASIFIED AS CARBON MONOXIDE

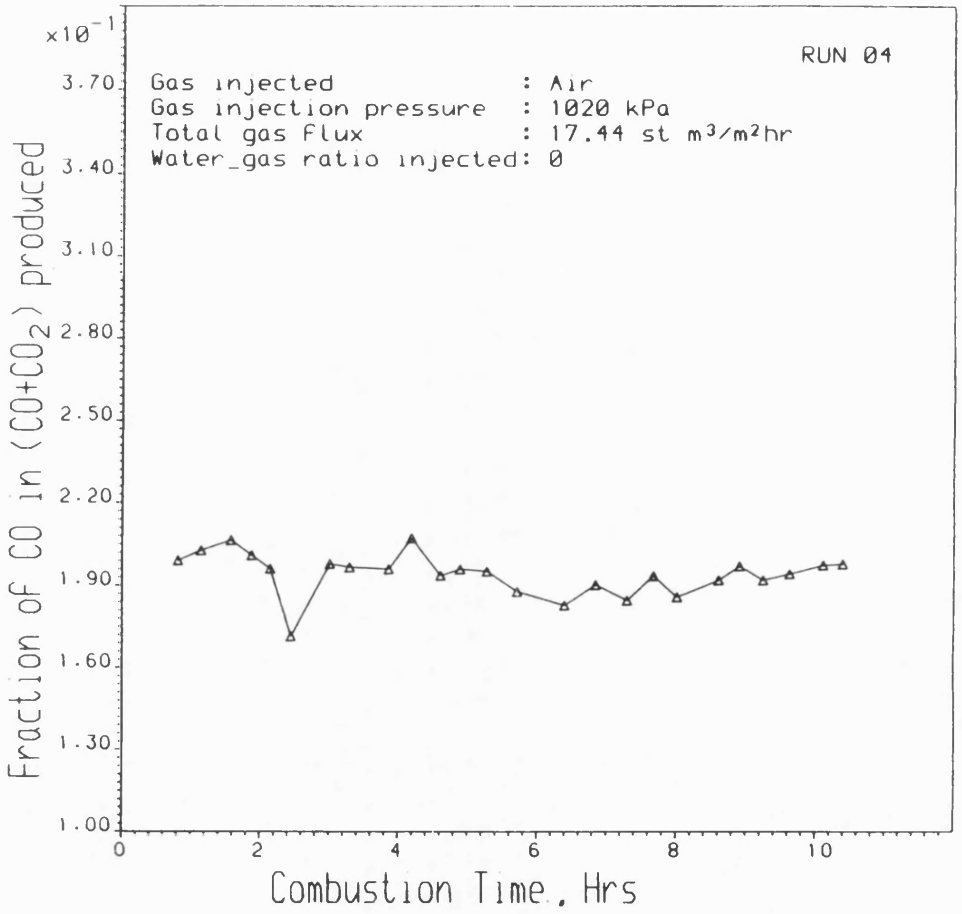

Figure 5.10 FRACTION OF CARBON GASIFIED AS CARBON MONOXIDE

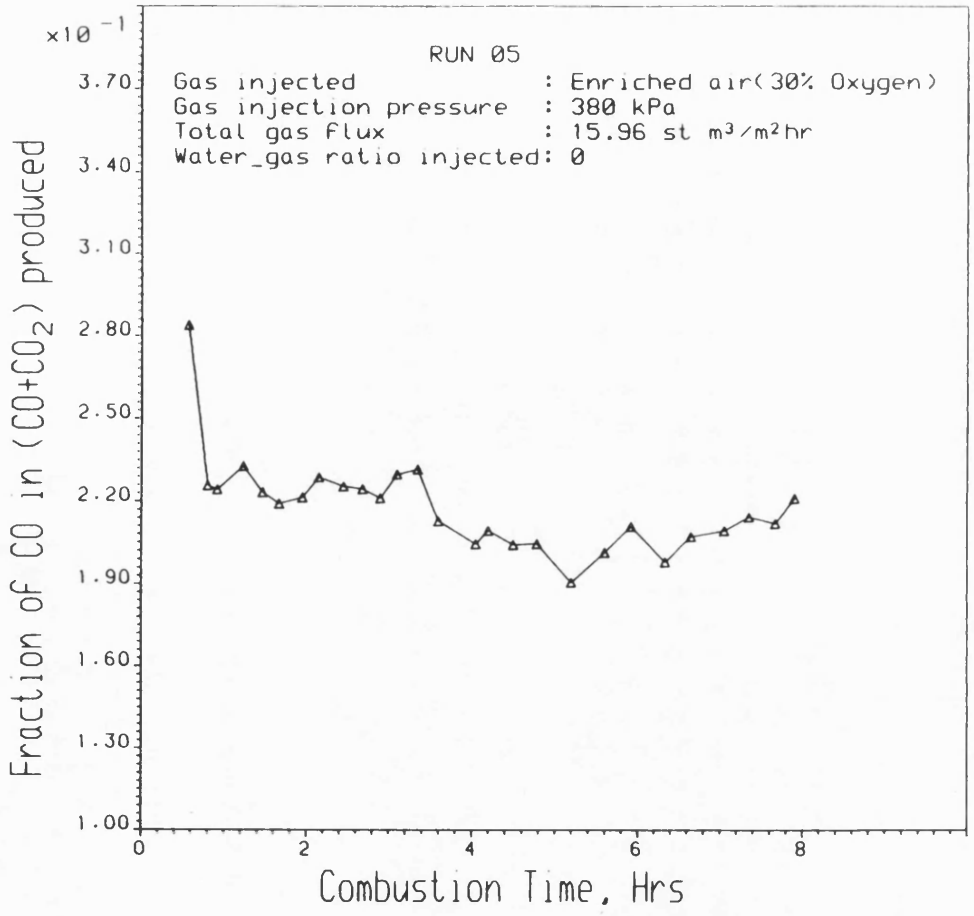

Figure 5.11 FRACTION OF CARBON GASIFIED AS CARBON MONOXIDE

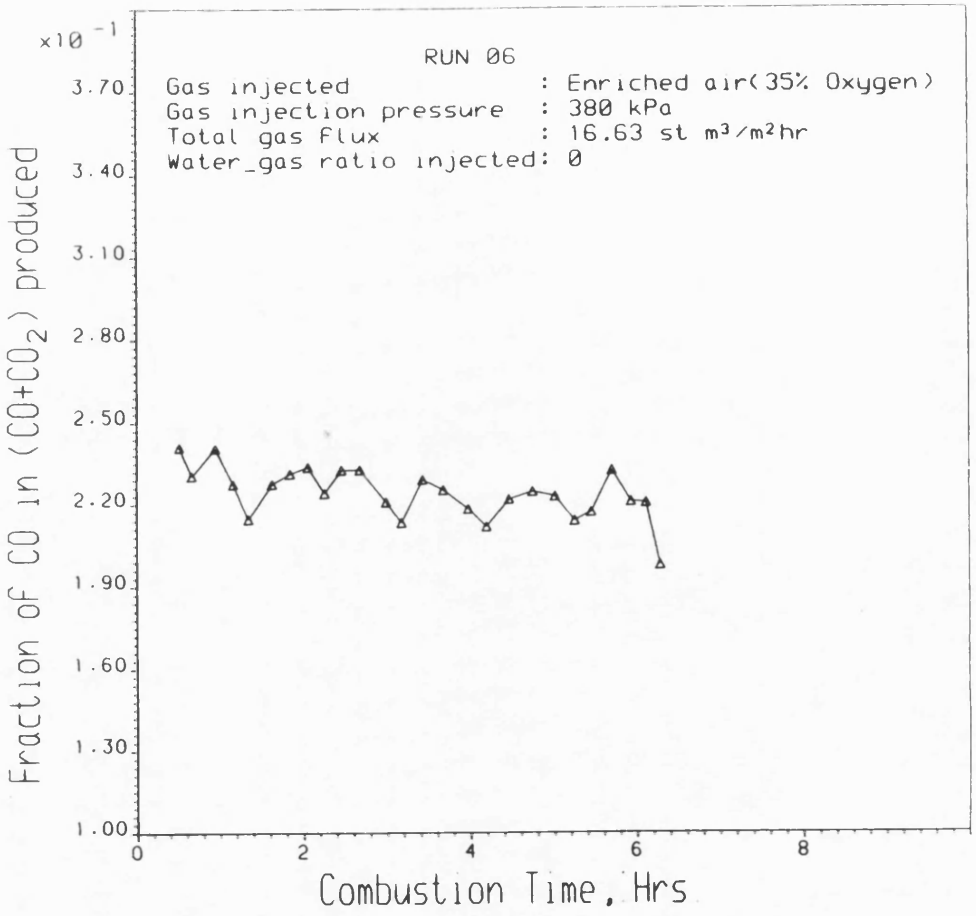

Figure 5.12 FRACTION OF CARBON GASIFIED AS CARBON MONOXIDE

characteristics which are attributable to change in fuel concentration, occurring at different combustion-front locations. This fuel concentration-time dependent is discussed in section 5.6.

The effect of injecting water and consequence production of steam on the combustion reaction is depicted in Figs. 5.13 to 5.18. The observed reduction in CO level is most evident in Figs. 5.19 to 5.24. Thus, the injection of water results in a lower fraction of carbon being gasified to carbon monoxide. Dietz et al. (1967) however reported that steam passes through the combustion front without affecting the combustion reaction. Skirrow et al. (1959) have shown that the presence of steam lowers the temperature at which CO is converted to CO_2, to about 688°F. This is well within the typical combustion zone temperatures. The mechanism of CO_2 production is therefore selectively influenced by steam formation and is believed to be due to the prevailing reaction kinetics as discussed in Chapter 6.

Table 5.3 shows that a substantial increase in the average level of CO and CO_2 concentration in the produced gas occurs during dry combustion when oxygen enrichment is increased. This is similar to that found by Hansel et al. (1982). The large increases in CO and CO_2 concentration that are achieved compared with using air as the oxidant gas suggests that there may be important benefits obtained when using enriched air.

The trend of average molar CO/CO_2 ratio as a function of oxygen enrichment, air injection pressure and WGR is shown in Figs. 5.25 to 5.27. The CO/CO_2 ratio increases with oxygen enrichment, but decreases with increasing air injection pressure. It also shows a decrease when the WGR is increased,

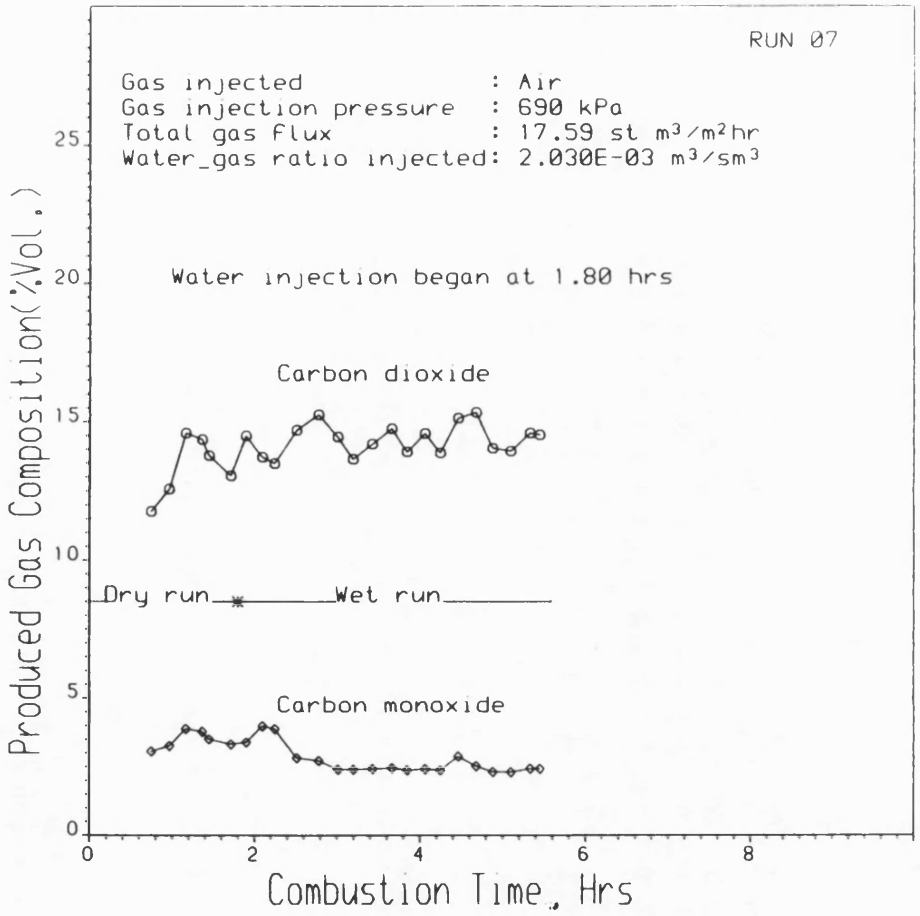

Figure 5.13 PRODUCED GAS COMPOSITION PROFILE

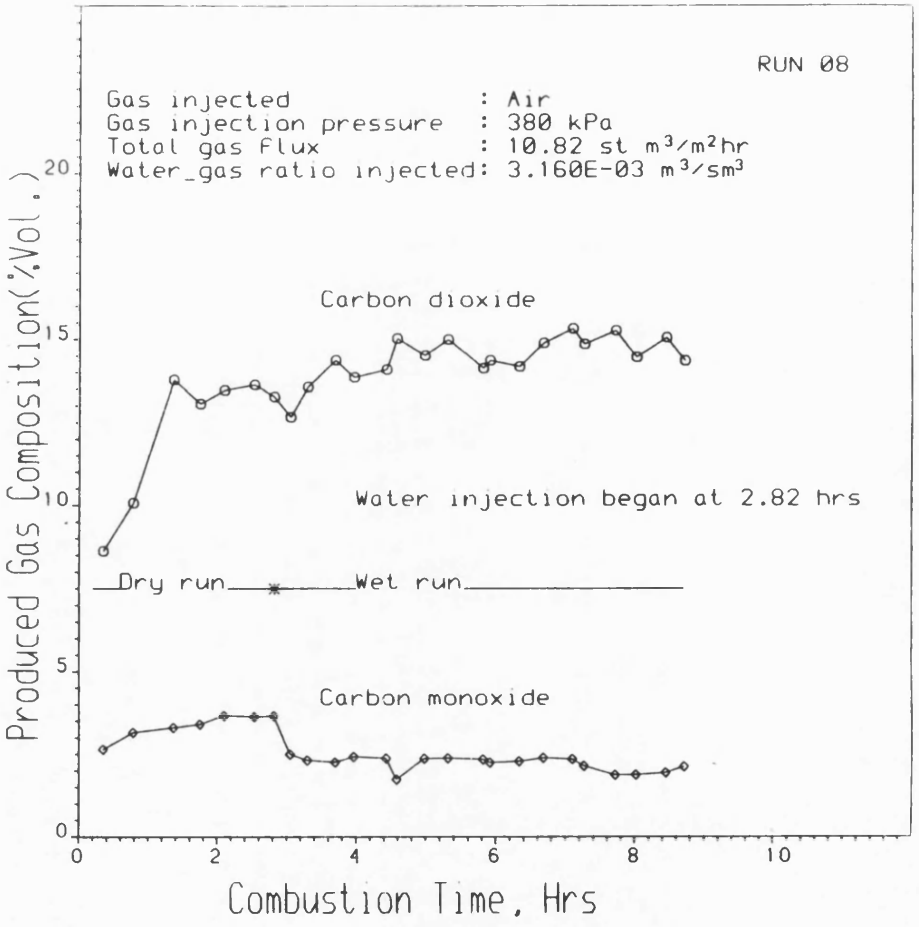

Figure 5.14 PRODUCED GAS COMPOSITION PROFILE

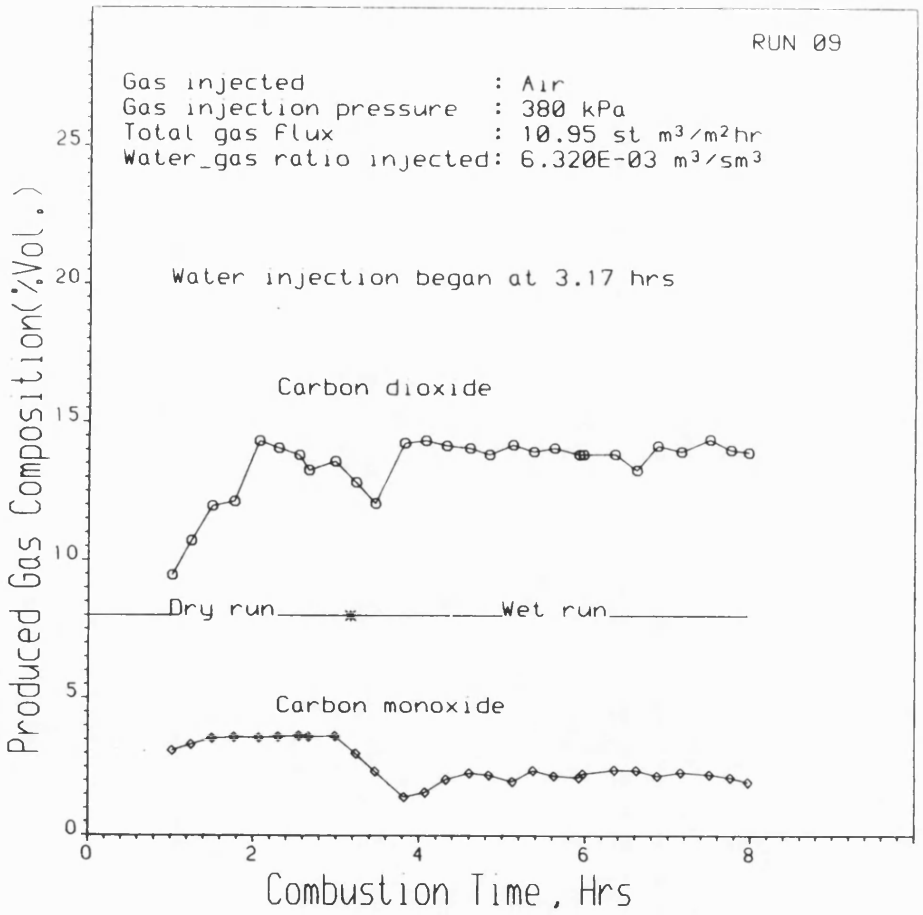

Figure 5.15 PRODUCED GAS COMPOSITION PROFILE

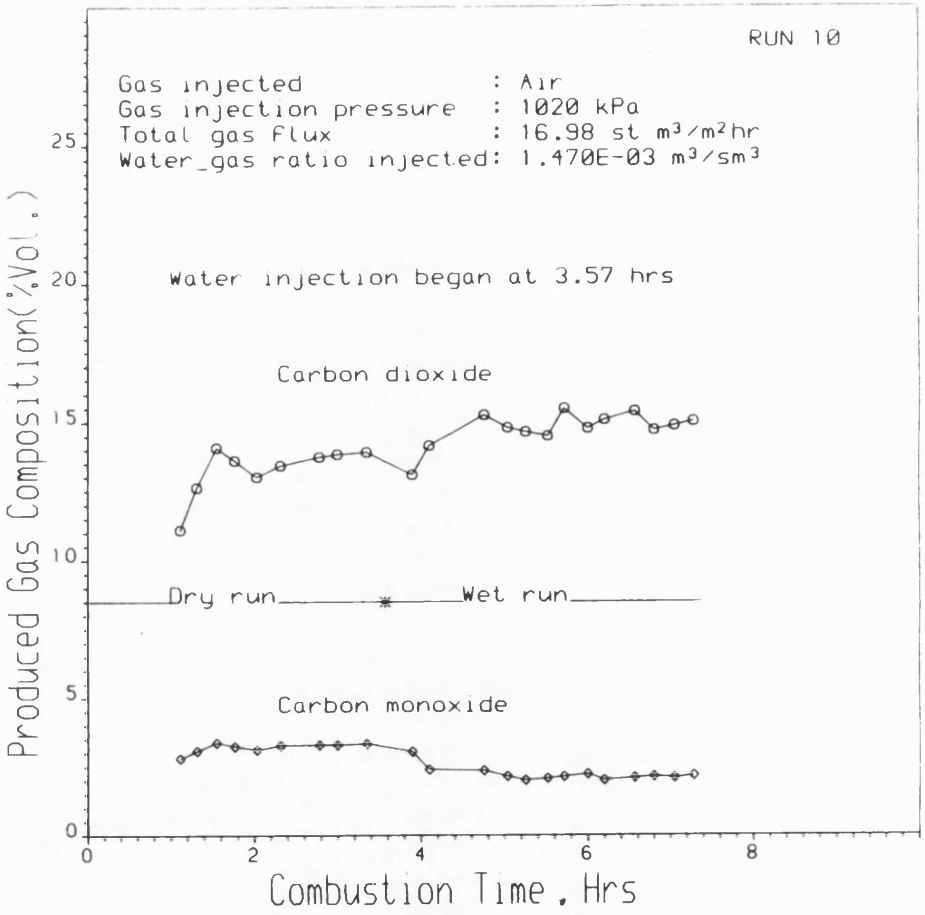

Figure 5.16 PRODUCED GAS COMPOSITION PROFILE

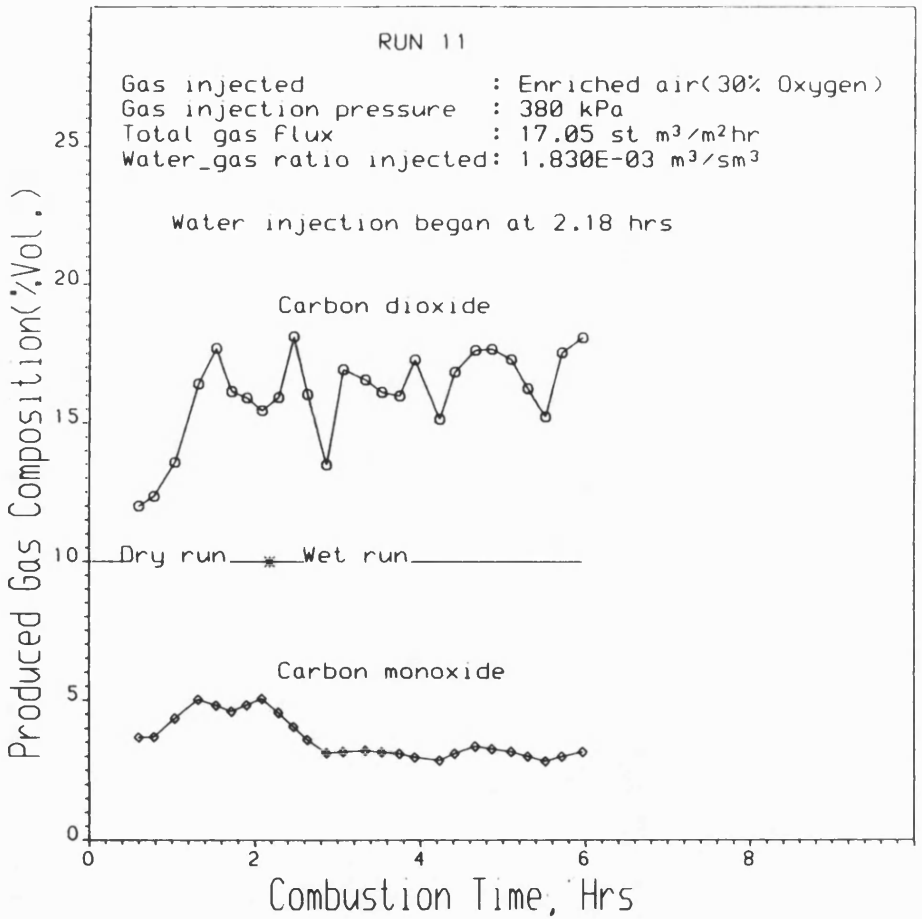

Figure 5.17 PRODUCED GAS COMPOSITION PROFILE

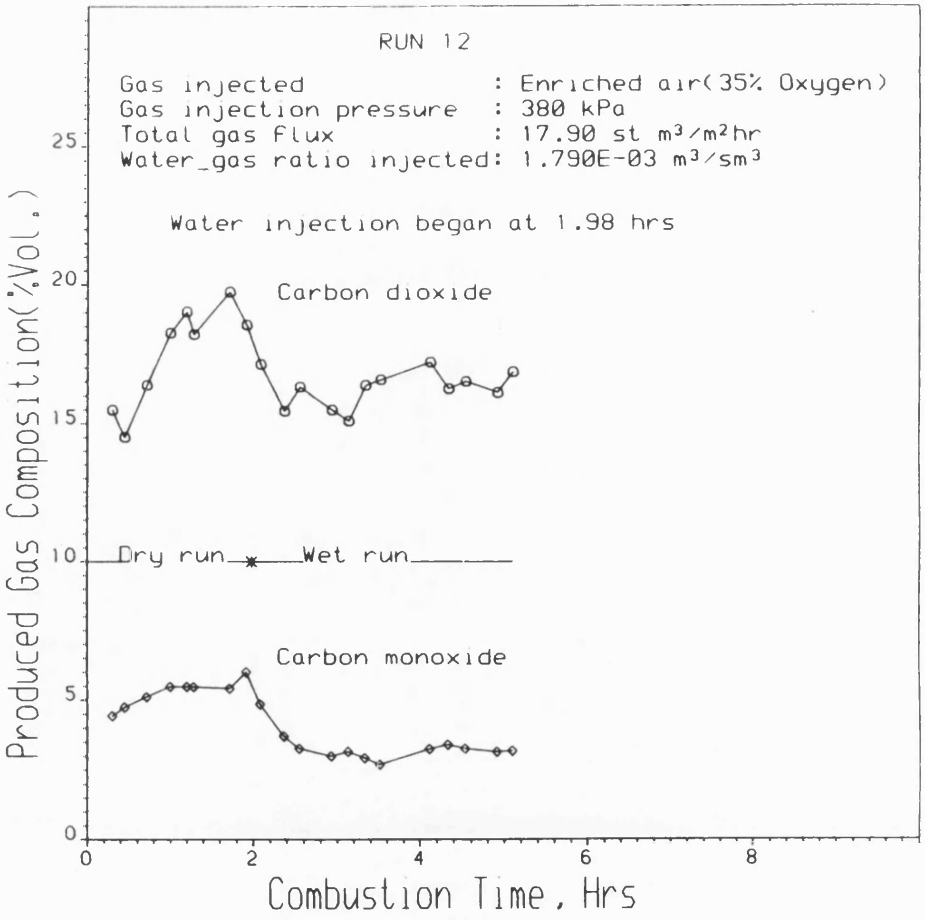

Figure 5.18 PRODUCED GAS COMPOSITION PROFILE

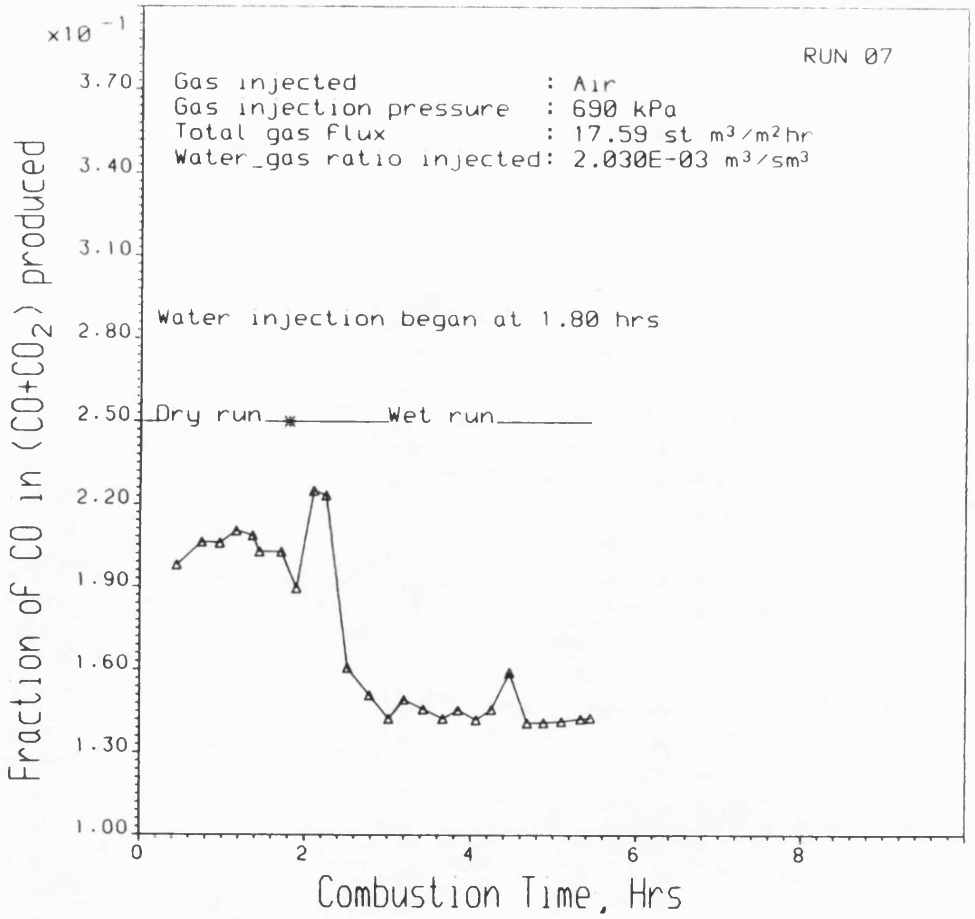

Figure 5.19 FRACTION OF CARBON GASIFIED AS CARBON MONOXIDE

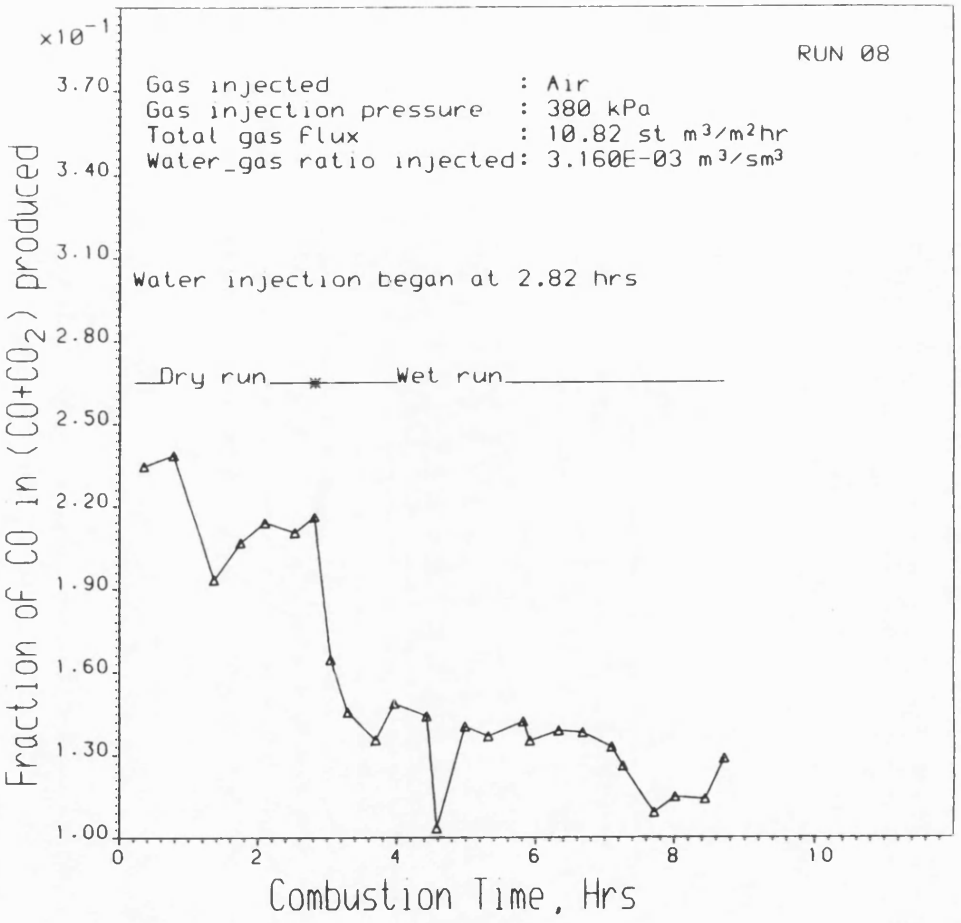

Figure 5.20 FRACTION OF CARBON GASIFIED AS CARBON MONOXIDE

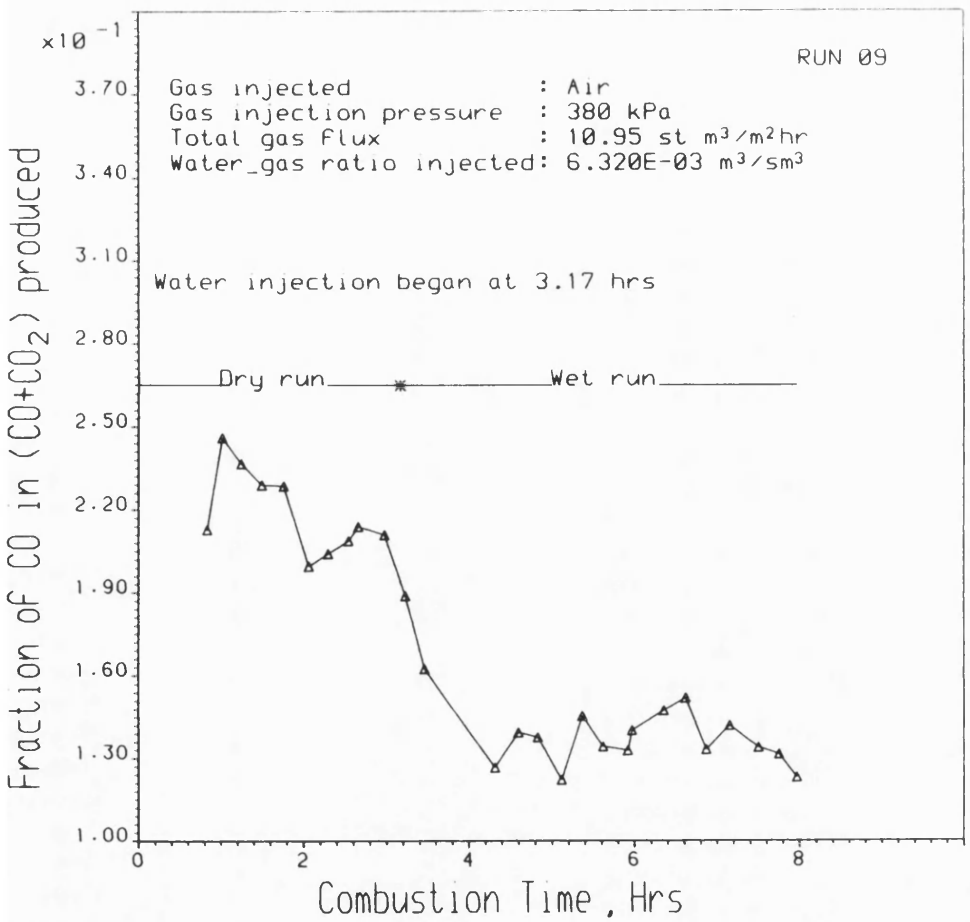

Figure 5.21 FRACTION OF CARBON GASIFIED AS CARBON MONOXIDE

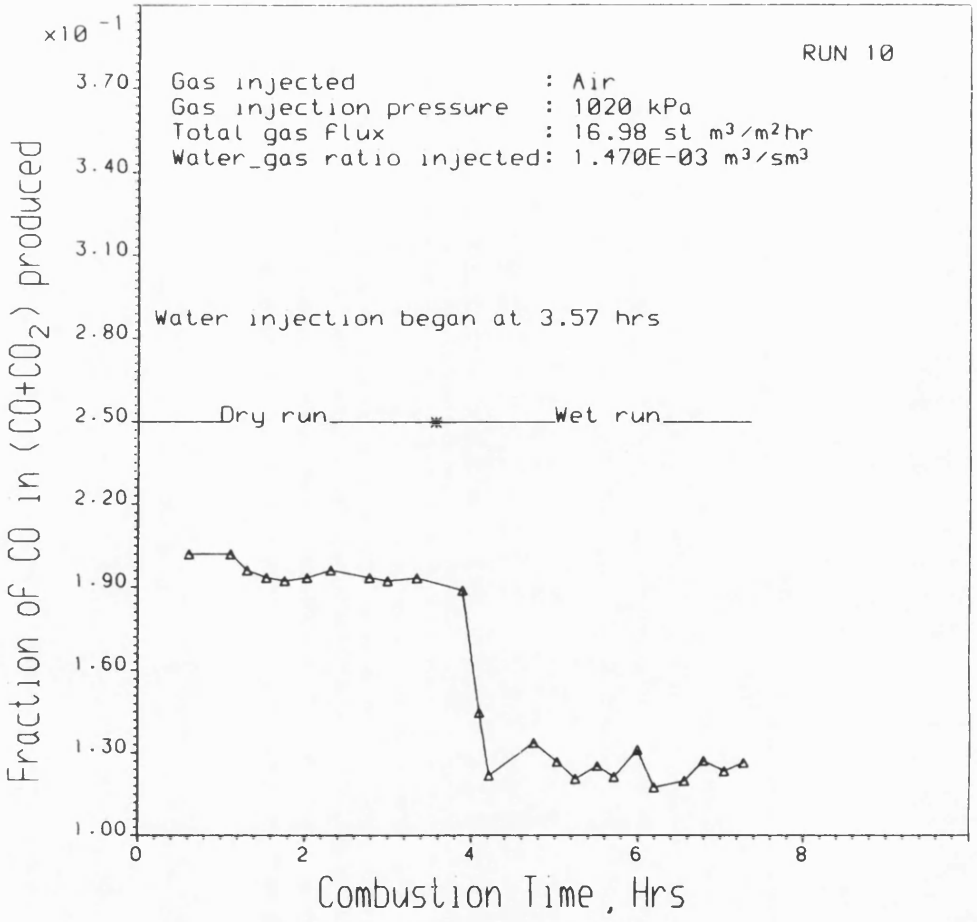

Figure 5.22 FRACTION OF CARBON GASIFIED AS CARBON MONOXIDE

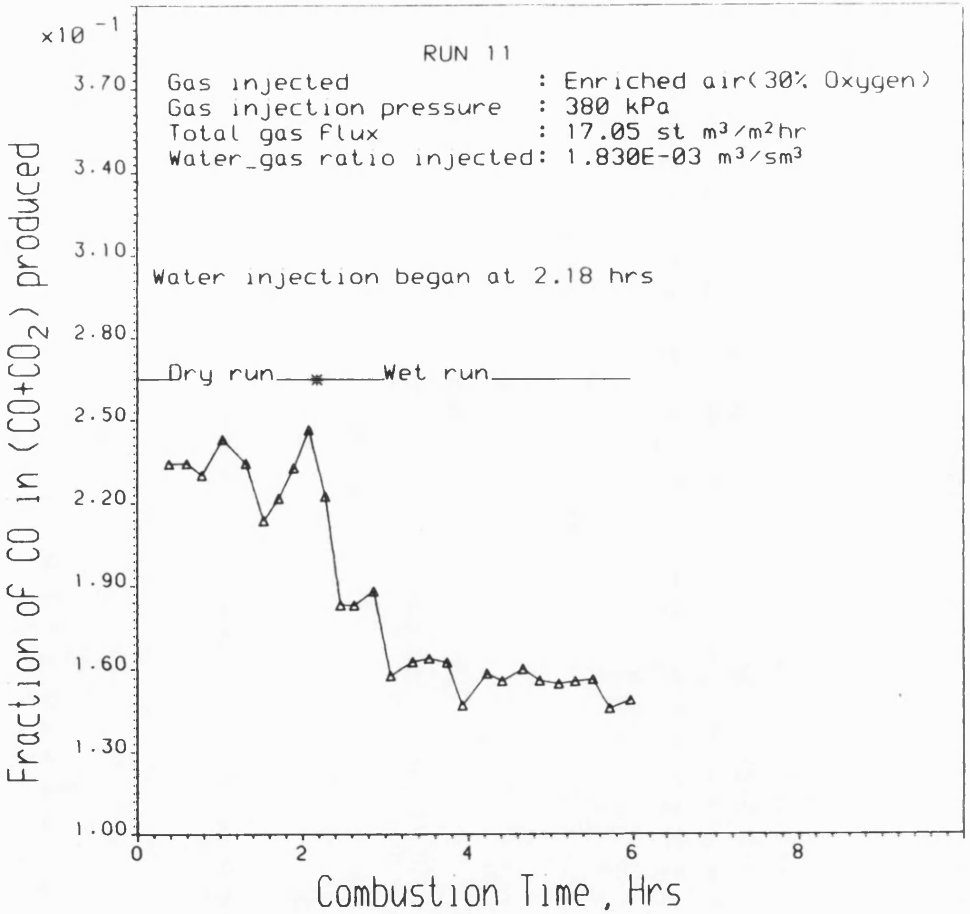

Figure 5.23 FRACTION OF CARBON GASIFIED AS CARBON MONOXIDE

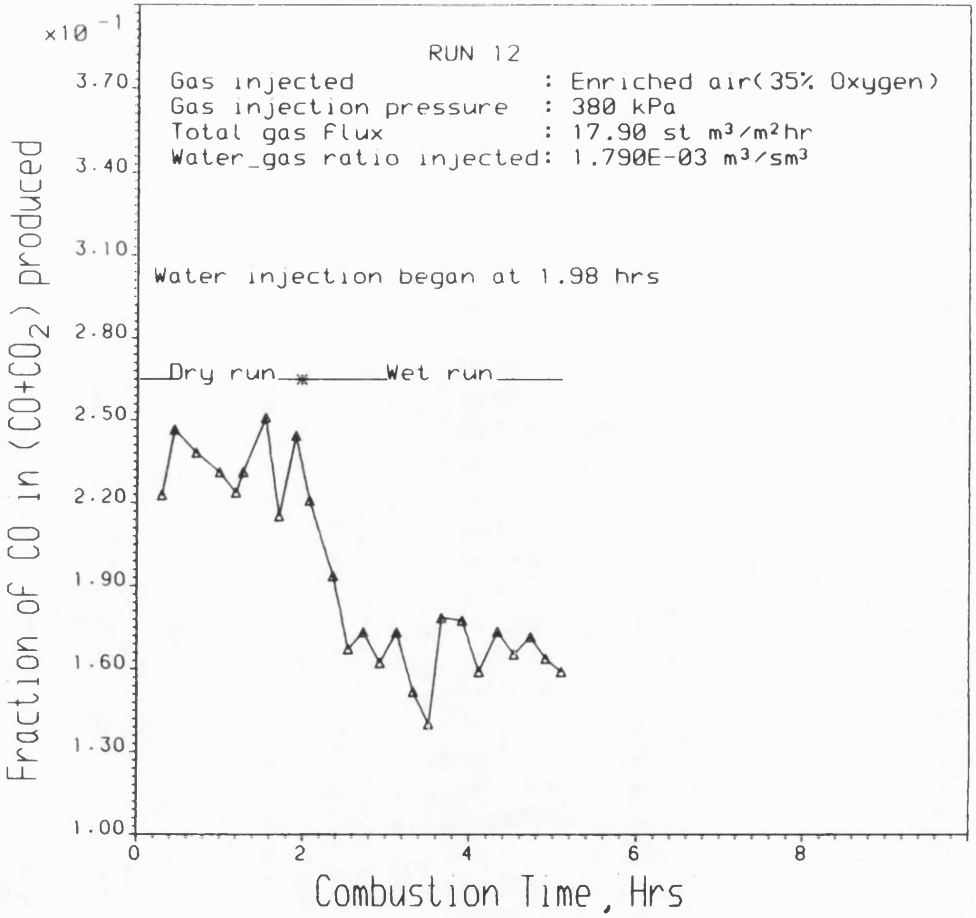

Figure 5.24 FRACTION OF CARBON GASIFIED AS CARBON MONOXIDE

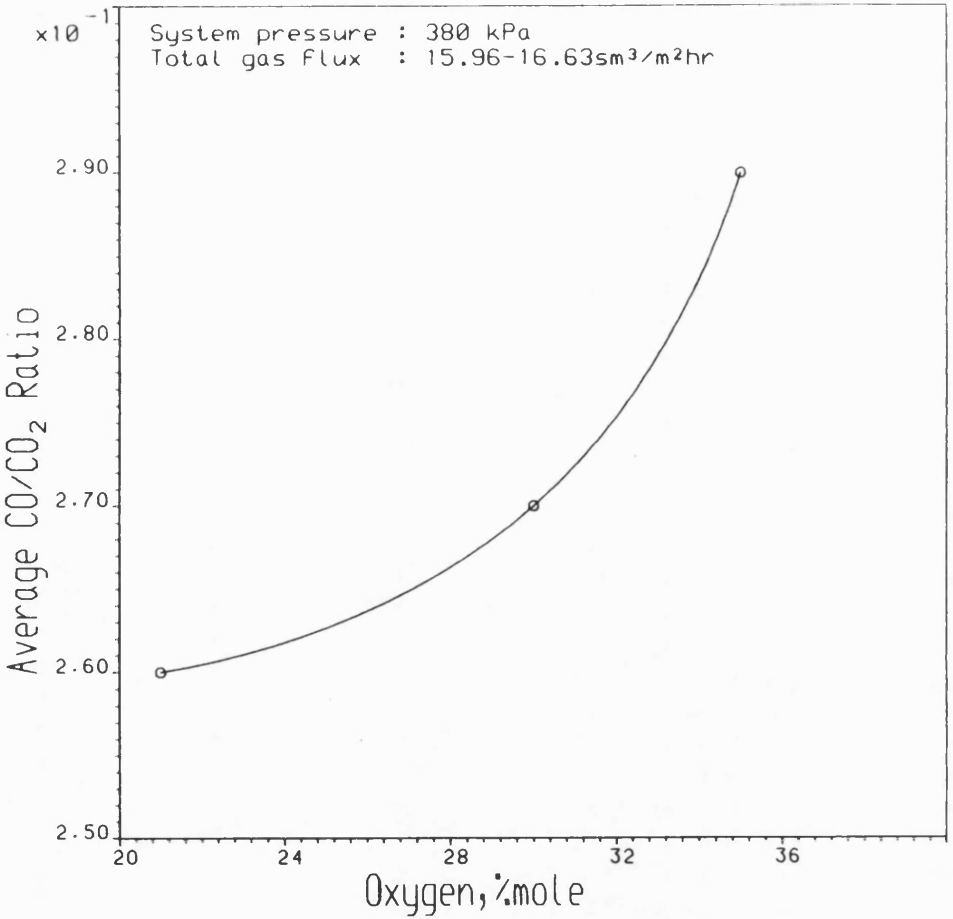

Figure 5.25 EFFECT OF OXYGEN ENRICHMENT OF AIR ON MOLAR CO/CO_2 RATIO IN THE PRODUCED GAS

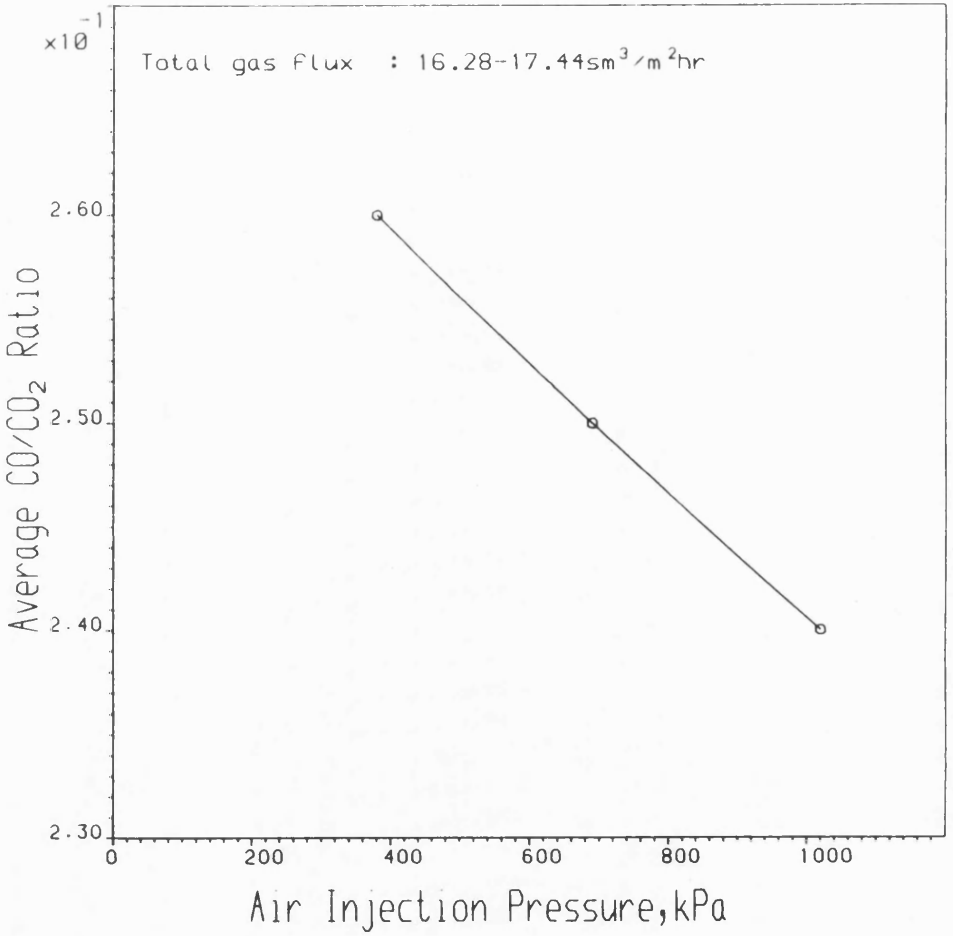

Figure 5.26 EFFECT OF AIR INJECTION PRESSURE ON MOLAR CO/CO_2 RATIO IN THE PRODUCED GAS

levelling off however at WGR=3.16m^3/Msm^3. The unusual increase in CO/CO_2 ratio with oxygen flux is due mainly to increase in combustion temperature which causes CO_2 formation to be suppressed in favour of CO. These trends are in agreement with those of Garon et al. (1974), Fassihi (1981) and Hansel et al. (1982). Since the amount of oxygen required to produce CO_2 is twice that of CO, it follows that under oxygen enrichment conditions, a lower volume of injected gas will be required. This could have important economic bearing on the development of future in-situ combustion project.

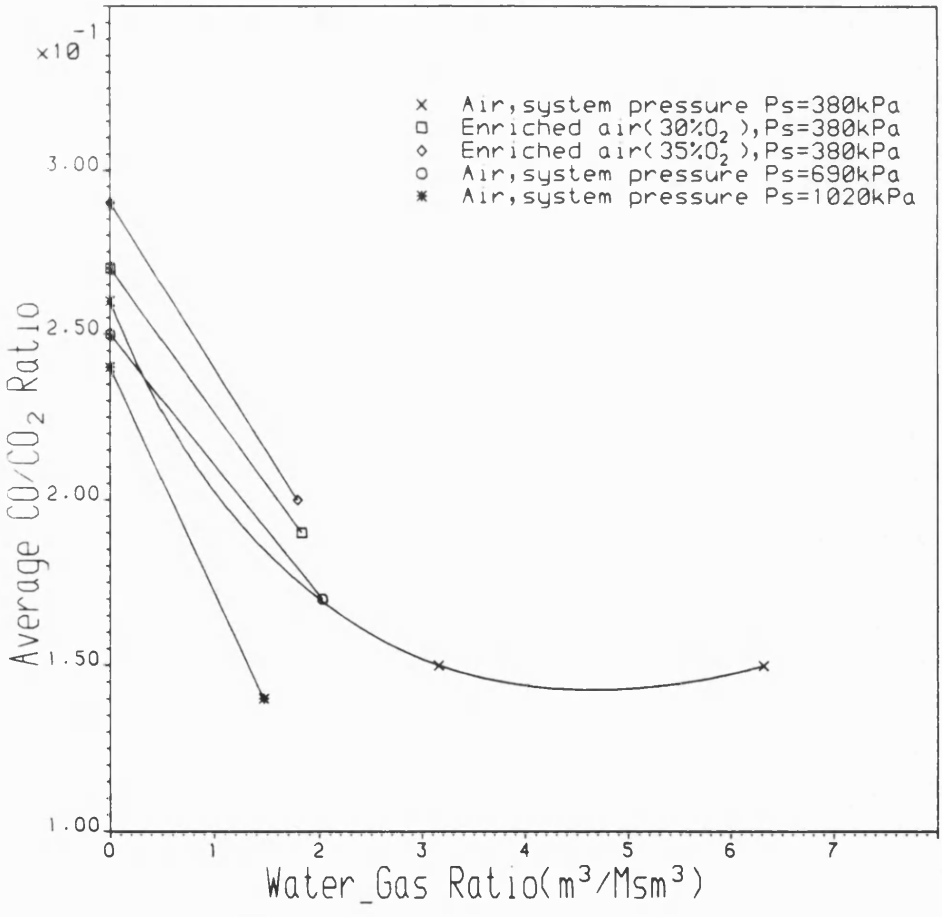

Figure 5.27 EFFECT OF WATER INJECTION ON MOLAR CO/CO_2 RATIO IN THE PRODUCED GAS

5.2 Combustion Tube Temperature Profile

5.2.1 Combustion Zone

The axial temperature profiles during dry combustion are shown in Figs. 5.28 to 5.33. A slight variation in peak temperatures is noticeable. This is due to the rate at which heat is generated by the exothermic combustion reaction compared with the heat losses from the combustion zone. Heat losses from the combustion zone is the result of radial conduction through the tube wall, combined with axial heat conduction and convection downstream to the steam zone. Under non-adiabatic combustion tube conditions, the radial heat loss is most critical. A simplified model of heat transfer taking place in the immediate neighbourhood of the combustion zone has already been described in section 3.2. An example calculation of the heat losses for Run 1 is given in Appendix B (Part B2). The analysis was repeated in a similar manner for Runs 2, 5 and 6. As reported in Table 5.2, Runs 1 and 2 were performed with air at different total gas fluxes while Runs 5 and 6 were performed at approximately the same total gas flux as Run 2, but with oxygen enrichment at 30 and 35 percent, respectively. These runs therefore demonstrate the effect of oxygen flux on the magnitude of radial heat loss. From a practical viewpoint of operating forward combustion project, oxygen fluxes greater than the minimum are often used, in order to compensate for any excessive heat losses, otherwise extinction of the combustion front could occur. (Parrish et al., 1965).

The radial heat loss as a percentage of the cumulative heat liberated for Runs 1, 2, 5 and 6 is shown in Figs. 5.34 to 5.37. It is apparent that the heat generated and the radial

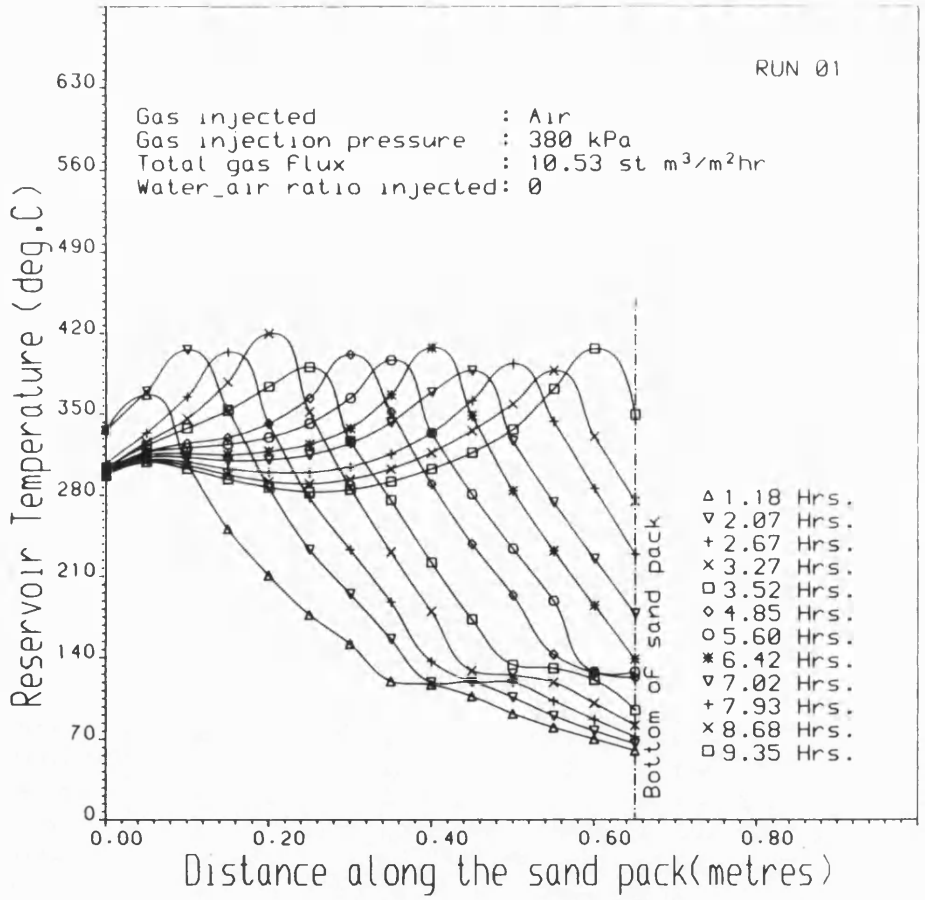

Figure 5.28 COMBUSTION TUBE AXIAL TEMPERATURE PROFILE

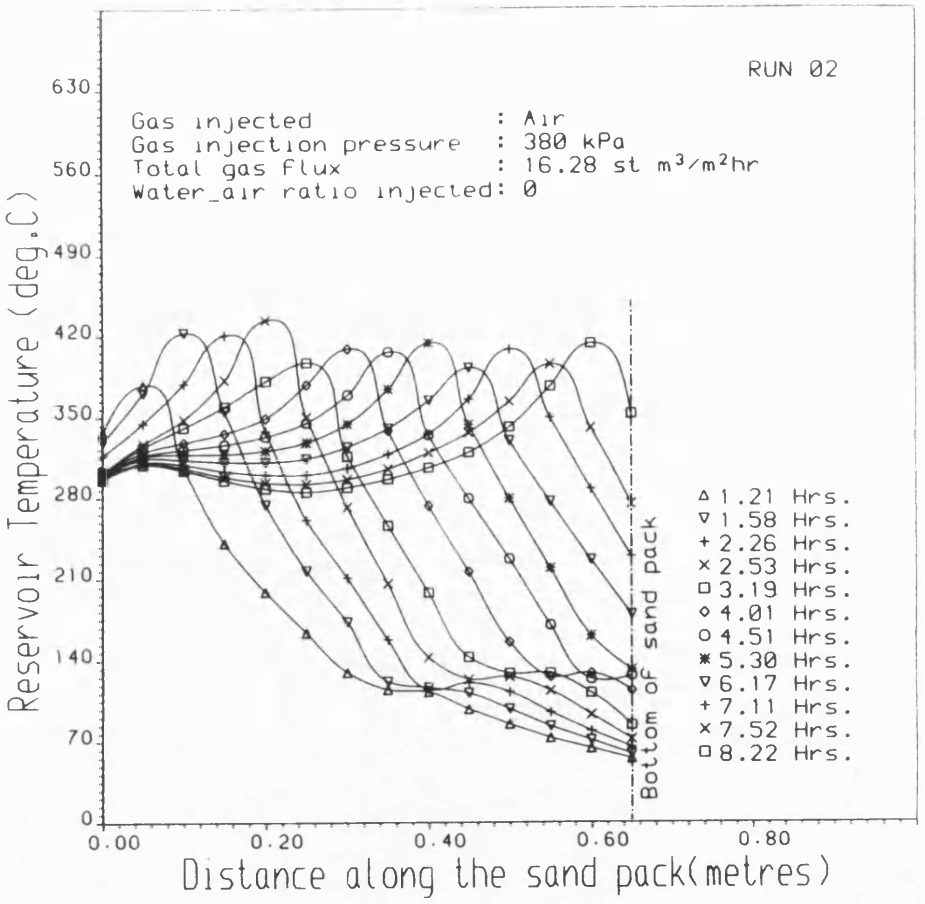

Fig. 5.29 COMBUSTION TUBE AXIAL TEMPERATURE PROFILE

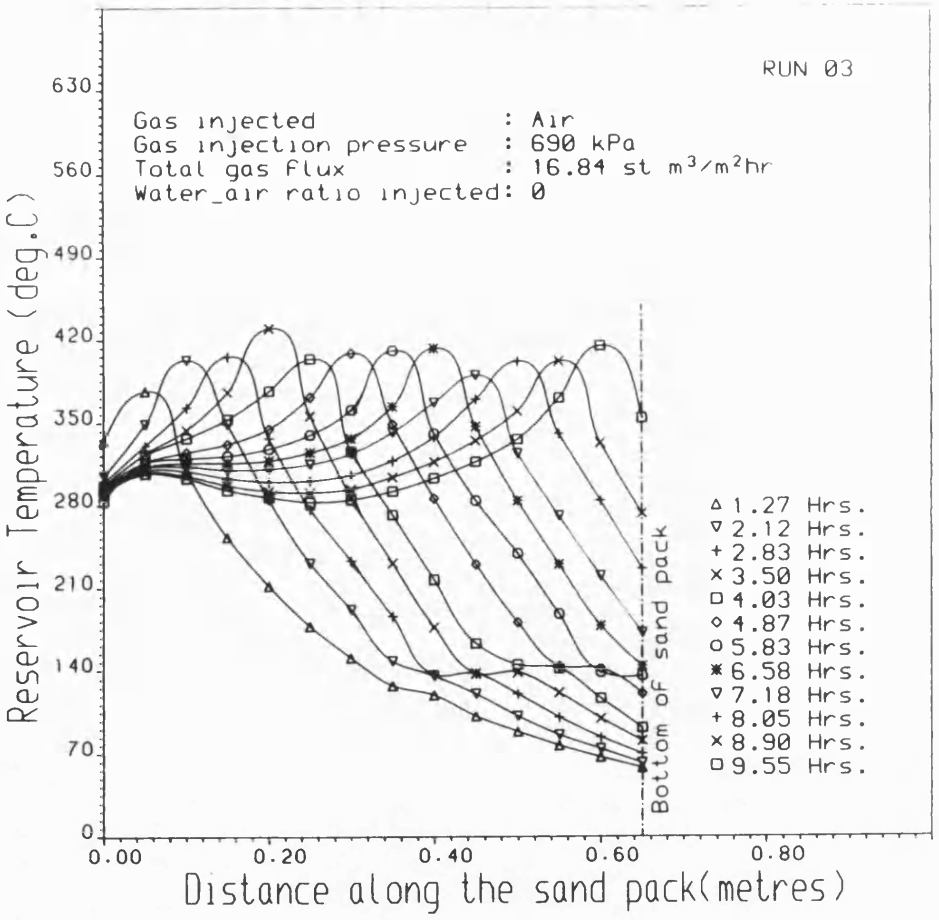

Fig. 5.30 COMBUSTION TUBE AXIAL TEMPERATURE PROFILE

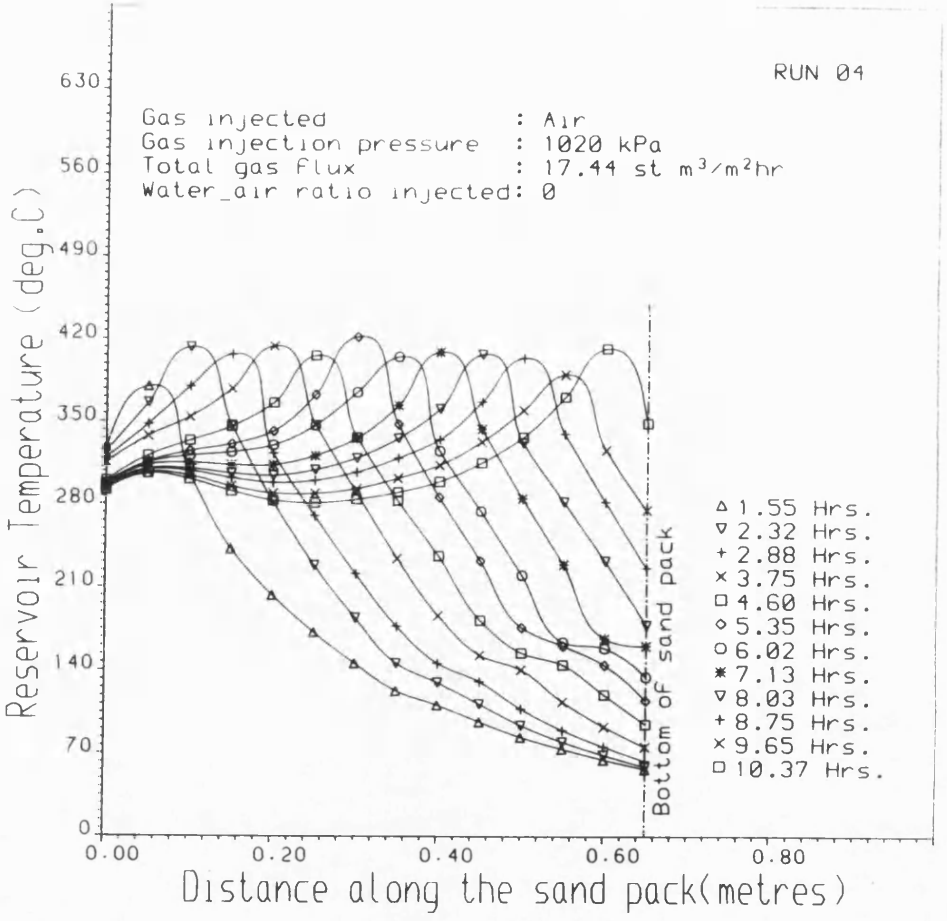

Fig. 5.31 COMBUSTION TUBE AXIAL TEMPERATURE PROFILE

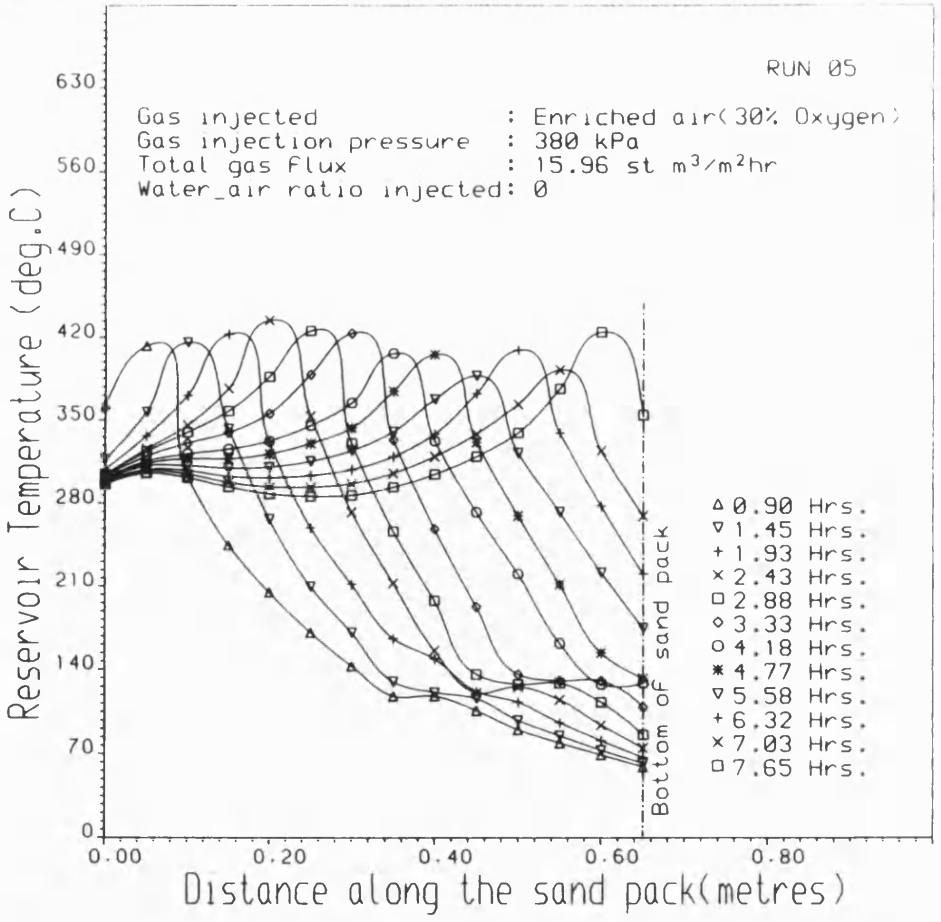

Fig. 5.32 COMBUSTION TUBE AXIAL TEMPERATURE PROFILE

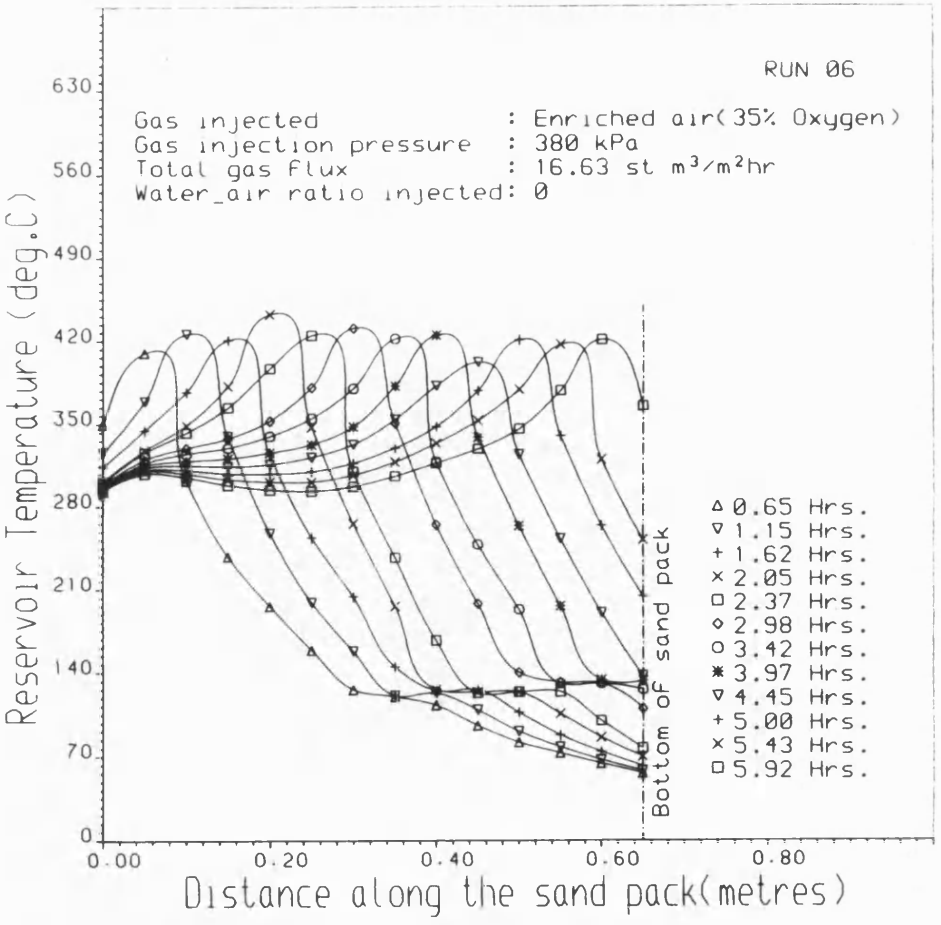

Fig. 5.33 COMBUSTION TUBE AXIAL TEMPERATURE PROFILE

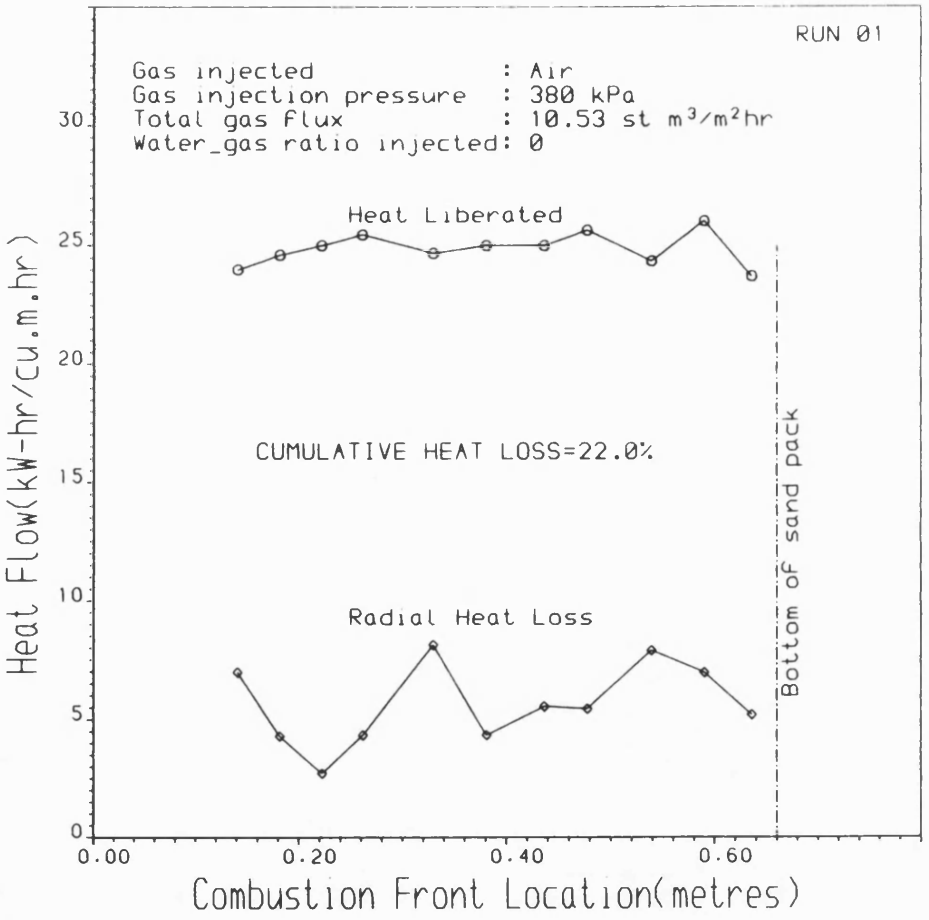

Figure 5.34 HEAT FLOW PROFILE IN COMBUSTION ZONE

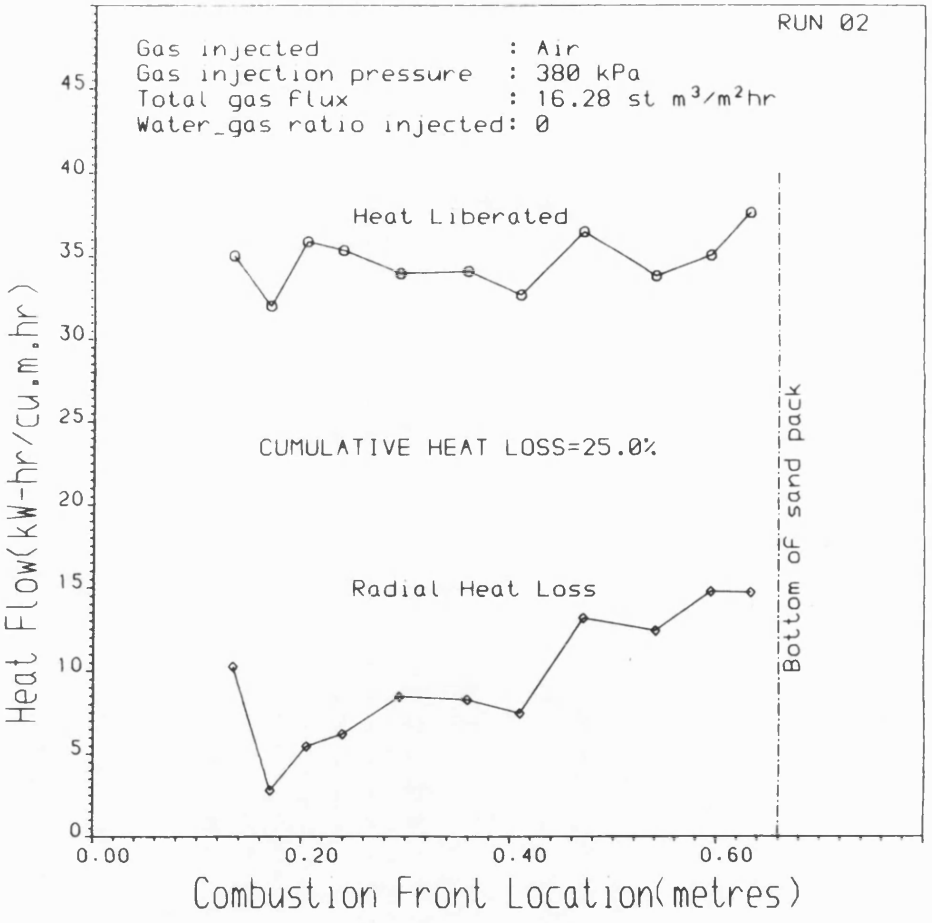

Figure 5.35 HEAT FLOW PROFILE IN COMBUSTION ZONE

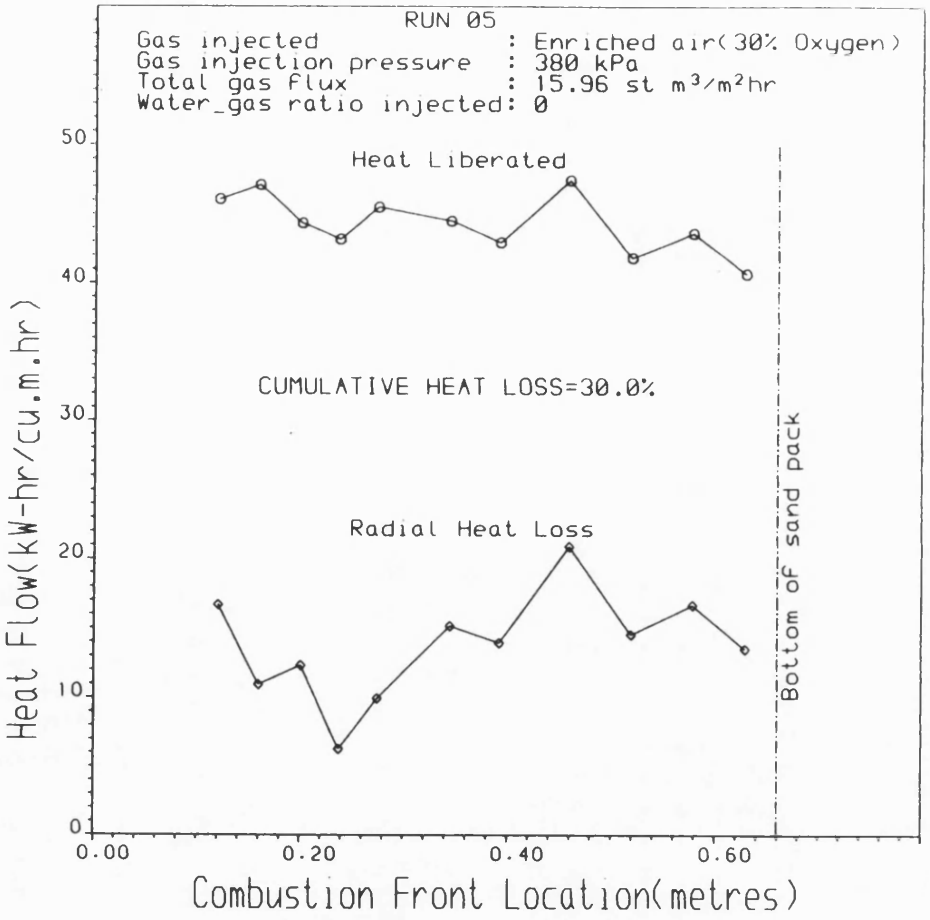

Figure 5.36 HEAT FLOW PROFILE IN COMBUSTION ZONE

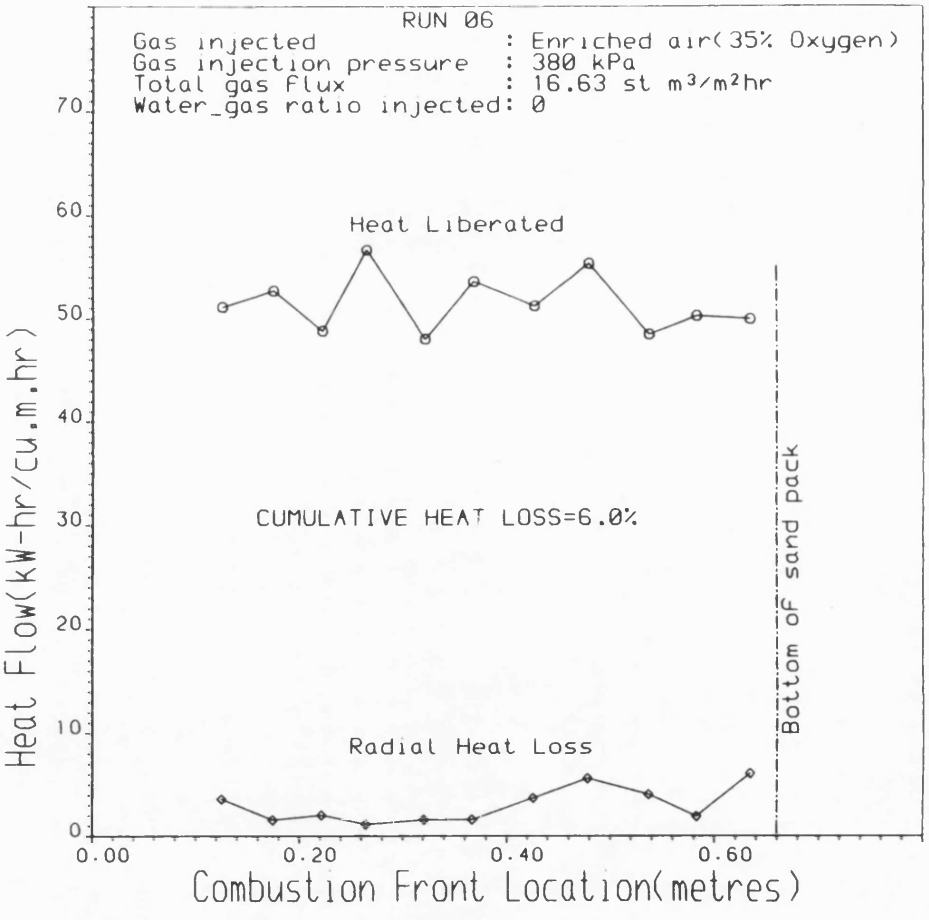

Figure 5.37 HEAT FLOW PROFILE IN COMBUSTION ZONE

heat losses are dependent on combustion front location. According to Burger and Sahuquet (1972), the heat released per unit mass of fuel burned at the combustion zone is a function of the H/C ratio of the fuel and CO/CO_2 ratio of the produced gas. The heats of formation of CO_2 and CO are respectively -94,052 and -26.416 cal/mol. at 25°C (Alderman et al., 1971), serving to illustrate that the amount of CO and CO_2 produced must significantly affect the heat generated. Therefore, any variation of the H/C or CO/CO_2 ratio will produce a corresponding change in the magnitude of heat generated as the combustion front propagates through the sand pack. On the other hand, radial heat loss is mainly a function of the radial temperature gradient prevailing at the combustion front and also the front velocity. For a fixed heat input by the wall heaters, the radial temperature gradient will depend on the heat transfer processes occurring in the vicinity of the combustion zone as well as the combustion reaction kinetics. Hence, for a given front velocity, variations in the radial temperature gradient, as shown in Figs. 5.38 to 5.41, give rise to a corresponding change in radial heat loss over the combustion tube. The net effect is to increase or decrease the observed peak temperature. Under adiabatic conditions, however, the radial heat loss is negligible so that axial conductive and convective heat transport is the principal mechanism of heat loss from the combustion zone.

The average heat generation rate and the net radial heat loss are represented as a function of the total oxygen flux in Figs. 5.42 and 5.43. The average heat generation rate increases very substantially with oxygen flux with and without oxygen enrichment. Figure 5.43 shows that the cumulative heat loss initially increases with oxygen flux using air and 30% oxygen

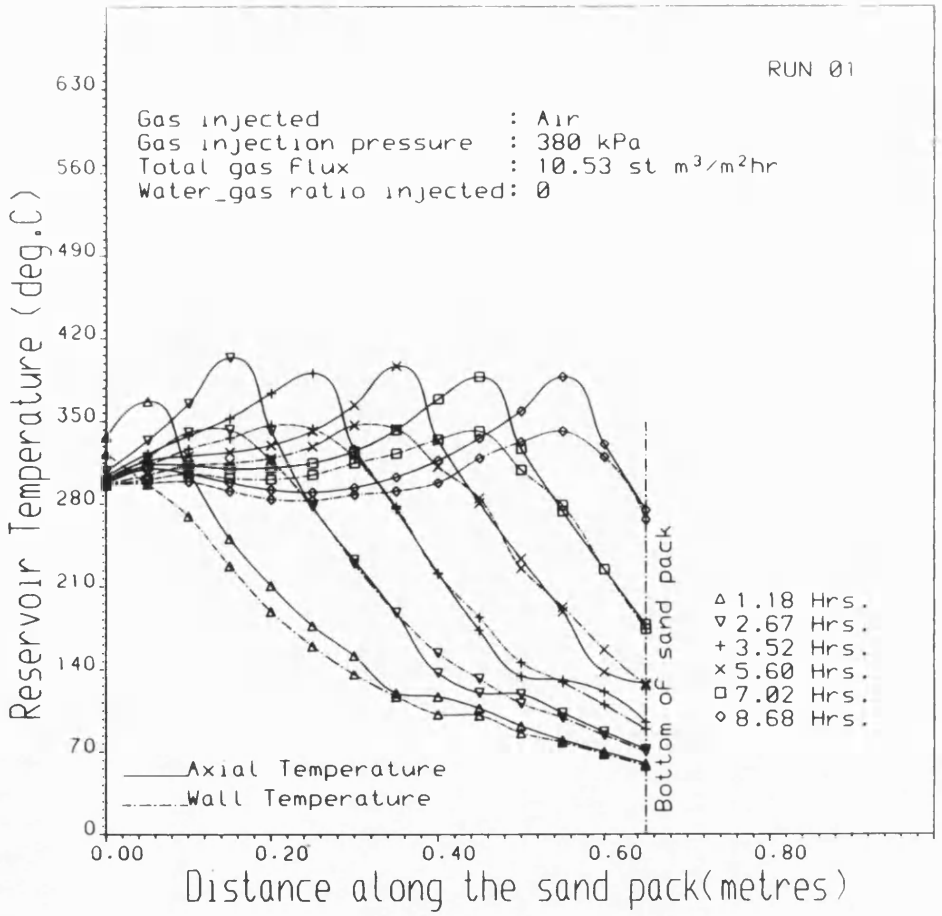

Figure 5.38 COMBUSTION TUBE AXIAL AND WALL TEMPERATURE PROFILES

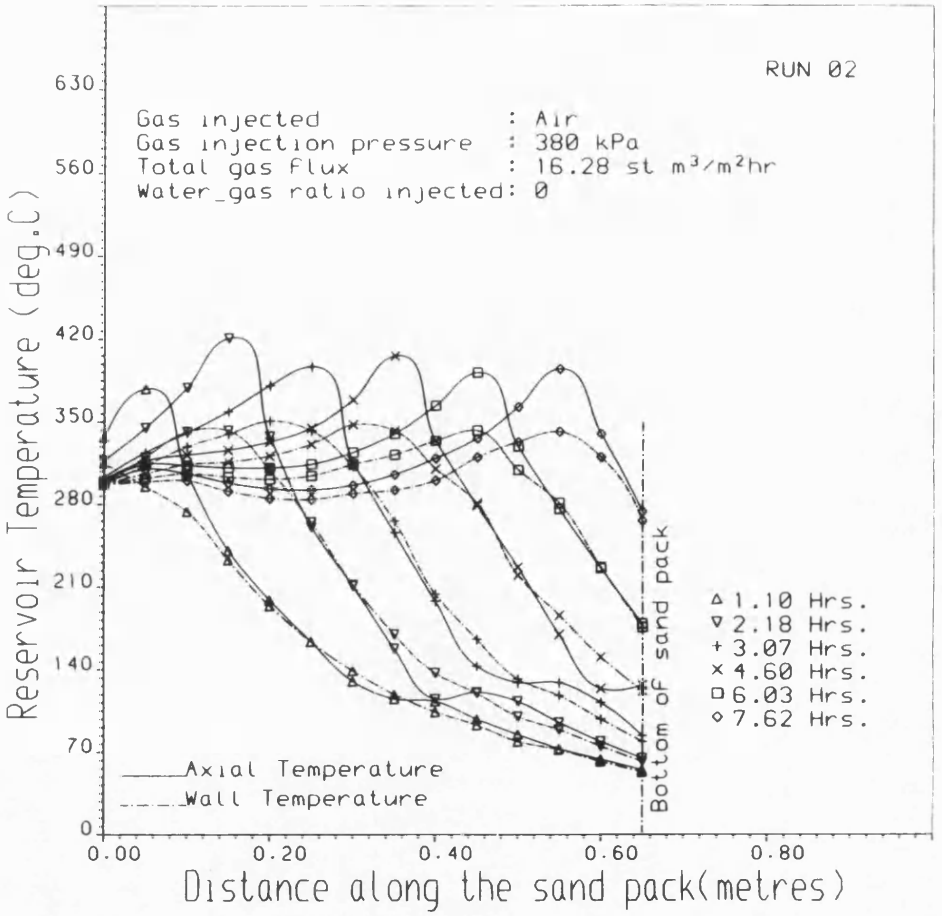

Figure 5.39 COMBUSTION TUBE AXIAL AND WALL TEMPERATURE PROFILES

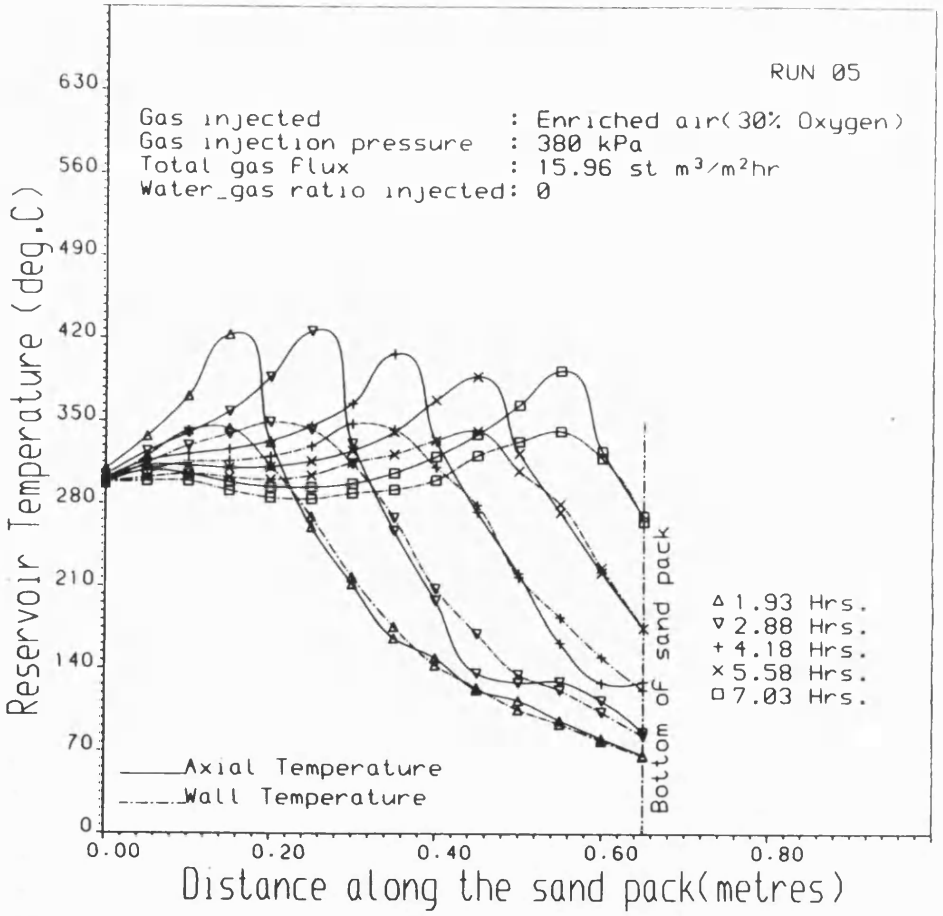

Figure 5.40 COMBUSTION TUBE AXIAL AND WALL TEMPERATURE PROFILES

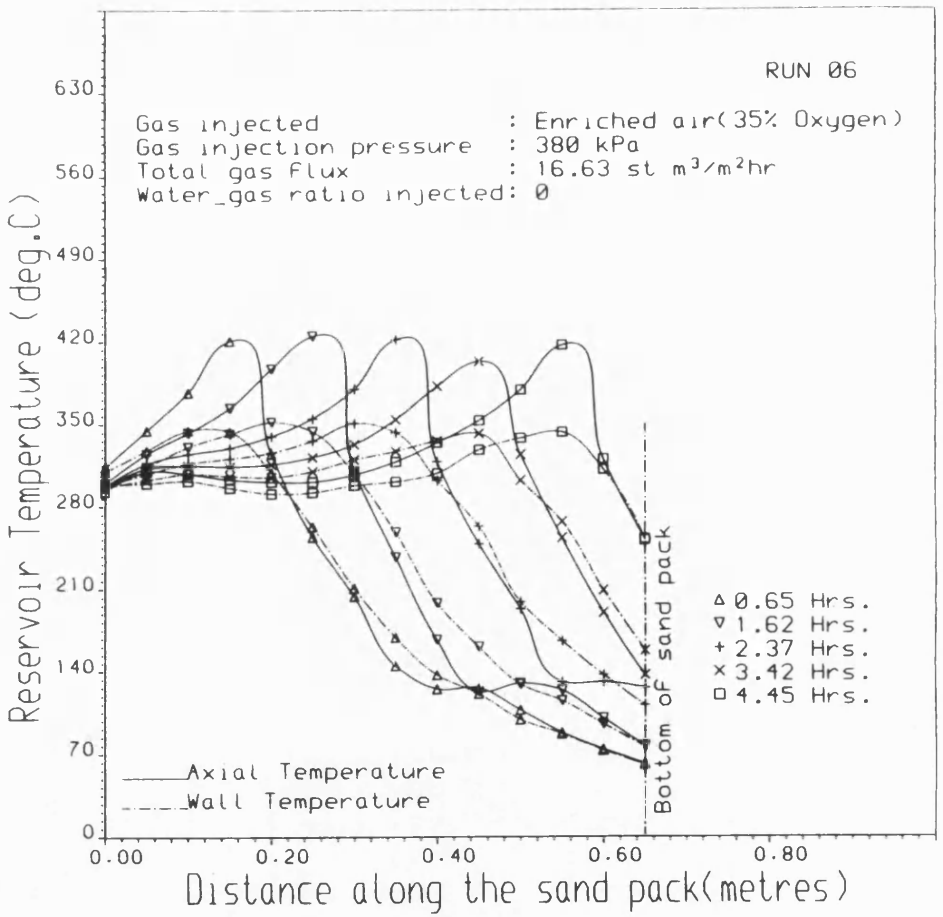

Figure 5.41 COMBUSTION TUBE AXIAL AND WALL TEMPERATURE PROFILES

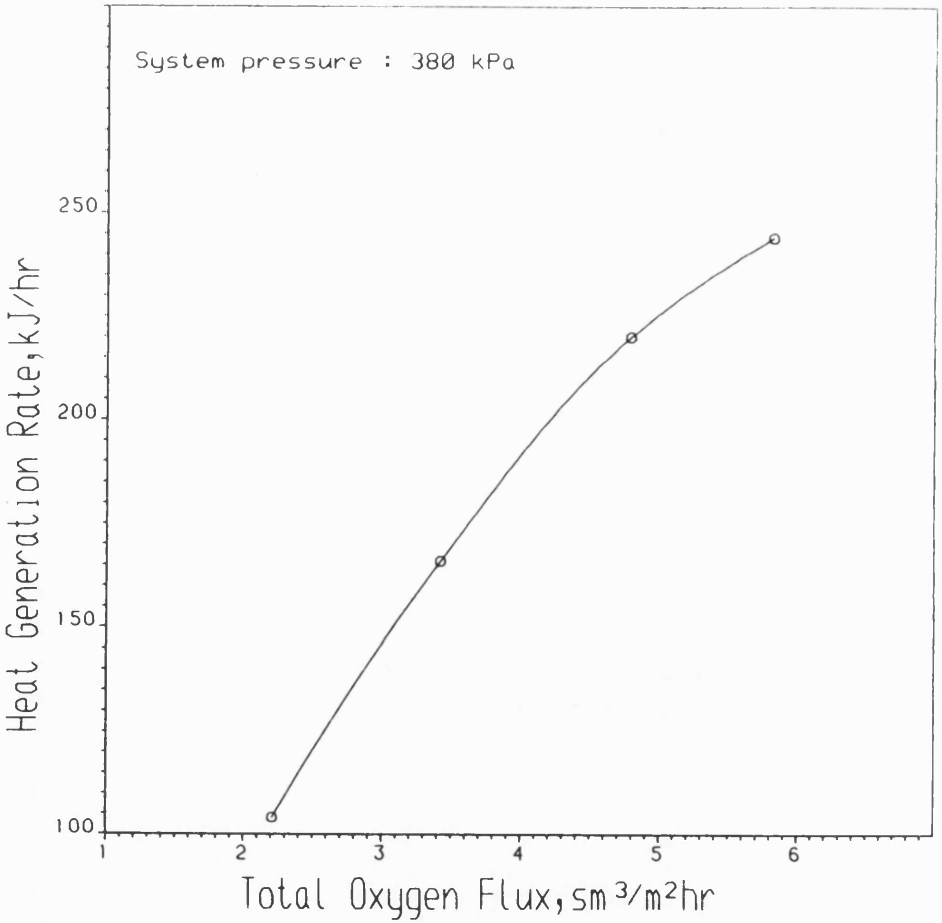

Figure 5.42 HEAT GENERATION RATE AS A FUNCTION OF TOTAL OXYGEN FLUX

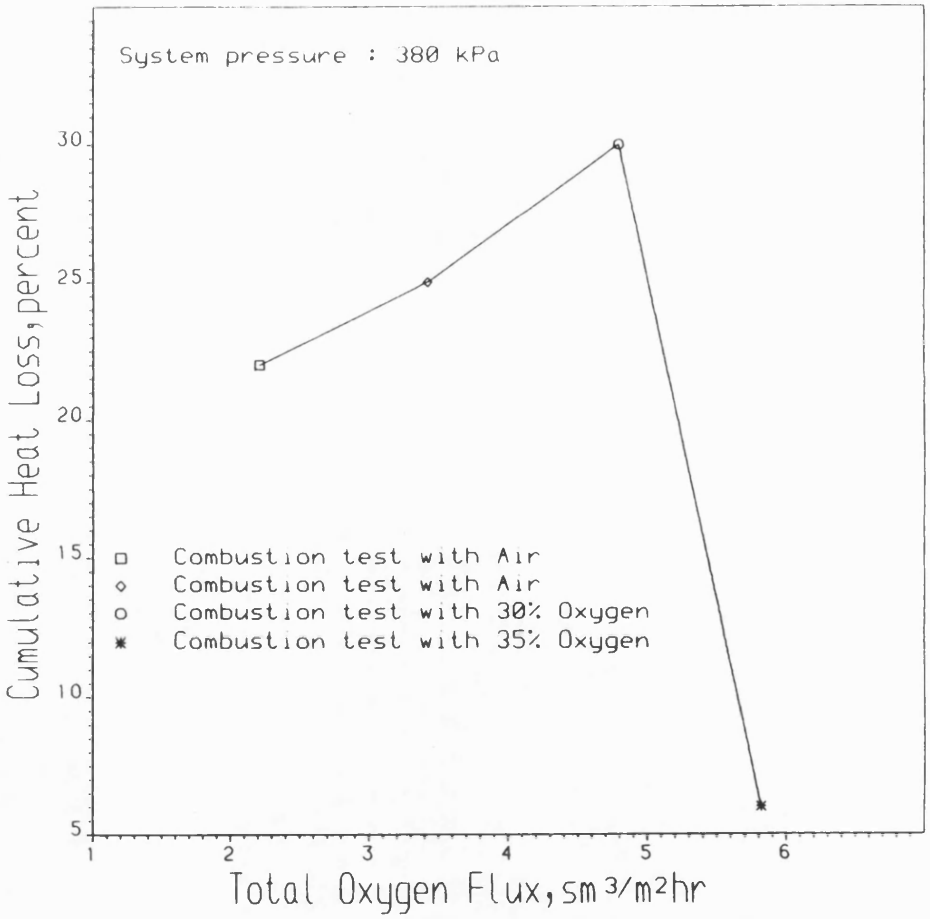

Figure 5.43 CUMULATIVE HEAT LOSS IN COMBUSTION ZONE AS A FUNCTION OF TOTAL OXYGEN FLUX

enrichment but decreases considerably with 35% O_2. This is considered to be due principally to an increase in fuel concentration which reduces the combustion-front velocity. Notice that the percent rise in the rate of heat generation from Runs 1 to 2 and 2 to 5 as shown in Table 5.3, exceeds the percent increase in combustion-front velocity and hence increased radial heat loss. The greatly increased front velocity at 35% O_2, however, caused a significant reduction in the radial heat loss. In-situ combustion with high oxygen enrichment may therefore benefit from a lower cumulative heat loss in addition to having higher heat generation rate. The increasing trend of the average peak tempearture with oxygen concentration shown in Table 5.3 is consistent with the findings of Hansel et al. (1982) and is believed to be due to the rate at which heat is generated compared with the radial heat loss.

With air-assisted combustion, the peak temperature is not significantly affected by increase in pressure, varying from only 406 to 410°C over the pressure range 380, 690 and 1020kPa. One explanation for this is that at higher injection pressures, the distillation rate of volatile components in the steam zone is lower. This means that more fuel is potentially available for combustion. In consequence, a high peak temperature would be expected, but the convective heat transport from the combustion zone also increases due to the larger fraction of nitrogen in the combustion gases. Thus, when this is combined with the radial heat loss by conduction, the net result is to suppress any increased temperature effect arising from higher fuel concentration. Similar insensitivity of combustion front peak temperature to air injection pressure has also been reported by Wilson et al. (1963) who conducted experiments up to 1,000 psig with a near-adiabatic combustion tube.

The wet combustion results, represented in Figs. 5.44 to 5.49 show that there is a lowering of combustion front peak temperature, due mainly to the combined effect of external heat losses and in-situ generated steam. Similar results were reported by Burger et al. (1973) and Garon et al. (1974). Ejiogu et al. (1979), however, observed higher peak temperatures during wet combustion compared with dry combustion. This was attributed to the additional heat input to the combustion zone by superheated steam which is produced when the injected water contacts the hot rock behind the combustion zone. They claimed that this increased the size of the steam zone. The resultant preheating reduced the rate of heat loss by decreasing the axial temperature gradient. In the normal wet combustion region to which Ejiogu's et al. resultsmainly apply, the superheated steam is always at a lower temperature than the combustion peak temperature before it enters the combustion zone. Some cooling effect is therefore expected to occur. As shown in Table 5.3, the average heat generation rate is higher for some wet combustion than for the corresponding dry combustion. This is due mainly to the combined effect of the higher molar CO_2/CO ratio and the atomic H/C ratio of the burned fuel, both parameters being reaction kinetics dependent. It seems more plausible therefore that if radial heat losses are minimized, then higher peak temperature in wet combustion than in the corresponding dry combustion could be expected in such cases.

The heat scavenging effect of the injected water is very evident from the much lower axial temperature profile behind the combustion front, compared with dry combustion, as shown in Figs. 5.50 to 5.55.

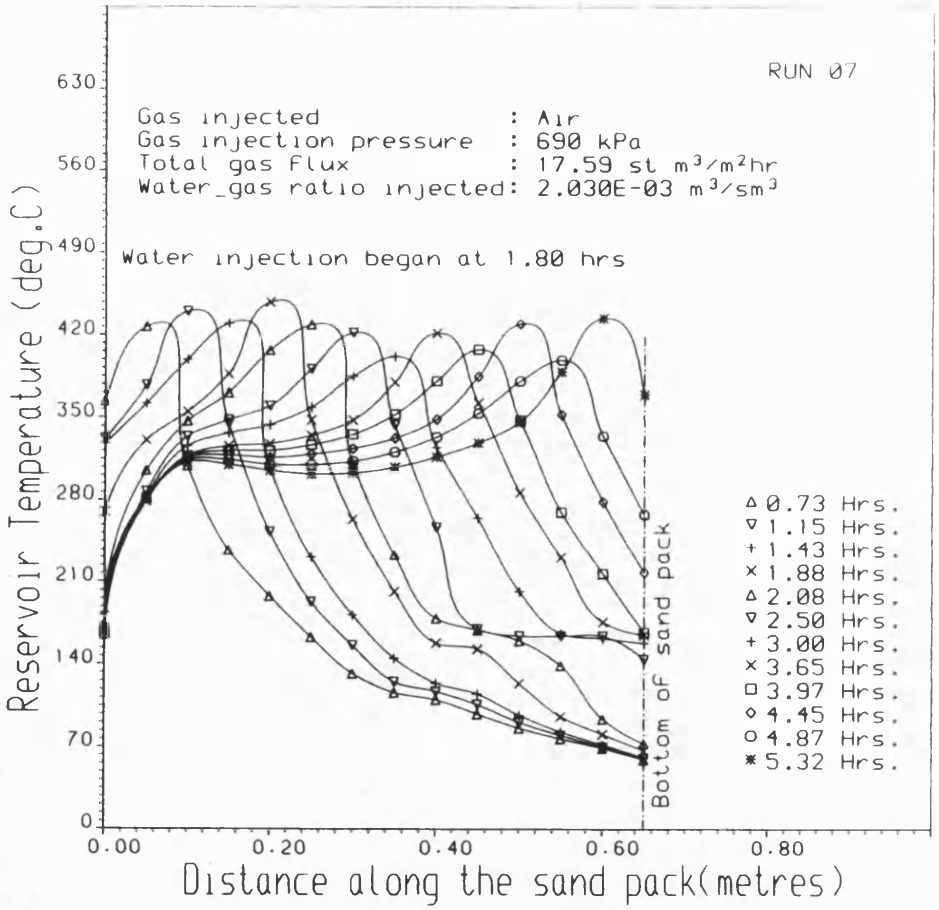

Fig. 5.44 COMBUSTION TUBE AXIAL TEMPERATURE PROFILE

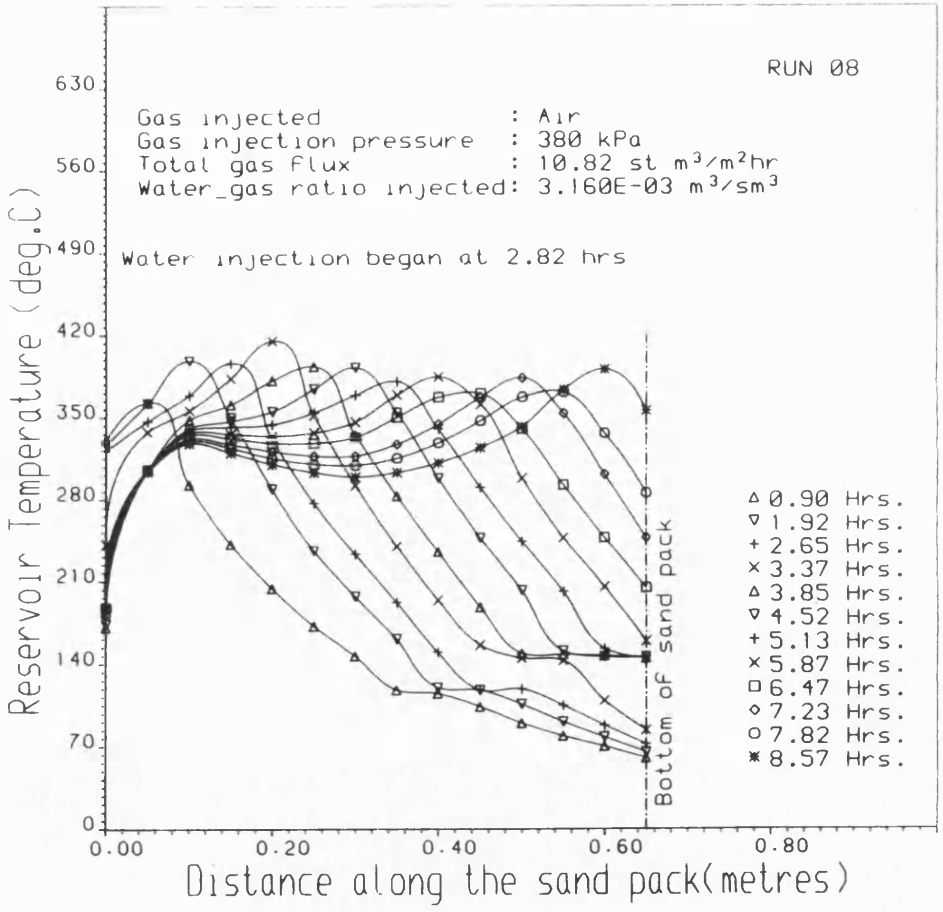

Fig. 5.45 COMBUSTION TUBE AXIAL TEMPERATURE PROFILE

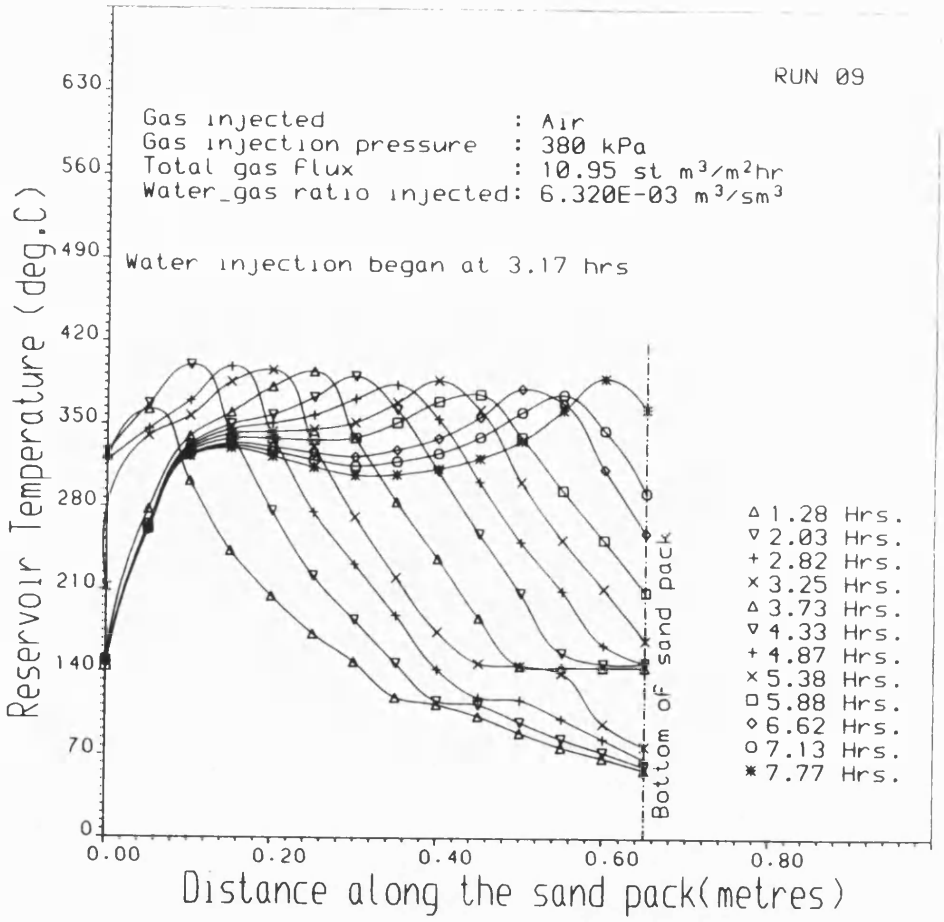

Fig. 5.46 COMBUSTION TUBE AXIAL TEMPERATURE PROFILE

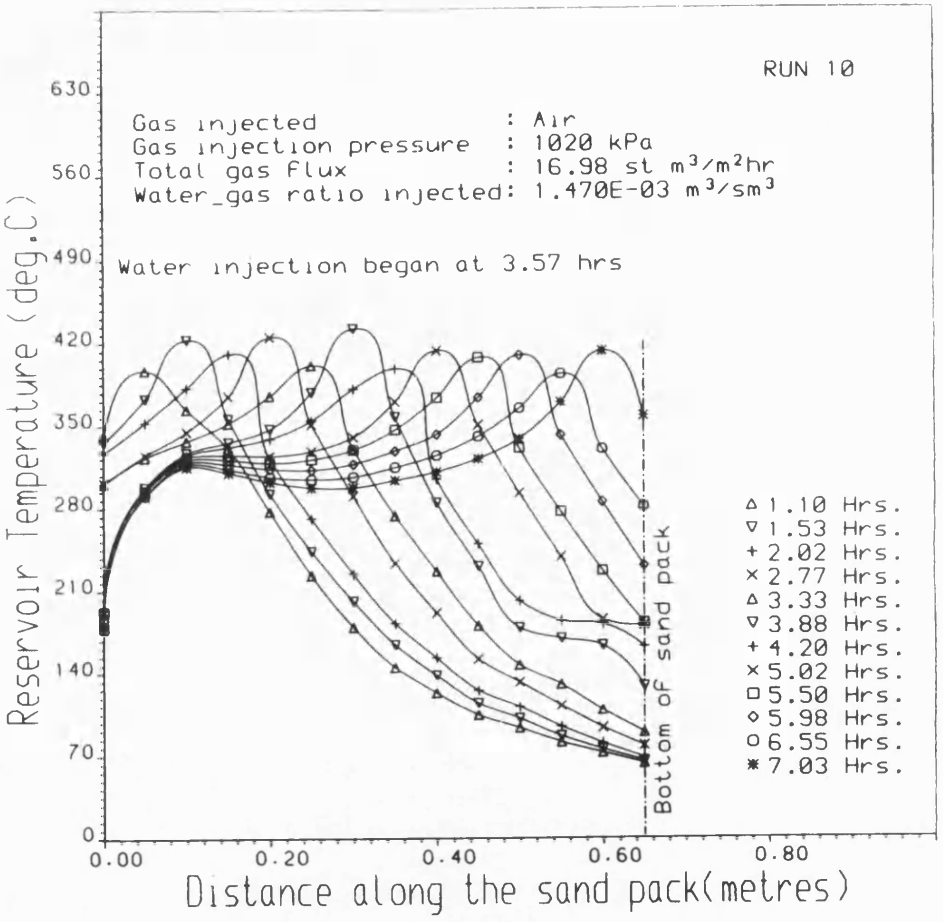

Figure 5.47 COMBUSTION TUBE AXIAL TEMPERATURE PROFILE

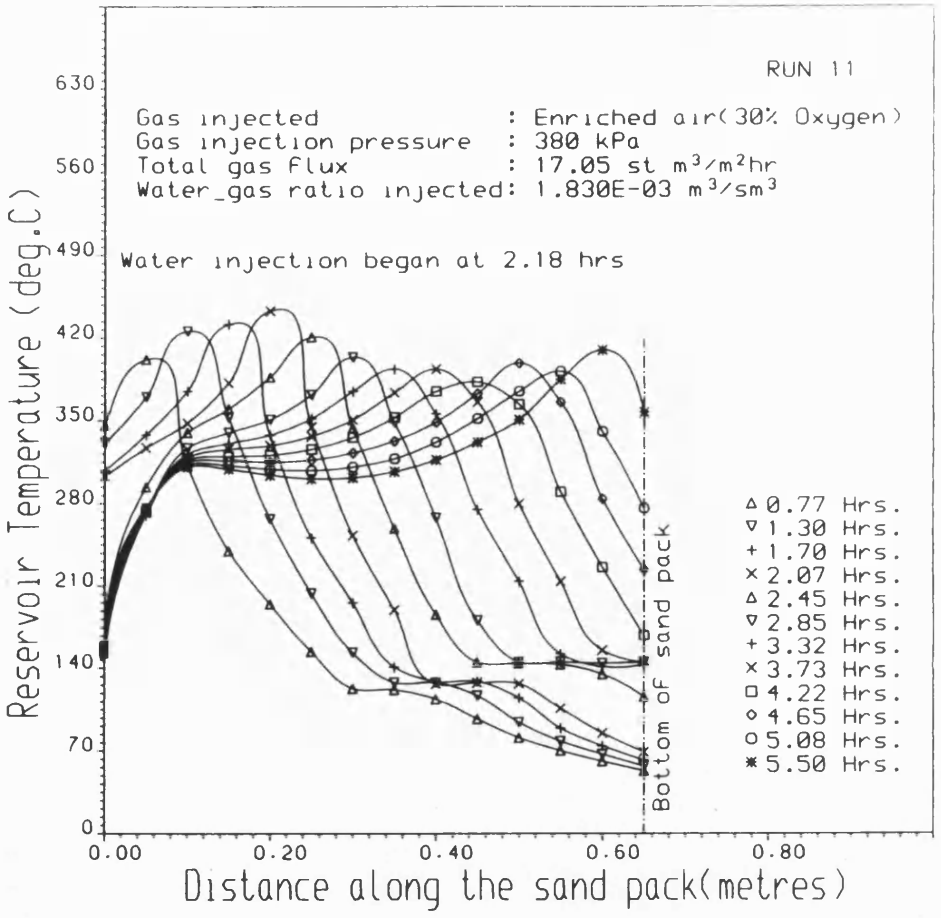

Fig. 5.48 COMBUSTION TUBE AXIAL TEMPERATURE PROFILE

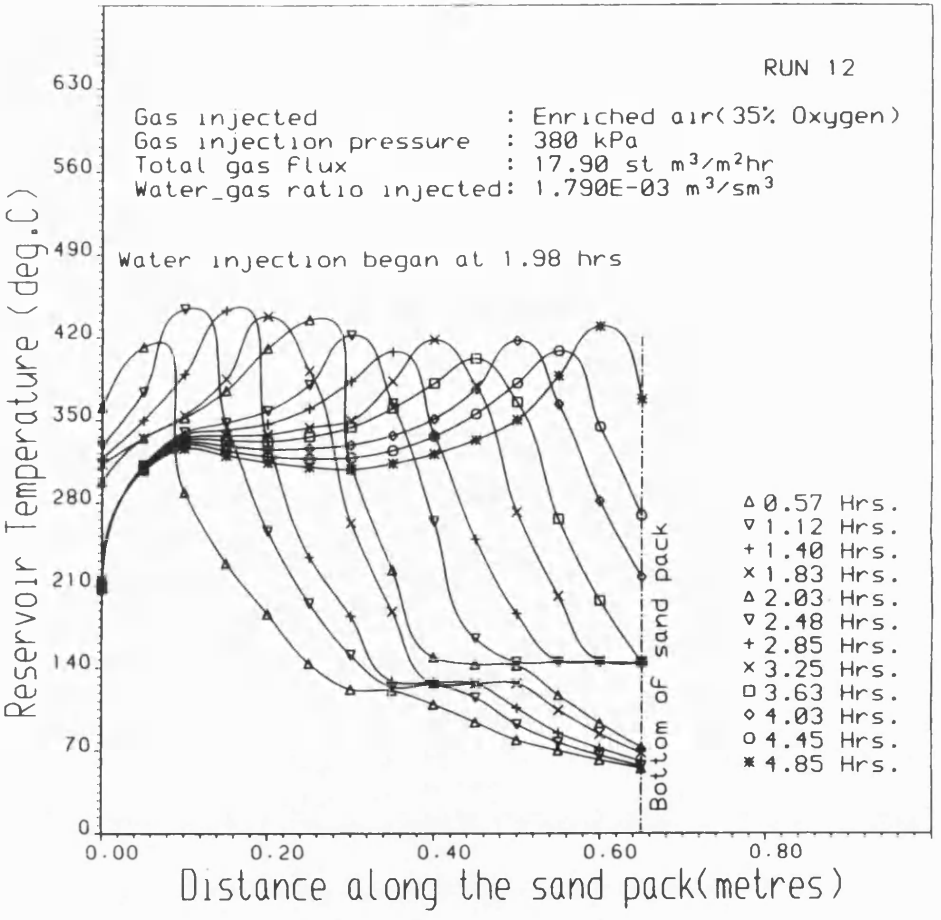

Fig. 5.49 COMBUSTION TUBE AXIAL TEMPERATURE PROFILE

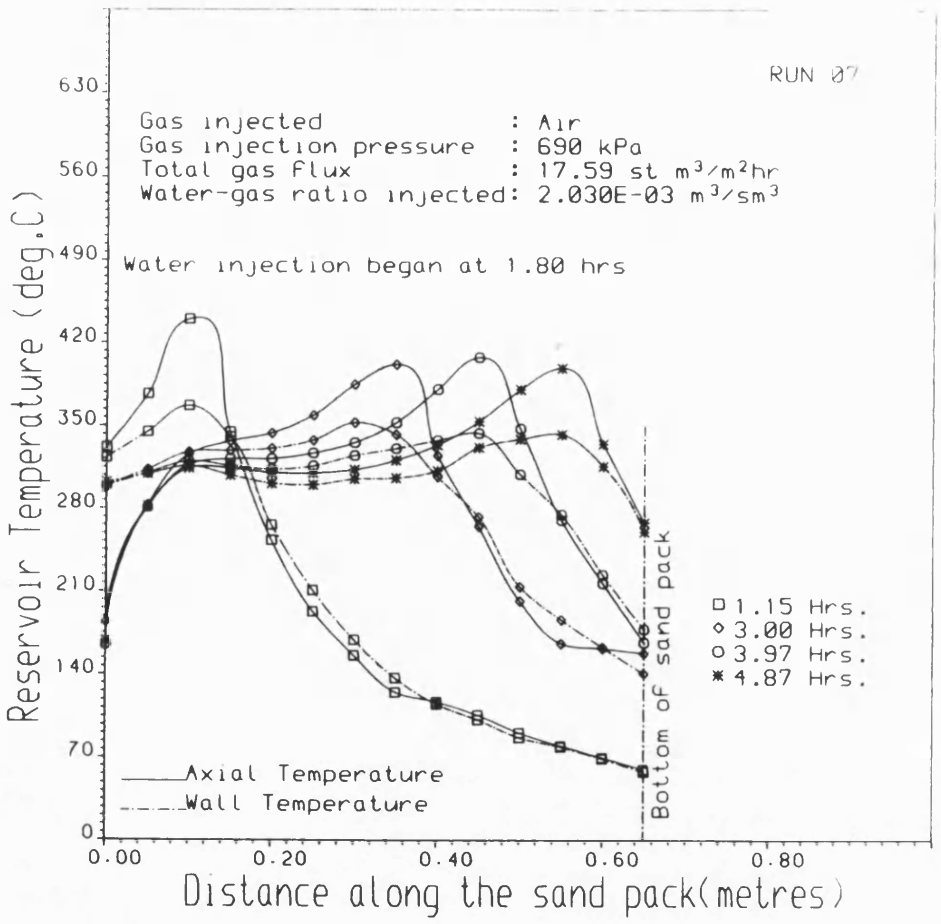

Figure 5.50 COMBUSTION TUBE AXIAL AND WALL TEMPERATURE PROFILES

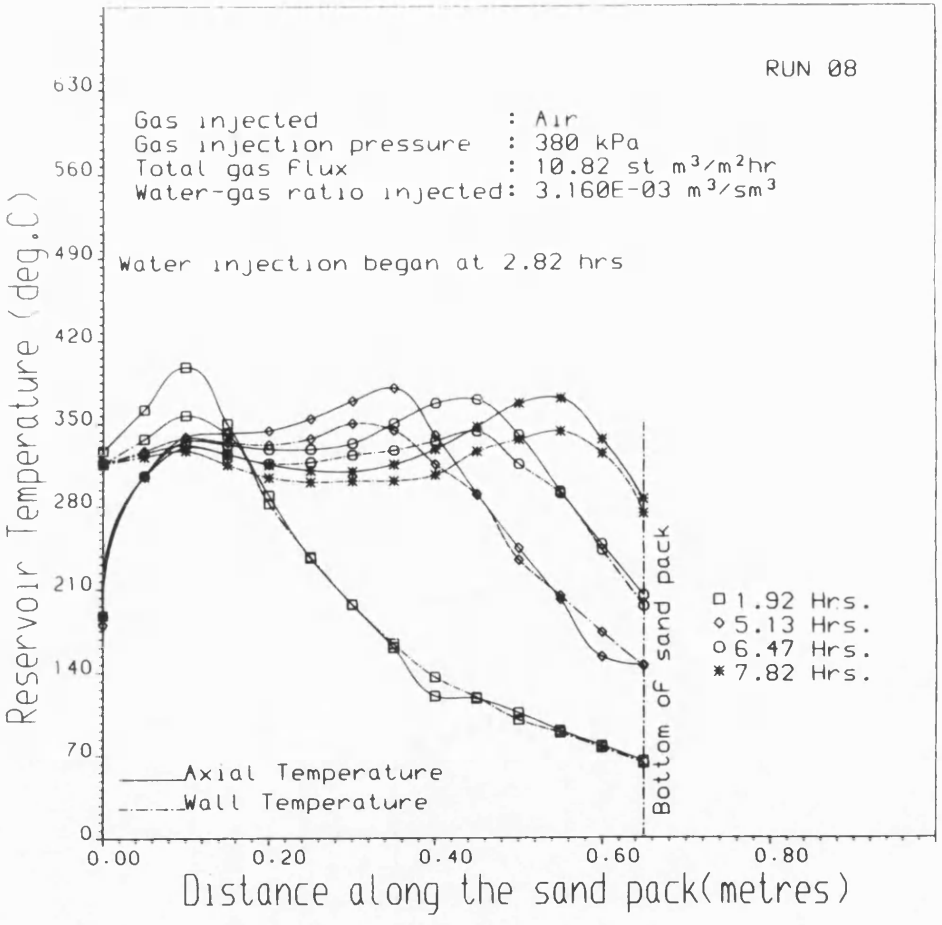

Figure 5.51 COMBUSTION TUBE AXIAL AND WALL TEMPERATURE PROFILES

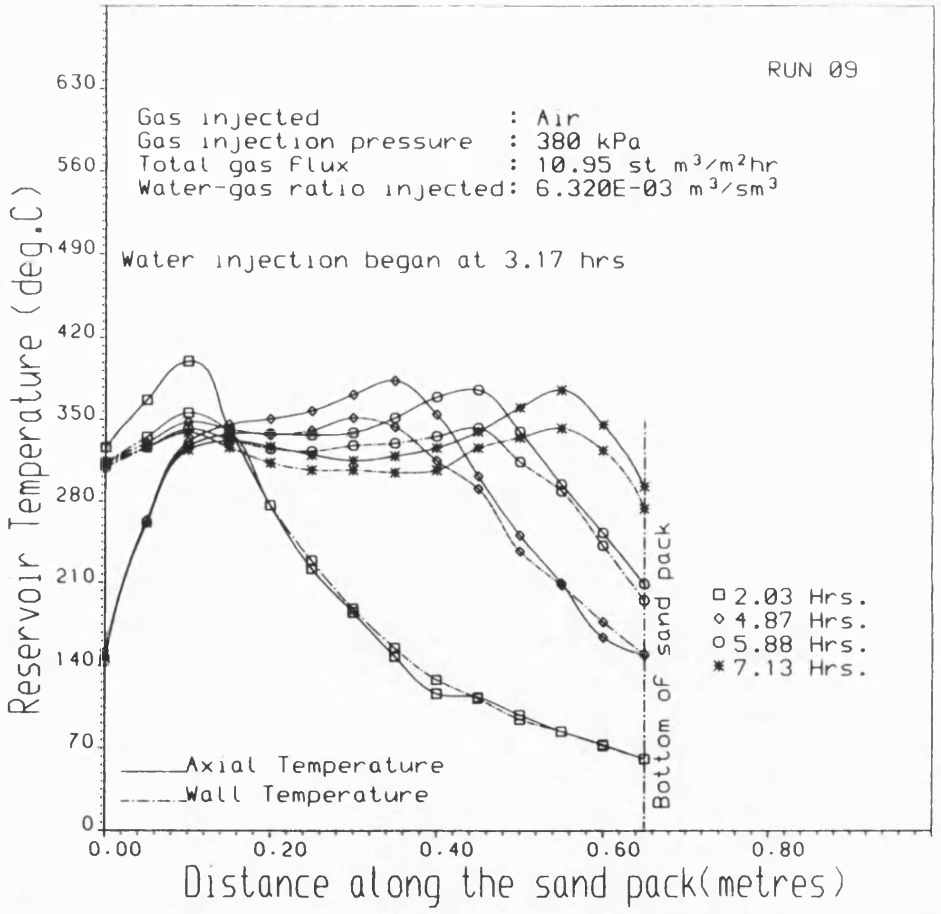

Figure 5.52 COMBUSTION TUBE AXIAL AND WALL TEMPERATURE PROFILES

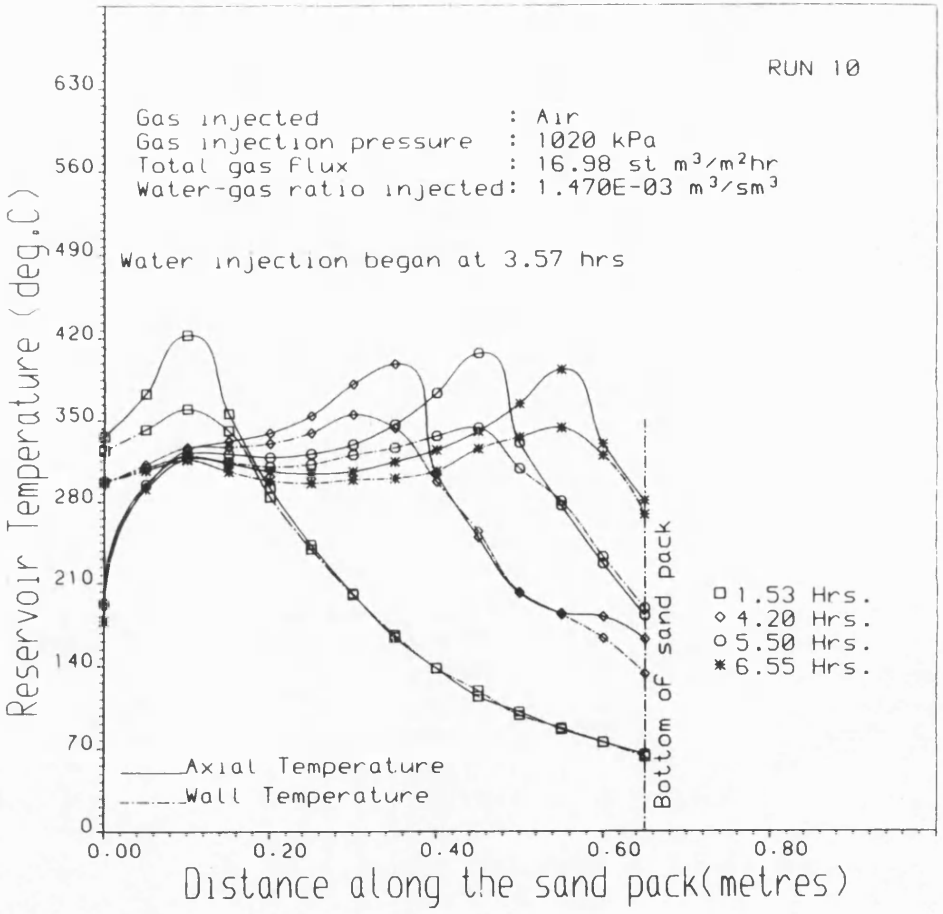

Figure 5.53 COMBUSTION TUBE AXIAL AND WALL TEMPERATURE PROFILES

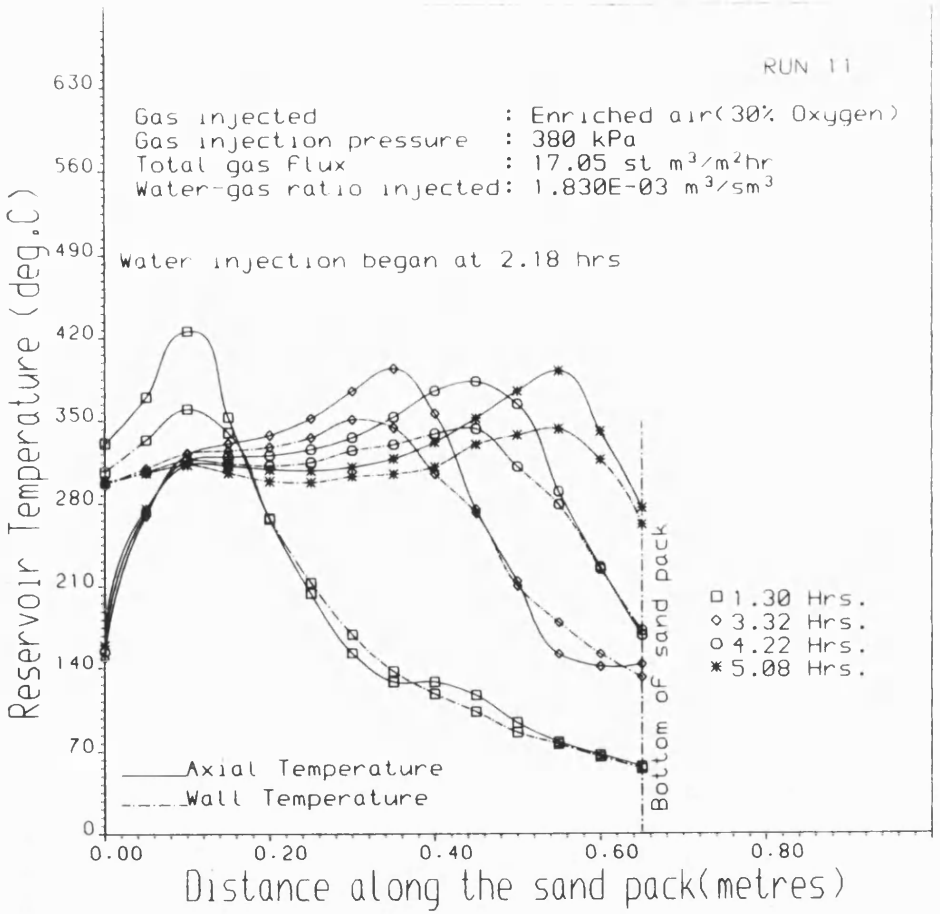

Figure 5.54 COMBUSTION TUBE AXIAL AND WALL TEMPERATURE PROFILES

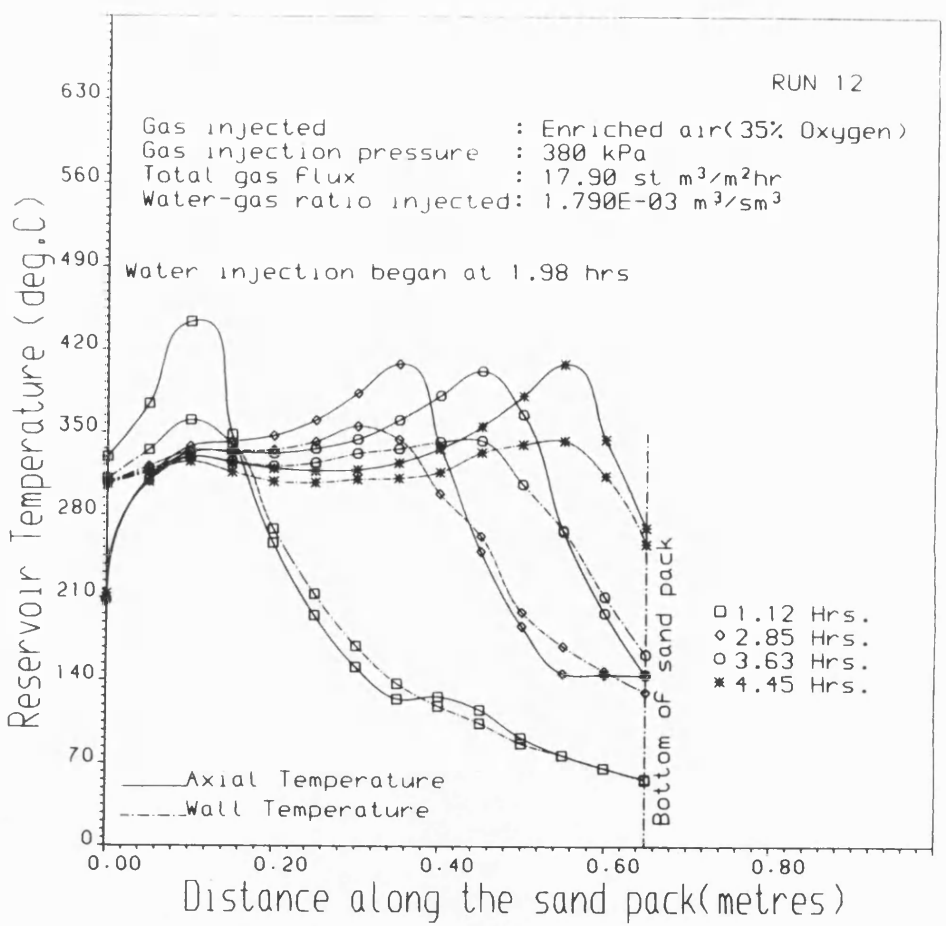

Figure 5.55 COMBUSTION TUBE AXIAL AND WALL TEMPERATURE PROFILES

5.2.2 Steam Zone

The characteristics of the steam zone are dependent on operating conditions.

Operating pressure

The effect of pressure on the steam zone is shown in Figs. 5.29 to 5.31. At 380kPa, the size of the steam zone eventually stabilises after 1.21 hours, during which the combustion front travelled a distance of 0.051m from the top of the sand pack. This contrasts with times of 2.83 and 6.02 hours, respectively at 690 and 1020kPa, for which the distances travelled by the combustion front were 0.152 and 0.356 metres. Thus, from the time of ignition the period required for the steam bank to stabilize is very dependent on system pressure, and is greatly increased at higher pressures. The influence of steam flooding therefore occurred at much later time for the higher pressure experiments. Since the fuel availability is affected by processes taking place in the steam zone, the stability of the in-situ combustion process itself will depend on the approach to stabilization of this zone. The maximum length of fully developed steam plateau observed is approximately 0.051m. This suggests that the length of this zone is not very sensitive to system pressure used in this study. The velocity of the steam zone for Runs 2 and 3 (380 and 690kPa) are 0.077 and 0.068 m/hr respectively. Insufficient data was obtained to estimate this for Run 4, owing to extended stabilisation period. The steam zone thus propagates faster at lower injection pressure, which is significant in relation to the rate of oil production.

Oxygen Enrichment

The use of oxygen enriched air results in larger steam zone. As shown in Figs. 5.32 and 5.33, the length of the

steam zone is approximately 0.102m using 30 and 35% oxygen compared with 0.051m using air (Fig. 5.29). Certainly, the higher steam production rate with enriched air is the main factor. The steam front velocities are estimated to be 0.077, 0.084 and 0.110m/hr respectively for air, 30% and 35% O_2. Both effects of larger steam zone size and increased velocity are likely to be important in promoting more efficient steam flooding during in-situ combustion.

Water Injection

Injection of water causes a continuous increase in the size of the steam zone up to the point of steam breakthrough, as shown in Figs. 5.44 to 5.49. The length of the steam zone remains constant at 0.051m during the dry combustion period (Fig. 5.45), but increases to 0.102m at 3.37hrs and further to 0.152m at 3.85hrs. Increasing size of the steam zone inevitably leads to its early breakthrough, but the overall effect may be beneficial from an oil production viewpoint.

It is also observed that the temperature of the steam plateau, for dry and wet combustion runs, is not constant. This variation will result in a non-uniform rate of vaporization and cracking of the oil.

5.3 Fuel Combustion Rate

The carbon combustion rate which is determined from the cumulative amount of carbon burned exhibits a linear trend for all the experiments (Figs. 5.56 to 5.61). Thus the carbon combustion rate became constant shortly after the combustion front is established. As shown in Table 5.3, the carbon combustion rate with air does not exhibit any particular trend with increasing

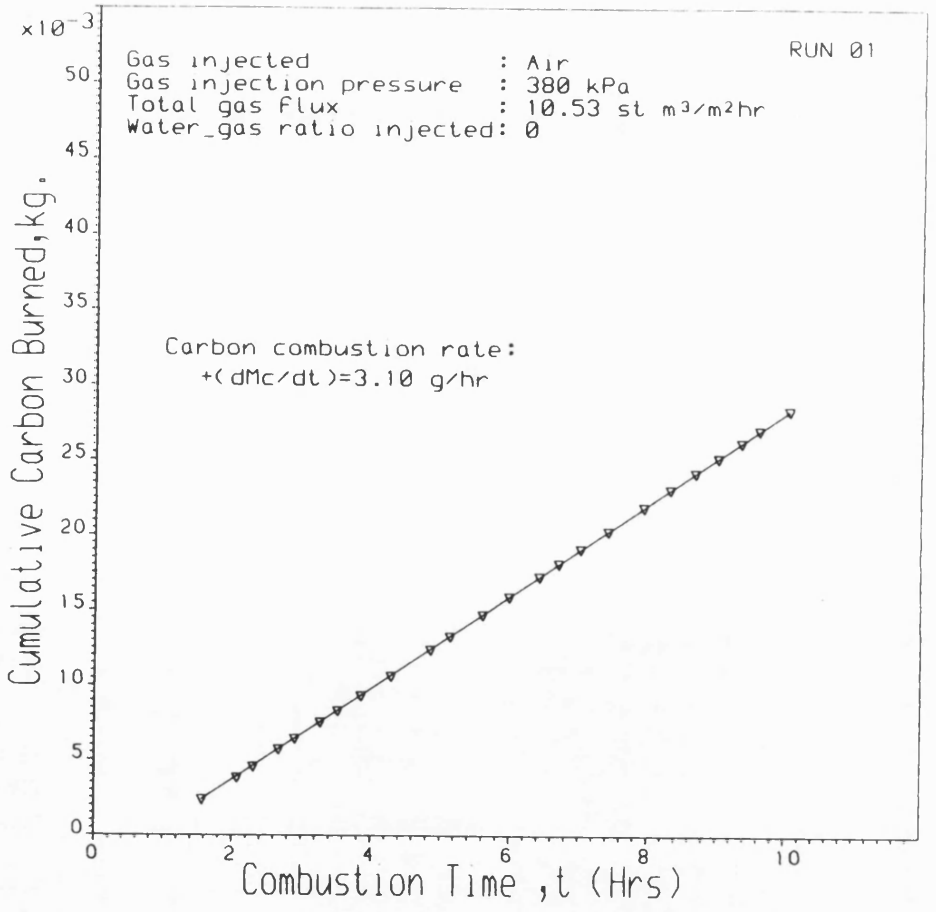

Figure 5.56 CUMULATIVE CARBON BURNED AS A FUNCTION OF COMBUSTION TIMES

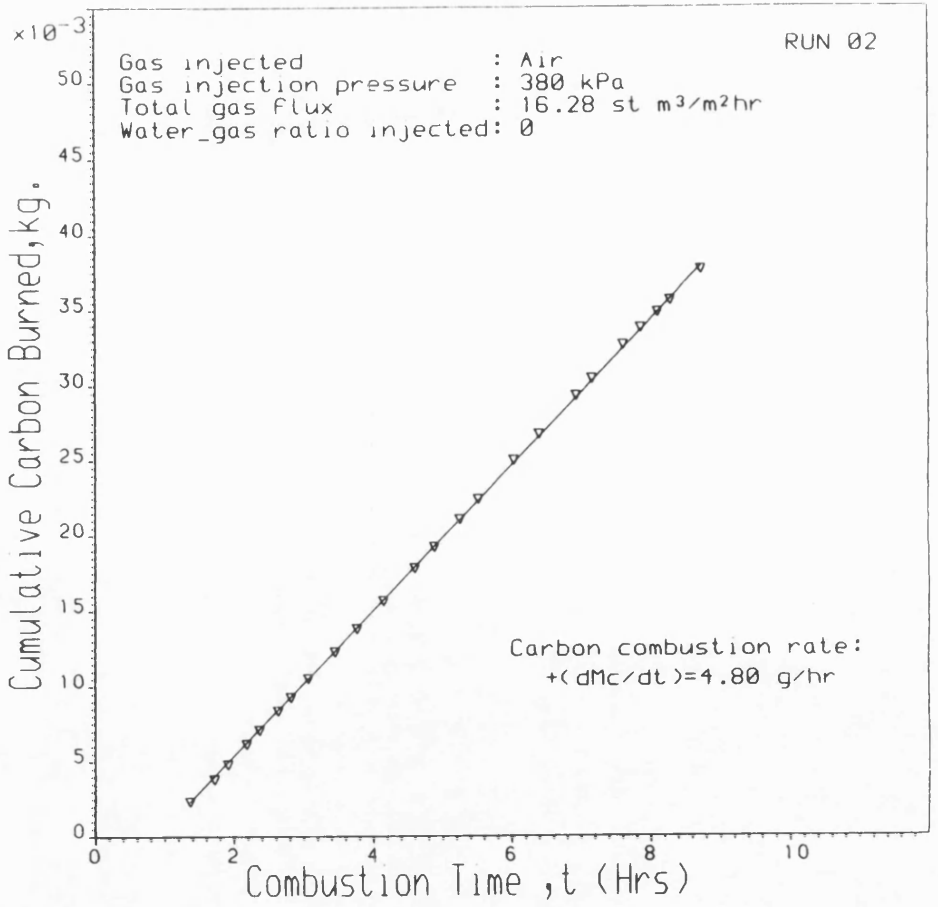

Figure 5.57 CUMULATIVE CARBON BURNED AS A FUNCTION OF COMBUSTION TIMES

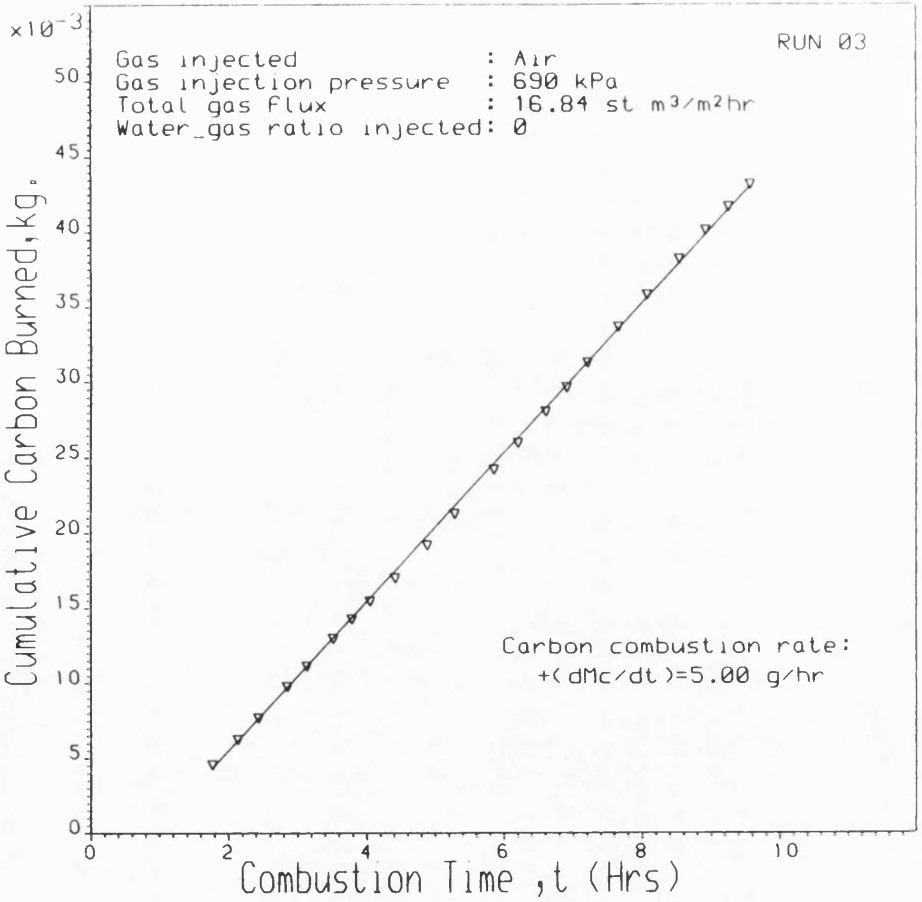

Figure 5.58 CUMULATIVE CARBON BURNED AS A FUNCTION OF COMBUSTION TIMES

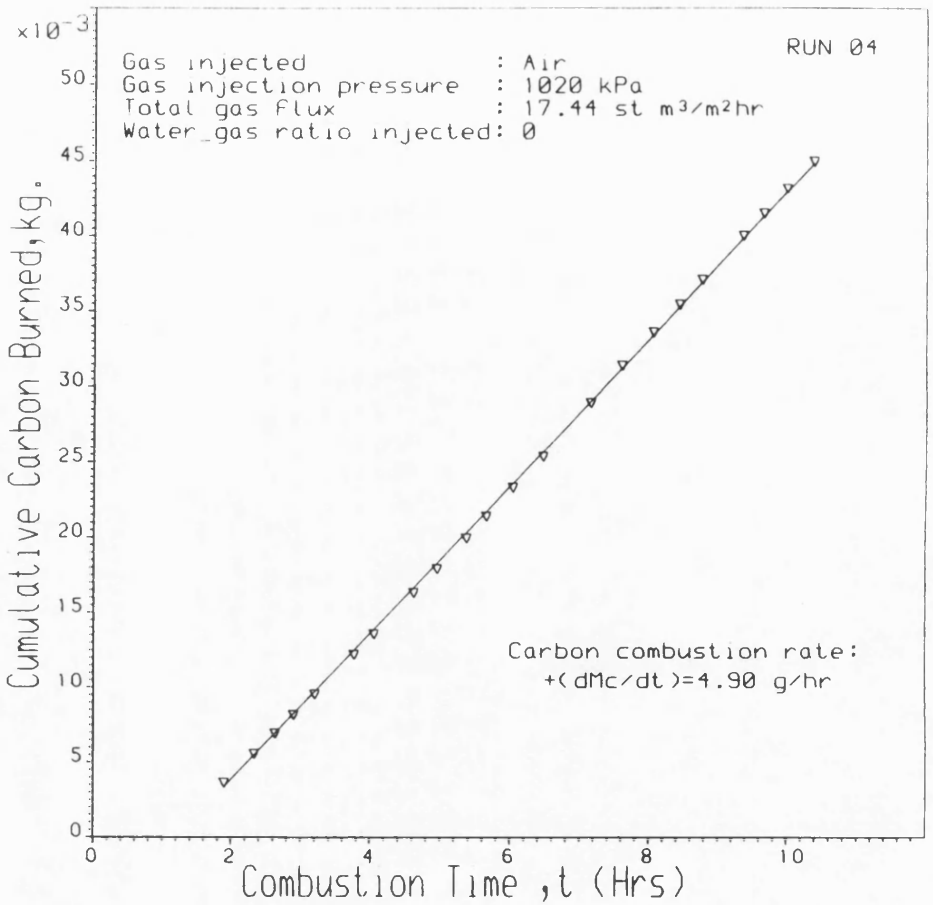

Figure 5.59 CUMULATIVE CARBON BURNED AS A FUNCTION OF COMBUSTION TIMES

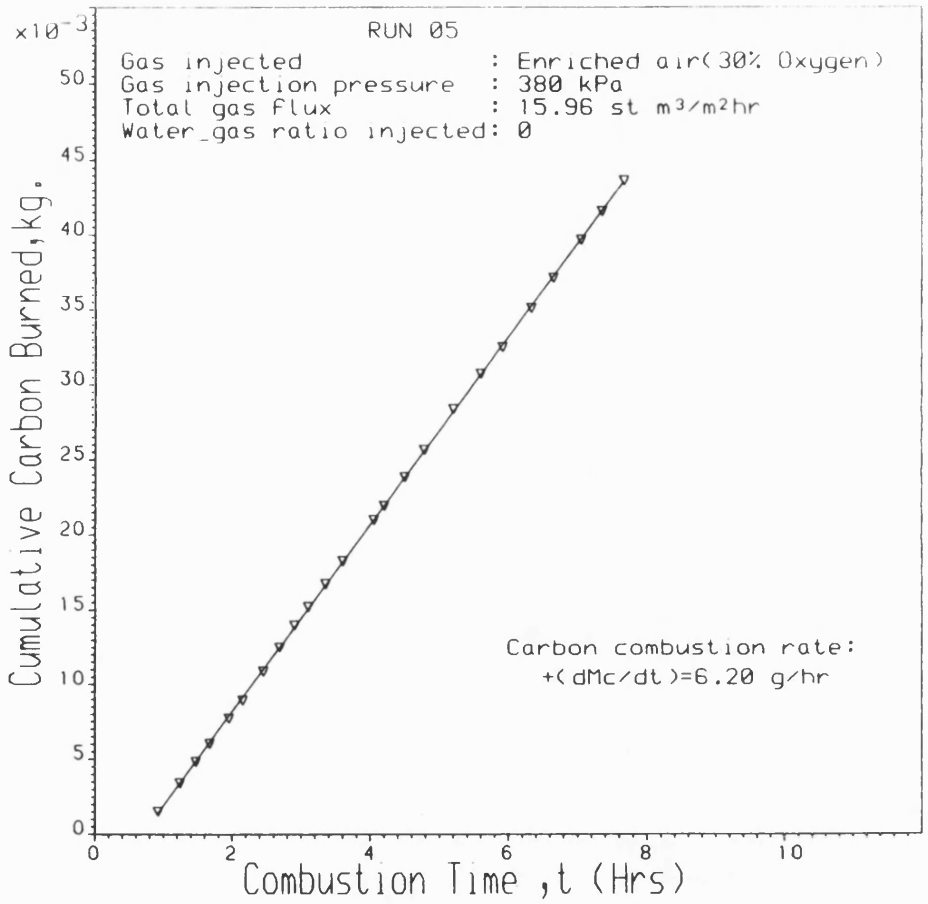

Figure 5.60 CUMULATIVE CARBON BURNED AS A FUNCTION OF COMBUSTION TIMES

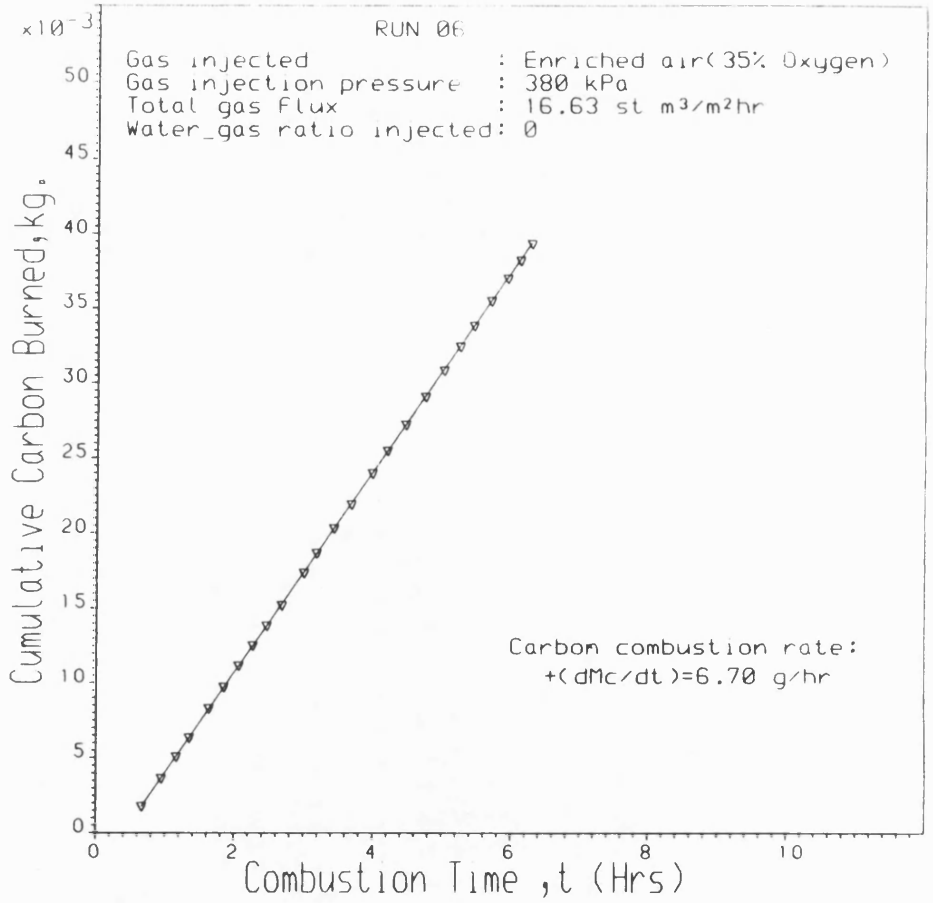

Figure 5.61 CUMULATIVE CARBON BURNED AS A FUNCTION OF COMBUSTION TIMES

pressure. However, there is a strong dependence on oxygen enrichment. Fig. 5.62 shows that there is a very substantial increase in carbon combustion rate with oxygen enrichment during the dry combustion. Increase in oxygen flux in the combustion zone will lead to increase in reaction rate. This aspect is considered later in chapter 6.

The carbon combustion rate only appears to be affected by water injection when enriched air is used. For example, 6.2g/hr of carbon is burned in Run 5 compared with 5.6g/hr at a water injection rate of 1.83m^3/Msm^3 in Run 11. Both runs were carried out using 30% O_2. A similar effect is obtained using 35% oxygen.

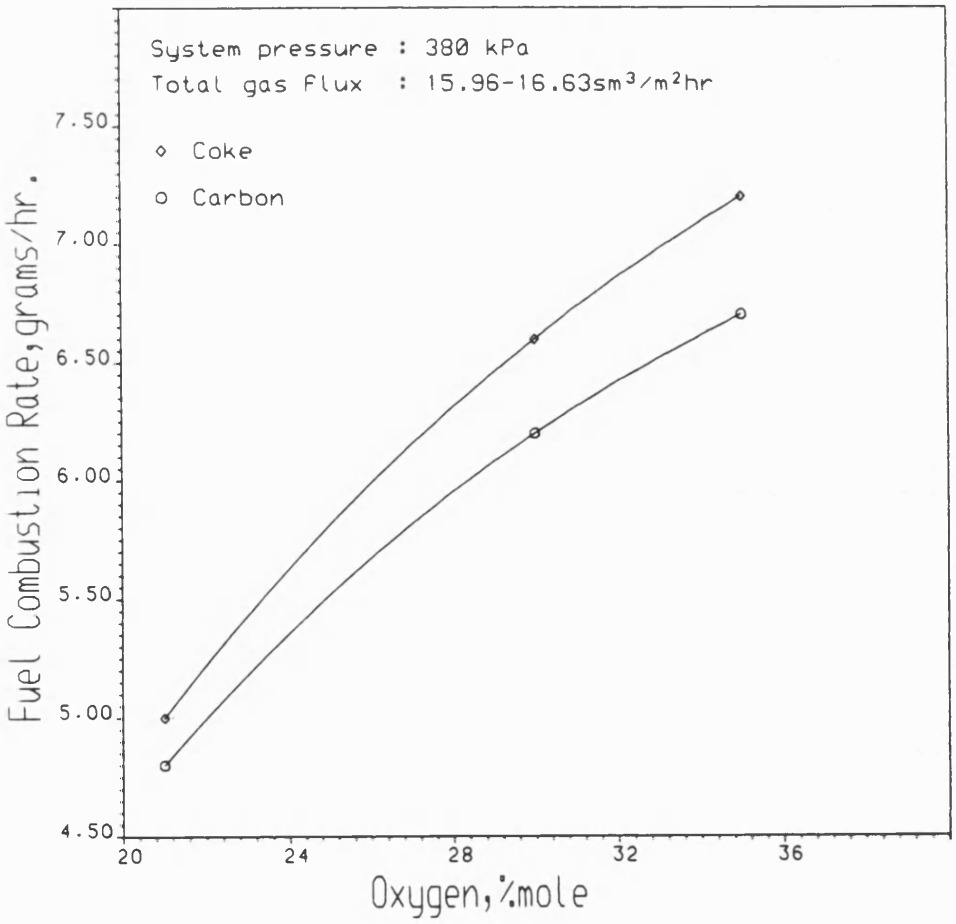

Figure 5.62 EFFECT OF OXYGEN ENRICHMENT OF AIR ON FUEL COMBUSTION RATE

5.4 Combustion-Front Velocity

A reference temperature level (700°F), known to be representative of combustion conditions, was used to determine the location of the combustion front. Figures 5.63 to 5.65 are typical plots of the distance-time relation, from which the average combustion-front velocity was determined. The linear trend indicates a stable combustion process. The non-uniform radial heat loss effect along the tube does not appear therefore to influence the stability of the combustion front. The normalized combustion-front velocity (velocity/gas flux) for different oxygen enrichment levels is shown in Fig. 5.66. The front velocity increases dramatically beyond 30% oxygen enrichment, which is due to greatly increased fuel consumption rate.

The effect of water injection on combustion-front velocity is depicted in Figs. 5.67 to 5.69. Evidently, any transient features of the wet combustion process that exist (stabilisation in the steam zone) do not appear to affect the steady propagation of the combustion front. However, the increased size of the steam zone causes greater vaporisation and increased cracking, which tends to reduce the fuel availability. The net effect of this, is an increased velocity of the combustion front. For example, in Run 8 (Fig. 5.67), the front velocity was 0.072m/hr before water injection and 0.080m/hr after water injection. In Run 10 and 12, the velocity increased from 0.078 and 0.110 to 0.094 and 0.128m/hr respectively. Furthermore, the front velocity is sensitive to the rate of water injection as shown in Fig. 5.70, with increasing effect at higher WAR. This trend is consistent with the findings of Burger et al. (1973) who reported the result of wet combustion test at 1100kPa. The front velocity increased respectively from 0.044 and 0.028 to

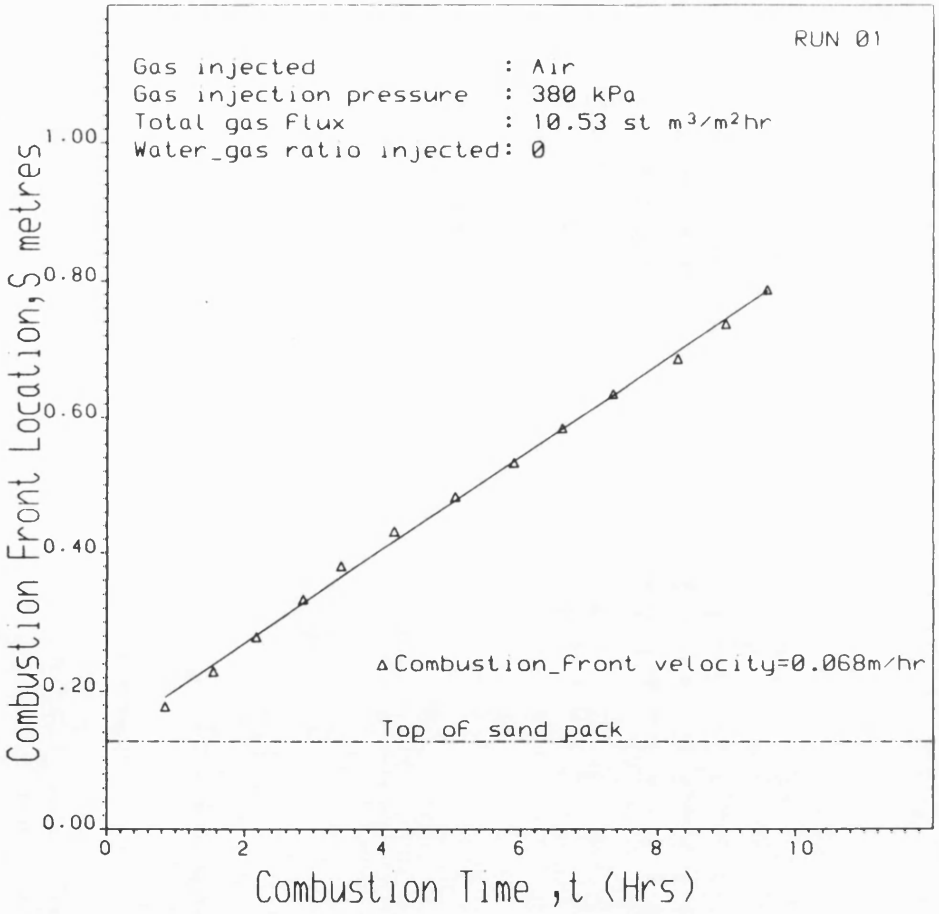

Fig. 5.63 DISTANCE-TIME RELATION OF COMBUSTION FRONT

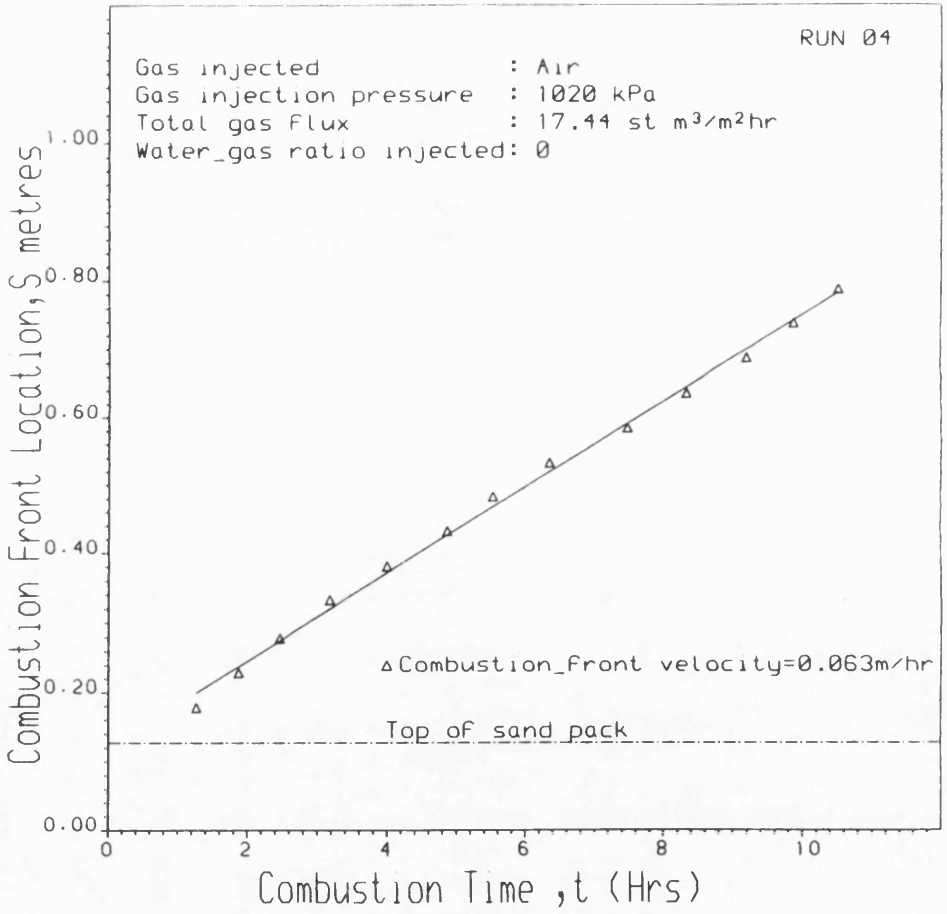

Fig. 5.64 DISTANCE-TIME RELATION OF COMBUSTION FRONT

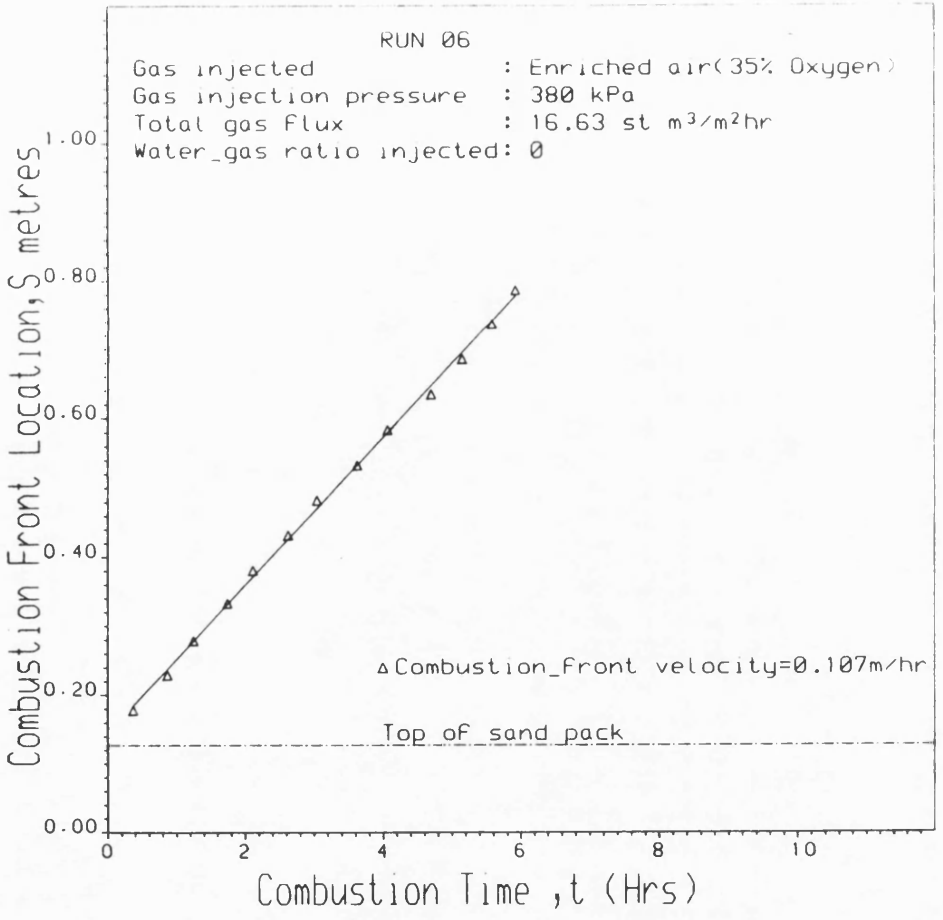

Fig. 5.65 DISTANCE-TIME RELATION OF COMBUSTION FRONT

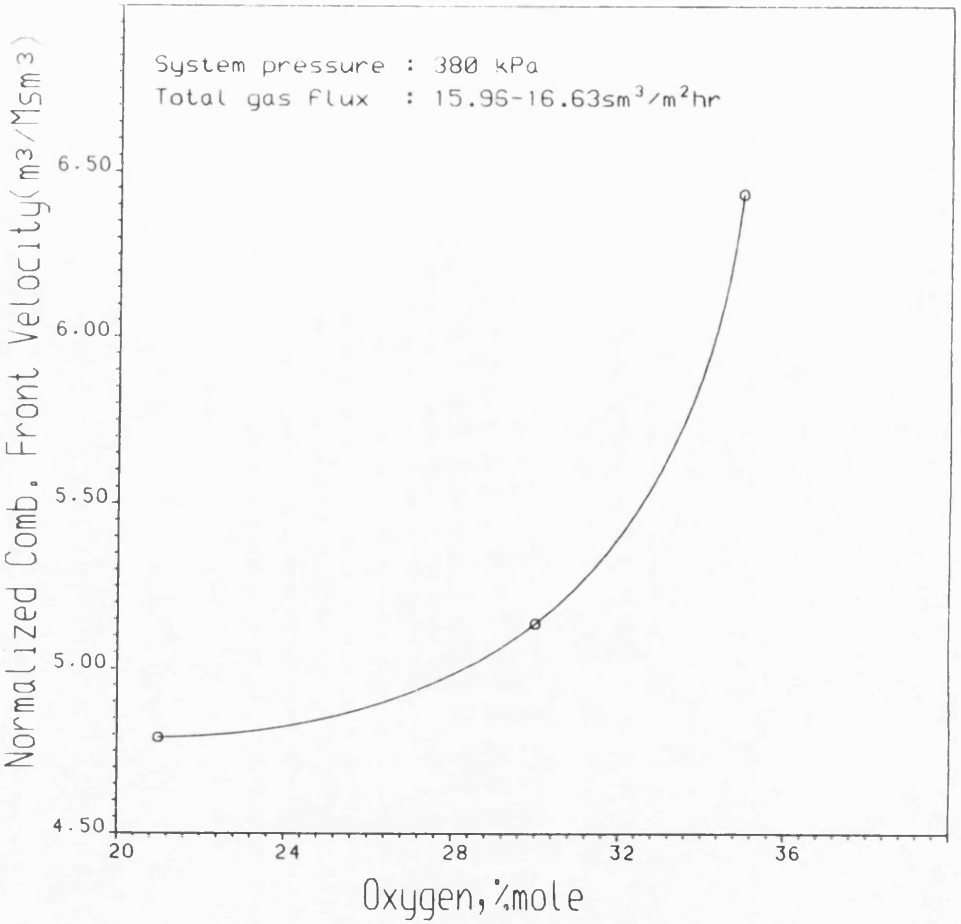

Figure 5.66 COMBUSTION FRONT VELOCITY AS A FUNCTION OF OXYGEN ENRICHMENT

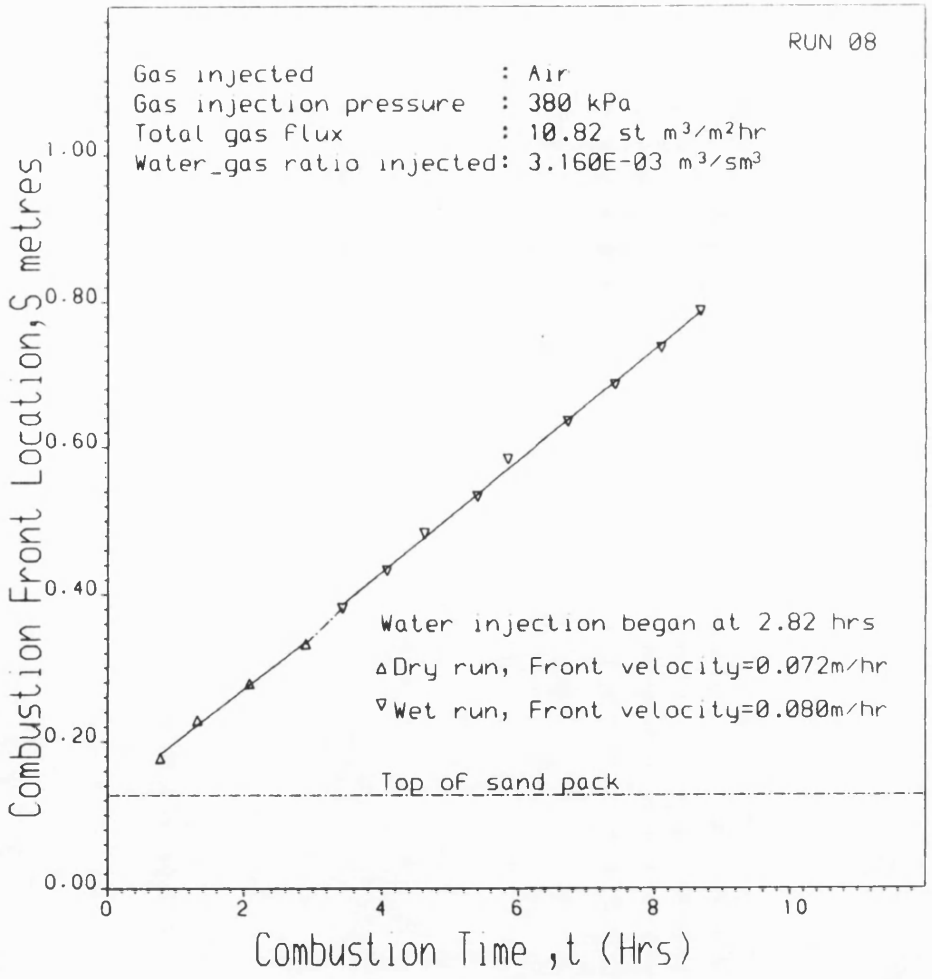

Fig. 5.67 DISTANCE-TIME RELATION OF COMBUSTION FRONT

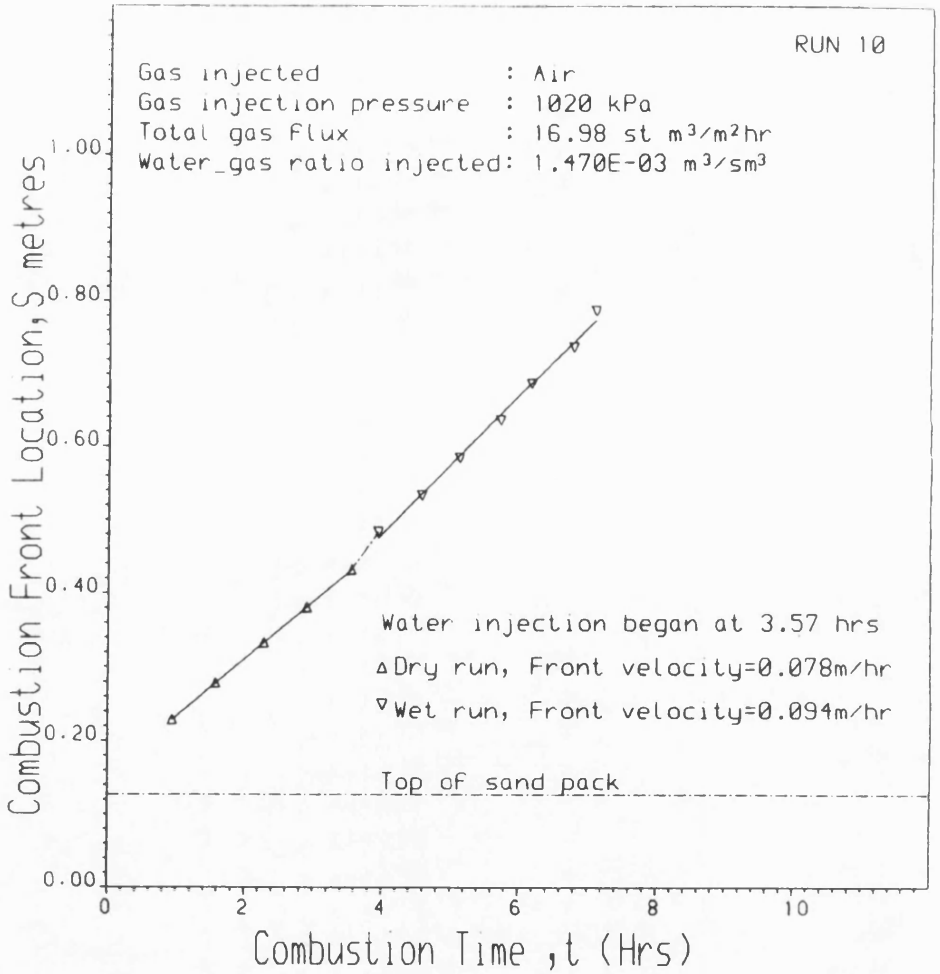

Fig. 5.68 DISTANCE-TIME RELATION OF COMBUSTION FRONT

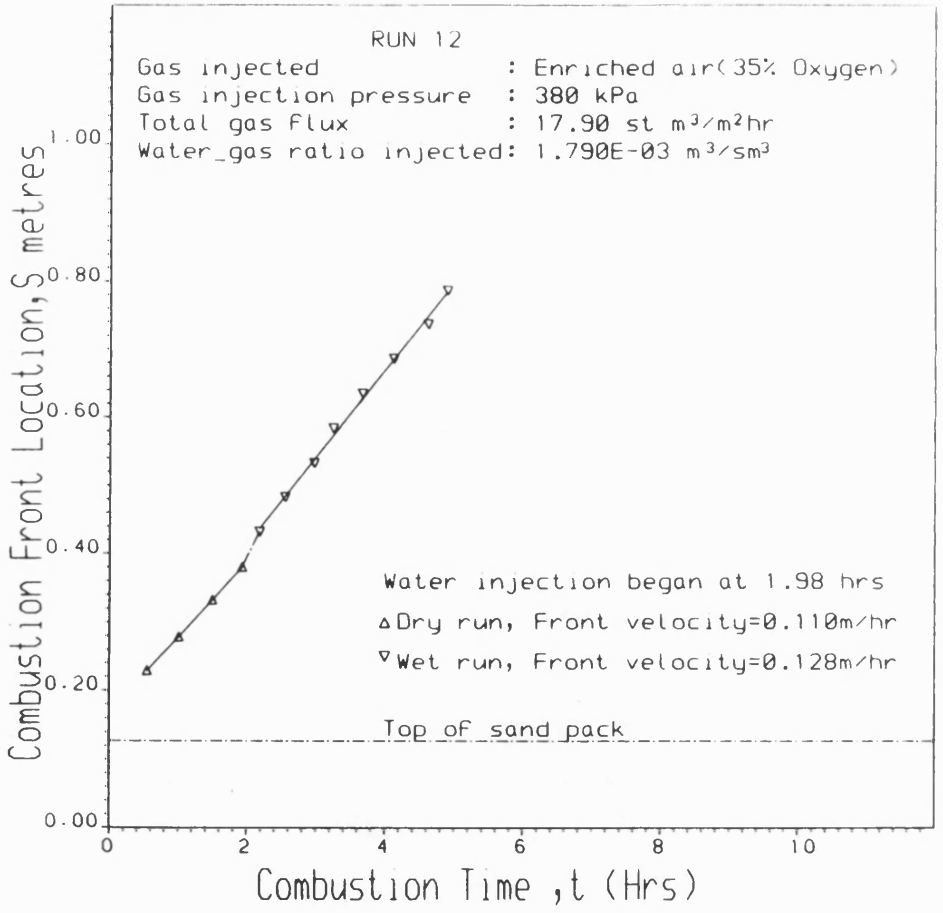

Fig. 5.69 DISTANCE-TIME RELATION OF COMBUSTION FRONT

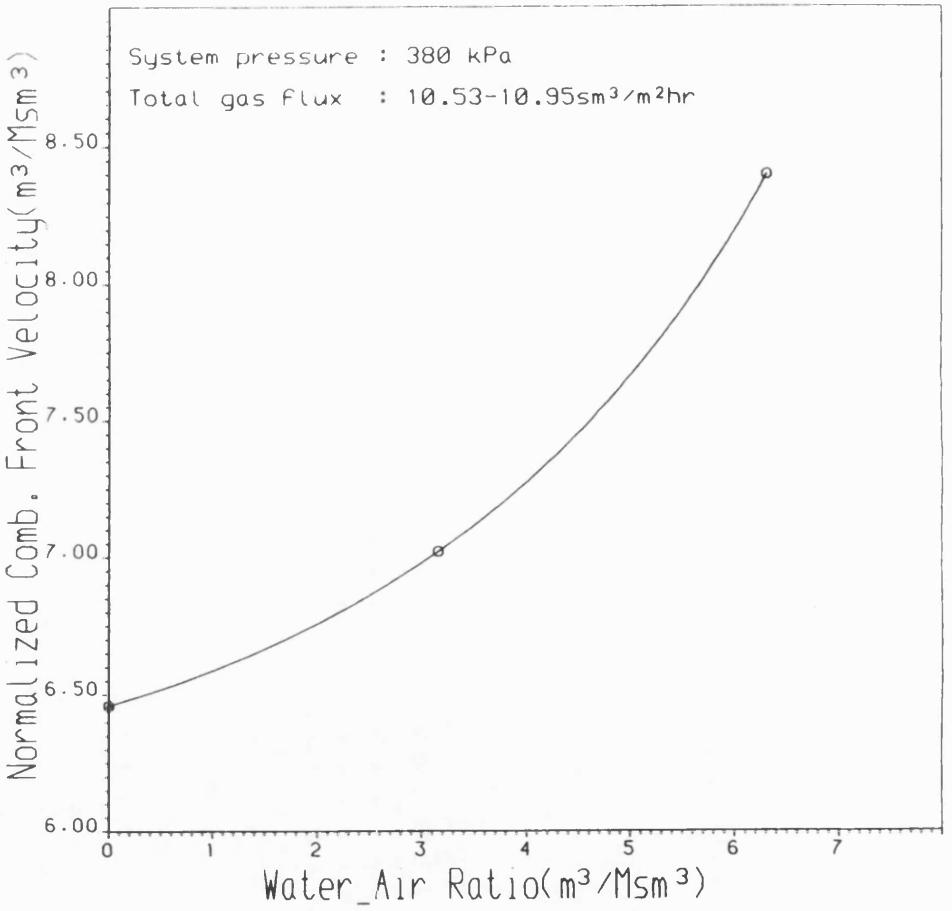

Figure 5.70 COMBUSTION FRONT VELOCITY AS A FUNCTION OF WATER_AIR RATIO

0.052 and 0.0526m/hr using WAR of 2.0 and 4.0m^3/Msm^3. Similar trends have also been reported by Dietz et al. (1967) and Alderman et al. (1971).

The significant decrease in the normalised front velocity with increasing operating pressure as shown in Fig. 5.71, can be explained in terms of increased fuel concentration and combustion time.

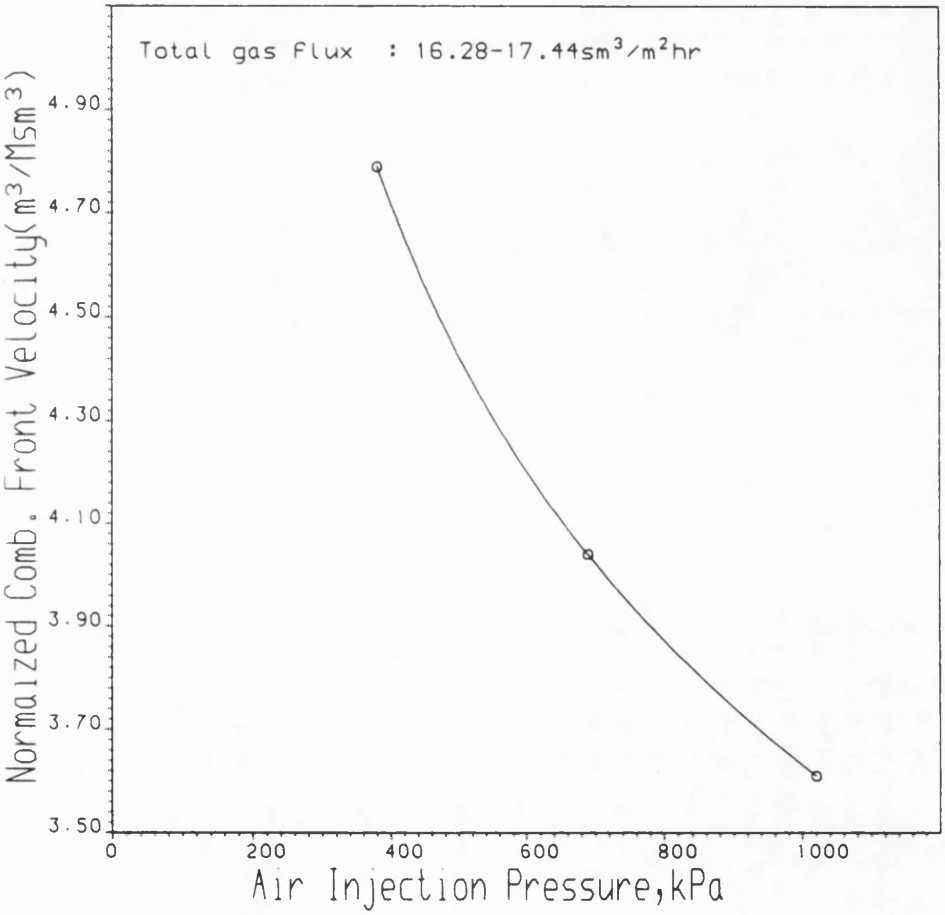

Figure 5.71 COMBUSTION FRONT VELOCITY AS A FUNCTION OF AIR INJECTION PRESSURE

5.5 Atomic Hydrogen - Carbon Ratio

Equation 5.1 presented below is used to compute the H/C ratio of the fuel burned (Nelson et al., 1961).

$$H/C = \frac{((YO_{2i} \times YN_2/YN_{2i}) - (YO_2 + YCO_2 + 0.5YCO))}{0.25(YCO + YCO_2)} \qquad 5.1$$

where YO_{2i} and YN_{2i} are the respective mole fractions of oxygen and nitrogen in the injected gas and YO_2, YCO and YCO_2 are the mole fractions of oxygen, carbon monoxide and carbon dioxide in the produced gas. The calculations are based on the assumption that all of the oxygen not observed in the exit gases reacts to form water. This is not strictly true because some of the oxygen may be consumed by low-temperature oxidation (LTO) reactions. It is for this reason that the computed H/C ratio is often referred to as an "apparent" value. Figures 5.72 to 5.77 show the trend of H/C ratio as a function of combustion time. The H/C ratio is not constant, but varies as the combustion front progresses down the combustion tube. This means that the chemical composition of the fuel must be changing. The average H/C ratios for the fuel in the dry runs (0.56 - 0.80) are much lower than the crude's (1.52). Therefore, the fuel burned is of heavier composition with little or no LTO effect occurring. A similar conclusion is valid for all of the wet runs, excepting Run 12 (Table 5.3). As shown in Fig. 5.77, the atomic H/C ratio for Run 12 is higher (wet phase) and the average value of 2.04 is also higher than that of the original crude. This is a clear indication that some LTO, and possibly, combustion of light hydrocarbons took place.

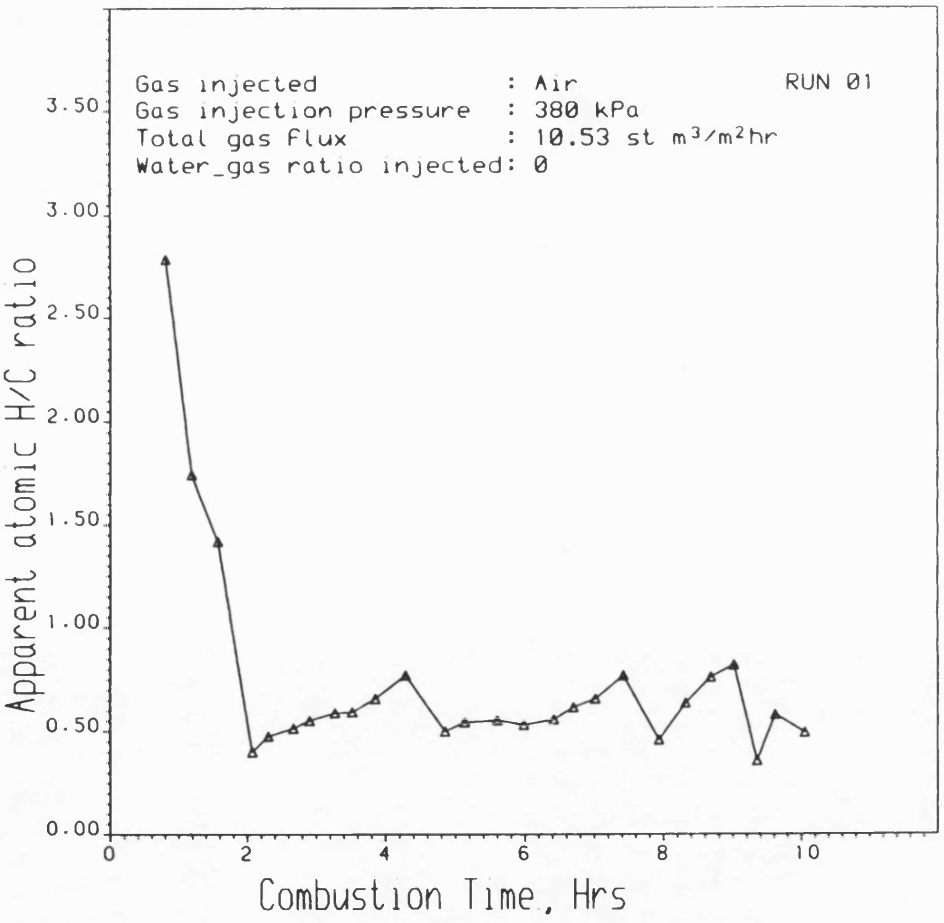

Fig. 5.72 APPARENT ATOMIC H/C RATIO OF FUEL BURNED

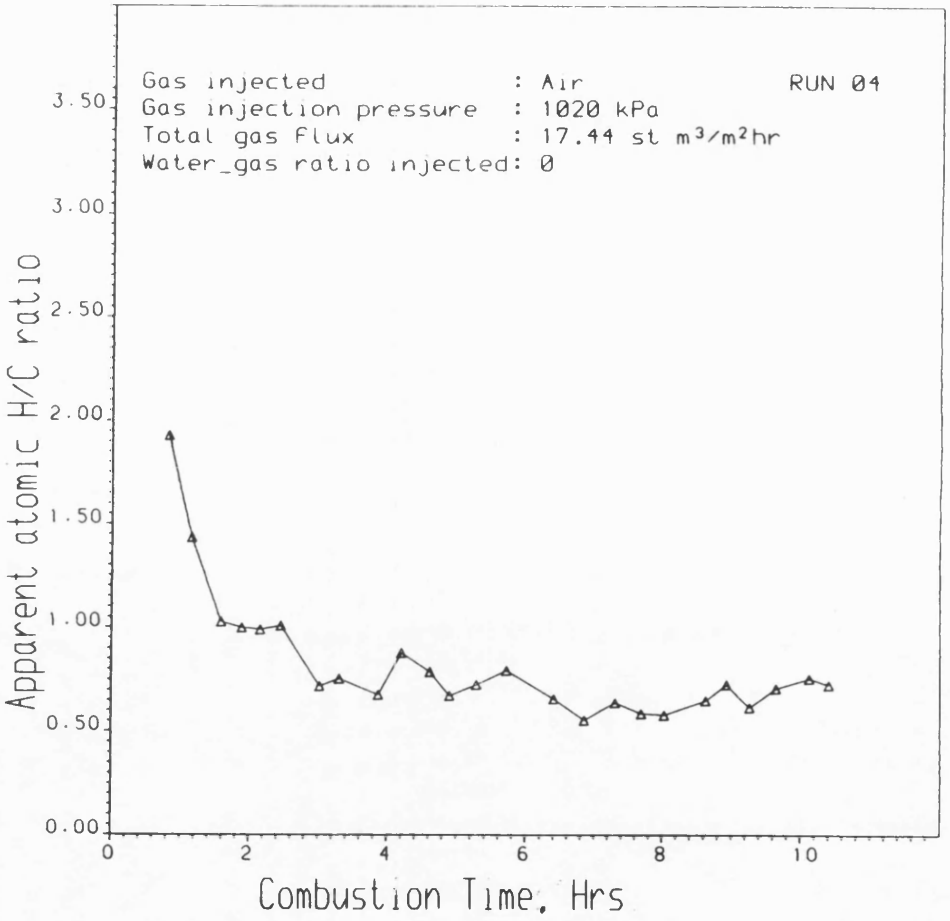

Fig. 5.73 APPARENT ATOMIC H/C RATIO OF FUEL BURNED

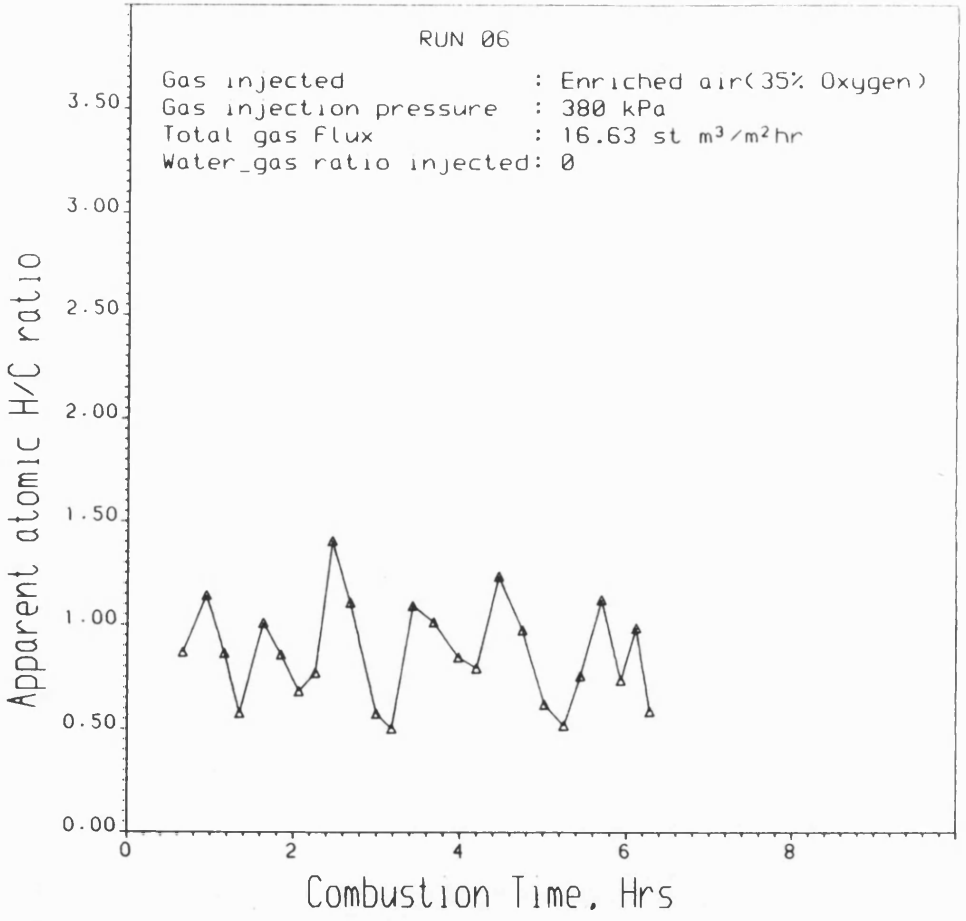

Fig. 5.74 APPARENT ATOMIC H/C RATIO OF FUEL BURNED

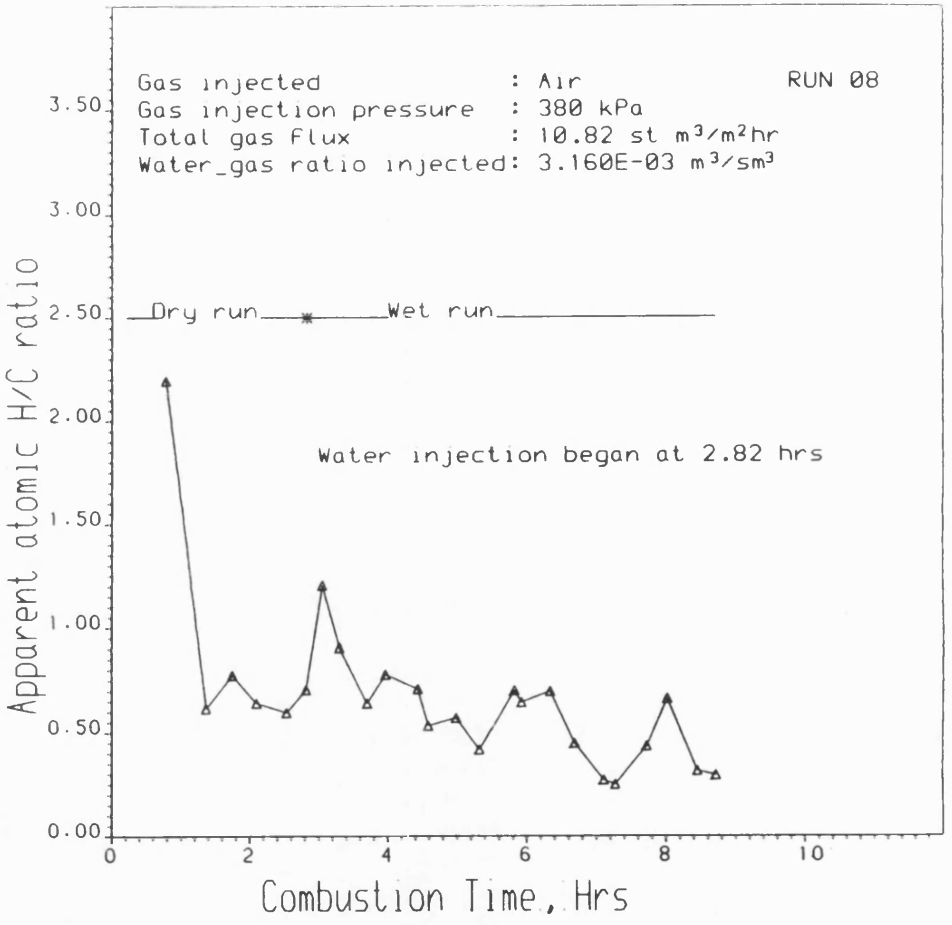

Fig. 5.75 APPARENT ATOMIC H/C RATIO OF FUEL BURNED

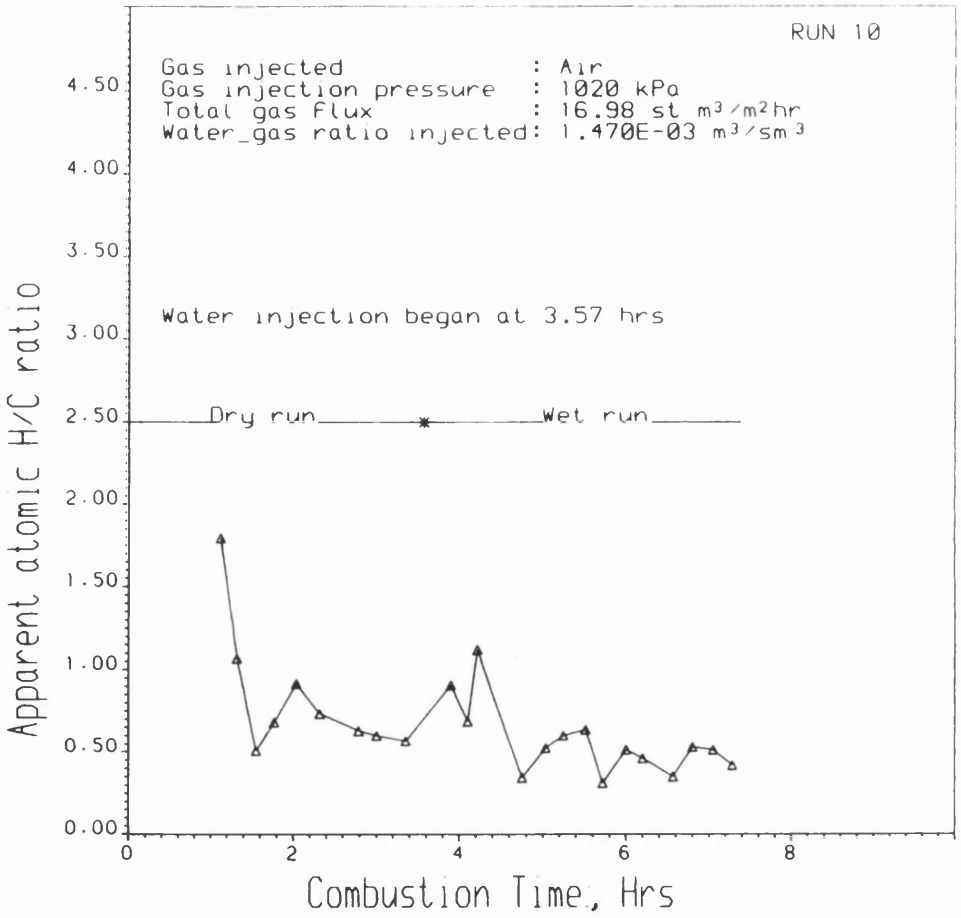

Fig. 5.76 APPARENT ATOMIC H/C RATIO OF FUEL BURNED

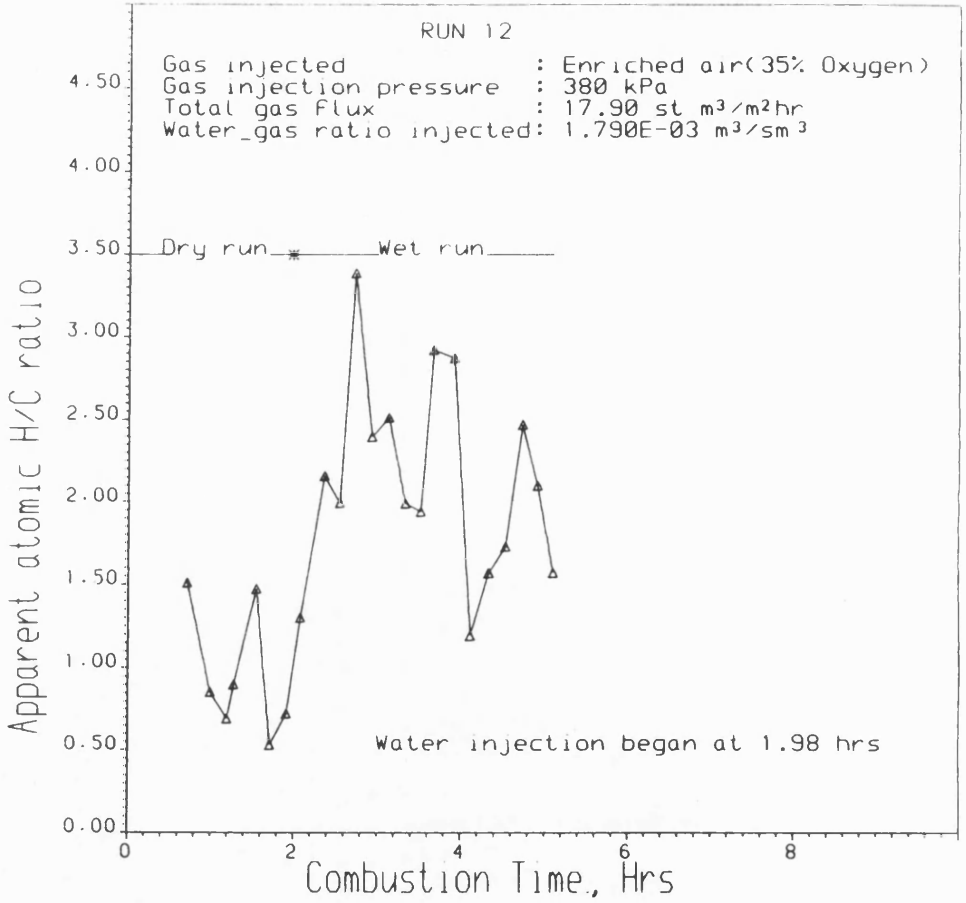

Fig. 5.77 APPARENT ATOMIC H/C RATIO OF FUEL BURNED

5.6 Fuel Consumption

For dry combustion, the trend of fuel consumption is shown in Figs. 5.78 to 5.80. Similar plots for wet combustion runs are presented in Figs. 5.81 to 5.83. All of the dry and wet combustion runs indicate that the fuel consumption is not constant. This is due to the variation in fuel availability arising principally from changes in characteristics of the porous medium and the oil in place. The drop in fuel consumption observed in Figs. 5.81 to 5.83, when water injection was initiated is the result of lower fuel availability, characteristics of a larger steam zone.

The calculated carbon consumption over the stabilised period is illustrated by the following example (Vossoughi et al., 1982): For Run 1,

$$\text{Average carbon consumption kg/m of tube} = \frac{\text{Carbon Combustion rate, kgC/hr}}{\text{Combustion velocity, m/hr}} \qquad 5.2$$

$$= 0.0031/0.068$$

$$= \underline{0.0456}$$

If the amount of sand per metre length of the tube is known, the average carbon consumption in kgC/100kg sand can be calculated.

Average carbon consumption, kgC/100kg sand

$$= \left(\frac{\text{Avg. carbon consumption, kgC/m of tube}}{\text{kg of sand packed/m of tube}}\right) \times 100 \qquad 5.3$$

$$= (0.0456/3.60906) \times 100$$

$$= \underline{1.263}$$

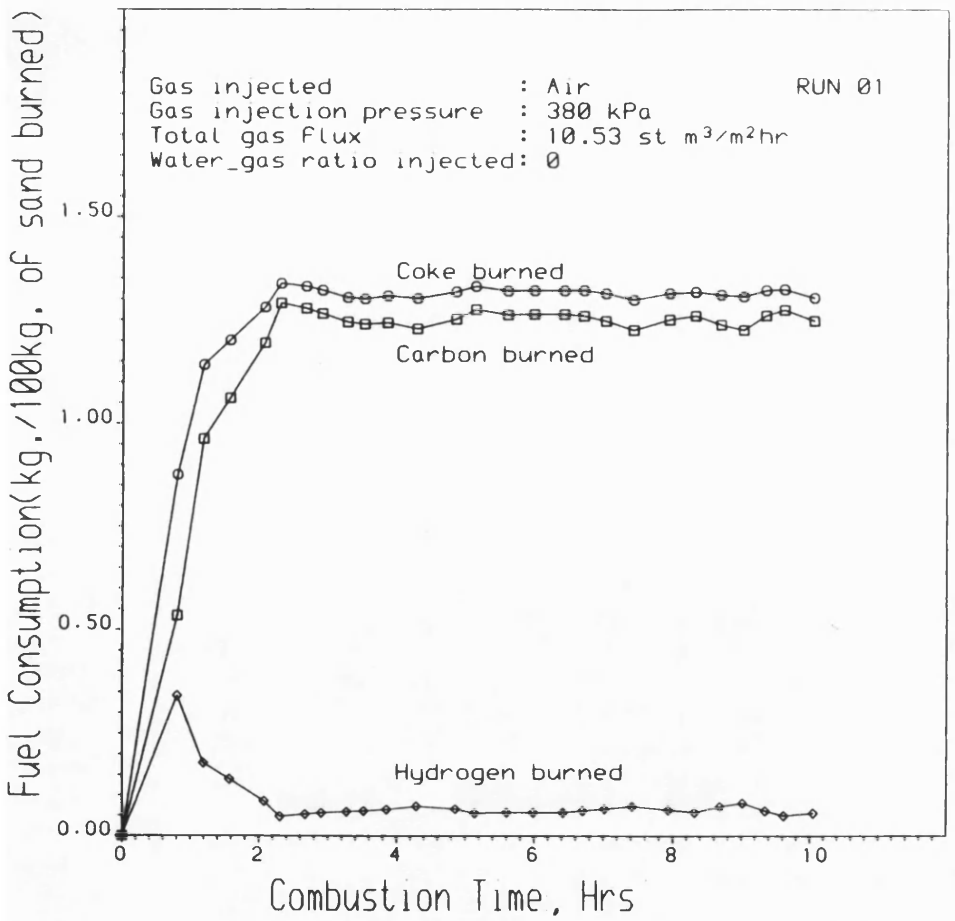

Figure 5.78 INSTANTANEOUS FUEL CONSUMPTION

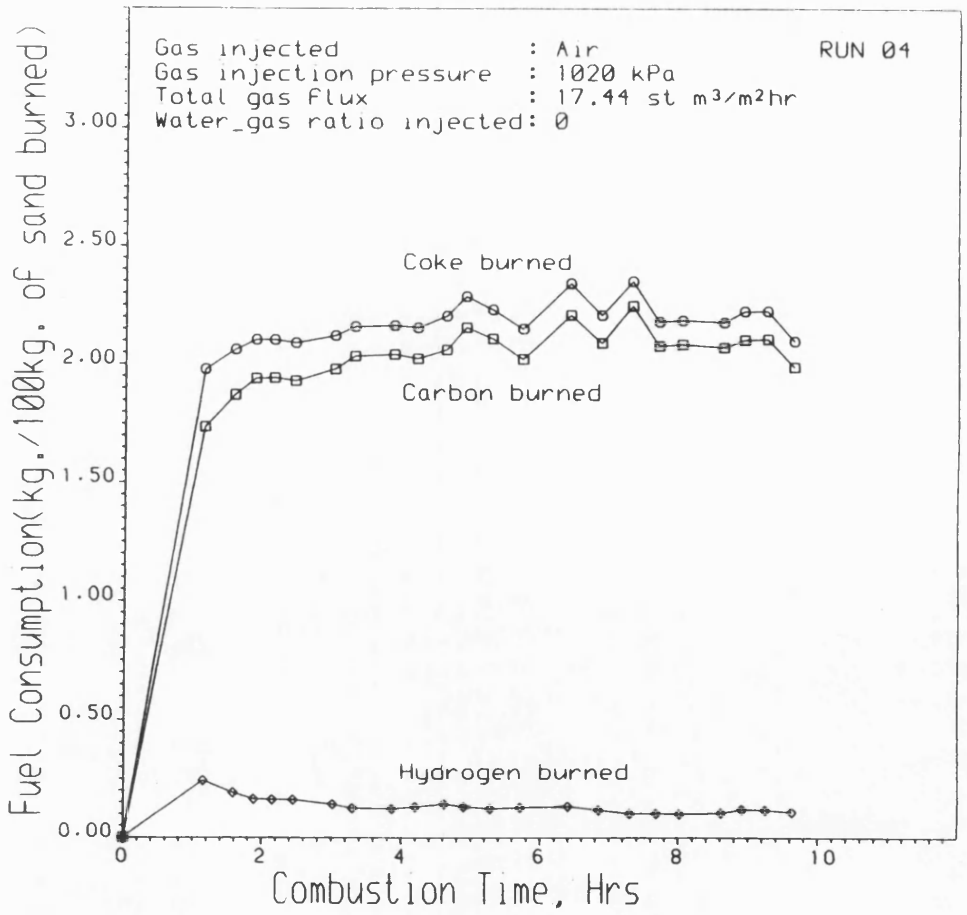

Figure 5.79 INSTANTANEOUS FUEL CONSUMPTION

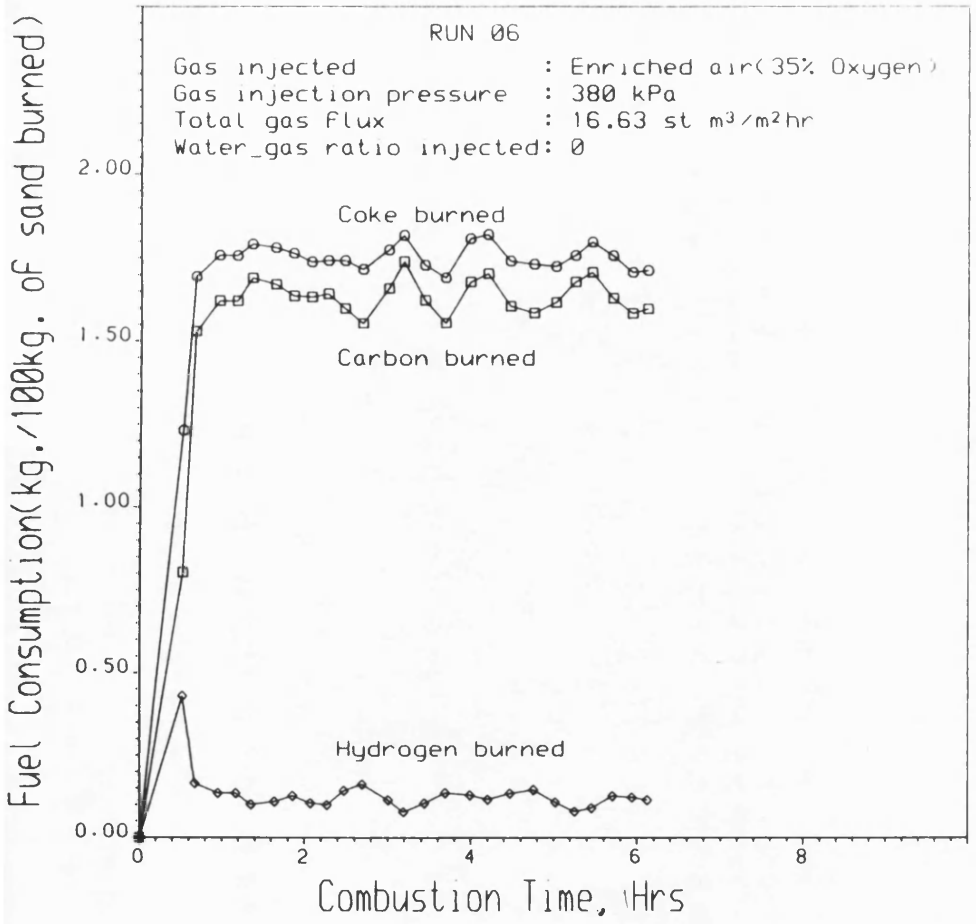

Figure 5.80 INSTANTANEOUS FUEL CONSUMPTION

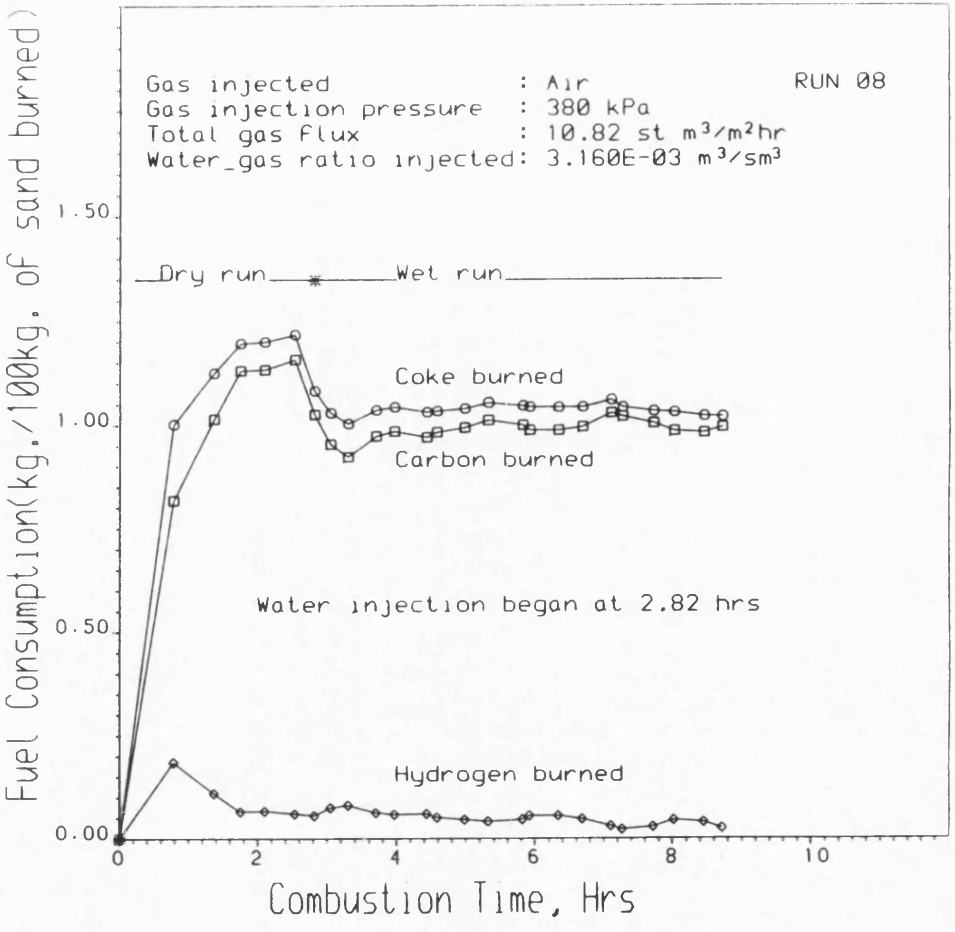

Figure 5.81 INSTANTANEOUS FUEL CONSUMPTION

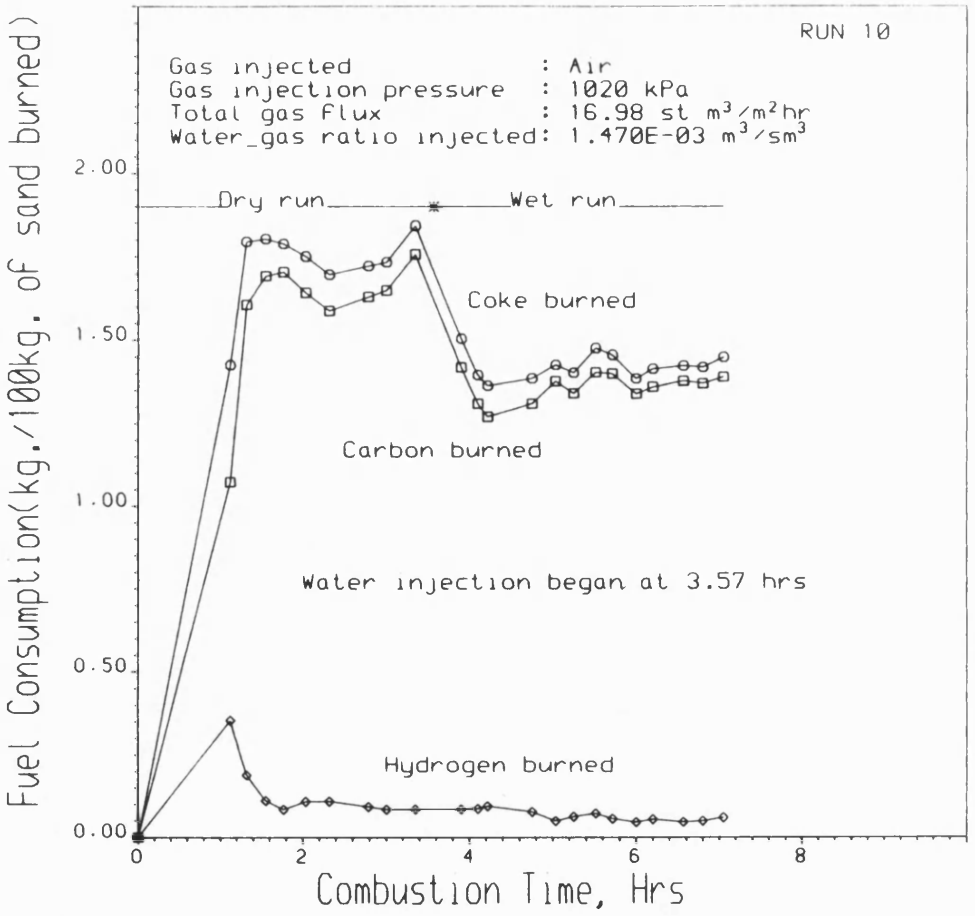

Figure 5.82 INSTANTANEOUS FUEL CONSUMPTION

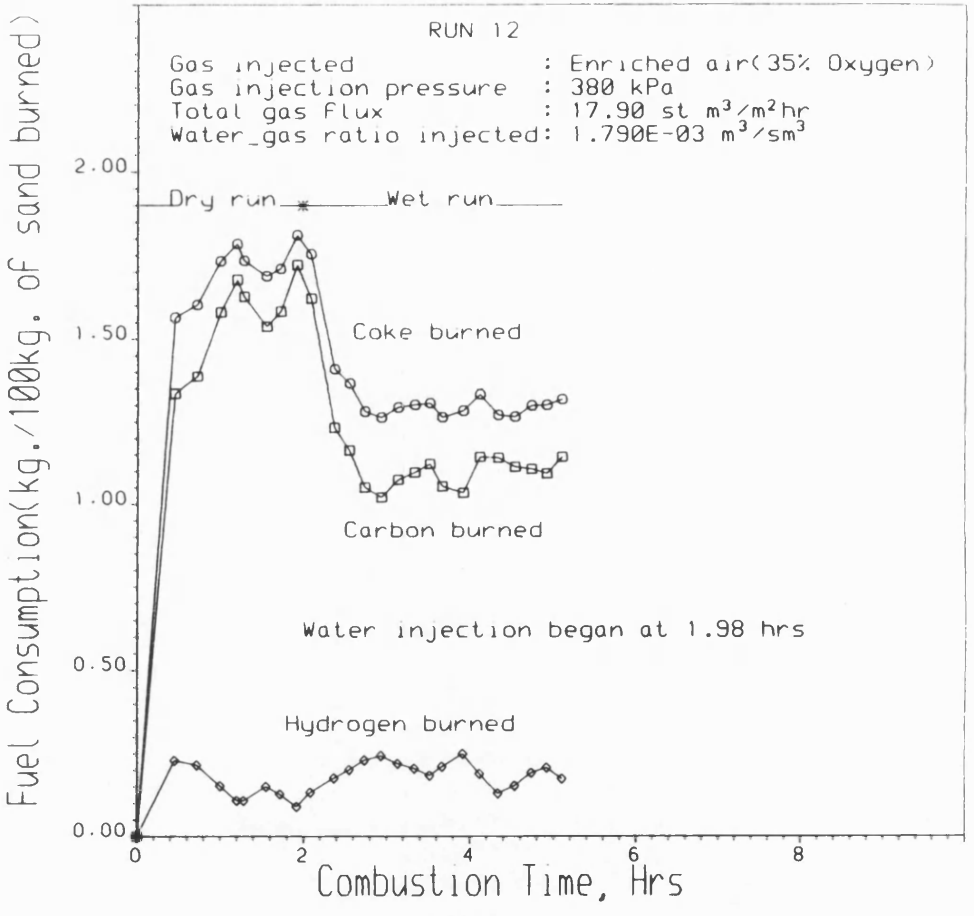

Figure 5.83 INSTANTANEOUS FUEL CONSUMPTION

Alternatively, carbon consumption can be expressed as kgC/m³ of reservoir swept, as follows:

Average carbon consumption, kgC/m³ reservoir volume

$$= \frac{\text{kgC/100kg sand}}{\text{Volume of formation (m}^3\text{)/100kg sand}} \qquad 5.4$$

$$= 1.263/0.08777$$

$$= \underline{14.392}$$

The corresponding coke burned can then be computed from the average carbon consumption and average H/C ratio:

Average coke consumed, in kg coke/100kg sand or kg coke/m³ reservoir

$$= \frac{\left[\begin{array}{l}\text{Avg. carbon consumption}\\ \text{in kgC/100kg sand}\\ \text{or kgC/m}^3\text{ reservoir}\end{array}\right]\left[12 + \left(\begin{array}{l}\text{Avg. apparent}\\ \text{H/C ratio}\end{array}\right)\right]}{12} \qquad 5.5$$

Thus, average coke consumed

$$= 1.263\ (12.56/12)$$

$$= \underline{1.32\text{kg/100kg sand}}$$

or $= 14.392(12.56/12)$

$$= \underline{14.99\text{kg/m}^3\text{ reservoir volume}}$$

The average fuel consumption computed for each run is reported in Table 5.3.

The carbon consumption for the dry runs varies from 1.26 to 2.07 kg/100kg sand. Values of 1 to 2 kgC/100kg sand have been reported by Flock et al. (1971) for air-assisted combustion. Hansel et al. (1982) however, reports a much lower

coke loading of only 1kg/100kg sand when using oxygen enrichment of 40% and above. The much lower coke loading in their case is attributable to the lighter crude oil (31°API) used.

There is a noticeable increase in fuel consumption resulting from increase in fuel availability with pressure as shown in Fig. 5.84. This is consistent with the results of Showalter (1963) and Fassihi (1981) and is caused by changes in the distillation properties of the crude oil. There is a reduced distillation effect at higher pressures so that more fuel is potentially available. In dry foward combustion, which is a fuel dominated process (Wilson et al., 1963), increased fuel consumption is therefore expected at higher operating pressures.

The pattern of fuel consumption does not reveal any particular trend with oxygen enrichment in the range 21 to 35% oxygen. Hansel et al., who investigated oxygen enrichment up to 95% O_2, similarly found that coke loadings were relatively invariant over this range.

Compared with dry combustion, the injection of water produces a substantial reduction in fuel consumption. Using a WAR = 1.47 m^3/Msm^3, for instance, fuel consumption is reduced by 35%. Figure 5.85 shows a typical dependence of fuel consumption on the magnitude of WAR used. The trend shows a continuous fall in fuel consumption with increasing water-air ratio. These results agree with those reported by Alderman et al. (1971), Burger et al. (1973), Ejiogu et al. (1979) and Moss (1982). The fuel consumption fundamentally determines the injected gas requirement, which is a key factor affecting the economic success of an in-situ combustion process.

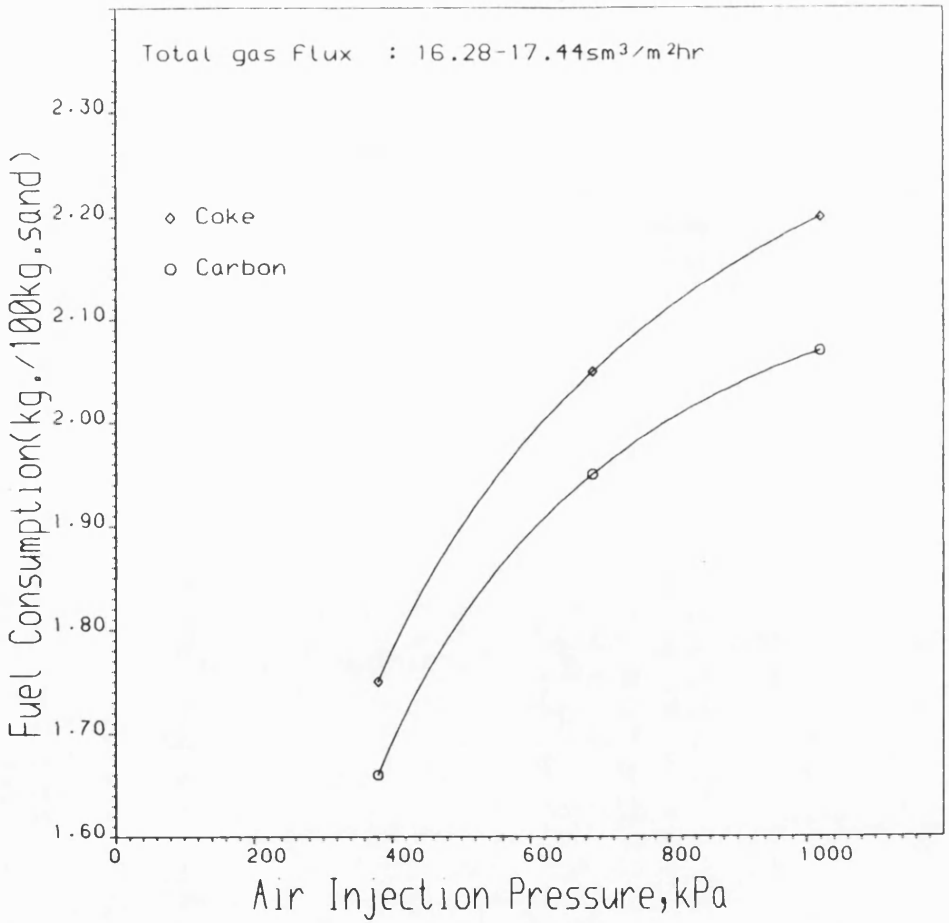

Figure 5.84 FUEL CONSUMPTION AS A FUNCTION OF AIR INJECTION PRESSURE

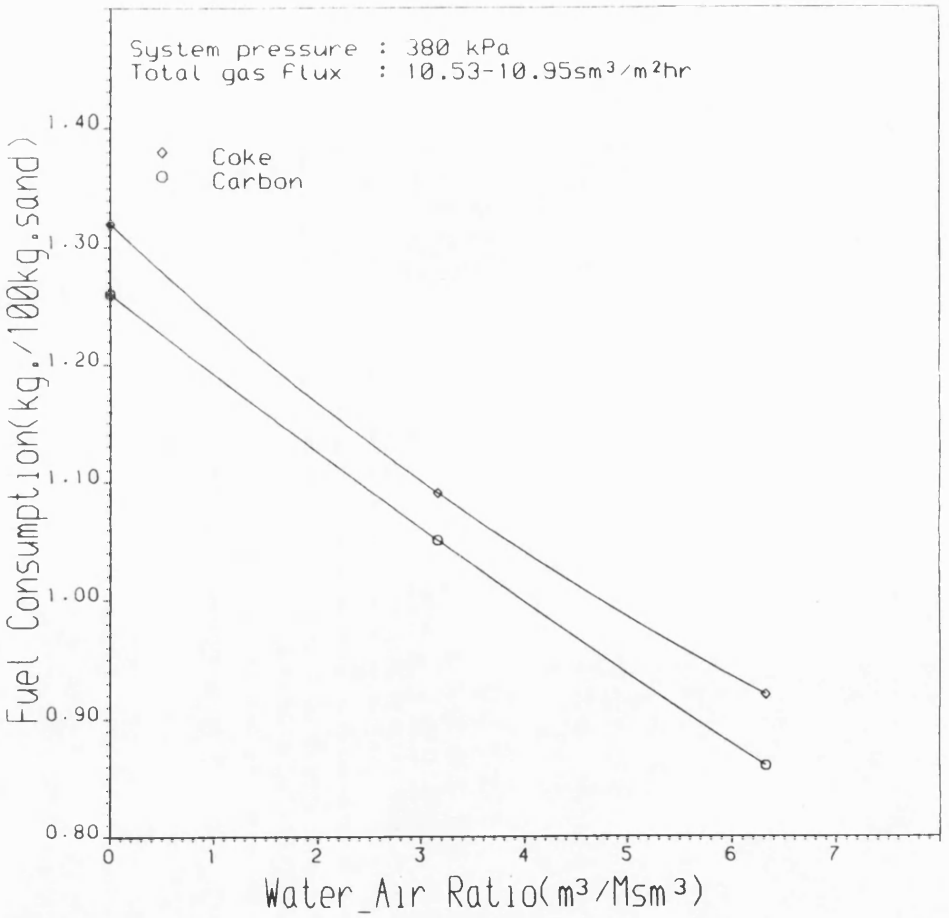

Figure 5.85 FUEL CONSUMPTION AS A FUNCTION OF WATER_AIR RATIO

5.7 Air Requirement

Air requirement is the volume of air (sm^3) required to burn a unit volume (m^3) of oil bearing formation. It is determined from the combustion-front velocity and total air flux as follows:

$$Ar = \frac{\text{Total air flux}}{\text{Combustion-front velocity}} \qquad 5.6$$

In practice, some air is stored in the burned volume. The stored air increases in proportion to the pressure in the burned zone. It may be approximated by the injection pressure (Prats, 1982). At low pressure, if the pressure drop through the reservoir is not exceedingly high, the stored quantity is small. At high pressures, however, the additonal air stored in the burned volume must be taken into account when calculating the total requirement as discussed by Prats. For the present purpose, the value of Ar determined from Equation 5.6 is considered to be adequate.

The other two parameters which are frequently used to measure the economic success of in-situ combustion project are Air-oil ratio (AOR) and Air-fuel ratio (AFR). Normally, the AOR is the volume (sm^3) of air required to produce 1kg of oil. That is,

$$AOR = Ar(1/Mo) \qquad 5.7$$

where Mo is the kg of oil produced per m^3 of reservoir volume.

The AFR is the volume (sm^3) of air required to burn 1kg of fuel as determined from Equation 5.8 (Nelson et al., 1961).

$$AFR = \frac{22.4YN_2(1 + (YO_{2i}/YN_{2i}))}{(12 + H/C)(YCO + YCO_2)} \qquad 5.8$$

The values of Ar, AOR and AFR obtained for each experiment are given in Table 5.3. The effect of operating pressure on these parameters is shown in Fig. 5.86. The AFR is not significantly affected by pressure, but there is a noticeable increase in the values of Ar and AOR with increase in pressure. Thus, shallower reservoirs will be more favourable candidates for forward combustion than those at greater depth.

The plots in Fig. 5.87 show a continuous fall in Gr, GOR and GFR with increasing oxygen concentration (G now replaces the symbol A to signify use of oxygen enrichment). The lower total gas injection requirement, obtained with oxygen enrichment is therefore a distinct advantage over the use of air. This is particularly important in heavy oil reservoirs, in which there is a correspondingly larger fuel deposition.

For wet combustion, there is a significant reduction in the values of Gr and GOR at all operating pressures, as shown in Figs. 5.88 to 5.90. The greatest reduction occurs at the highest pressure. However, there is a small increase in the gas-fuel ratio with water injection, but only for the two cases with oxygen enrichment (Fig. 5.91). This agrees with Moss's (1982) results which reveal that greater amounts of oxygen are used for producing compounds other than carbon oxides. The general trend of Gr and GOR with water injection, observed in this study is consistent with the findings of Dietz et al. (1967), Garon et al. (1974) and Ejiogu et al. (1979).

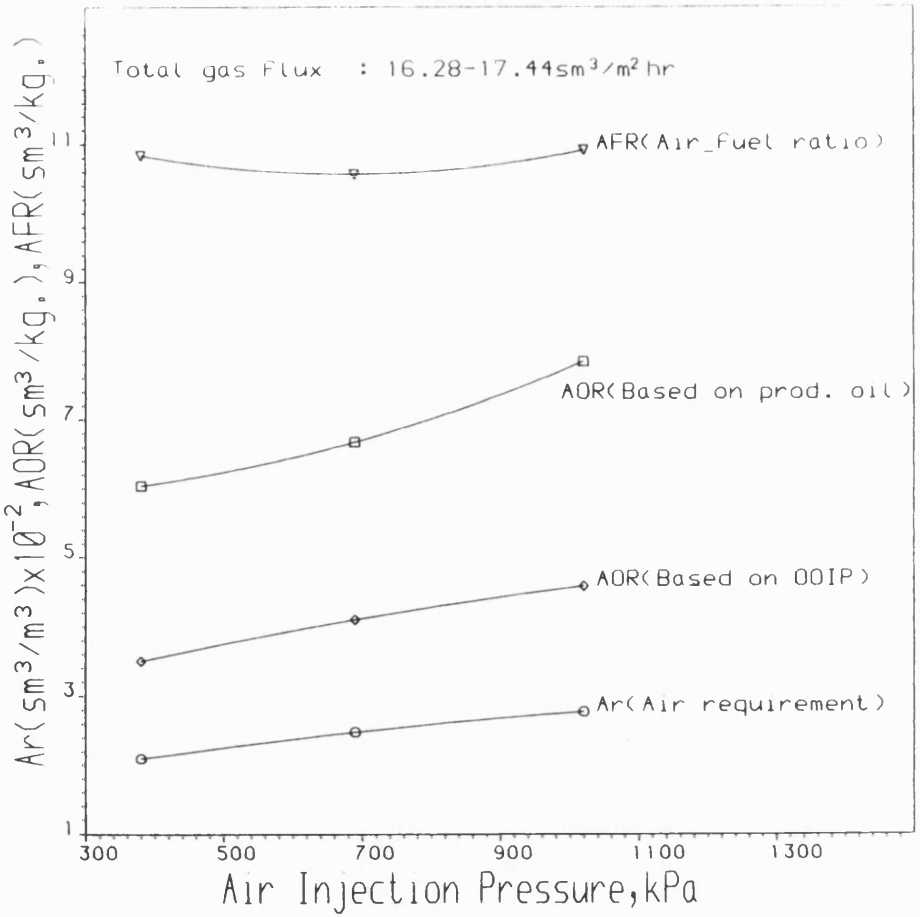

Figure 5.86 AIR REQUIREMENT AS A FUNCTION OF AIR INJECTION PRESSURE

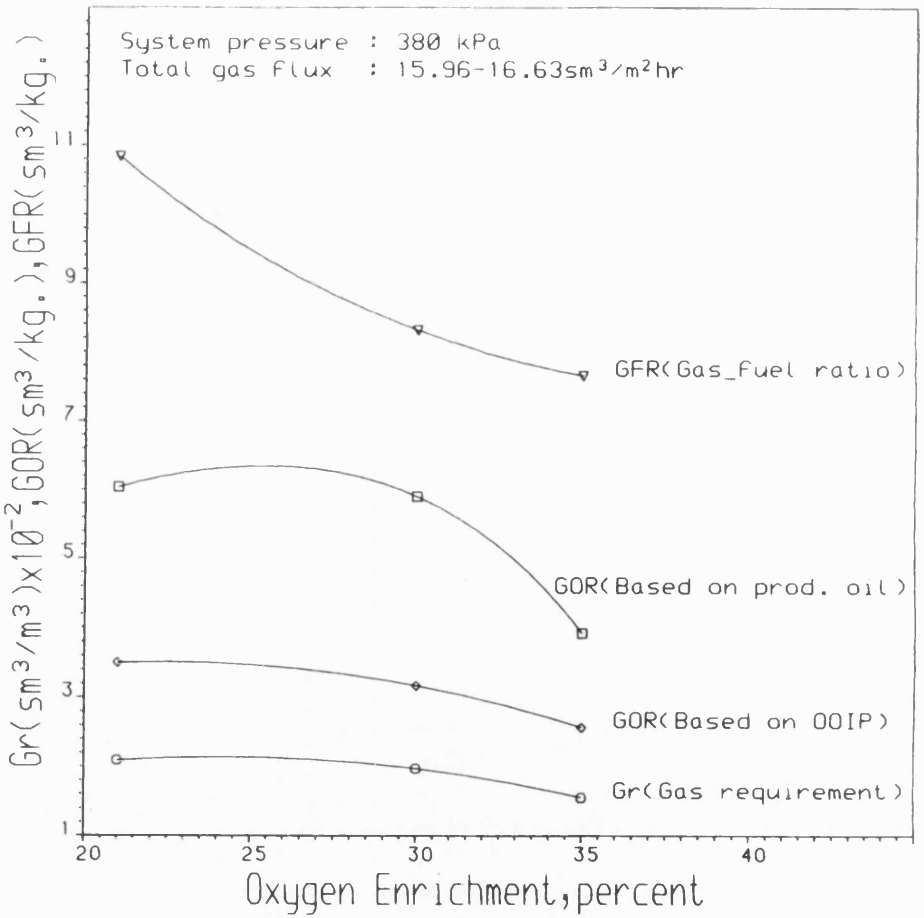

Figure 5.87 GAS REQUIREMENT AS A FUNCTION OF OXYGEN ENRICHMENT

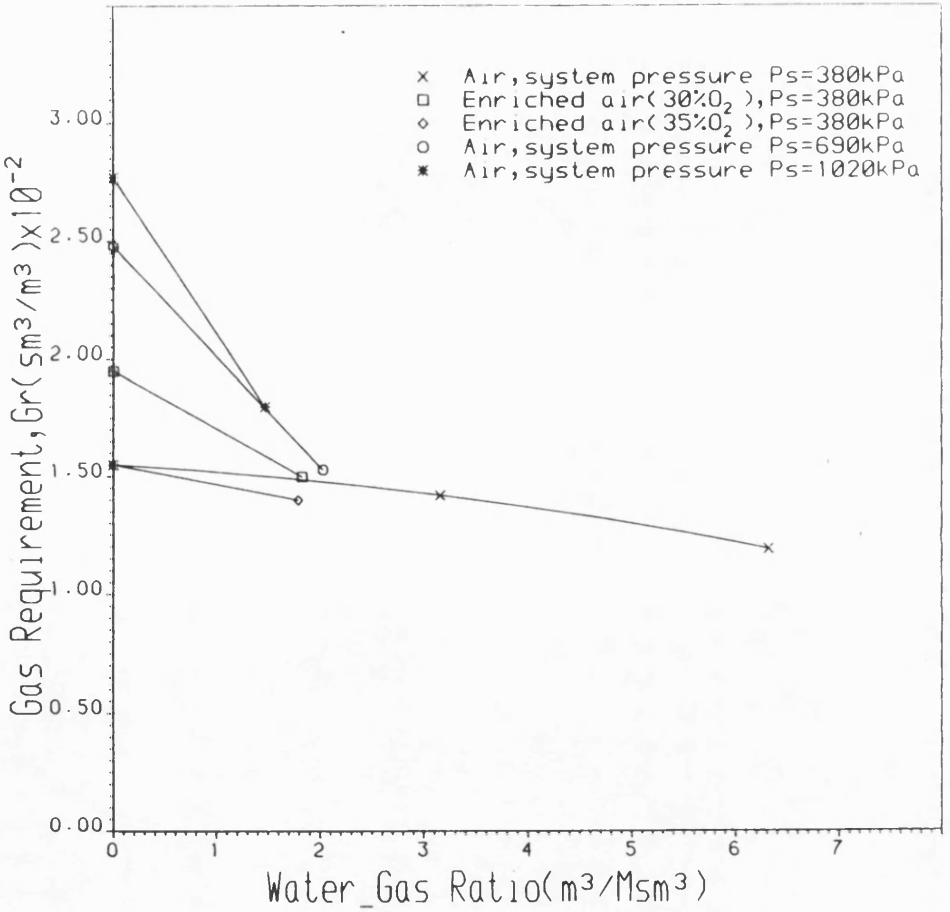

Figure 5.88 EFFECT OF WATER INJECTION ON GAS REQUIREMENT

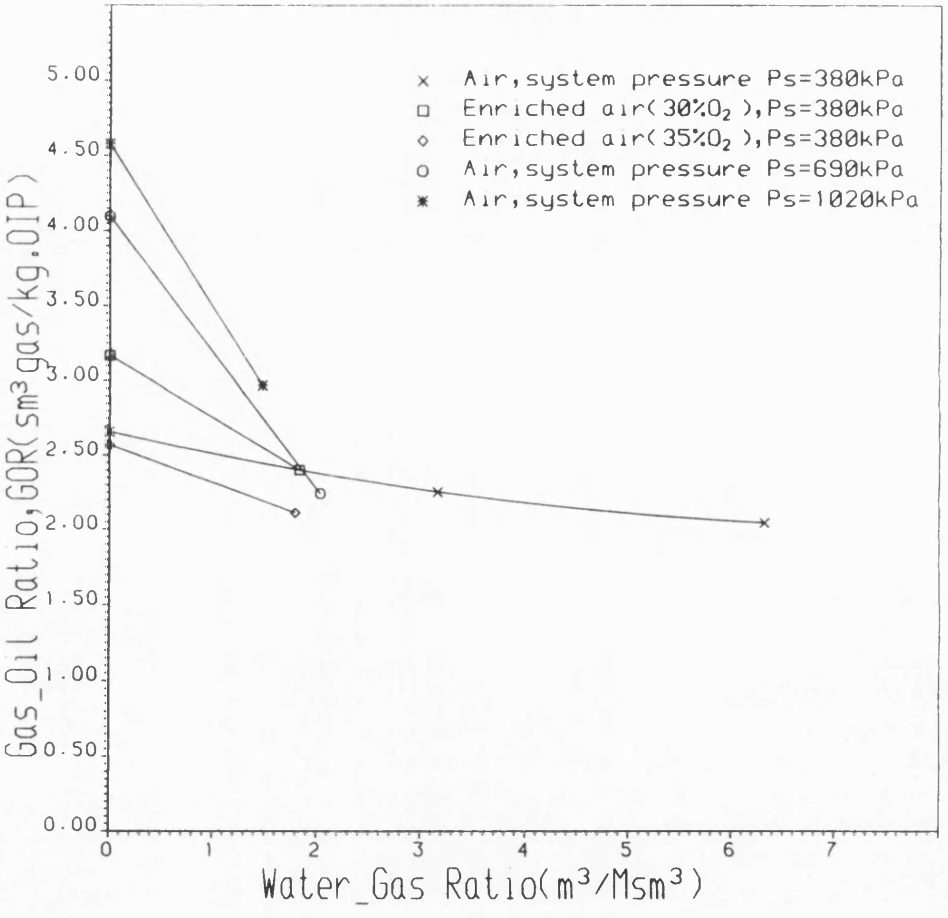

Figure 5.89 EFFECT OF WATER INJECTION ON GAS_OIL RATIO

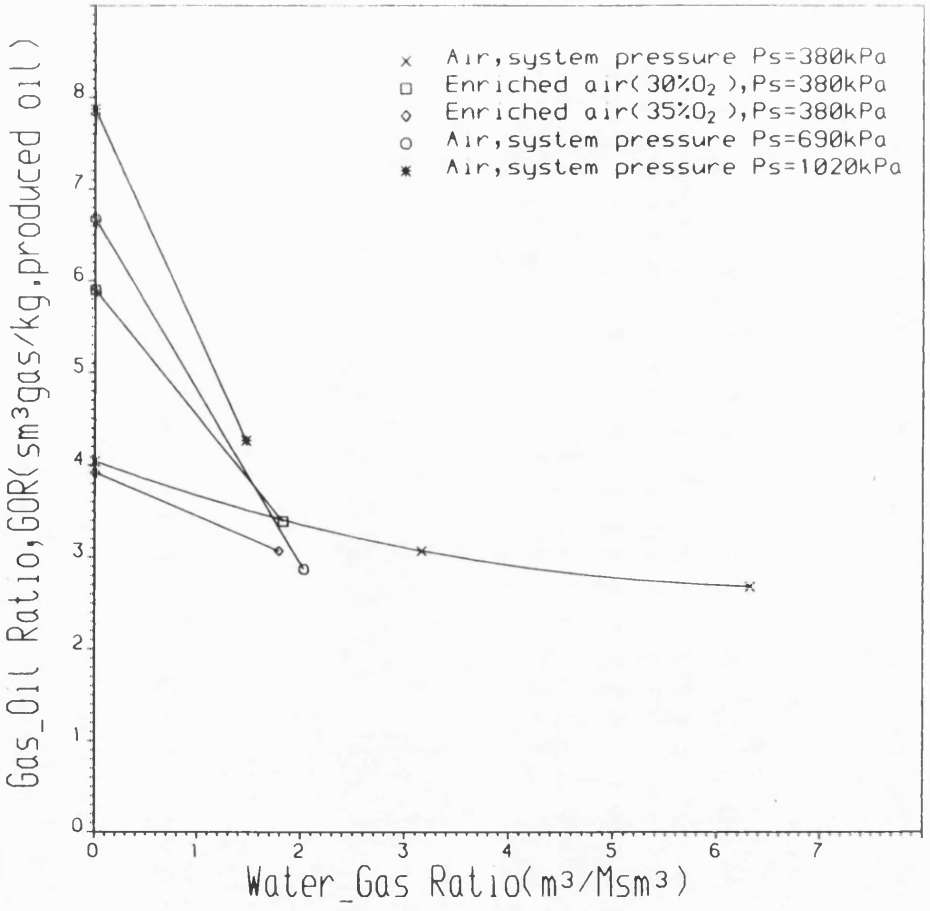

Figure 5.90 EFFECT OF WATER INJECTION ON GAS_OIL RATIO

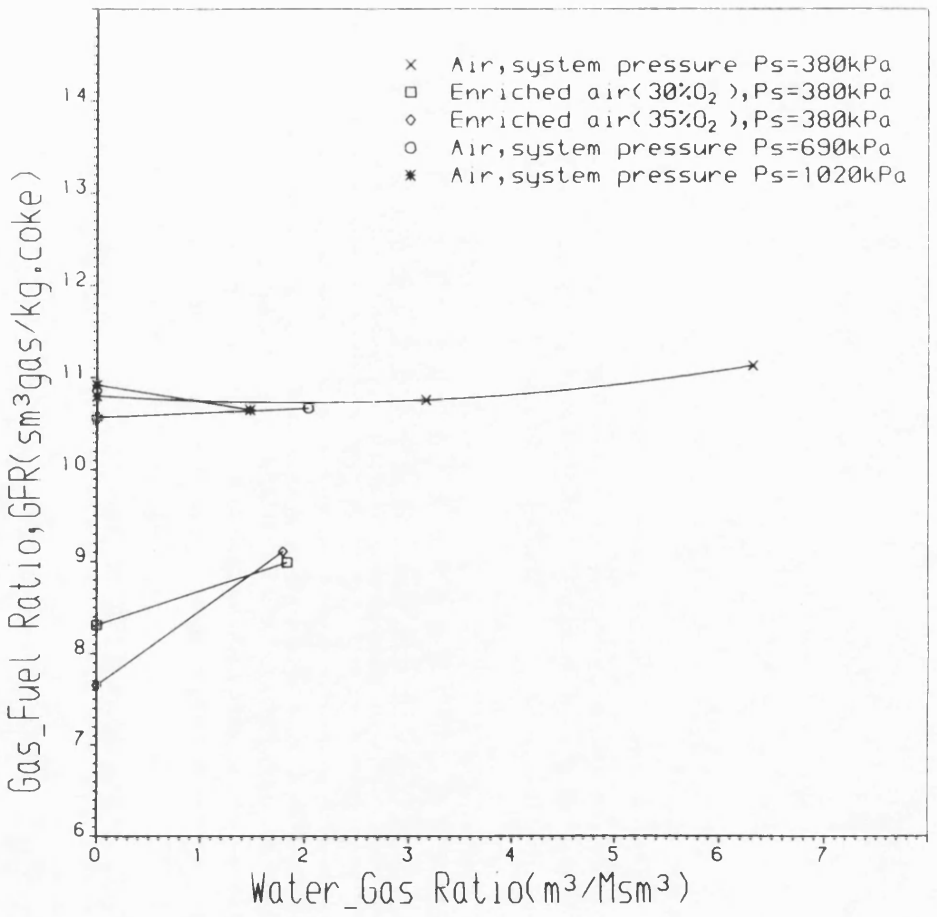

Figure 5.91 EFFECT OF WATER INJECTION ON GAS_FUEL RATIO

5.8 Oxygen Utilisation

Oxygen utilisation is a measure of the efficiency of the combustion process. Table 5.3 shows that approximately 100 percent oxygen utilisation is obtained during the stabilised periods for the dry runs, at all operating pressures and gas fluxes investigated. The value obtained for the majority of wet combustion runs is however, about 1 percent lower. A similar trend was reported by Moss (1982), who obtained 97 percent oxygen utilisation in wet combustion compared with 99 percent in dry forward combustion. With wet combustion, the steam which is produced tends to restrict the diffusion path for the oxygen to the fuel surface. This will inevitably lead to increased oxygen channelling.

5.9 Conclusions

The combustion characteristics of Maya crude under dry and wet combustion conditions are summarised as follows:

1. Combustion-front velocity increases significantly with oxygen enrichment and water injection rate. The fuel concentration increases with increasing pressure, reducing the velocity of the combustion front.

2. Increased oxygen enrichment of the oxidant gas leads to higher levels of CO and CO_2 in the produced gas, with a corresponding increase in the molar CO/CO_2 ratio. The CO/CO_2 decreases, however, as the pressure and water injection rate are increased.

3. The combustion front peak temperature increases when using enriched air, but is reduced by water injection. Peak temperature is not affected by change in pressure.

4. In wet combustion, heat, which is scavenged from the burned zone, is carried forward, causing a lengthening of the steam zone. The extent of the steam zone does not depend on pressure, but is significantly affected by oxygen enrichment.

5. The carbon combustion rate achieves a constant value as soon as a stable combustion front begins to propagate through the sand pack. It increased significantly with oxygen enrichment, but is reduced by water injection, particularly when enriched air is used.

6. The chemical composition of the fuel burned, as indicated by the H/C ratio, varies during combustion. Generally, the average H/C ratios for dry combustion runs and for the majority of wet combustion are much less than that of the original crude. This indicates that the fuel burned has a heavier composition and that little or no LTO effects occurred.

7. The air requirement and GOR increase with operating pressure. However, both parameters decrease substantially with oxygen enrichment and WGR. The GFR is not sensitive to change in pressure but decreases with oxygen enrichment. The increase in gas-fuel ratio with water injection suggests that greater amounts of oxygen was consumed by LTO reactions.

Chapter 6

ANALYSIS OF IN-SITU COMBUSTION REACTION KINETICS

The kinetic data obtained from three dry and two wet combustion runs are analysed to obtain overall rate expressions describing the rate of carbon combustion. The occurence of LTO reaction is not significant, due mainly to high oxygen utilisation (>98%) at the combustion zone. The cracking reaction (fuel deposition) however, although very competitive with fuel combustion reaction, has a lower influence on the overall process behaviour and is therefore, as the LTO reaction, not considered. The major influence of combustion reaction kinetics on the process behaviour is through its effect on the combustion-front velocity. In addition to this, the amount of fuel consumed will also significantly affect the ultimate recovery of oil.

In this investigation, the porous medium properties were essentially the same for each run and the total pressure was maintained constant at 380kPa. The oxygen concentration was varied from 21 to 35% and in the wet runs, WGR's of 1.79 and 1.83m^3/Msm^3 were used. The main objective is to determine the effect of oxygen enrichment under dry and wet combustion conditions.

The proposed model for the carbon combustion rate, as given in section 3.13, is:

$$-Rc = kC_c^m P_{O_2}^n \qquad 6.1$$

Introducing the Arrhenius relation, we have

$$-Rc = A_r \exp(-E/RT) C_c^m P_{O_2}^n \qquad 6.2$$

The procedure for determining numerical values of the reaction orders m and n, the Arrhenius constant, A_r and the activation energy E from the kinetic data, are explained overleaf:

6.1 Instantaneous Carbon Concentration

The instantaneous carbon concentration of the reacting fuel within the porous medium is determined by computing detailed material balance for the products of combustion. The cumulative carbon burned Cb in kg/100kg sand at any time t is first determined from:

$$Cb = \frac{1.2 \times 10^3}{22.4} \int_0^t \frac{F(t)(YCO_2(t) + YCO(t))dt}{S_1 V_b t} \qquad 6.3$$

where $F(t)$ = instantaneous exit gas flow rate, sm^3/hr

V_b = avg. combustion front velocity, m/hr

S_1 = sand pack density, kgsand/m length of tube

$YCO_2(t)$, $YCO(t)$ = instantaneous concentration of CO_2 and CO of the produced gas

The instantaneous carbon concentration of the reacting fuel, Cc is then obtained by substracting the carbon burned from the initial carbon content of the bed. (N.B. tt = stabilized combustion period)

$$Cc = \int_0^{tt} Cbdt + Cbo - \int_0^t Cbdt \qquad 6.4$$

The quantity Cbo represents the amount of unburned fuel remaining in the bed at the end of the combustion run. Figures 6.1 to 6.5 represent computed values of Cb and Cc as a function of combustion time. The amount of carbon burned steadily increases while the cumulative carbon concentration of the reacting fuel correspondingly decreases with combustion time.

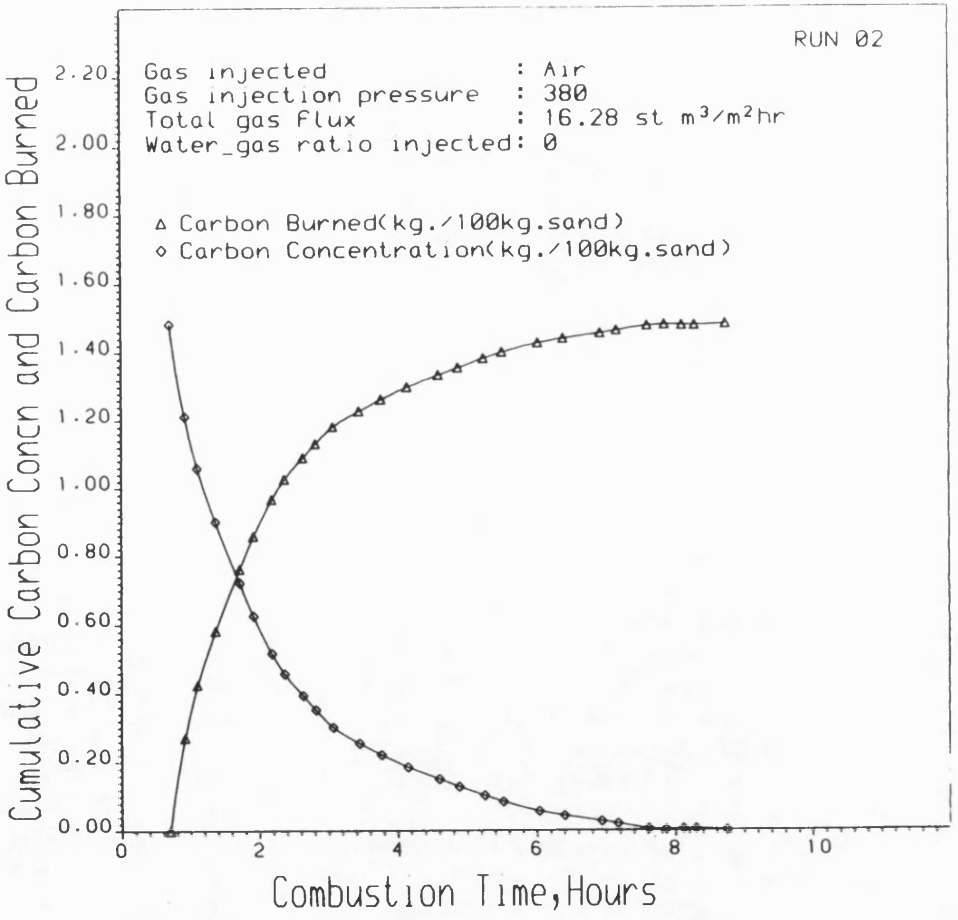

Fig. 6.1 CARBON CONCENTRATION AND CARBON BURNED AS A FUNCTION OF COMBUSTION TIME

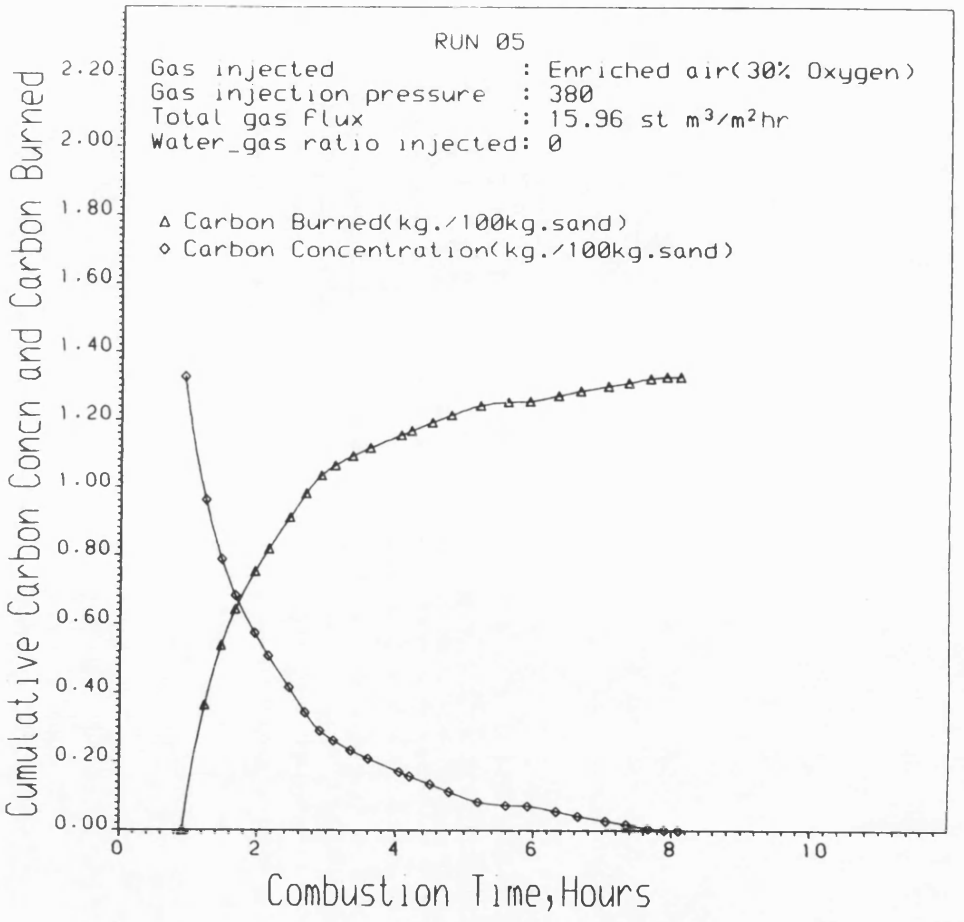

Fig. 6.2 CARBON CONCENTRATION AND CARBON BURNED AS A FUNCTION OF COMBUSTION TIME

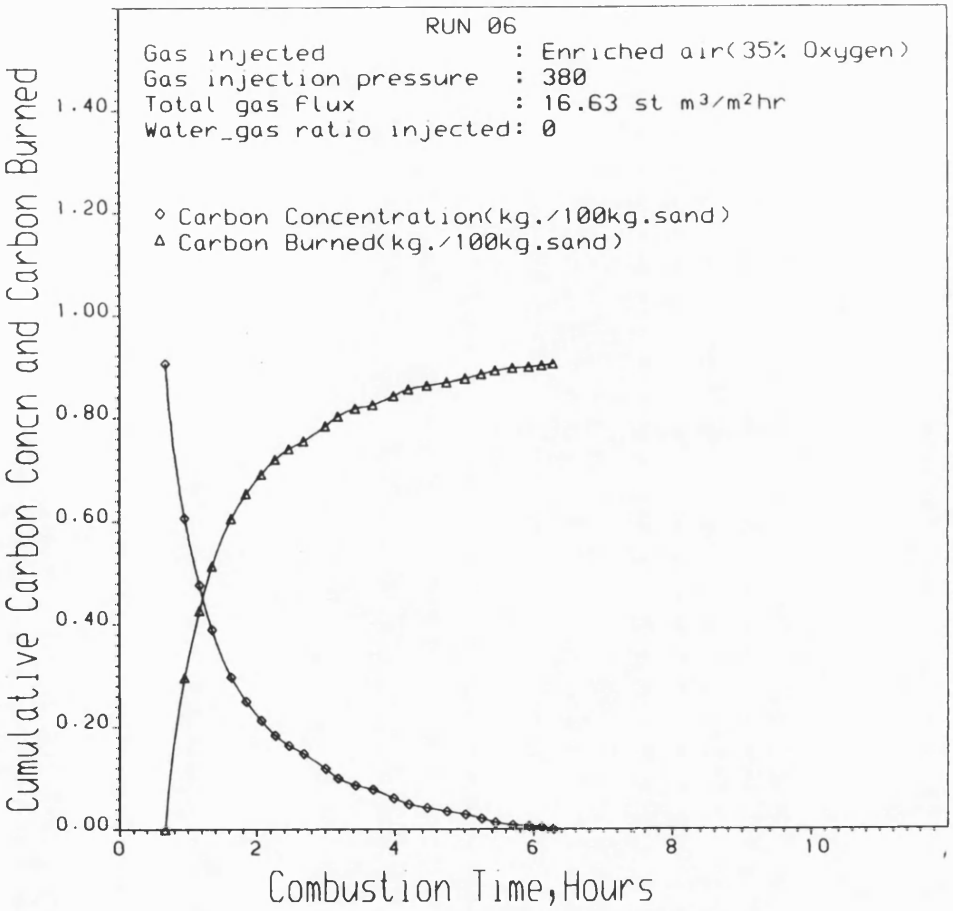

Fig. 6.3 CARBON CONCENTRATION AND CARBON BURNED AS A FUNCTION OF COMBUSTION TIME

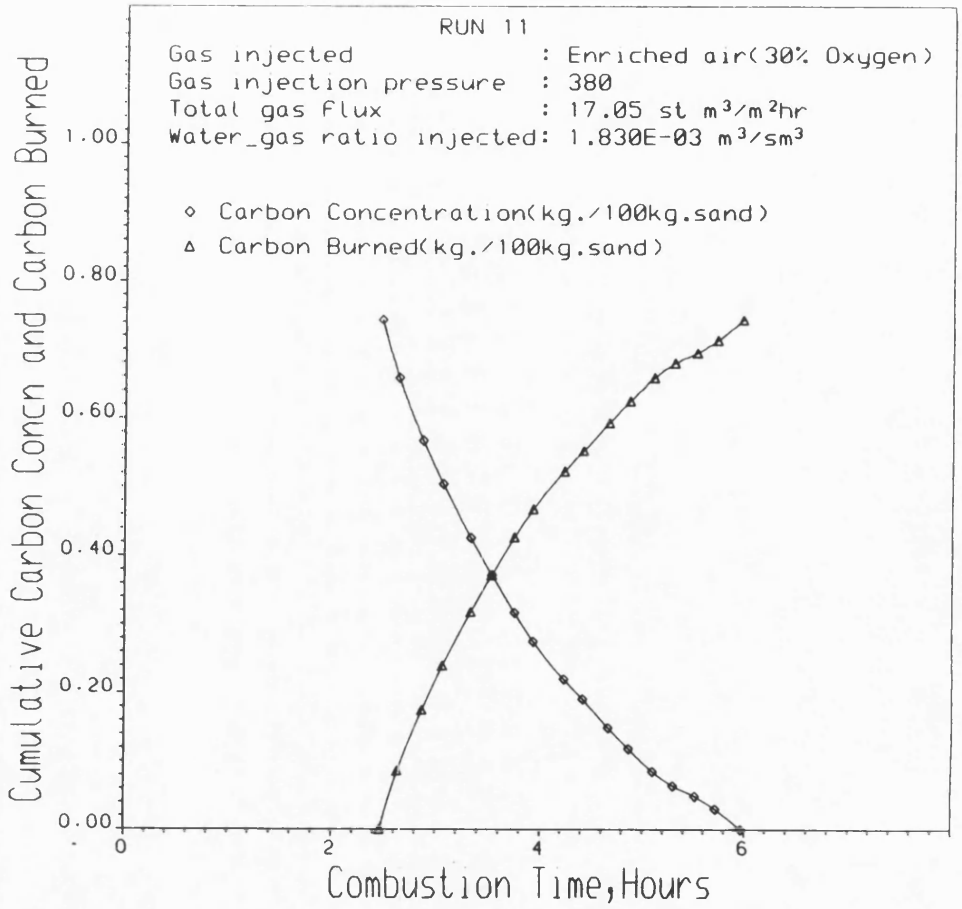

Fig. 6.4 CARBON CONCENTRATION AND CARBON BURNED AS A FUNCTION OF COMBUSTION TIME

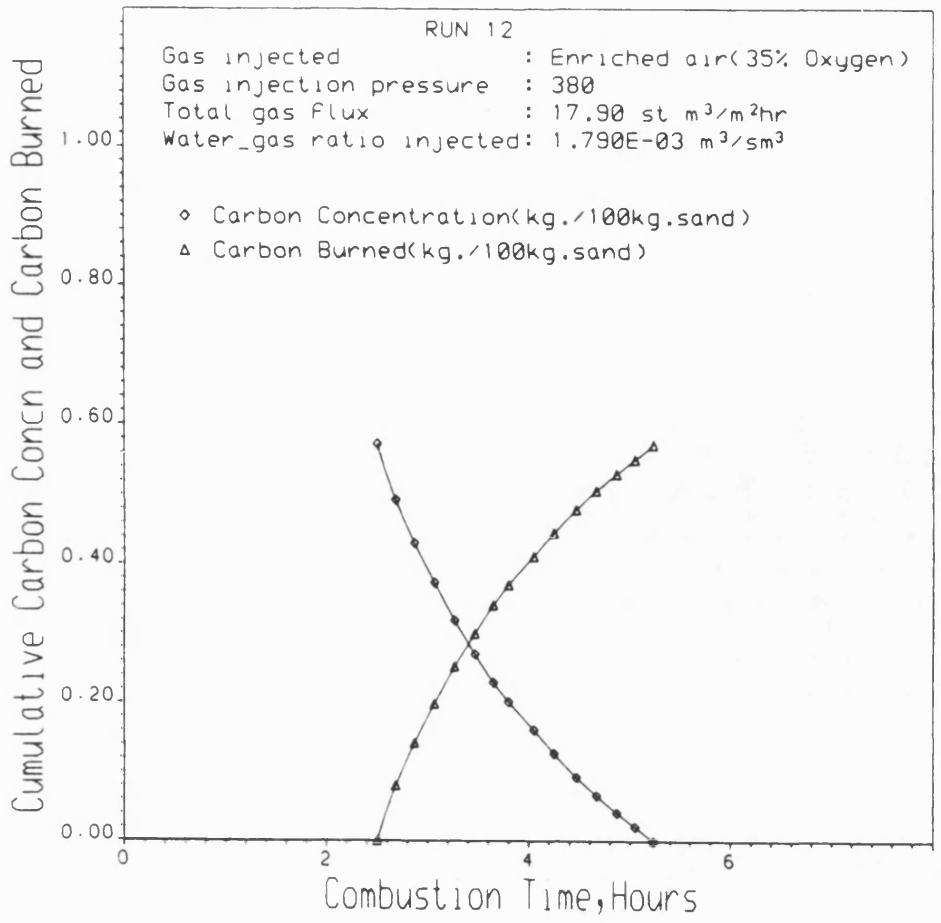

Fig. 6.5 CARBON CONCENTRATION AND CARBON BURNED AS A FUNCTION OF COMBUSTION TIME

6.2 Rate Equation for Non-Isothermal Combustion

The carbon combustion rate, -Rc(kg/100kg sand hr) is determined by numerical differentiation of carbon concentration profiles in Figs. 6.1 to 6.5. Equation 6.2 relates isothermal combustion rate to the carbon concentration. For isothermal combustion, this relationship is normally determined by a regression analysis of the values of log(-Rc) and logCc in order to obtain the value of m, the reaction order with carbon concentration (Dabbous, 1971; Bousaid, 1967). However, this approach is not strictly valid for non-isothermal operation. Therefore, Equation 6.2 is arranged as follows:

$$-Rc = A_r Po_2^n Cc^m \exp(-E/RT) \qquad 6.5$$

Since the quantity $A_r Po_2^n$ is constant for each combustion

experiment (performed at constant partial pressure of oxygen), Equation 6.5 can be expressed in the form:

$$\log_e(-Rc) = \log_e(A_r Po_2^n) + m\log_e Cc - E/RT \qquad 6.6$$

A multi-linear regression analysis of the values of $\log_e(-Rc)$, $\log_e Cc$ and 1/T was used to obtain the values of the kinetic parameters m, E and the constant $A_r Po_2^n$. The resulting "Rate equations" are given in Table 6.1.

TABLE 6.1 NON-ISOTHERMAL COMBUSTION KINETIC DATA

RUN 2			RUN 5			RUN 6			RUN 11			RUN 12		
Peak Temp.	Carbon Concn. Cc	$-Rc = \frac{dCc}{dt}$	Peak Temp.	Carbon Concn. Cc	$-Rc = \frac{dCc}{dt}$	Peak Temp.	Carbon Concn. Cc	$-Rc = \frac{dCc}{dt}$	Peak Temp.	Carbon Concn. Cc	$-Rc = \frac{dCc}{dt}$	Peak Temp.	Carbon Concn. Cc	$-Rc = \frac{dCc}{dt}$
°K	kg.C / 100kgsand	kg.C / 100kgsand hr	°K	kg.C / 100kgsand	kg.C / 100kgsand hr	°K	kg.C / 100kgsand	kg.C / 100kgsand hr	°K	kg.C / 100kgsand	kg.C / 100kgsand hr	°K	kg.C / 100kgsand	kg.C / 100kgsand hr
696	0.722450	0.102718	686	1.32657	0.17467	683	0.90468	0.13907	694	0.74364	0.21247	695	0.57250	0.20945
694	0.517390	0.078791	689	0.78837	0.13185	699	0.47713	0.14025	677	0.56825	0.18331	681	0.43085	0.18205
707	0.394000	0.071415	696	0.57389	0.12132	694	0.29801	0.09809	667	0.42555	0.16160	691	0.31995	0.16968
670	0.302030	0.053144	708	0.41552	0.11854	709	0.11891	0.08322	667	0.31667	0.14286	675	0.23003	0.14528
682	0.221470	0.044441	699	0.29098	0.08896	695	0.08569	0.05207	656	0.22016	0.12701	690	0.16099	0.13605
679	0.149610	0.036051	697	0.23322	0.07710	698	0.06091	0.04618	672	0.14916	0.11474	681	0.09284	0.11010
687	0.101560	0.029017	680	0.15871	0.05069	694	0.02870	0.02867	665	0.08502	0.09310	702	0.04108	0.09003
665	0.056110	0.018652	679	0.11278	0.04300	690	0.01347	0.01617	683	0.04861	0.08102			
681	0.026930	0.012824	683	0.05478	0.03101	694	0.00589	0.01283						
668	0.005140	0.004536	666	0.02663	0.01836									
686	0.004430	0.004396	698	0.00483	0.01120									
Rate Equation: $-Rc = 1.697Cc^{0.60}e^{-1842/T}$			Rate Equation: $-Rc = 4.241 \times 10^{2} Cc^{0.51}e^{-5480/T}$			Rate Equation: $-Rc = 1.203 \times 10^{6} Cc^{0.53}e^{-10880/T}$			Rate Equation: $-Rc = 1.551Cc^{0.34}e^{-1315/T}$			Rate Equation: $-Rc = 2.219Cc^{0.33}e^{-1515/T}$		

Figures 6.6 to 6.10 compare the experimental combustion rates with those predicted by the rate equations. There is a good agreement over the entire range of carbon concentrations and combustion peak temperatures. The rate equations therefore enable the variation of carbon combustion rate with carbon concentration to be determined at any given combustion front peak temperature condition within the range encountered in each combustion run. With this approach, it is possible to derive isothermal reaction kinetic information from the non-isothermal combustion data.

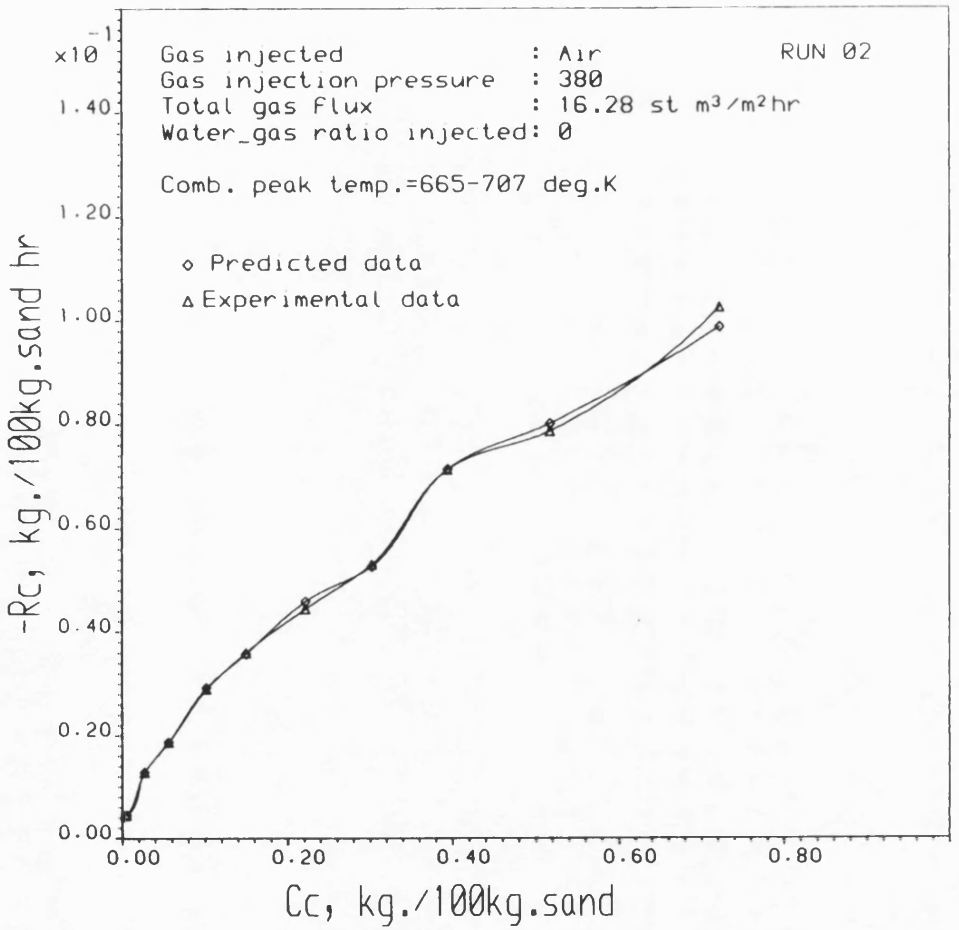

Fig. 6.6 CARBON COMBUSTION RATE AS A FUNCTION OF CARBON CONCENTRATION (non-isothermal condition)

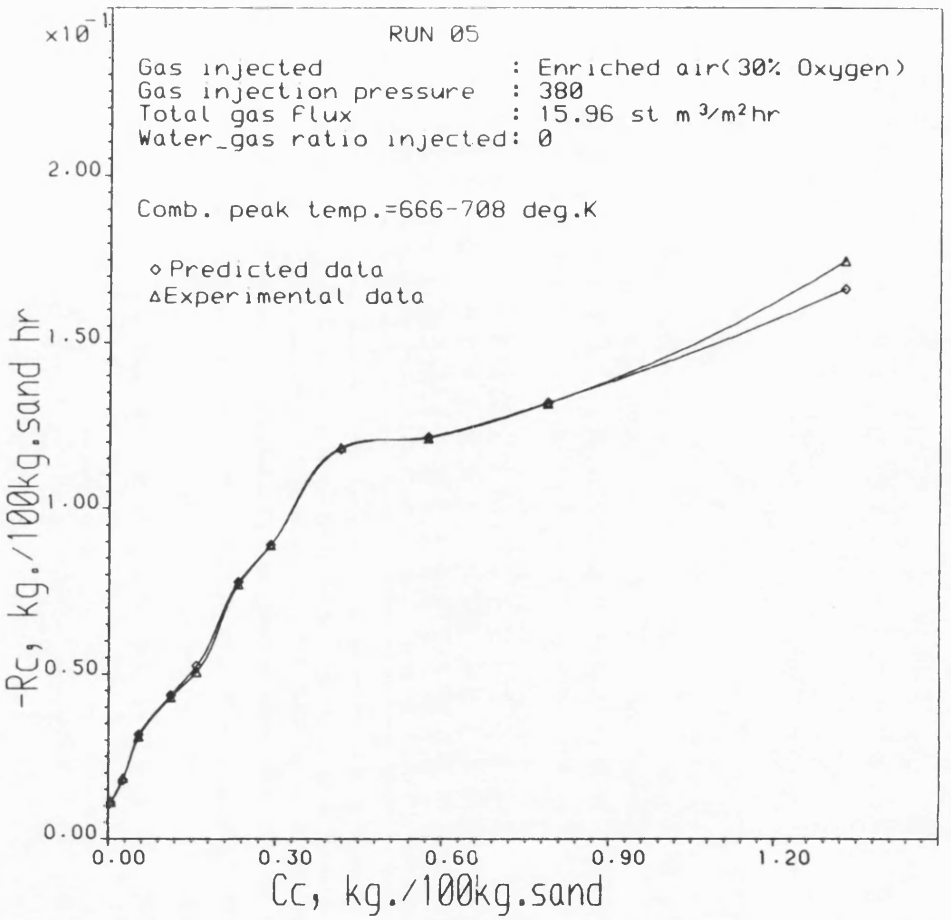

Figure 6.7 CARBON COMBUSTION RATE AS A FUNCTION OF CARBON CONCENTRATION (non-isothermal condition)

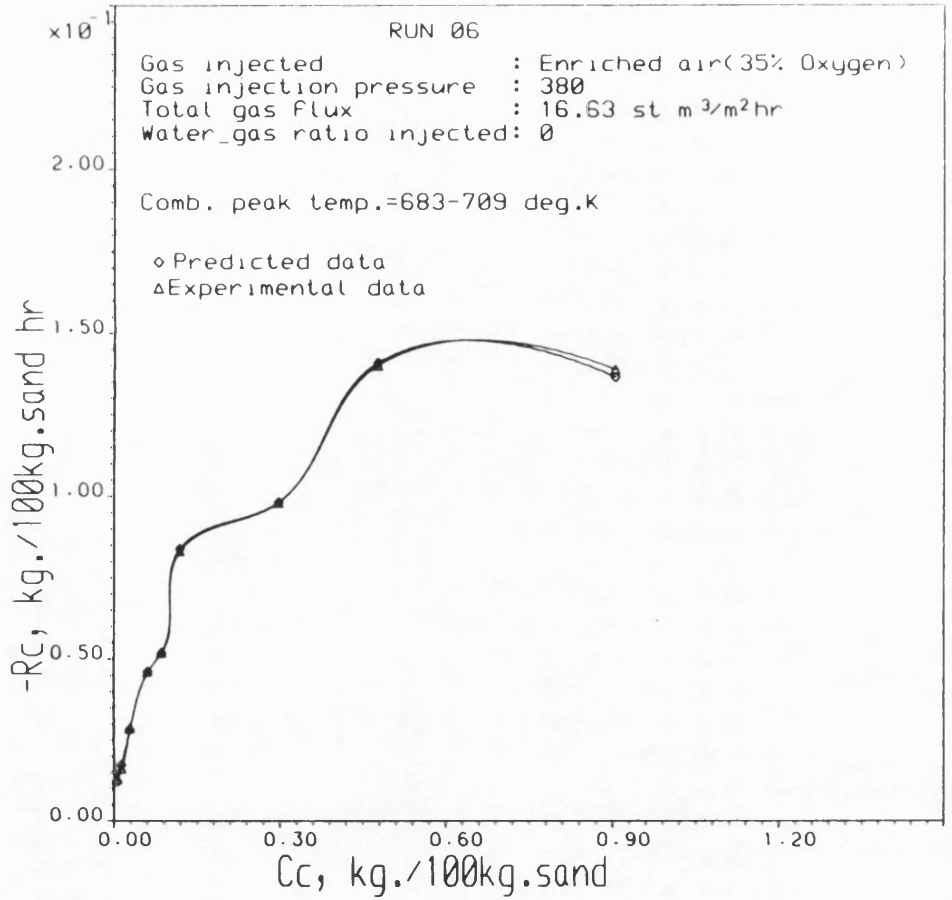

Figure 6.8 CARBON COMBUSTION RATE AS A FUNCTION OF CARBON CONCENTRATION (non-isothermal condition)

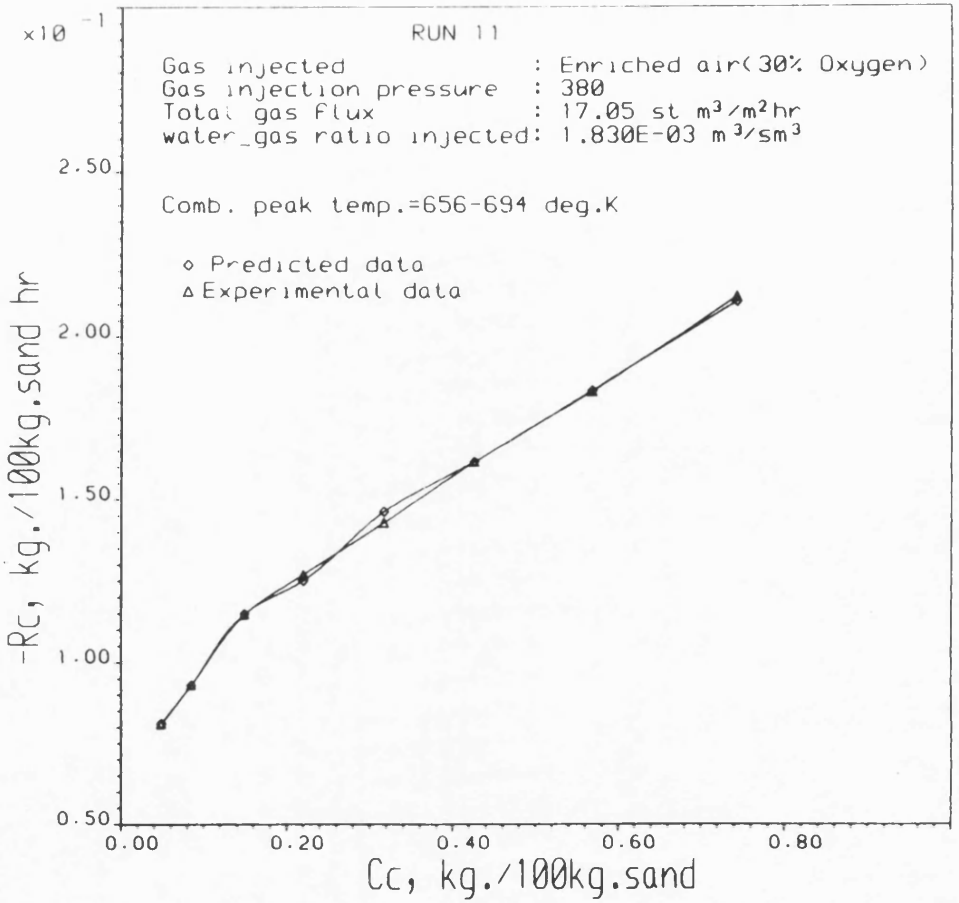

Figure 6.9 CARBON COMBUSTION RATE AS A FUNCTION OF CARBON CONCENTRATION (non-isothermal condition)

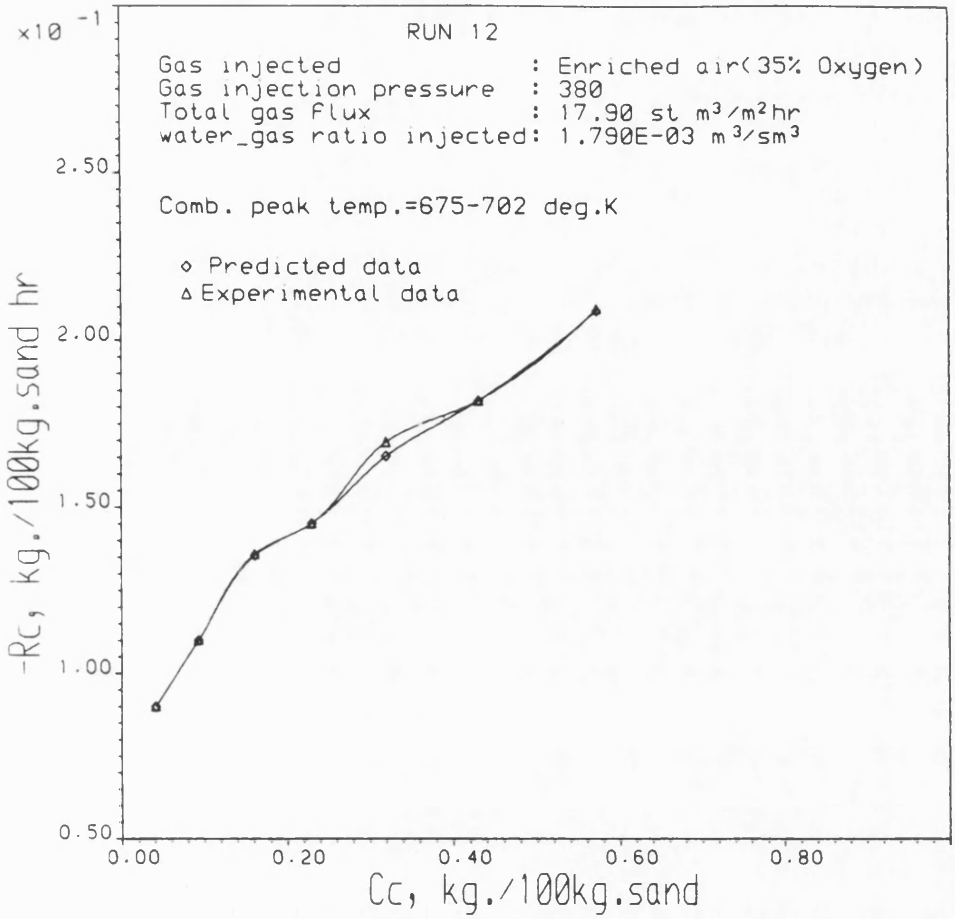

Figure 6.10 CARBON COMBUSTION RATE AS A FUNCTION OF CARBON CONCENTRATION (non-isothermal condition)

6.3 Isothermal Kinetic Parameters

6.3.1 Reaction Order 'm'

The order m on carbon concentration under isothermal condition at 690°K is determined from the computational results for Runs 2, 5 and 6. The average oxygen partial pressure for each run was respectively 79.8, 114 and 133 kPa. Figure 6.11 shows the trend of carbon combustion rate with carbon concentration at the three partial pressures. Similar trends for the wet combustion runs are also shown in Fig. 6.12. The concave curve characteristic indicates a non-first order dependence of the reaction rate on carbon concentration. Furthermore, the reaction rate increases with oxygen partial pressure.

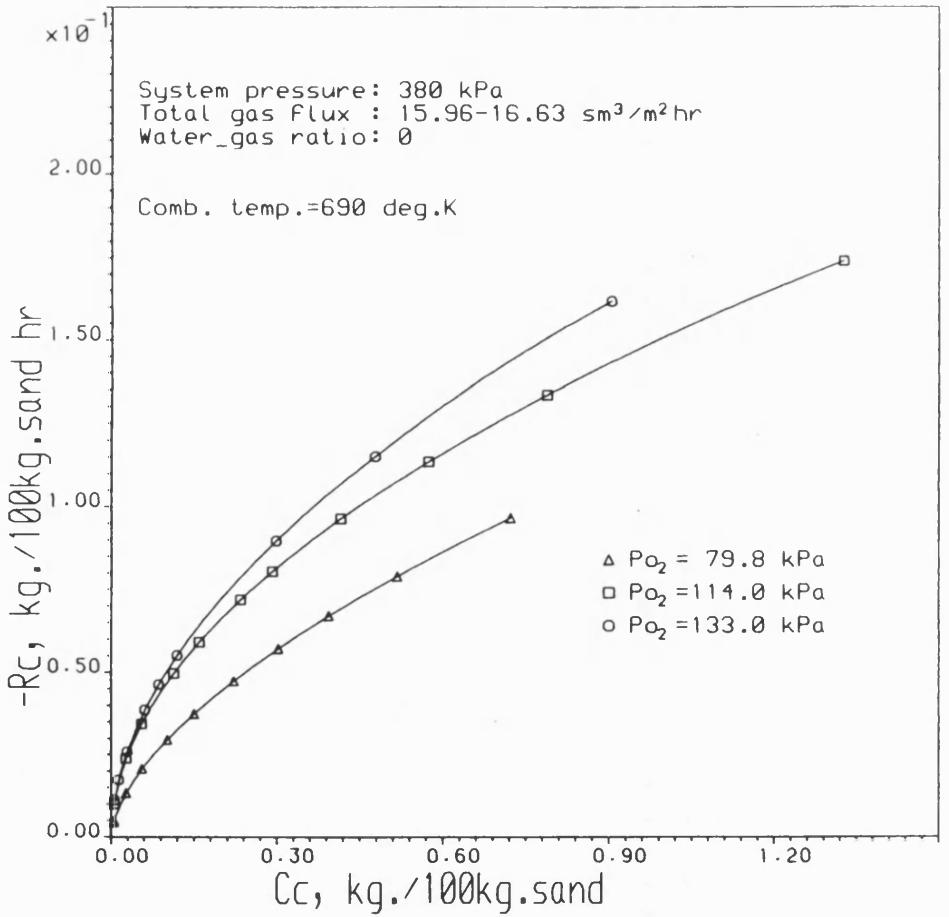

Figure 6.11 CARBON COMBUSTION RATE AS A FUNCTION OF CARBON CONCENTRATION (isothermal condition)

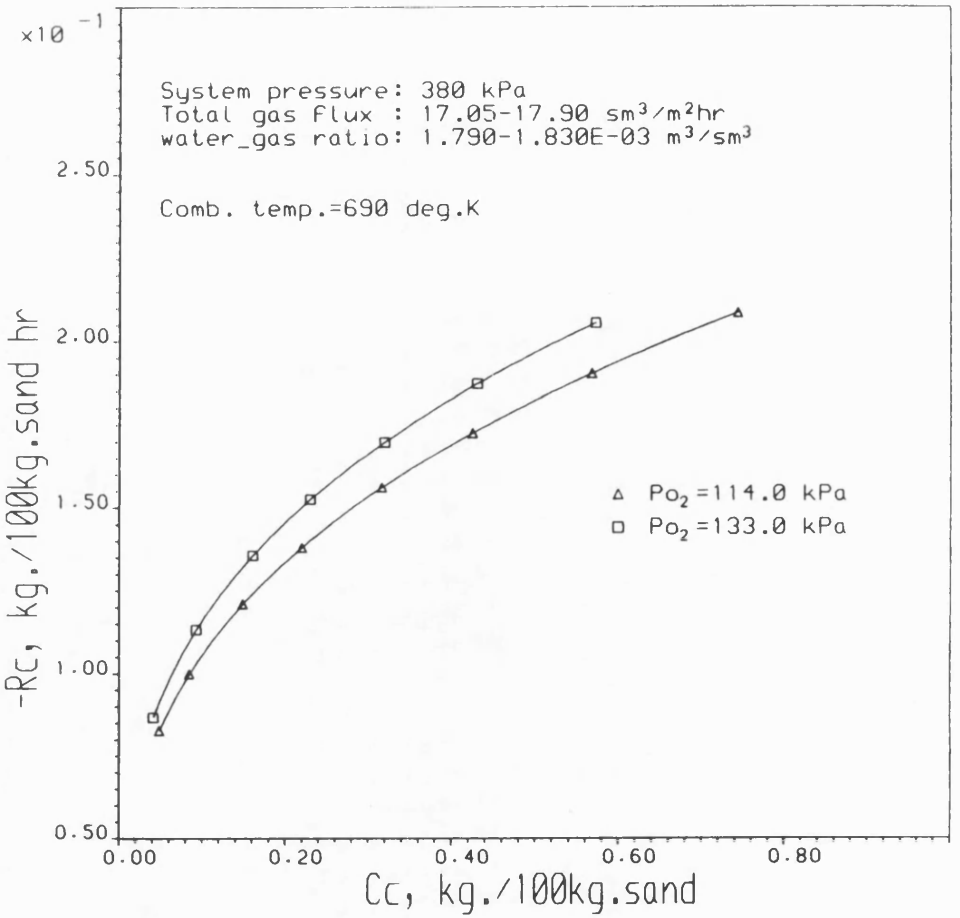

Figure 6.12 CARBON COMBUSTION RATE AS A FUNCTION OF CARBON CONCENTRATION (isothermal condition)

At a fixed oxygen partial pressure and combustion temperature, Equation 6.1 becomes:

$$\log(-Rc) = \log(kP_{O_2}^{n}) + m\log Cc \qquad 6.7$$

A linear regression of the values of log(-Rc) and logCc was used to obtain the values of m in Table 6.2 and the plots are illustrated in Figs. 6.13 and 6.14. The values of m obtained by this procedure are exactly the same as those given in Table 6.1 for the non-isothermal condition. Each combustion run shows different carbon reaction order. Since the same crude oil (Maya, 22.8 API) and sand-clay mixture were used for experiment, the difference must be attributable to the oxygen partial pressure and the gas flux. The general lowering of carbon reaction order during wet combustion, compared with dry combustion is attributed to steam which was generated by water injection, that is, the presence of steam exerts controlling effect on the reaction mechanism.

TABLE 6.2 ISOTHERMAL COMBUSTION KINETIC DATA

ISOTHERMAL CONDITION : 690°K									
RUN 2		RUN 5		RUN 6		RUN 11		RUN 12	
Po_2 = 79.8kPa		Po_2 = 114kPa		Po_2 = 133kPa		Po_2 = 114kPa		Po_2 = 133kPa	
Cc	-Rc	Cc	-Rc	Cc	-Rc	Cc	-Rc	Cc	-Rc
0.72245	0.09665	1.32657	0.17409	0.90468	0.16181	0.74364	0.20863	0.57250	0.20565
0.51739	0.07903	0.78837	0.13358	0.47713	0.11521	0.56825	0.19044	0.43085	0.18734
0.39400	0.06706	0.57389	0.11364	0.29801	0.08973	0.42555	0.17266	0.31995	0.16992
0.30203	0.05713	0.41552	0.09642	0.11891	0.05509	0.31667	0.15620	0.23003	0.15249
0.22147	0.04738	0.29098	0.08043	0.08569	0.04629	0.22016	0.13809	0.16099	0.13565
0.14961	0.03740	0.23322	0.07186	0.06091	0.03862	0.14916	0.12102	0.09284	0.11324
0.10156	0.02961	0.15871	0.05908	0.02870	0.02590	0.08502	0.10002	0.04108	0.08667
0.05611	0.02070	0.11278	0.04965	0.01347	0.01733	0.04861	0.08275		
0.02693	0.01330	0.05478	0.03438	0.00589	0.01117				
0.00514	0.00490	0.02663	0.02381						
0.00443	0.00448	0.00485	0.01001						
Carbon reaction order: m = 0.60		Carbon reaction order: m = 0.51		Carbon reaction order: m = 0.53		Carbon reaction order: m = 0.34		Carbon reaction order: m = 0.33	

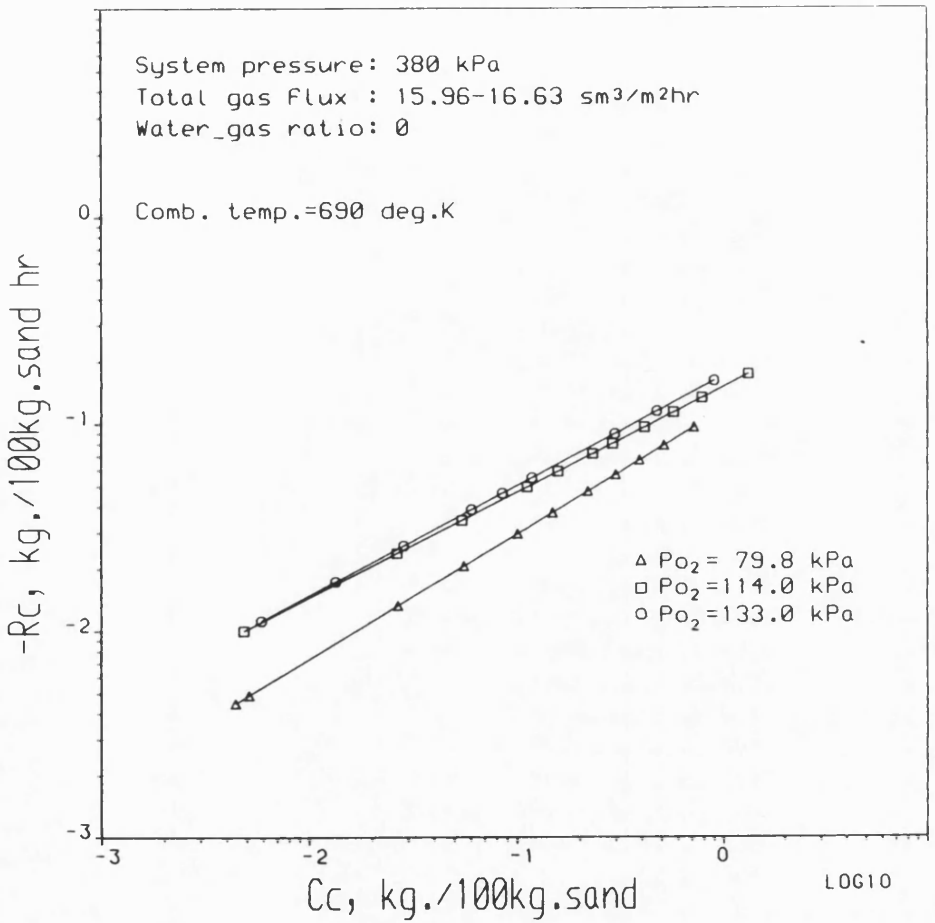

Figure 6.13 CARBON COMBUSTION RATE AS A FUNCTION OF CARBON CONCENTRATION (isothermal condition)

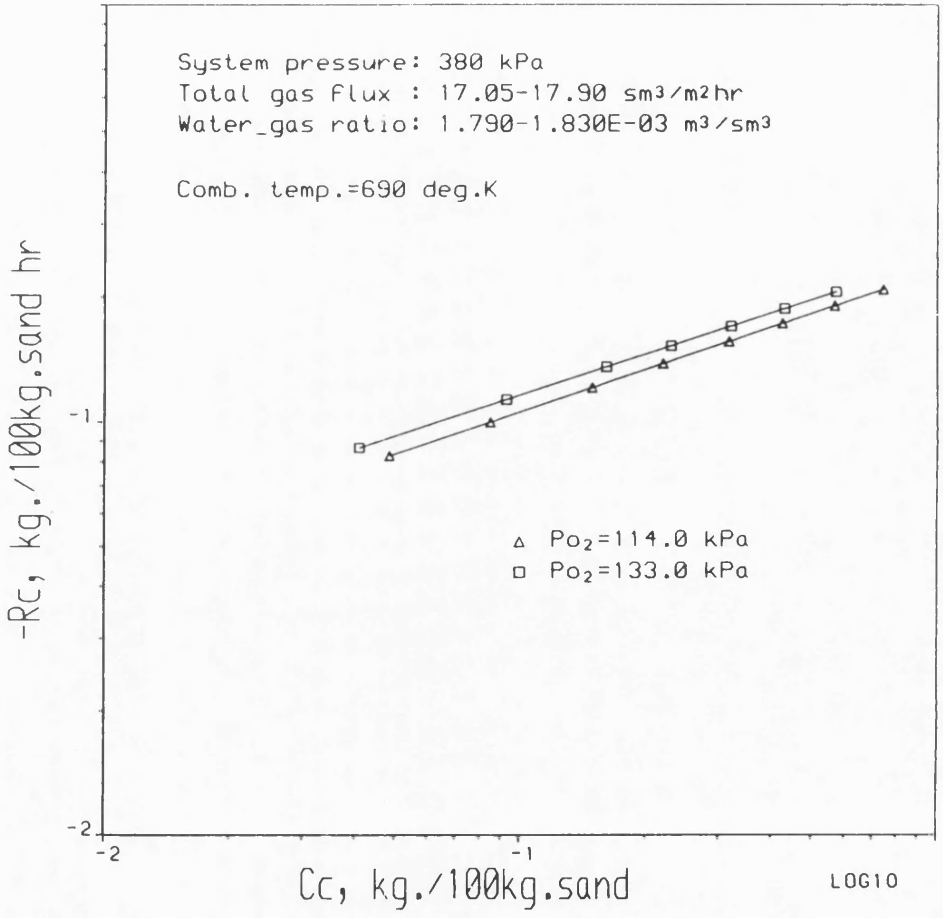

Figure 6.14 CARBON COMBUSTION RATE AS A FUNCTION OF CARBON CONCENTRATION (isothermal condition)

6.3.2 Reaction Order, n

The order n, on the average oxygen partial pressure was determined for the same isothermal condition of 690°K as previously. Equation 6.1 is now expressed as:

$$\log(-Rc/Cc^{m}) = \log k + n\log Po_2 \qquad 6.8$$

Thus, the effect of variation in carbon concentration on the combustion rate is thereby eliminated. With the value of m determined previously, $-Rc/Cc^{m}$ as a function of oxygen partial pressure is obtained from Figs. 6.11 and 6.12. The values for the dry combustion runs are shown in Fig. 6.15 and those for the wet combustion runs in Fig. 6.16. The slopes of these lines are obtained by regression analysis and are given in Table 6.3. Figures 6.17 to 6.21 demonstrate the validity of the method since the value of n satisfies the reaction model for each combustion run. The value of n = 0.72 obtained for the dry runs when compared to n = 0.45 for the wet runs clearly indicates an increased role of diffusion (of oxygen) in wet combustion reaction.

6.3.3. Activation Energy and Arrhenius Constant

Four representative combustion peak temperatures are chosen to calculate the reaction rate constants from Equation 6.1, which is written in the form:

$$k = \frac{-Rc}{Cc^{m}\, Po_2^{n}} \qquad 6.9$$

These values are given in Table 6.4. A regression analysis was used to fit the computed values of k against reciprocal absolute temperature, according to Arrhenius relation.

$$\log k = \log A_r - E/2.303RT \qquad 6.10$$

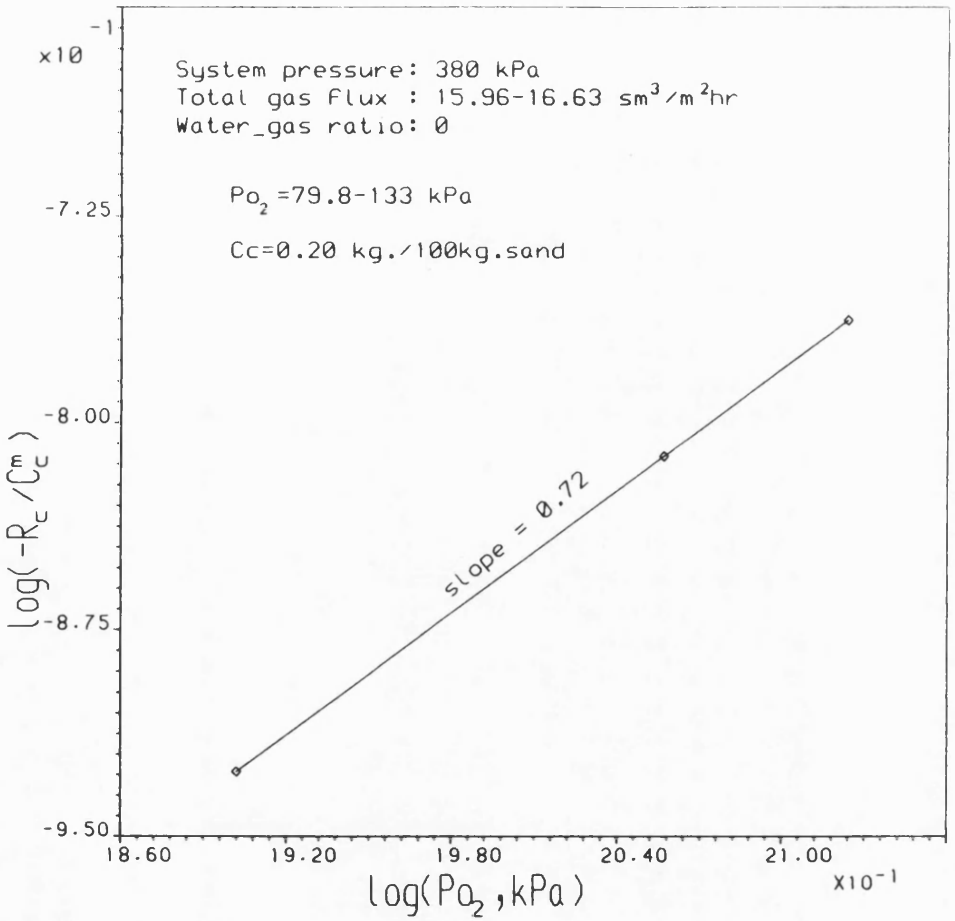

Figure 6.15 EFFECT OF OXYGEN PARTIAL PRESSURE ON CARBON COMBUSTION RATE

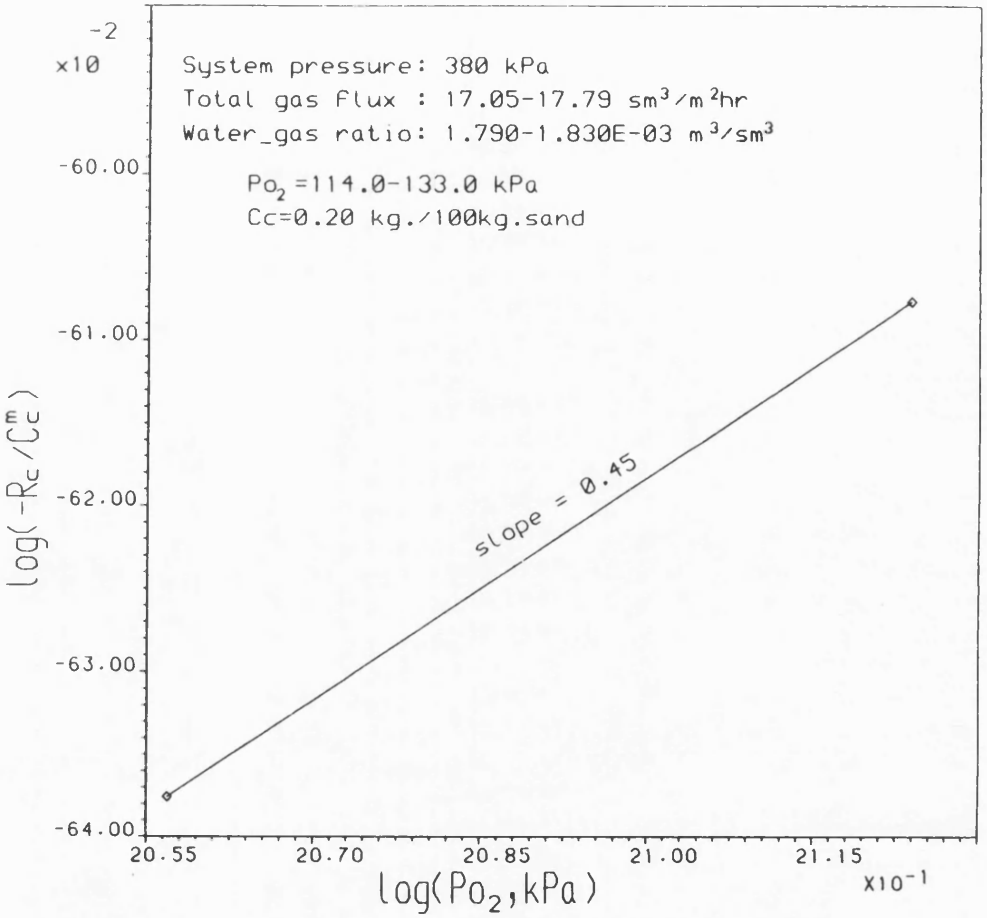

Figure 6.16 EFFECT OF OXYGEN PARTIAL PRESSURE ON CARBON COMBUSTION RATE

TABLE 6.3 ISOTHERMAL KINETIC PARAMETERS

ISOTHERMAL CONDITION: 690°K								
RUN	Cc	-Rc	m	$-Rc/Cc^m$	Po_2	$\log(-Rc/Cc^m)$	$\log Po_2$	n
2	0.200	0.0446	0.60	0.1176	79.8	-0.9296	1.9020	0.72
5	0.200	0.0665	0.51	0.1508	114.0	-0.8217	2.0569	0.72
6	0.200	0.0726	0.53	0.1706	133.0	-0.7679	2.1239	0.72
11	0.200	0.1337	0.34	0.2307	114.0	-0.6370	2.0569	0.45
12	0.200	0.1457	0.33	0.2469	133.0	-0.6074	2.1239	0.45

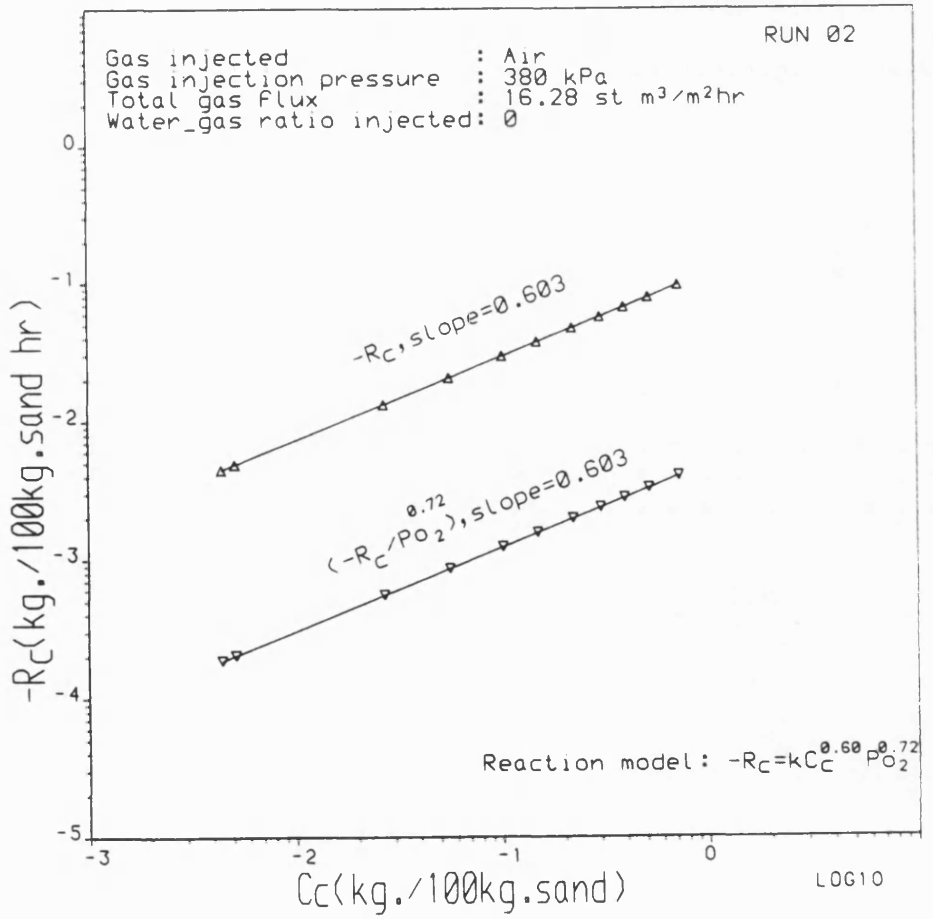

Figure 6.17 EFFECT OF CARBON CONCENTRATION ON COMBUSTION RATE

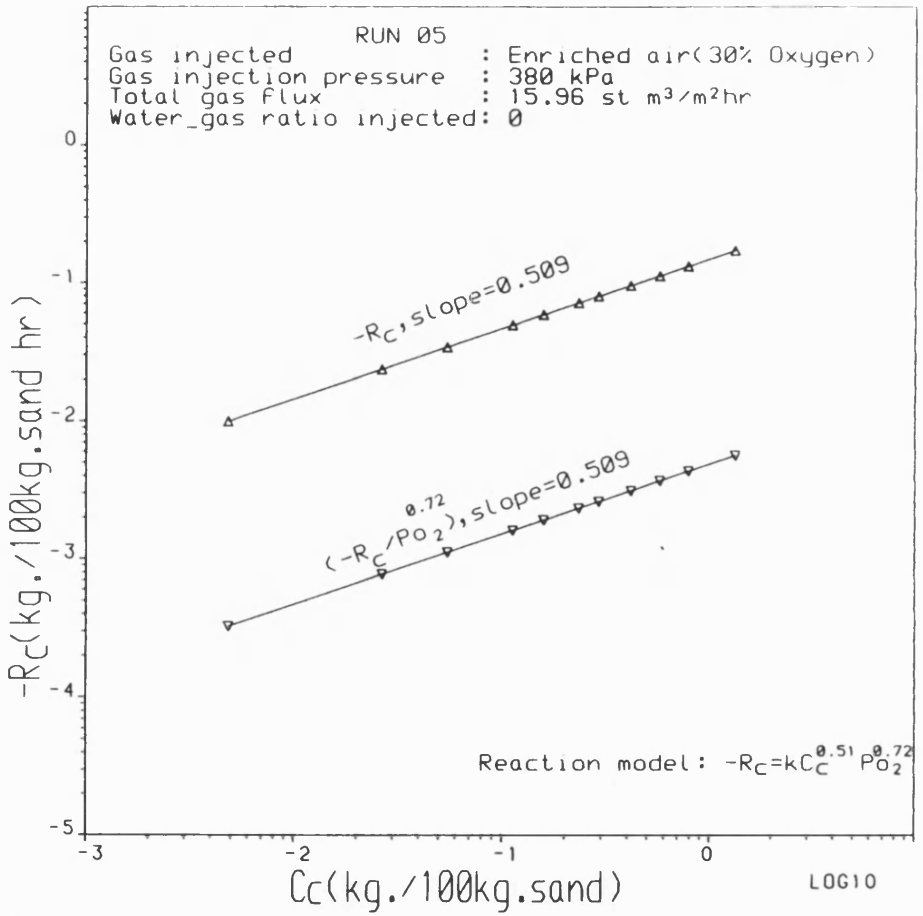

Figure 6.18 EFFECT OF CARBON CONCENTRATION ON COMBUSTION RATE

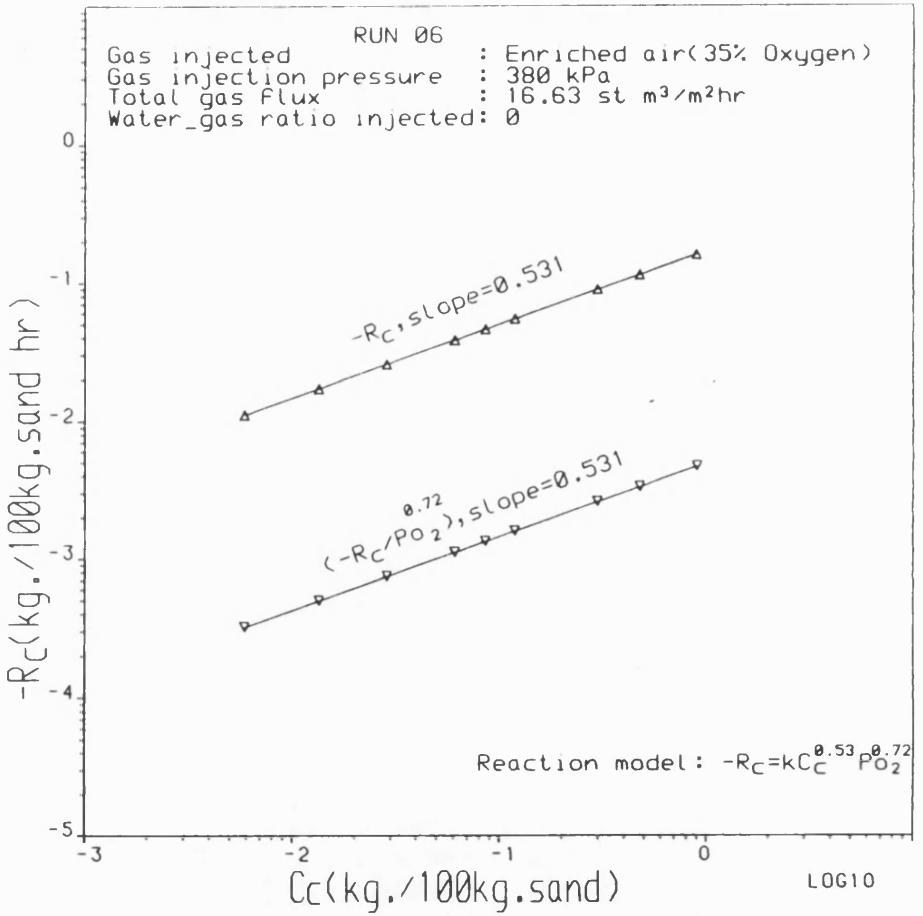

Figure 6.19 EFFECT OF CARBON CONCENTRATION ON COMBUSTION RATE

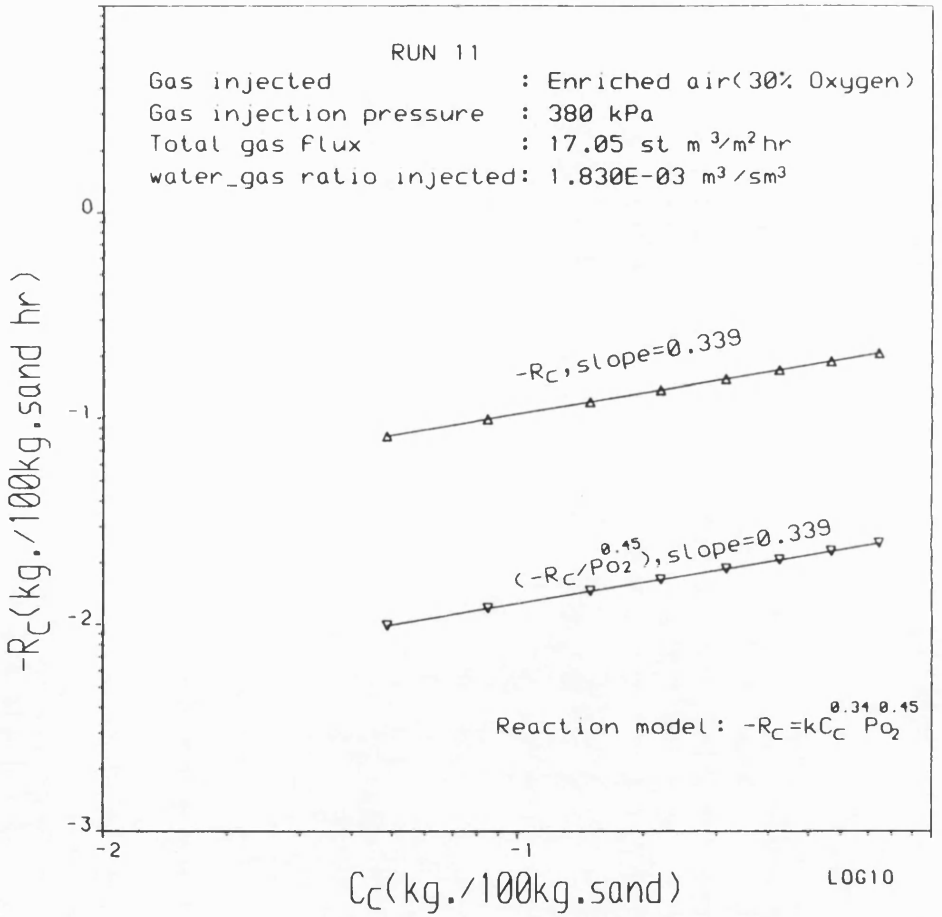

Figure 6.20 EFFECT OF CARBON CONCENTRATION ON COMBUSTION RATE

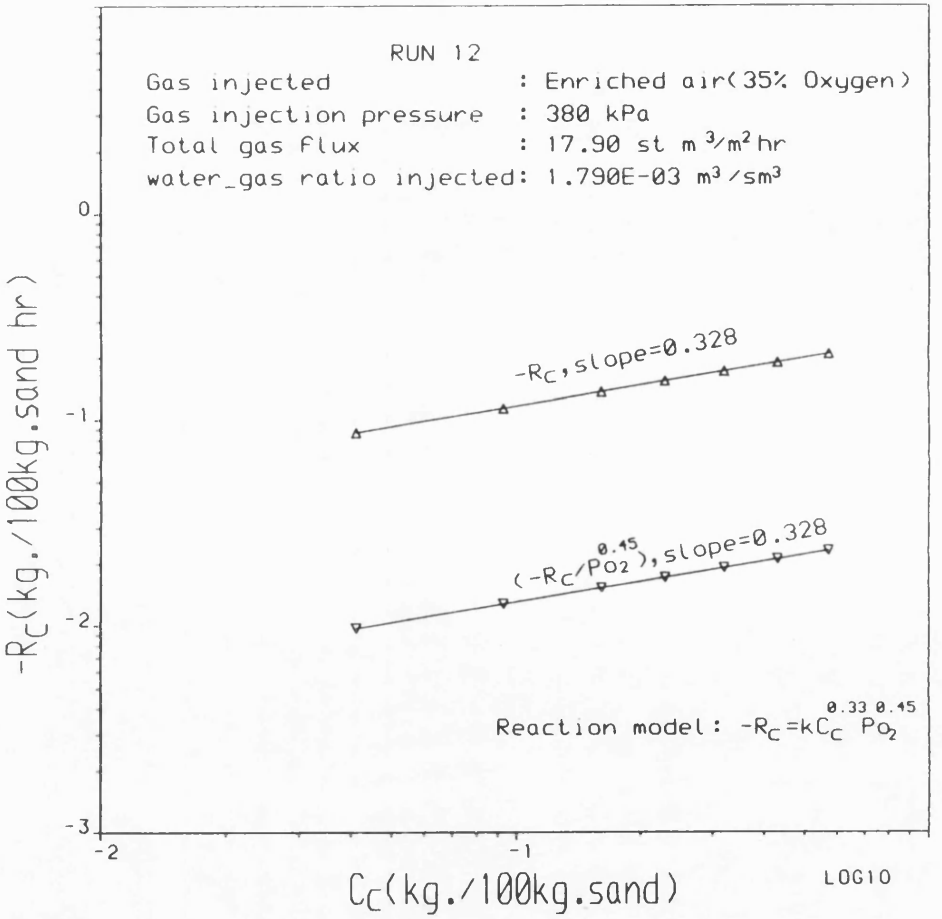

Figure 6.21 EFFECT OF CARBON CONCENTRATION ON COMBUSTION RATE

TABLE 6.4 COMBUSTION REACTION RATE CONSTANTS

DRY COMBUSTION				WET COMBUSTION		
Combustion Peak Temp. °K	Reaction Rate Constant, k			Combustion Peak Temp. °K	Reaction Rate Constant, k	
	Run 2	Run 5	Run 6		Run 11	Run 12
685	4.840×10^{-3}	4.612×10^{-3}	4.410×10^{-3}	675	27.255×10^{-3}	27.172×10^{-3}
690	4.935×10^{-3}	4.888×10^{-3}	4.948×10^{-3}	680	27.637×10^{-3}	27.611×10^{-3}
695	5.031×10^{-3}	5.175×10^{-3}	5.543×10^{-3}	685	28.018×10^{-3}	28.051×10^{-3}
700	5.127×10^{-3}	5.475×10^{-3}	6.198×10^{-3}	690	28.399×10^{-3}	28.491×10^{-3}

$$\text{Reaction Rate Constant, } k = \frac{-Rc}{Cc^{m} Po_2^{n}}$$

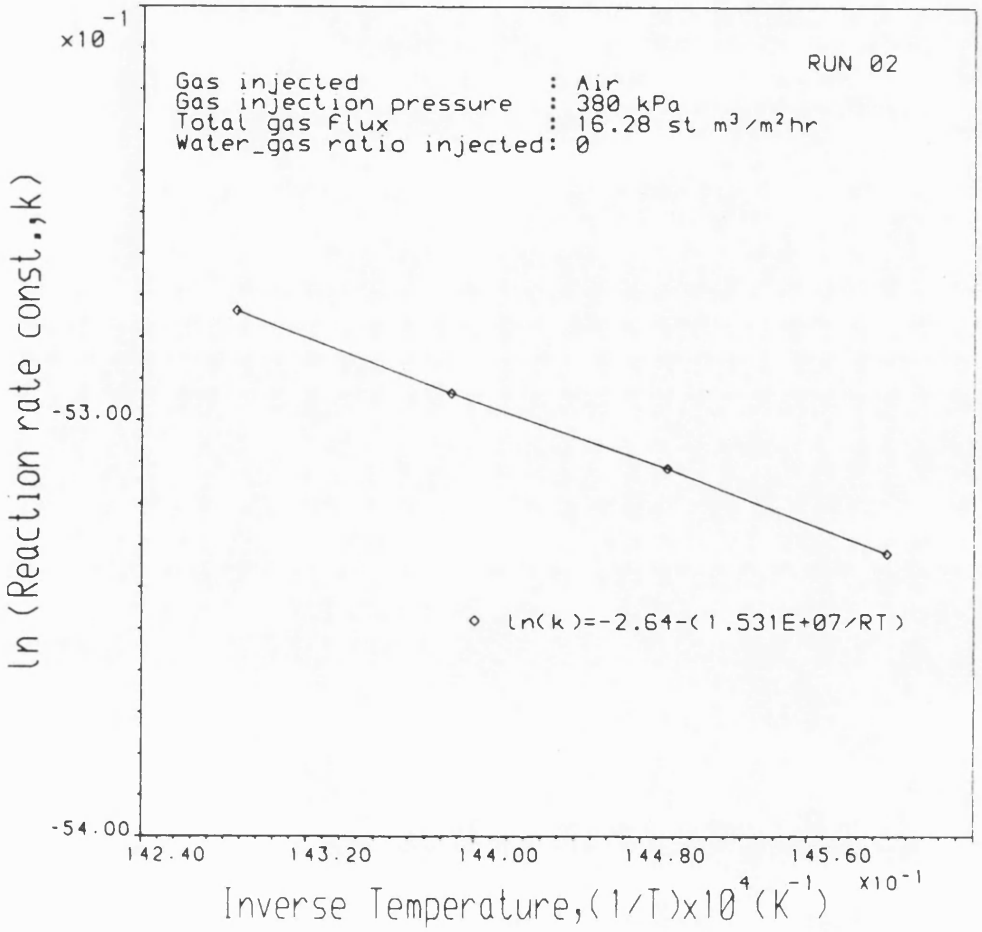

Figure 6.22 ARRHENIUS PLOT FOR COMBUSTION REACTIONS

The activation energy and the Arrhenius constant were calculated from the regression equation and the Arrhenius plots are shown in Figs. 6.22 to 6.26.

6.4 Comparison of Kinetic Parameters

The kinetic parameters obtained in this study are summarised in Table 6.5. The reaction order m and n with respect to carbon concentration and oxygen partial pressure, lie within the range of those reported by other workers in Table 6.6, and the activation energies are also of the same order. However, the Arrhenius constant cannot be compared because of the difference in the values of m and n. The difference that results in the numerical values of the kinetic parameters obtained in this study compared with those reported in Table 6.6 are attributed to the different sand pack properties and the operating parameters used. The presence of clay in the sand, is known to have a catalytic effect, reducing the activation energy in addition to causing a fractional order dependence of the reaction rate on carbon concentration (Fassihi, 1981). Also, the use of precoked oils in combustion kinetic studies does not simulate the flow and heat transfer found in in-situ combustion. Furthermore, the lower peak temperatures obtained in this study has a reducing effect on the kinetic parameters.

6.5 Controlling Mechanism

Figure 6.27 shows the variation of the reaction rate constant (expressed as k/C_c^m) with the level of oxygen enrichment for various combustion peak temperatures. Between 21 to 30%, the diffusion rate of oxygen has a reducing effect on the reaction rate constant. Above 30% O_2, however, the trend is

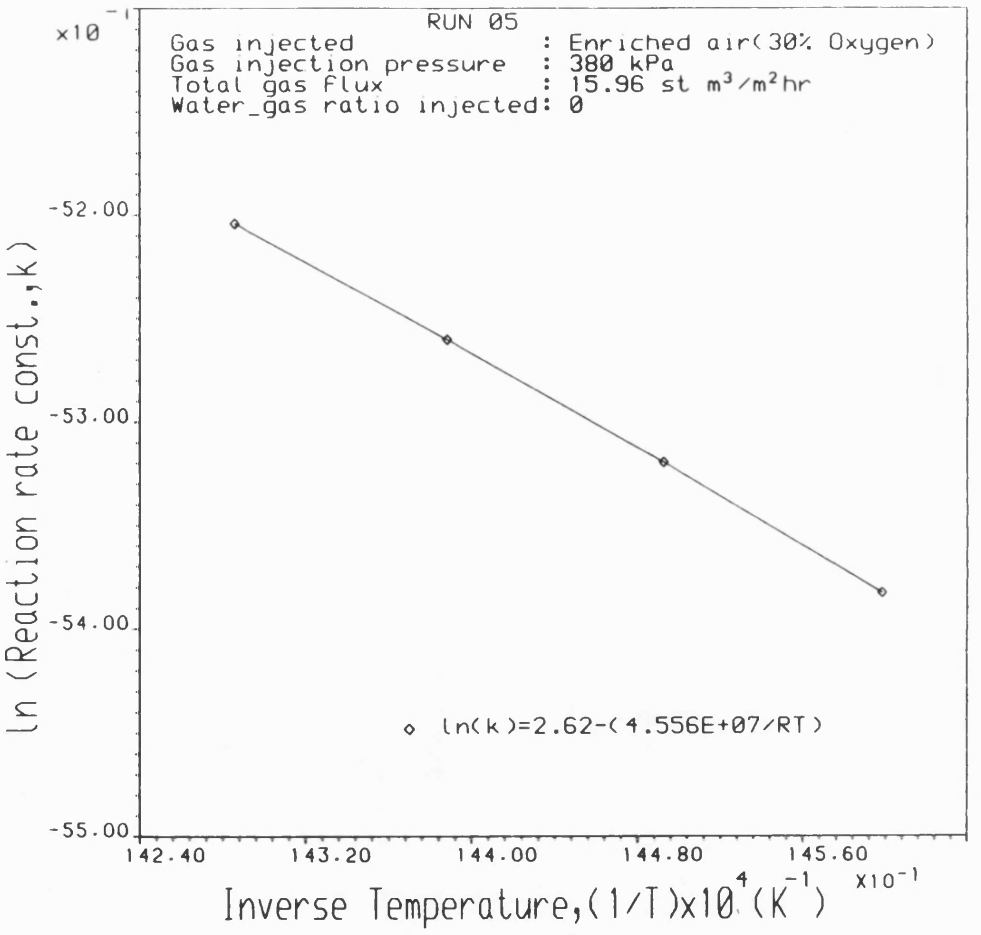

Figure 6.23 ARRHENIUS PLOT FOR COMBUSTION REACTIONS

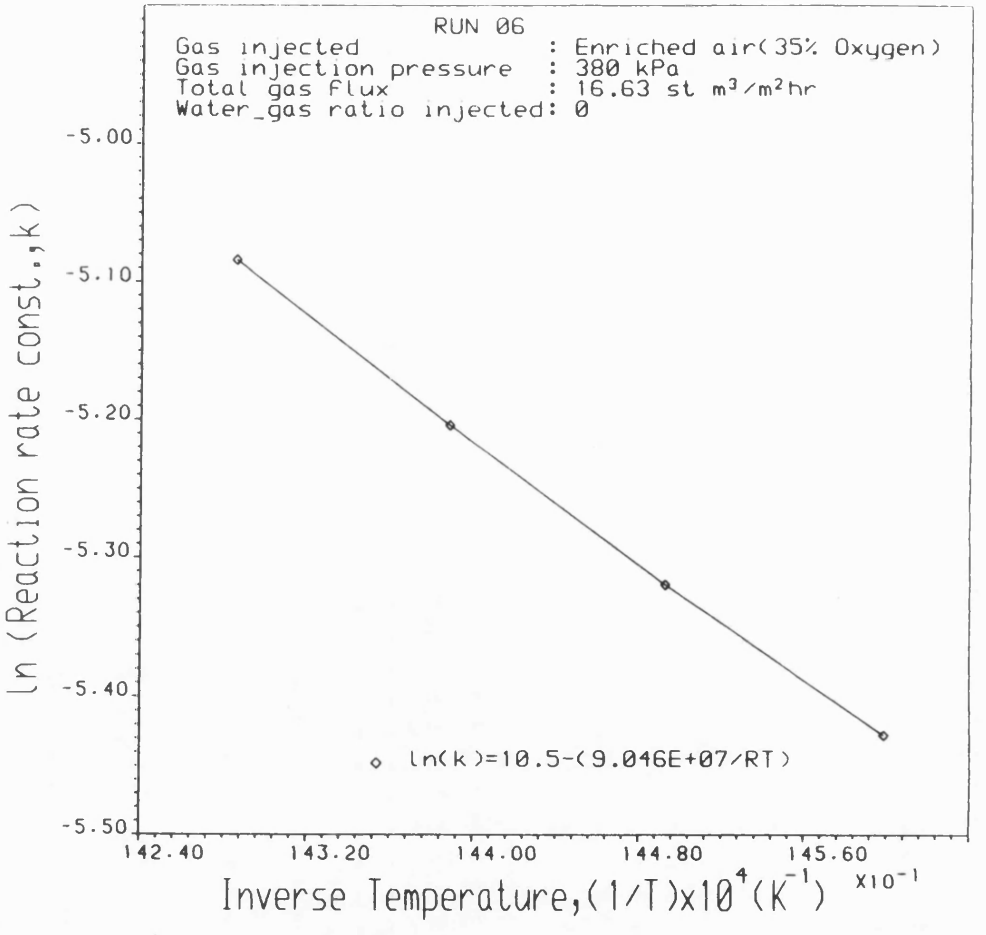

Figure 6.24 ARRHENIUS PLOT FOR COMBUSTION REACTIONS

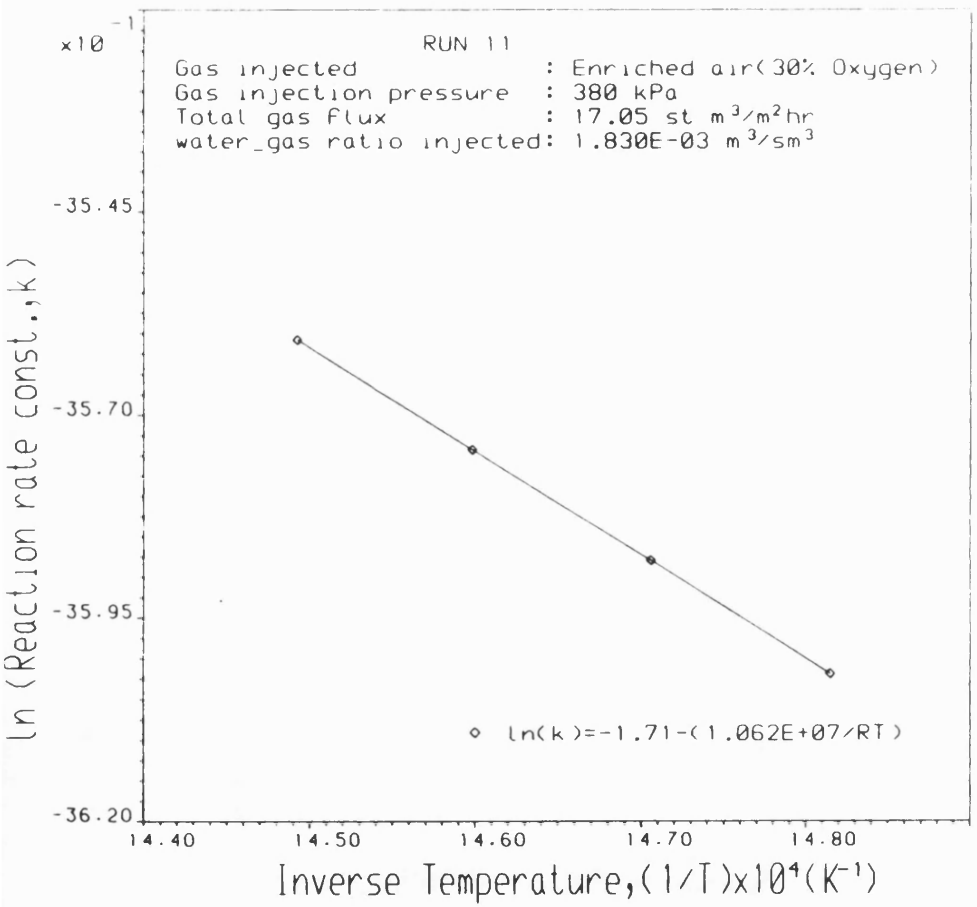

Figure 6.25 ARRHENIUS PLOT FOR COMBUSTION REACTIONS

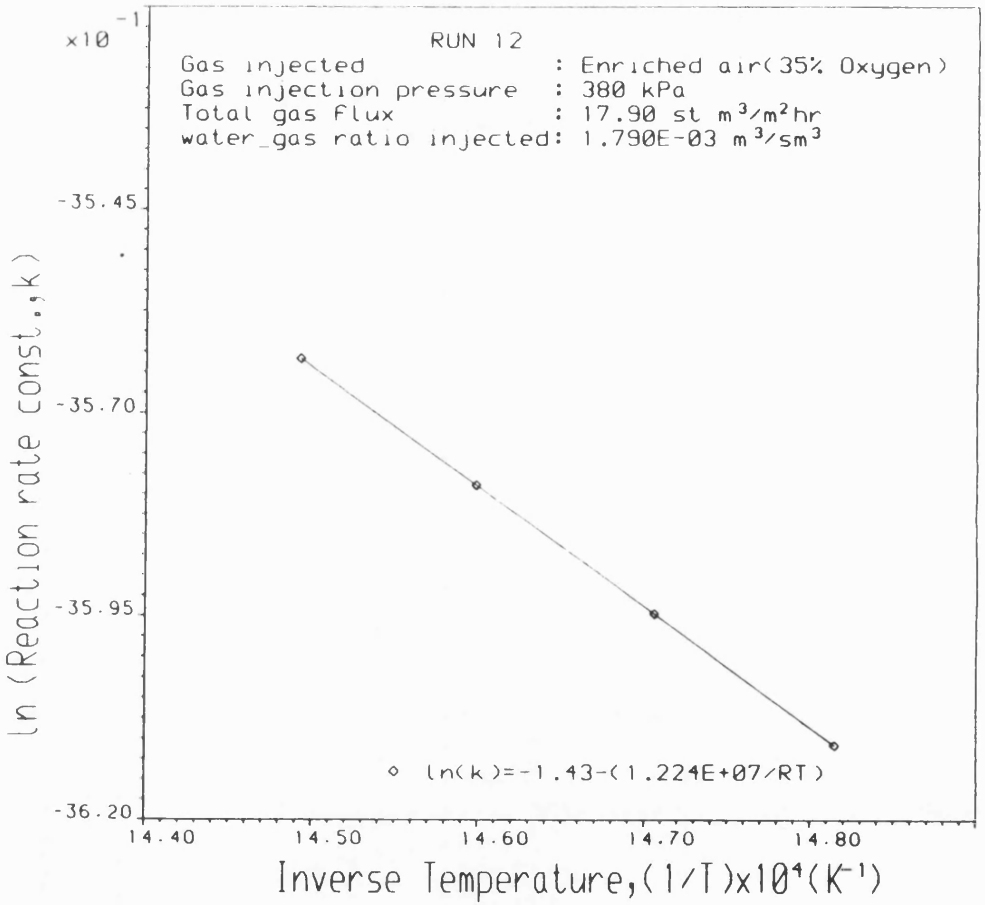

Figure 6.26 ARRHENIUS PLOT FOR COMBUSTION REACTIONS

TABLE 6.5 SUMMARY OF COMBUSTION REACTION KINETIC PARAMETERS

RUN NO.	OPERATING PARAMETERS					KINETIC PARAMETERS					
	SYSTEM PRESSURE	TOTAL GAS FLUX	OXYGEN INJECTED	OXYGEN PARTIAL PRESSURE	WATER-GAS RATIO	$ArPo_2^n$	CARBON REACTION ORDER, m	OXYGEN REACTION ORDER, n	A_r	E	AVG. PEAK TEMP.
	kPa	sm^3/m^2hr	% mole	kPa	m^3/Msm^3	$\frac{(kg/100kg)^{1-m}}{hr}$			$\frac{(kg/100kg)^{1-m}}{(kPa)^n hr}$	J/kgmole	°K
2	380	16.28	21	79.8	0.00	1.671	0.60	0.72	7.136×10^{-2}	1.531×10^{7}	683
5	380	15.96	30	114	0.00	4.157×10^{2}	0.51	0.72	1.374×10^{1}	4.556×10^{7}	689
6	380	16.63	35	133	0.00	1.228×10^{6}	0.53	0.72	3.632×10^{4}	9.046×10^{7}	696
11	380	17.05	30	114	1.83	1.524	0.34	0.45	1.809×10^{-1}	1.062×10^{7}	673
12	380	17.90	35	133	1.79	2.161	0.33	0.45	2.393×10^{-1}	1.224×10^{7}	688

Reaction Model: $-Rc = A_r \exp(-E/RT) C_C^m P_{O_2}^n$

TABLE 6.6 COMBUSTION REACTION RATE (Fassihi, 1981)

$$-Rc^{(1)} = A_r \exp(-E/RT) P_{O_2}^n C_C^m$$

AUTHORS	CRUDE TYPE	REACTOR BED	A_r (1/Pa.s)	E(J/kgmole)	m	n	P(kPa)	Avg. Combustion Peak Temp °K
Lewis, et al. (1954)	Metallurgical Coke	Fluidized	7.4×10^{-2}	12.14×10^{7}	1	1	1×10^{2}	n.a
	Hardwood Charcoal	Fluidized	2.0×10^{-3}	6.650×10^{7}	1	1	1×10^{2}	n.a
	Graphite	Fluidized	1.3×10^{3}	20.580×10^{7}	1	1	1×10^{2}	n.a
Weisz and Goodwin (1966)	Coke(3)	Sand Pack	6.67×10^{5}(4)	15.73×10^{7}	1	0(4)	1×10^{2}	n.a
Weijdema (1968)	n.a(2)	Sand Pack	n.a	12.55×10^{7}	n.a	n.a	4×10^{3}	n.a
Bousaid and Ramey (1968)	13.9°API	Berea Sand 170-230 mesh	2.37×10^{-3}	6.190×10^{7}	1	1	3×10^{2}	755
	13.9°API	80%Berea, 20% clay	2.43×10^{-4}	4.840×10^{7}	1	1	5×10^{2}	877
	22.1°API	Berea Sand	9.14×10^{-3}	5.980×10^{7}	2	1	2×10^{2}	744
Dabbous and Fulton (1974)	19.90°API precoked	Berea Sand 60mesh	1.38×10^{-3}	5.890×10^{7}	2	1	2×10^{2}	713
Thomas, et al. (1979)	27°API	Sand quarry	3.0×10^{1}	5.880×10^{7}	1	1(5)	1×10^{4}	n.a
		Kaolimite (5%)	1.8×10^{1}	5.880×10^{7}	1	1(5)	2.8×10^{4}	n.a
			4.84×10^{1}	5.880×10^{7}	1	1(5)	4.8×10^{4}	n.a
Fassihi (1981)	11.2°API	Sand pack no clay	4×10^{4}	12.000×10^{7}	1	0.58	166	700
	11.2°API	Sand pack 5% clay	260	6.100×10^{7}	0.4	0.55	137	700
	10.1°API	Sand pack	2×10^{6}	13.300×10^{7}	1	0.23	195	720
	18.5°API	Sand pack	6×10^{5}	13.500×10^{7}	1	0.66	253	756

(1) Rc = g carbon burned/100g sand s
(2) n.a = not available
(3) Obtained from chromatographic decolorization of heavy oil (percolation); It was purged at 430°C with nitrogen to remove residual liquid
(4) This is obtained at high oxygen partial pressure. If a first order dependence on oxygen partial pressure is assumed, the A_r would be 31.3
(5) Here m is the exponent of $(\phi \ell \rho_f)$ where: $(\phi \ell \rho_f)$ = fuel laid down minus fuel burnt

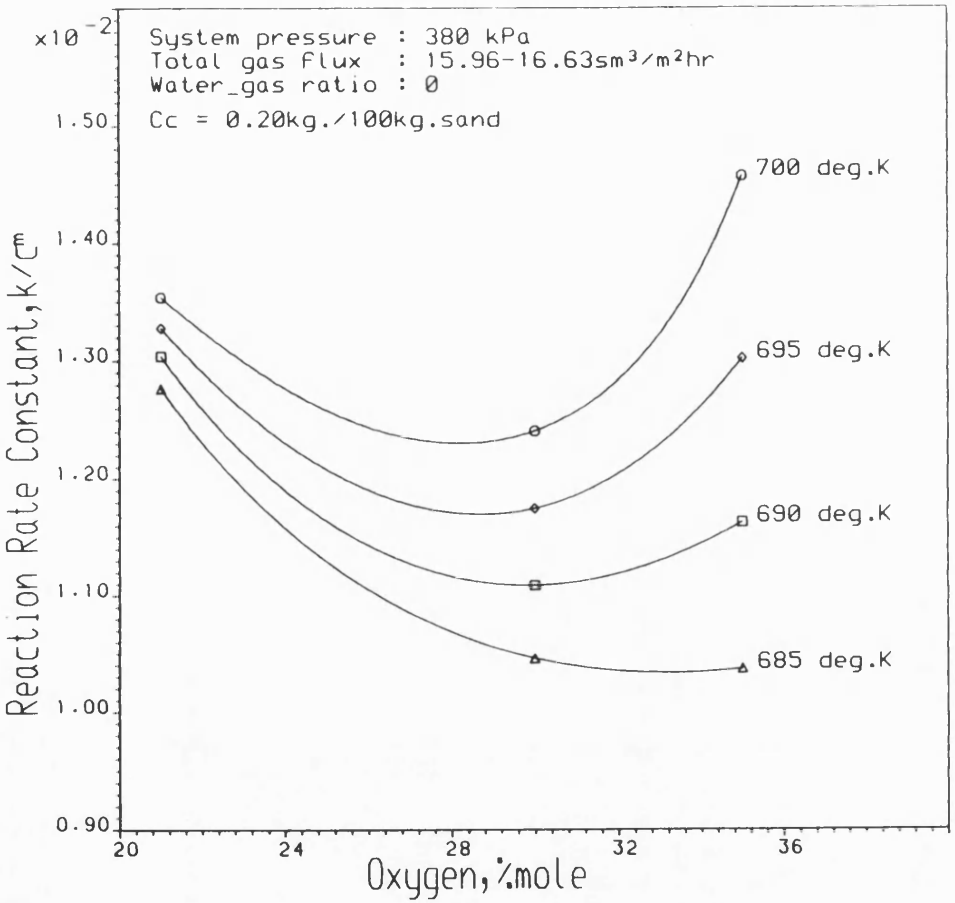

Figure 6.27 EFFECT OF OXYGEN ENRICHMENT OF AIR ON REACTION RATE CONSTANT

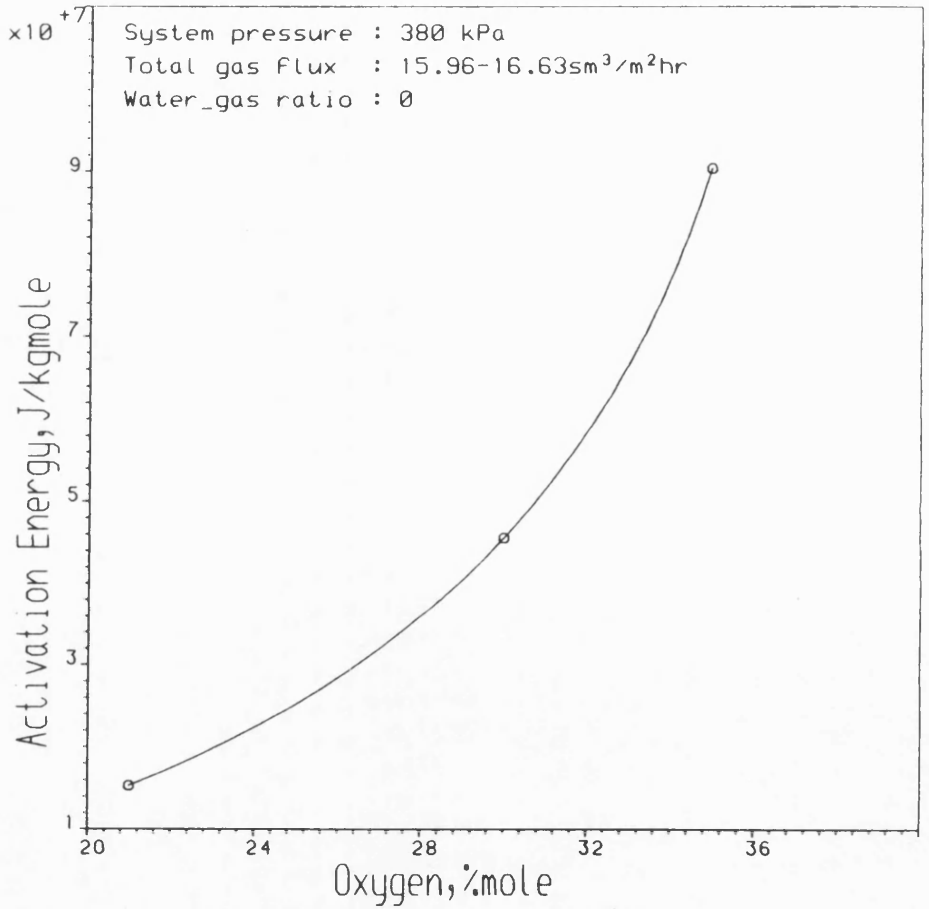

Figure 6.28 EFFECT OF OXYGEN ENRICHMENT OF AIR ON ACTIVATION ENERGY

reversed. The overall trend is dependent on peak temperature. As shown in Fig. 6.28, the activation energy increases quite rapidly with oxygen enrichment but is believed to be due mainly to higher combustion front peak temperature with higher oxygen concentration. The increase of the activation energy with average peak temperature, observed in this study is typical of a kinetically controlled process (Pusch, 1976). This is in agreement with the findings of Bousaid (1967) and Fassihi et al. (1984). Bousaid reported that an increase in gas flux at a combustion temperature of 1120°F resulted in a small decrease in the reaction rate constant, while it had a negligible effect at 900°F. Fassihi et al. also found that a twofold increase in the air flow rate did not cause any change in reaction rate constant and so as Bousaid concluded that the overall rate of combustion process was kinetically controlled.

In wet combustion, however, the activation energy is lower than for the dry combustion, as shown in Table 6.5. For an oxygen partial pressure of 114kPa and WGR of 1.83m^3/Msm^3, E reduces from 4.556×10^7 to 1.062×10^7 J/kgmole, which is a reduction of more than 75%. At oxygen partial pressure of 133kPa and WGR = 1.79, the reduction is more than 85%. The lower activation energy in wet combustion is therefore mainly due to the increased role of oxygen diffusion. This effect is illustrated in Figs. 6.29 and 6.30. When chemical reaction is no longer controlling, the variation of reaction rate constant with temperature becomes insignificant (Martin et al; 1958), which is precisely the case for the wet combustion reaction. It is therefore concluded that chemical reaction rate is controlling during dry combustion but this shifts to a gas diffusion control mechanism in wet combustion.

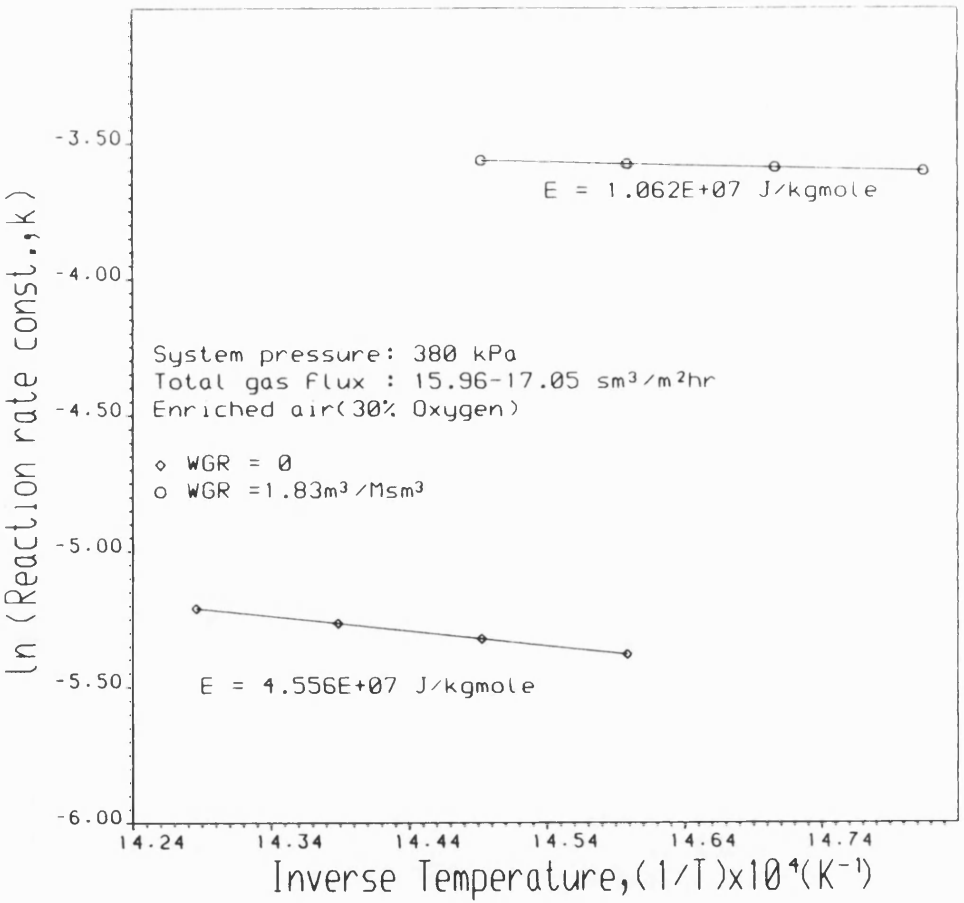

Figure 6.29 ARRHENIUS PLOT FOR WET AND DRY COMBUSTION

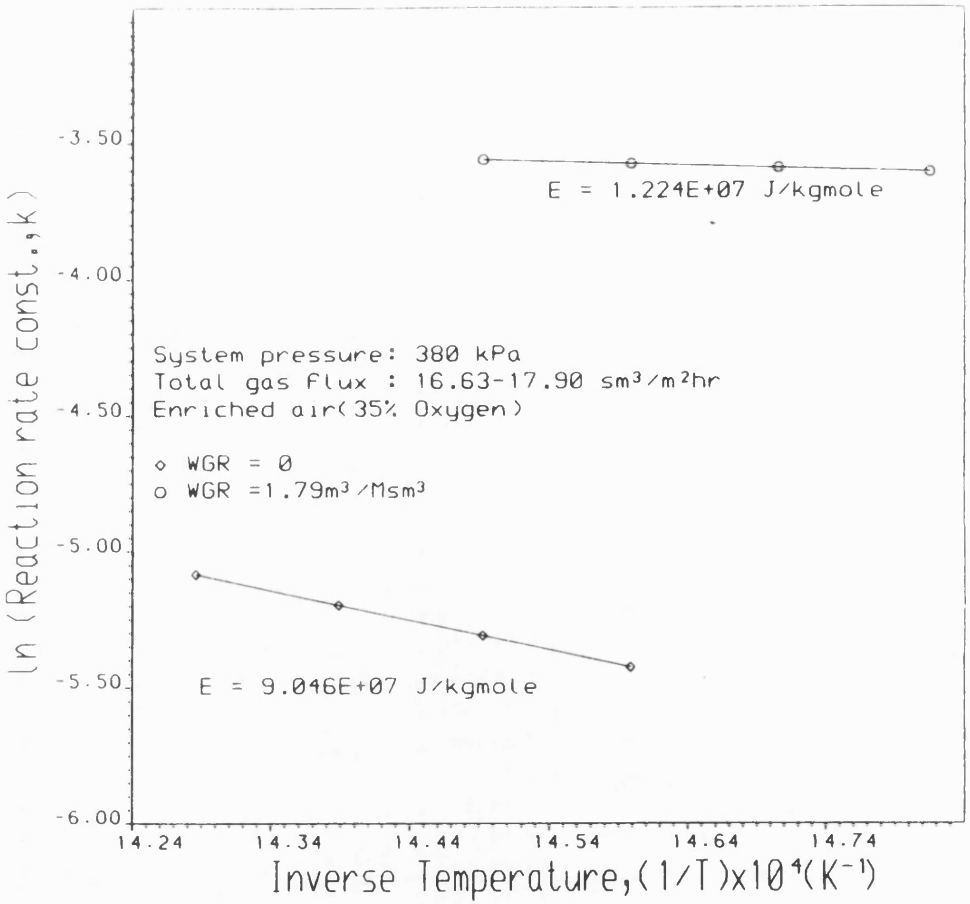

Figure 6.30 ARRHENIUS PLOT FOR WET AND DRY COMBUSTION

Pusch (1976) has observed that the reaction rate in wet combustion (above 300°C) was almost independent of temperature, that is, the chemical reaction rate does not control the process. According to Pusch, the presence of steam causes large areas of the fuel surface to be inaccessible to oxygen. Each oxygen molecule arriving at the free active sites of the fuel surface is then able to react with the carbon atoms. Hence the overall rate of combustion is determined by the rate at which oxygen is able to diffuse to the fuel surface and not by chemical reaction rate.

6.6 Conclusions

From the analysis of the combustion reaction kinetics during dry and wet in-situ combustion, the following conclusions are made.

1. The combustion reaction rate is dependent upon carbon concentration, oxygen partial pressure and combustion peak temperature. In dry combustion, the reaction order with respect to oxygen partial pressure was $n = 0.72$, with order on carbon concentration lying between 0.5 and 0.6. The values obtained for wet combustion were lower, respectively $n = 0.45$ and m between 0.3 and 0.4

2. The reaction rate constant and combustion temperature data were adequately described by Arrhenius kinetics. The activation energy for dry combustion runs shows a significant increase with oxygen enrichment and the average combustion peak temperature. This indicates that for dry combustion, the reaction rate is kinetically controlled and gas diffusion effects are minimal.

3. In wet combustion there is a very significant reduction in the activation energy due to the increased role of oxygen diffusion.

4. The kinetic parameter values obtained in this study were found to be very sensitive to the operating condition selected. This strongly indicates that in order to simulate actual reservoir condition, kinetic data must be obtained using reservoir rock material at the specific reservoir conditions.

Chapter 7

RECOVERY AND PROPERTIES OF THE PRODUCED OIL

The oil recovery data obtained from six dry and six wet combustion experiments are analysed to determine the effect of air injection pressure, oxygen enrichment and water-gas ratio (WGR) on oil recovery efficiency during forward in-situ combustion. These parameters have a major effect on oil recovery through their influence on the size and velocity of the steam zone. The steam zone velocity determines how quickly the zone mobilizes and displaces the oil ahead of the combustion front. On the other hand, the size of the steam zone affects the rate of vaporization and cracking of the oil and hence the fuel concentration. The maximum amount of oil recovered will depend to a significant extent on the fuel concentration.

The physical properties and simulated distillation data are obtained from analysis of the original crude and produced oil. The original oil properties are modified by thermal cracking and oxidation reaction products. The former alters the distillation characteristics of the oil while at sufficiently high pressures, CO_2 can promote swelling of the oil and viscosity reduction.

In this investigation, the experiments were performed at pressures of 380, 690 and 1020kPa, oxygen enrichment of 21% (air), 30% and 35% O_2, with the WGR varying from 1.47 to 6.32 m^3/Msm^3. The main objective was to compare the cumulative recovery of the produced oil under the operating conditions selected and also to investigate any upgrading of the produced oil.

7.1 Liquid Production

TABLE 7.1 IN-SITU COMBUSTION OIL RECOVERY

RUN NO	PROCESS CONDITIONS							RECOVERY DATA			
	SYSTEM PRESSURE	INJECTED GAS ANALYSIS		TOTAL GAS FLUX	WGR	LIQUID SATURATION		ORIGINAL OIL IN PLACE	TOTAL OIL PRODUCED	OVERALL OIL RECOVERY	OIL CONSUMED AS FUEL
	kPa	$\%N_2$	$\%O_2$	sm^3/m^2hr	m^3/Msm^3	So_I %PV	Sw_I %PV	grams	grams	%wt	grams
01	380	79.0	21.0	10.53	0.0	22.2	17.2	122.26	80.23	66	30.21
02	380	79.0	21.0	16.28	0.0	24.4	19.1	124.89	79.30	63	40.32
03	690	79.0	21.0	16.84	0.0	25.6	19.5	126.46	77.46	61	48.98
04	1020	79.0	21.0	17.44	0.0	25.6	19.7	126.32	73.60	58	52.70
05	380	70.0	30.0	15.96	0.0	25.5	19.8	128.17	68.88	54	49.40
06	380	65.0	35.0	16.63	0.0	26.7	20.7	126.58	83.03	66	42.49
07	690	79.0	21.0	17.59	2.03	26.8	20.7	127.32	99.16	78	26.40
08	380	79.0	21.0	10.82	3.16	26.0	20.0	126.97	93.25	73	26.22
09	380	79.0	21.0	10.95	6.32	22.9	17.6	122.71	93.62	76	22.40
10	1020	79.0	21.0	16.98	1.47	27.0	20.9	127.97	88.98	69	37.33
11	380	70.0	30.0	17.05	1.83	27.7	21.7	128.74	91.20	71	34.00
12	380	65.0	35.0	17.90	1.79	27.2	21.1	129.44	88.83	69	32.00

Table 7.1 gives a summary of oil recovery data. The liquid production as a function of combustion time for the dry combustion runs are presented in Figs. 7.1 to 7.6, together with the water cut (percent cumulative water produced). No liquid was produced during the first 2 hours due to low initial oil and water saturations. This delay period was necessary in order to build up oil and water saturations downstream of the combustion zone. The production profiles are characterised by a high water cut during the early stages of production, followed by an increased oil production rate. This production pattern is believed to be due to a combined effect of increased volume of water resulting from combustion and higher water mobility.

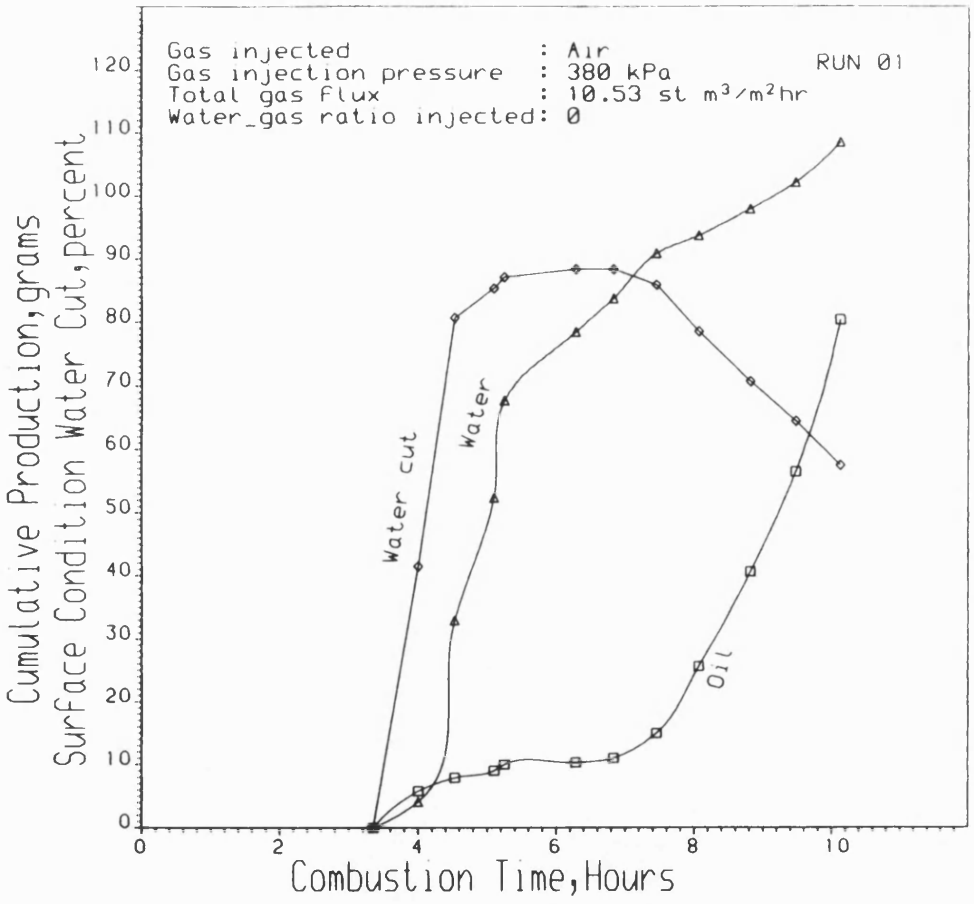

Figure 7.1 LIQUID PRODUCTION HISTORY

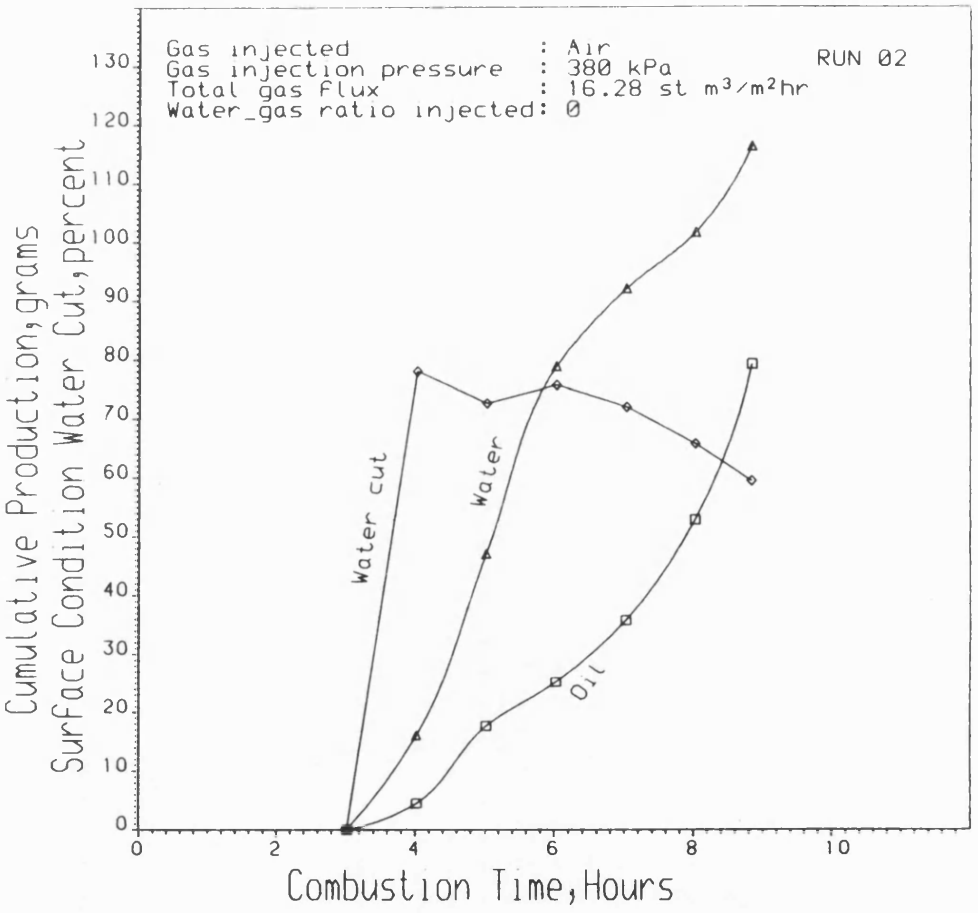

Figure 7.2 LIQUID PRODUCTION HISTORY

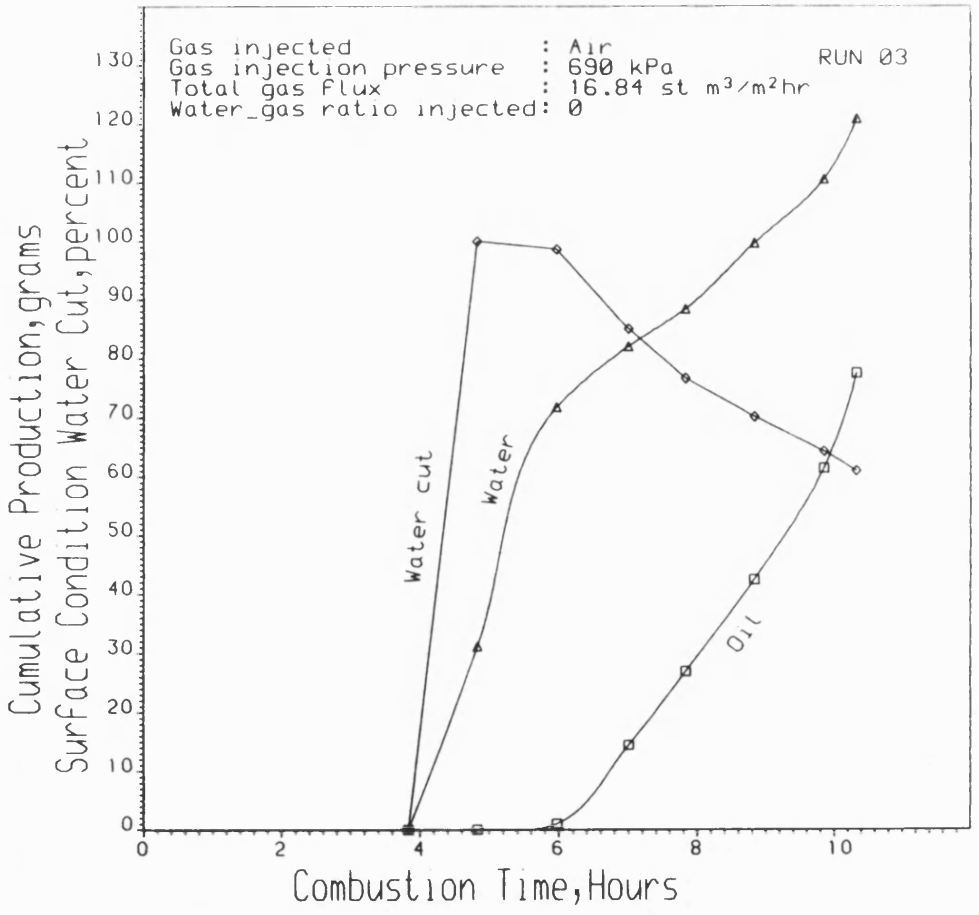

Figure 7.3 LIQUID PRODUCTION HISTORY

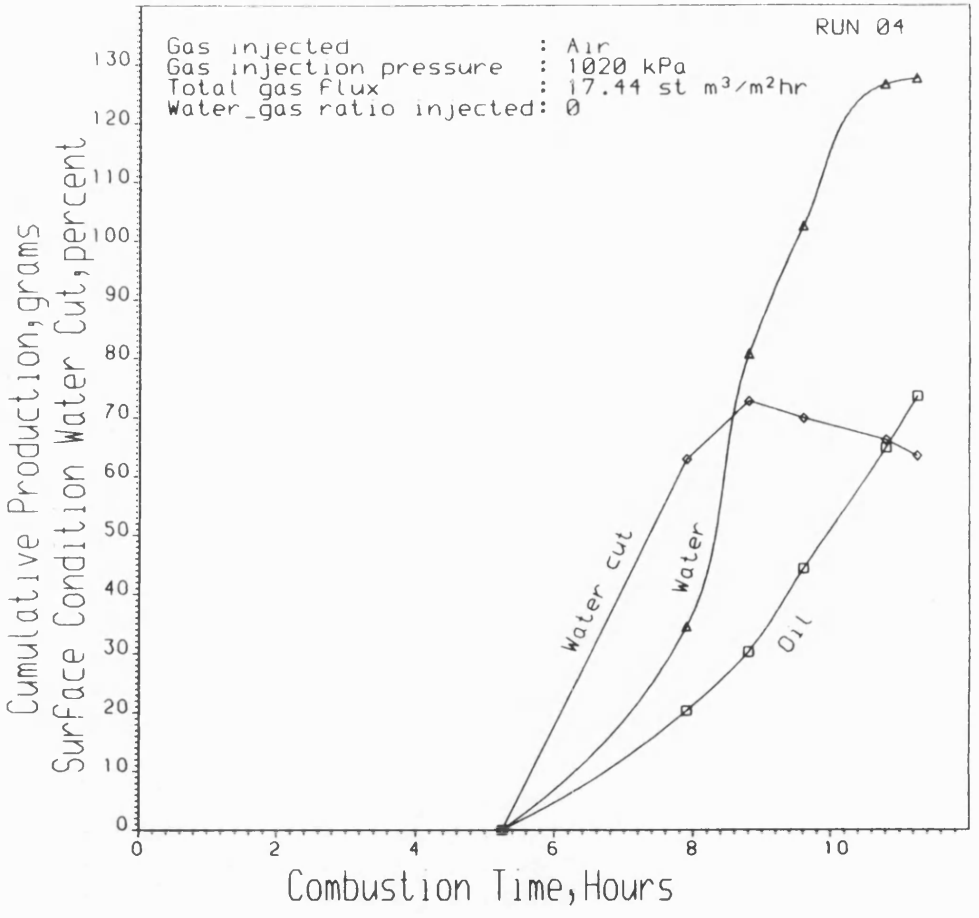

Figure 7.4 LIQUID PRODUCTION HISTORY

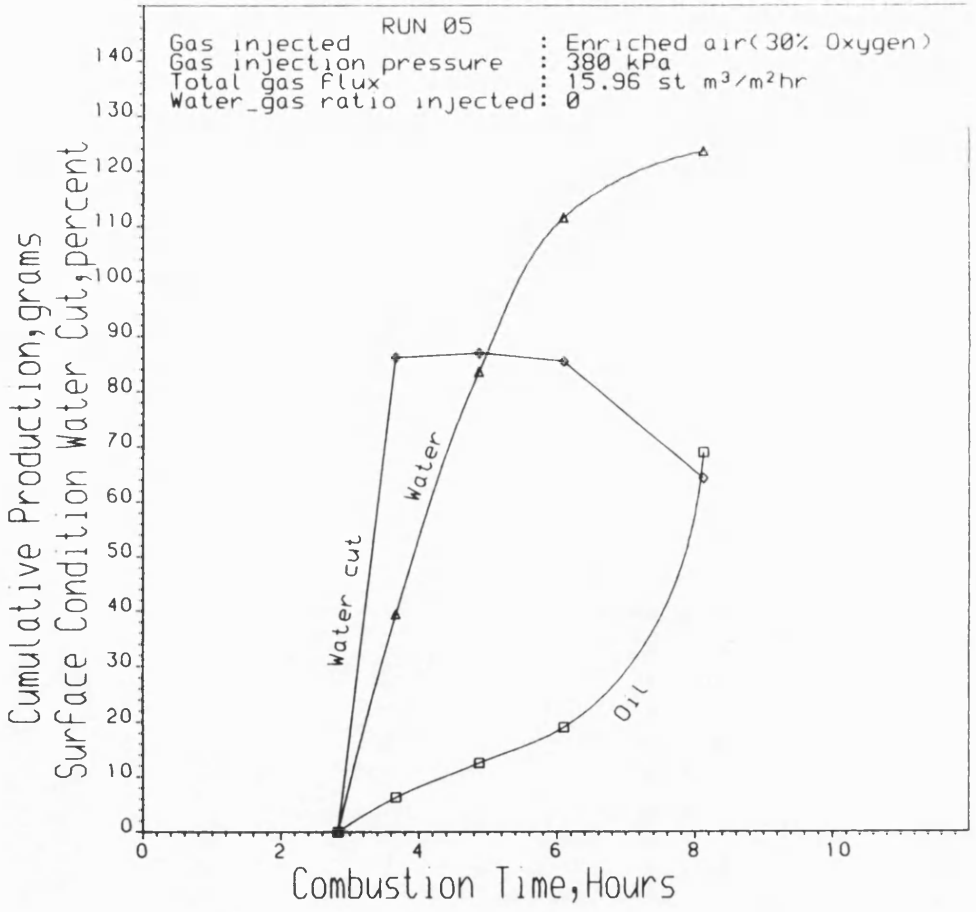

Figure 7.5 LIQUID PRODUCTION HISTORY

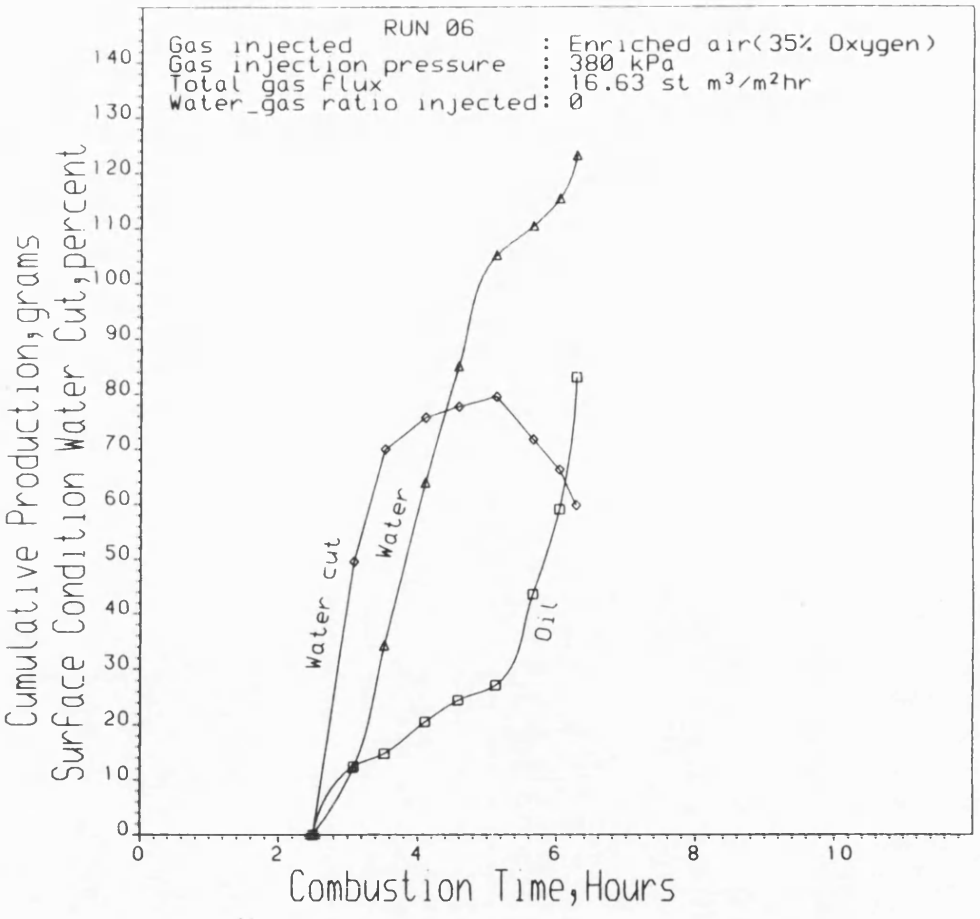

Figure 7.6 LIQUID PRODUCTION HISTORY

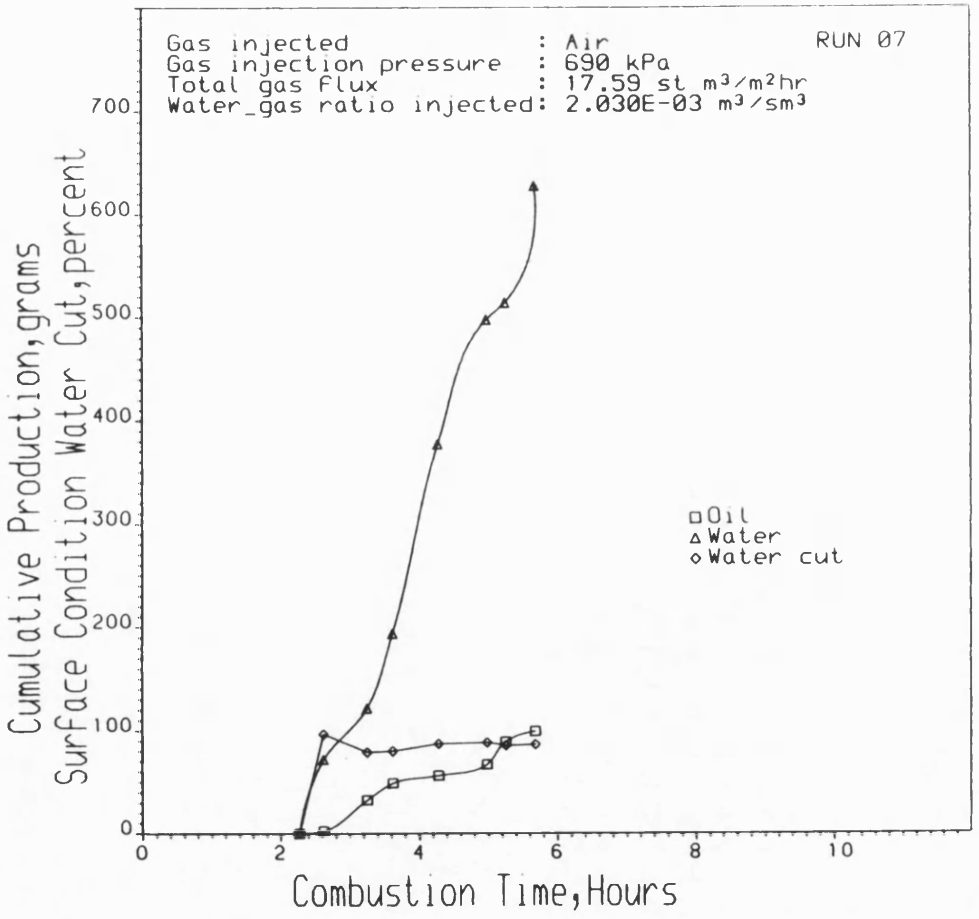

Figure 7.7 LIQUID PRODUCTION HISTORY

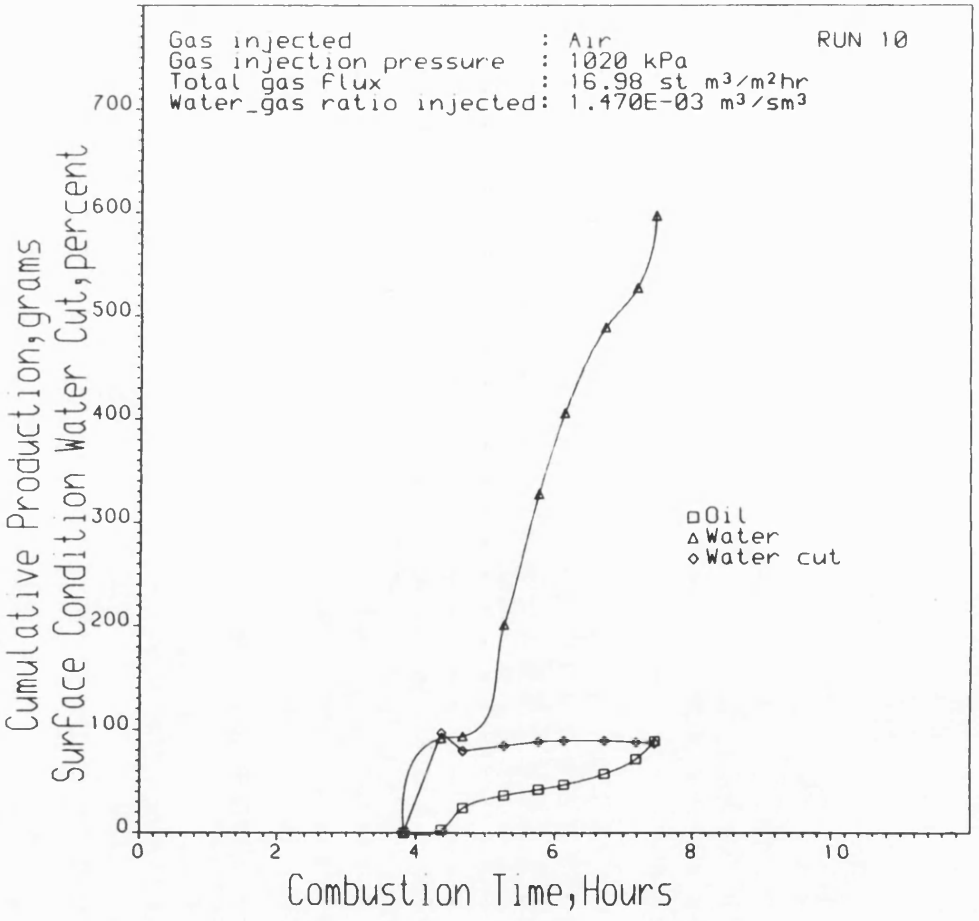

Figure 7.8 LIQUID PRODUCTION HISTORY

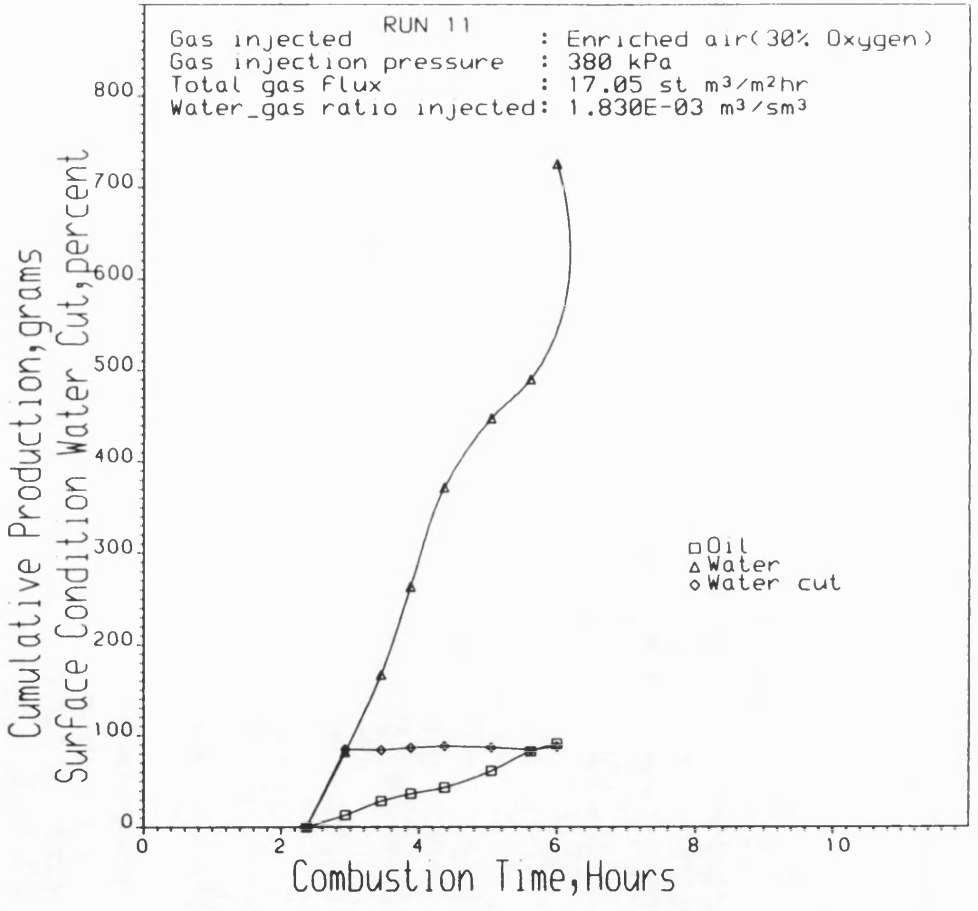

Figure 7.9 LIQUID PRODUCTION HISTORY

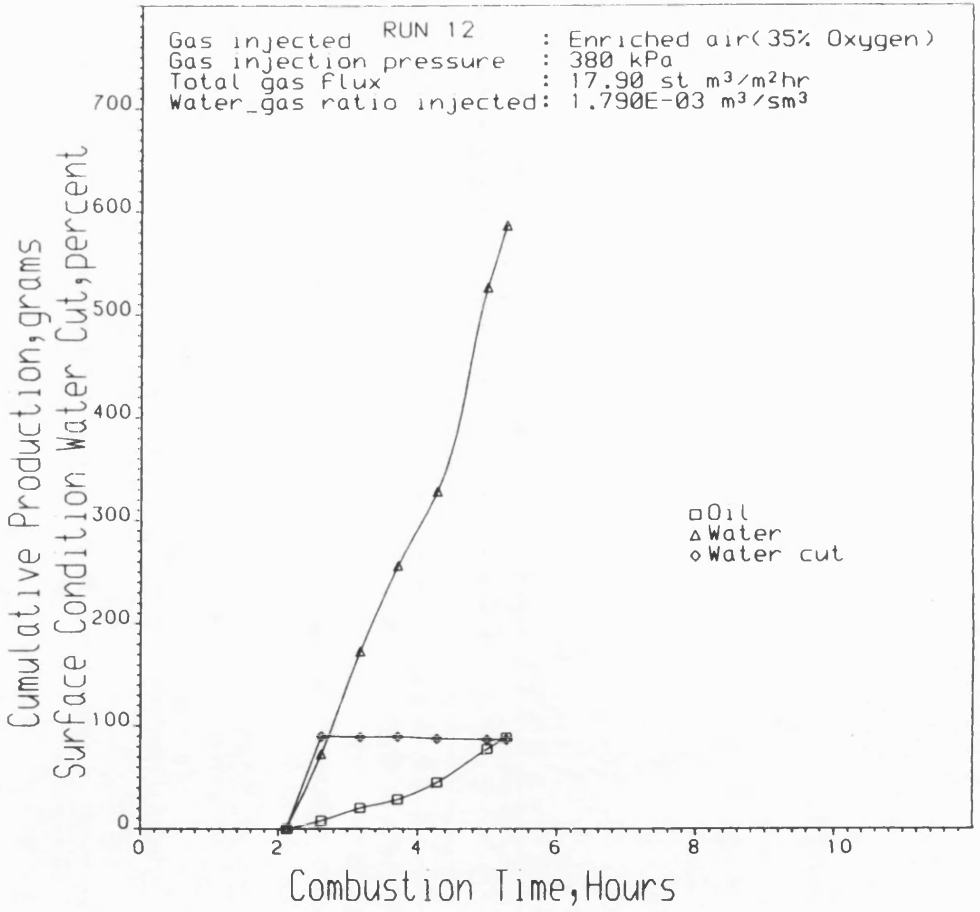

Figure 7.10 LIQUID PRODUCTION HISTORY

Figures 7.7 to 7.10 show typical cumulative liquid production histories for the wet combustion runs. With continuous water injection, the water cut remains relatively constant at a high level, up to 85% w/w. This is in contrast to the pattern in dry combustion in which the water cut shows a general decline from the peak value.

Operating Pressure

Figure 7.11 shows the effect of air injection pressure on the cumulative oil recovery.

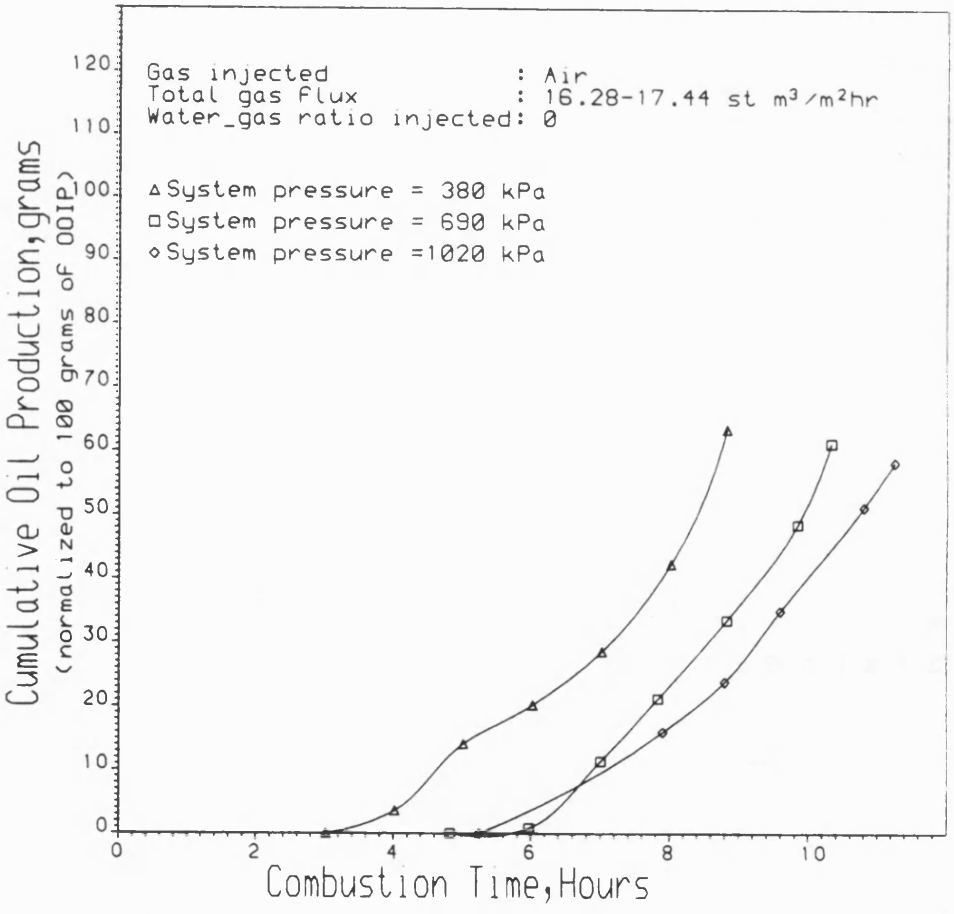

Figure 7.11 EFFECT OF PRESSURE ON CRUDE OIL RECOVERY

The oil production begins much earlier at the lowest pressure used. This is probably due to earlier stabilisation and increased rate of

propagation of the steam zone (Section 5.2), which promotes more rapid build-up of the oil bank and faster displacement towards the production end of the tube. Overall, the rate at which oil is produced is similar at each pressure, with the indication of an increase towards the end of the run for the lower pressure cases. However, the increased fuel concentration at higher pressures results in a slightly lower overall recovery, respectively, 63, 61 and 58% at 380, 690 and 1020 kPa.

Oxygen Enrichment

Figure 7.12 shows the cumulative oil production at different oxygen enrichment levels. At 21% O_2, oil production first starts at 3.02 hours, but then reduces to 2.83 and 2.50 hours with 30% and 35% O_2, respectively. This effect is attributed to the higher velocity of the steam zone as oxygen enrichment increases. Except for the time separation between the curves at 35% oxygen and the lower oxygen levels, there is no dramatic difference in the production pattern. However, there is an earlier onset of greatly increased production rate at the 35% oxygen level. Significantly, also, the highest overall oil recovery is obtained in the shortest period using 35% O_2. This is believed to be due to the combined effect of increased size and velocity of the steam zone which promotes more efficient steam flooding (section 5.2.2). The trend observed in the overall oil recovery is consistent with the pattern of fuel consumption described in section 5.6.

Water Injection

Figures 7.13 to 7.16 show that more oil is recovered with water injection compared to dry combustion.

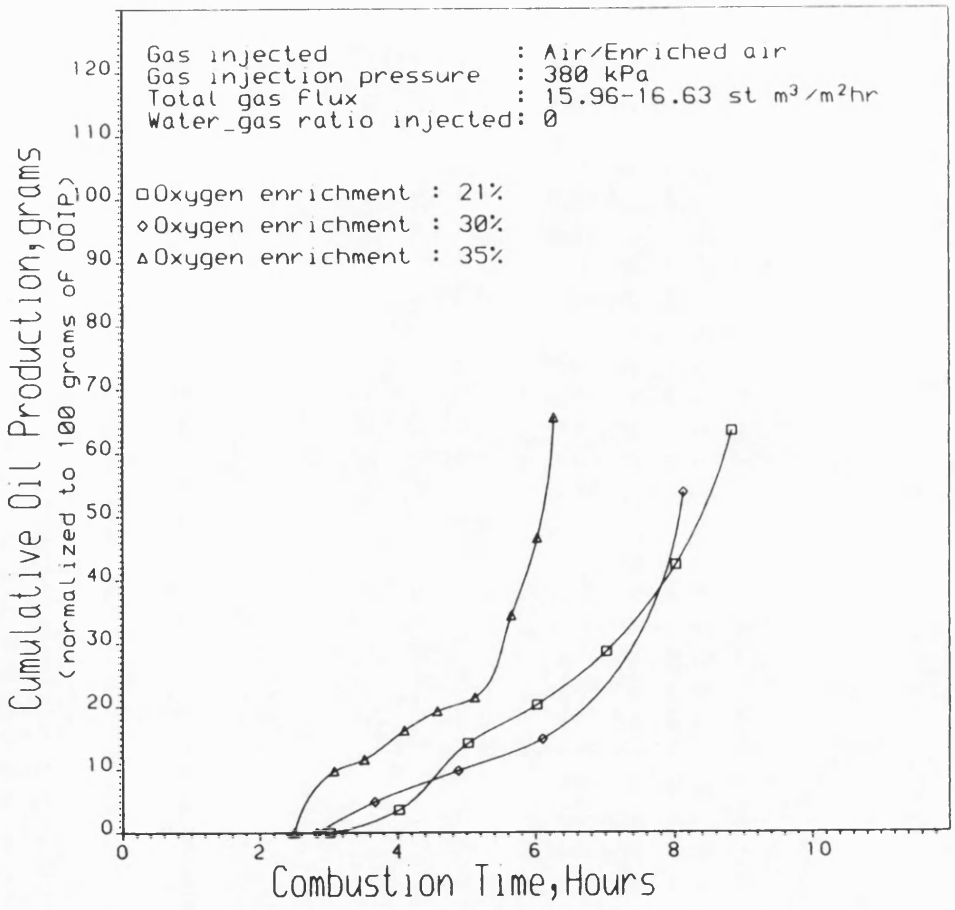

Figure 7.12 EFFECT OF OXYGEN ENRICHMENT ON CRUDE OIL RECOVERY

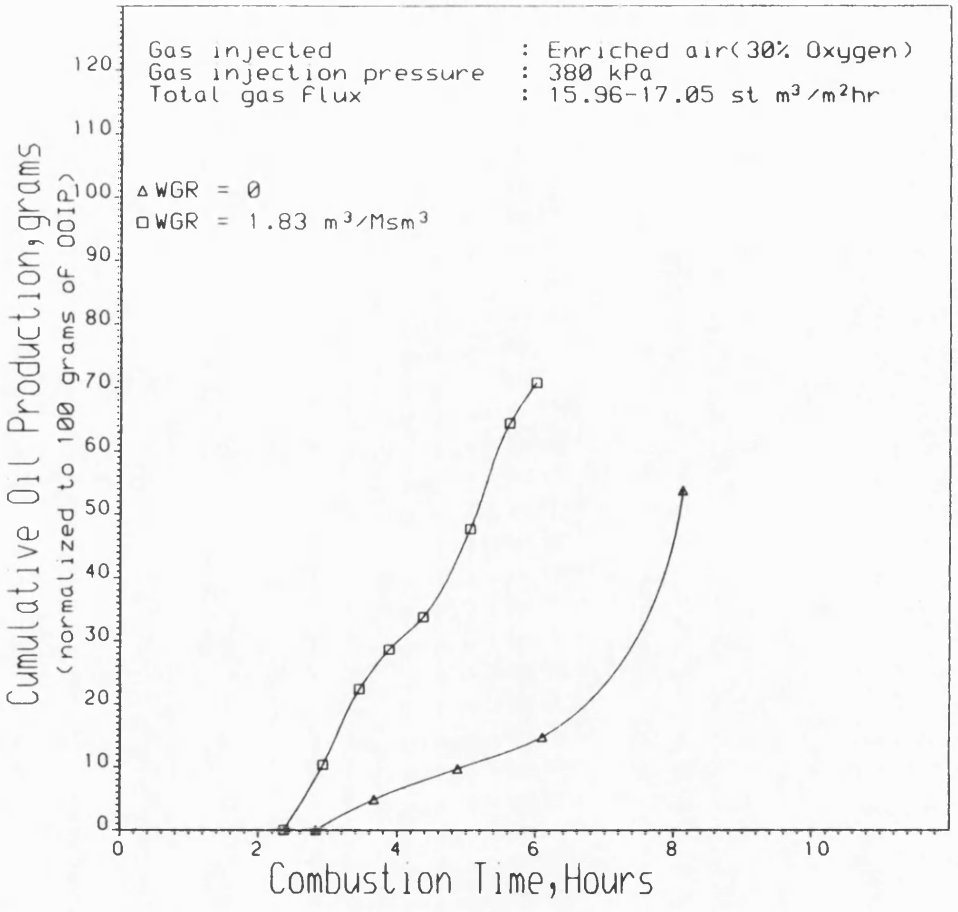

Figure 7.13 EFFECT OF WATER INJECTION (WITH AIR) ON CRUDE OIL RECOVERY

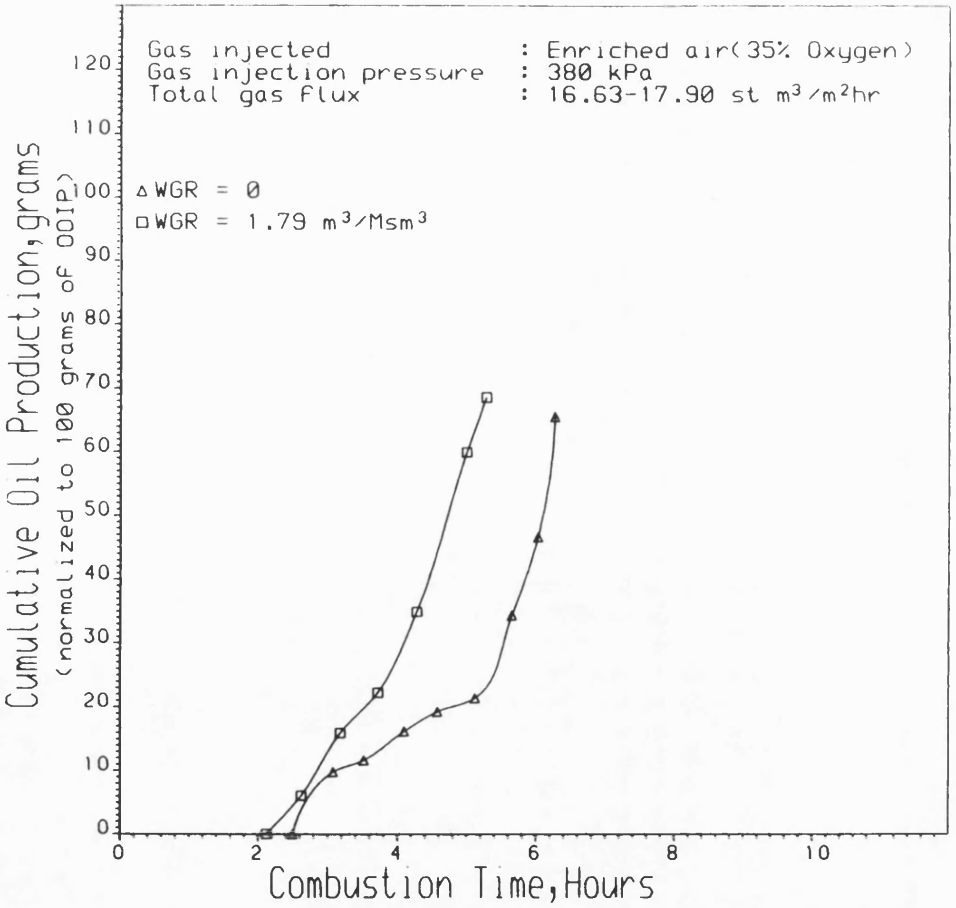

Figure 7.14 EFFECT OF WATER INJECTION (WITH AIR) ON CRUDE OIL RECOVERY

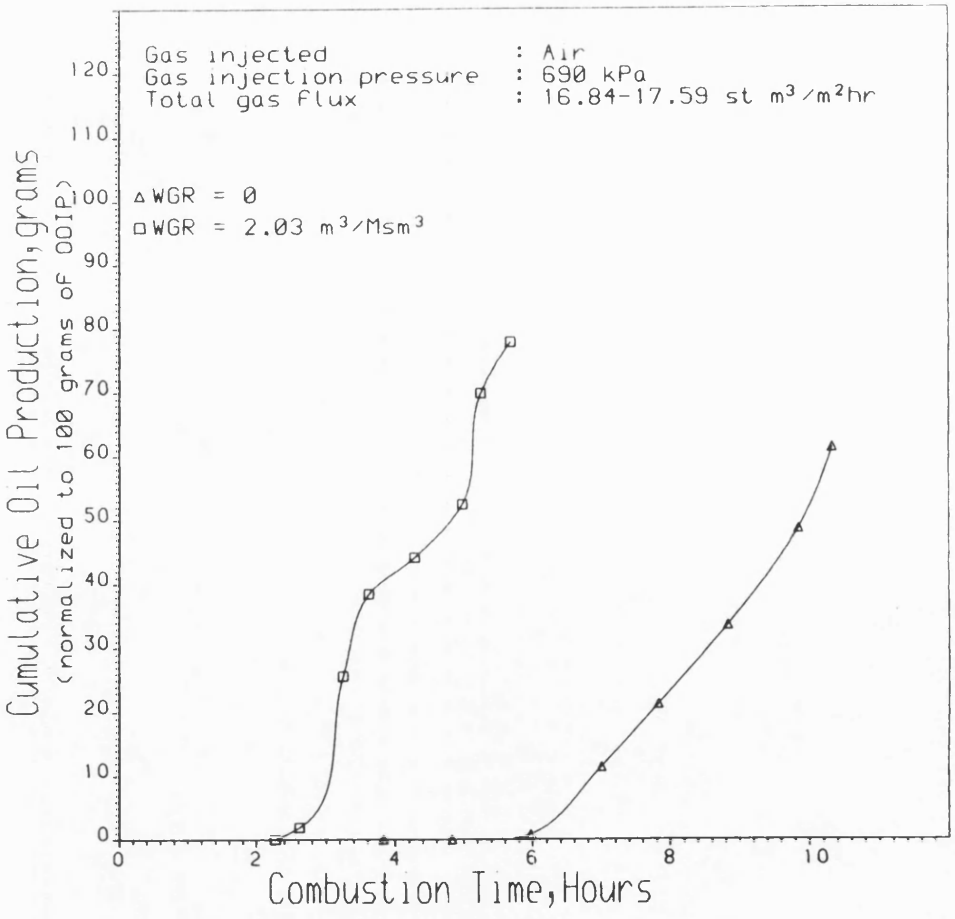

Figure 7.15 EFFECT OF WATER INJECTION (WITH AIR) ON CRUDE OIL RECOVERY

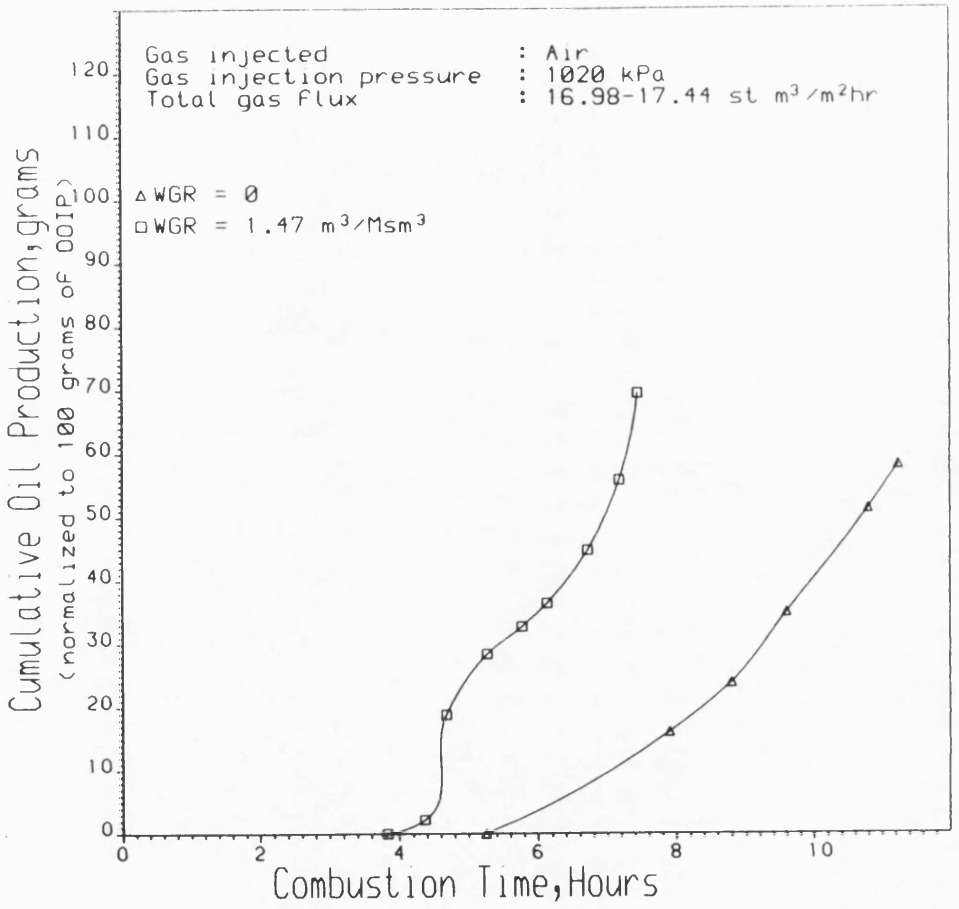

Figure 7.16 EFFECT OF WATER INJECTION (WITH AIR) ON CRUDE OIL RECOVERY

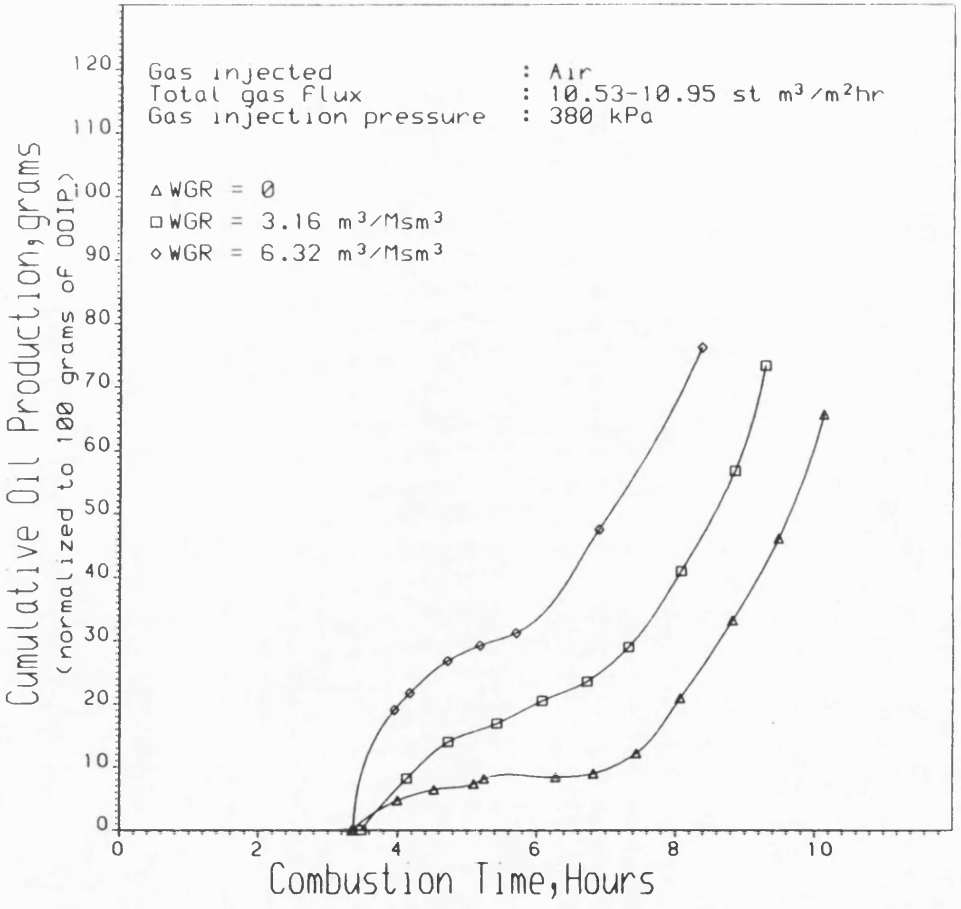

Figure 7.17 EFFECT OF WATER INJECTION RATE ON CRUDE OIL RECOVERY

Typically, at an injection pressure of 690kPa, the overall recovery increases from 61% in Run 3 (WGR = 0) to 78% in Run 7 (WGR = 2.03). At 1020kPa, with a WGR of 1.47m^3/Msm^3, the recovery increases by 11% in Run 10 compared with Run 4 (WGR = 0). The decrease in fuel concentration during wet combustion is the main factor affecting oil production. Furthermore, in wet combustion, oil production starts earlier and is accompanied by a higher overall production rate than in dry combustion. The incremental effect of water injection rate is further detailed in Fig. 7.17. It is, however, noticeable that the start of oil production is not significantly different with water injection, even though high WGR's were used. This can be attributed to late commencement of water injection in these cases, taking place at 2.82 and 3.17 hours respectively, for WGR = 3.16 and 6.32 m^3/Msm^3. Nevertheless, there is a substantial increase in the rate of oil production with increasing WGR, though the rates eventually became approximately the same. The overall oil recovery also shows a significant increase as indicated by the terminal values. This trend agrees with the findings of Alderman et al. (1971).

7.2 Liquid Mass Balances

Table 7.2 gives a summary of the liquid mass balance for each combustion run. Appendix C contains a sample calculation of the mass balance for Run 10. The difference in oil balance varies from 0.02g in Run 3 to 11.82g in Run 1, corresponding to error of 0.01 to 9.67 percent. The error in the water balance, however, varies from -2.66 percent in Run 11 to 12.21 percent in Run 10. The maximum error in the overall liquid balance for the dry and wet combustion runs is 10.42 percent.

TABLE 7.2 IN-SITU COMBUSTION LIQUID MASS BALANCES

RUN NO:-	01	02	03	04	05	06	07	08	09	10	11	12
OIL BALANCE												
Initial Oil in sand pack, g	122.26	124.89	126.46	126.33	128.17	126.48	127.32	126.97	122.71	127.97	128.74	129.44
Oil produced as liquid, g	80.23	79.30	77.46	73.60	68.88	83.03	99.16	93.25	93.62	88.98	91.20	88.83
Oil consumed as fuel, g	30.21	40.32	48.98	52.70	49.40	42.49	26.40	26.22	22.40	37.33	34.00	32.00
Oil produced as gas, g	0.00	0.22	0.00	0.00	0.00	0.17	0.00	0.00	0.00	0.06	0.00	0.69
Residual H-C in sand pack, g	0.00	0.00	0.00	0.00	0.00	0.00	1.70	4.52	5.67	1.02	1.59	3.54
Total, g	110.44	119.84	126.44	126.30	118.28	125.69	127.26	123.99	121.69	127.39	126.79	125.06
Difference, g	11.82	5.05	0.02	0.03	9.89	0.89	0.06	2.98	1.02	0.58	1.95	4.38
Percent error in balance	9.67	4.04	0.01	0.02	7.71	0.71	0.05	2.35	0.83	0.45	1.51	3.38
WATER BALANCE												
Initial water in sand pack, g	103.50	106.61	104.85	105.72	108.52	107.17	107.18	106.58	103.00	107.73	109.94	109.60
Water injected, g	0.00	0.00	0.00	0.00	0.00	0.00	578.20	901.60	1586.00	558.60	565.95	490.00
*Combustion Water, g	16.85	24.32	24.07	33.91	28.21	29.04	13.53	13.37	14.54	43.13	31.07	36.09
Total, g	120.35	130.93	128.92	139.63	136.73	136.21	698.91	1021.55	1703.54	709.46	706.96	635.69
Produced water, g	108.50	116.41	120.92	127.69	123.60	123.20	627.42	924.14	1606.52	597.51	726.30	587.33
Residual water in sand pack, g	0.00	0.00	0.00	0.00	0.00	0.00	0.00	0.00	0.00	25.29	0.00	0.00
Total, g	108.50	116.41	120.92	127.69	123.60	123.20	627.42	924.14	1606.52	622.80	726.30	587.33
Difference	11.85	14.52	8.00	11.94	13.13	13.01	71.49	92.41	97.02	86.65	-19.34	48.36
Percent error in balance	9.85	11.09	6.21	8.55	9.60	9.55	10.23	9.05	5.69	12.21	-2.66	7.61
OVERALL PERCENT ERROR	9.76	7.65	3.14	4.50	8.69	5.29	8.66	8.31	5.37	10.42	-2.08	6.89

* Water generated by combustion

Discrepancies in the liquid mass balance are due to the cumulative errors arising from the measured data. For example, errors resulted from manual control of the exit gas flow rate, particularly in the low range (0-0.98sm^3/hr), and also the use of average values of produced gas compositions in calculating the total volume of gas injected, and carbon and hydrogen consumed. As shown in Appendix C, a small error is incurred by using nitrogen as the tie component due to accumulation of small volume of injected gas in the burned zone. It was assumed that the produced gas was saturated with water at 0°C but this also contributes a very small error (see Appendix C). Water generated by combustion was calculated from the oxygen balance, assuming that all of the oxygen not observed in the exit gases reacted to form water. This assumption is not strictly valid, but since high oxygen utilisation is obtained in this study, the amount consumed by LTO reactions is only of a small order.

Losses due to liquid handling, during downstream separation constitute another source of error. The extraction procedure for determining liquid saturations in the post-burn sand uses very small fractions of the material. The procedure requires very careful and accurate measurement, and so, any small error incurred will be compounded when the saturation values are applied to sand pack. This is probably the major source of error in the liquid mass balances.

7.3 Properties of Produced Oil

Table 7.3 provides a summary of the physical properties of the original crude and the produced oils. The specific gravities, viscosities (at 100°F) and the molal average boiling points were determined experimentally. These were used to estimate the API gravity, molecular weight and C/H weight ratio.

The simulated distillation data obtained for each oil were used to generate the boiling point distribution curves presented in Figs. 7.18 to 7.29. From these curves, the molal average boiling points, corresponding to 50% temperature distribution point, were estimated. Inspection of these curves reveals that a small fraction of the lightest components and a few percent (up to 10% in some cases) of the heaviest components were consumed by combustion. In addition, the produced oil contains appreciably more material in the gasoline range (Bpt. $\leq$ 235°C), which lowers the molal average boiling points compared to the original crude.

The API gravity, molecular weight and the Carbon-to-hydrogen weight ratio for each oil are determined from the nomograph in Fig. 7.32. As shown in Table 7.3, the produced oils have higher API gravities, but lower viscosities and molecular weights than the original crude. Furthermore, the C/H weight ratio is also reduced. Figures 7.30 and 7.31 depict the viscosities of the original crude and the produced oils as a function of temperature, as estimated from Fig. 7.33. All of these trends are in agreement with those reported by Penberthy (1967), Omar Allag (1978) and Jon T.

Moss (1982). They clearly reveal that the oil produced by in-situ combustion is upgraded compared to the original oil in place.

TABLE 7.3 PHYSICAL PROPERTIES OF ORIGINAL AND PRODUCED OIL

SAMPLE	SPECIFIC GRAVITY	VISCOSITY at 100°F Cp	AVG. MOLAL BOILING POINT °C	GASOLINE RANGE %VOL.	API gravity Degrees	MOLECULAR WEIGHT	C/H WEIGHT RATIO
IN-PLACE OIL	0.917	40.0	275.4	29.6	22.8	204	7.87
PRODUCED OIL:							
RUN 01	0.883	13.0	204.6	69.2	28.7	151	7.54
RUN 02	0.854	5.5	231.6	56.6	34.2	178	6.92
RUN 03	0.867	7.8	197.5	69.3	31.7	148	7.28
RUN 04	0.863	6.8	187.0	67.9	32.5	142	7.26
RUN 05	0.861	6.6	216.2	58.5	32.8	164	7.10
RUN 06	0.886	14.5	237.0	49.8	28.2	178	7.45
RUN 07	0.866	7.5	231.8	54.4	31.9	176	7.20
RUN 08	0.870	8.4	181.2	68.6	31.1	137	7.43
RUN 09	0.875	9.9	211.4	61.4	30.2	157	7.38
RUN 10	0.883	13.0	206.0	61.0	28.7	153	7.54
RUN 11	0.867	7.6	233.0	50.1	31.7	177	7.12
RUN 12	0.861	6.6	169.8	80.5	32.8	128	7.33

7.4 Conclusions

The main conclusions concerning the recovery and properties of the produced oil under dry and wet combustion conditions are as follows:

1. Generally, the start of oil production is dependent upon the operating parameters (and the initial oil saturation). Lower operating pressure and increasing level of oxygen enrichment in the injected gas favour an early start of oil production. Similar

behaviour is obtained with water injection, but this depends on how soon after ignition, water injection begins.

2. The liquid production pattern in dry combustion is characterised by a high water cut (65 - 100% w/w) during the early stages of production, which is then followed by an increase in the oil production rate. During wet combustion, the water cut is maintained at a relatively constant level, reaching as high as 85% w/w.

3. Water injection results in increased oil recovery due to a reduction in the fuel concentration. Typically, at 1020 kPa, the overall recovery increases from 58% (WGR = 0) to 69% using WGR = 1.47m^3/Msm^3. It also shows an increasing trend with increasing WGR. However, the trend is reversed as combustion tube pressure increases. An increase of up to 3% in oil recovery is also obtained at 35% oxygen enrichment compared with air.

4. The rate of oil recovery initially shows an increase with water injection but the rates for different WGR's tend to equalise during later stages of combustion. The rate of oil recovery is also higher when 35% O_2 is used compared with air, but decreased with increasing pressure.

5. The combustion of heavy components leads to an upgrading of the produced oil. This is evidenced by an increase in the C_5 to C_{13} content, higher API gravity, reduced viscosity, lower molecular weight and a decreased C/H weight ratio.

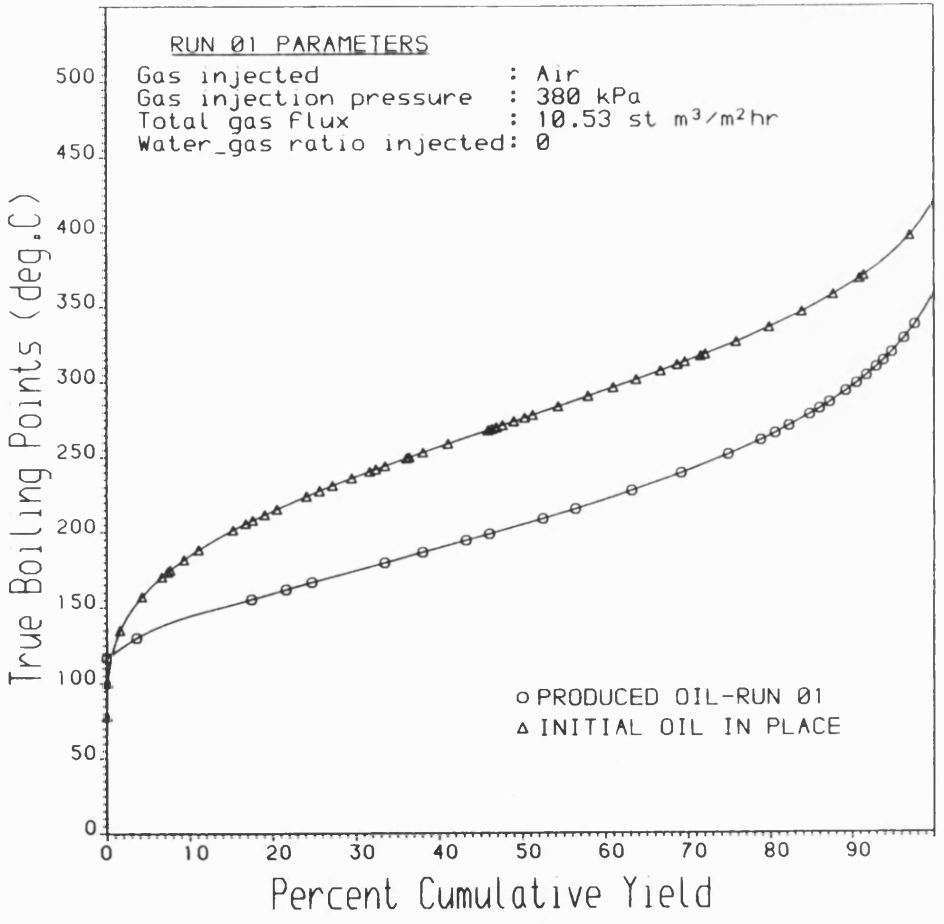

Figure 7.18 SIMULATED BOILING POINT DISTRIBUTION CURVE OF MAYA CRUDE

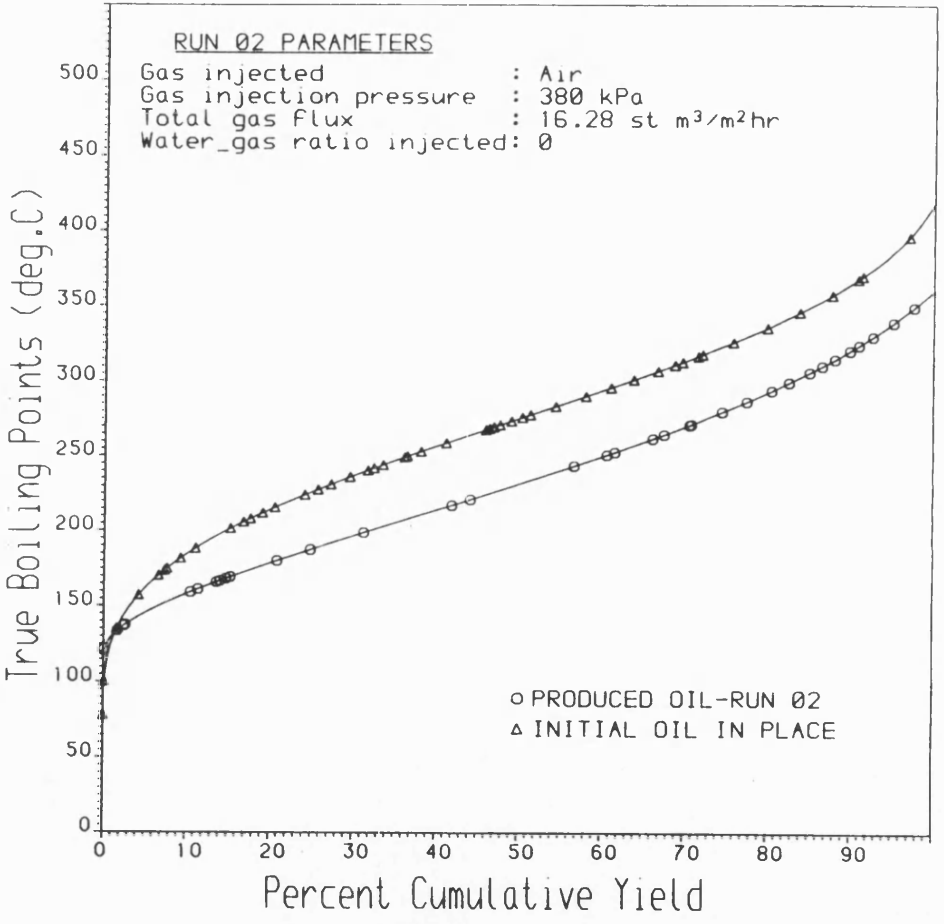

Figure 7.19 SIMULATED BOILING POINT DISTRIBUTION CURVE OF MAYA CRUDE

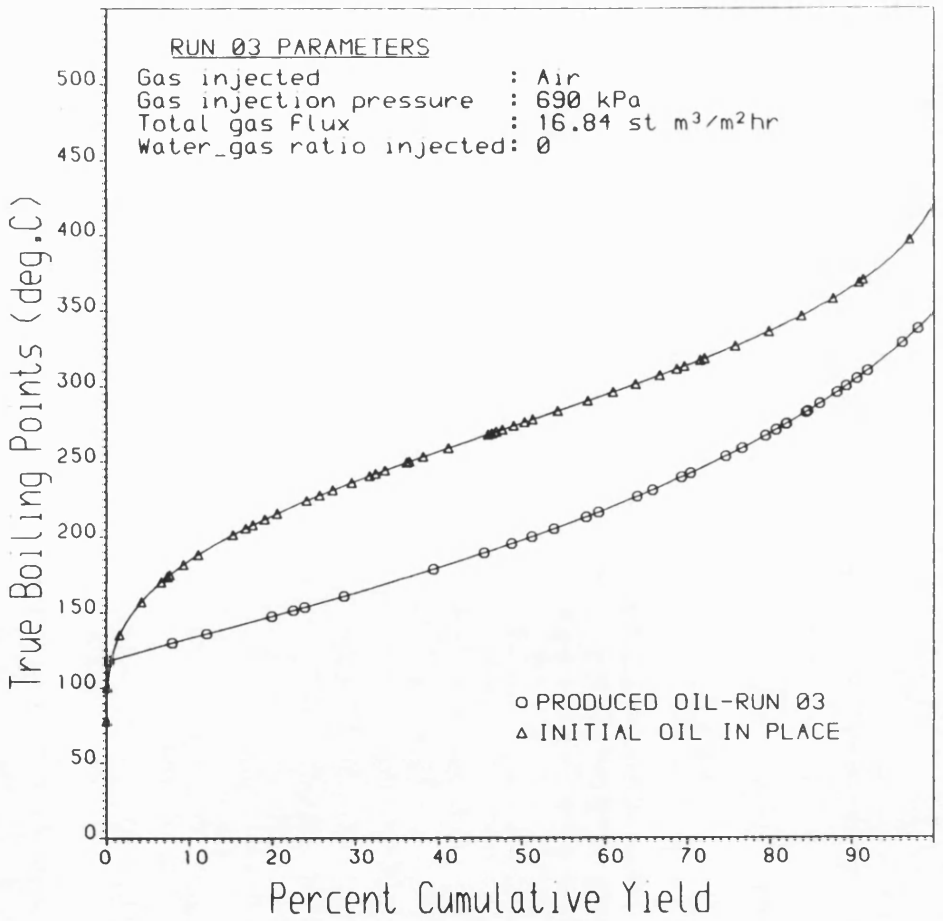

Fig. 7.20 SIMULATED BOILING POINT DISTRIBUTION CURVE OF MAYA CRUDE

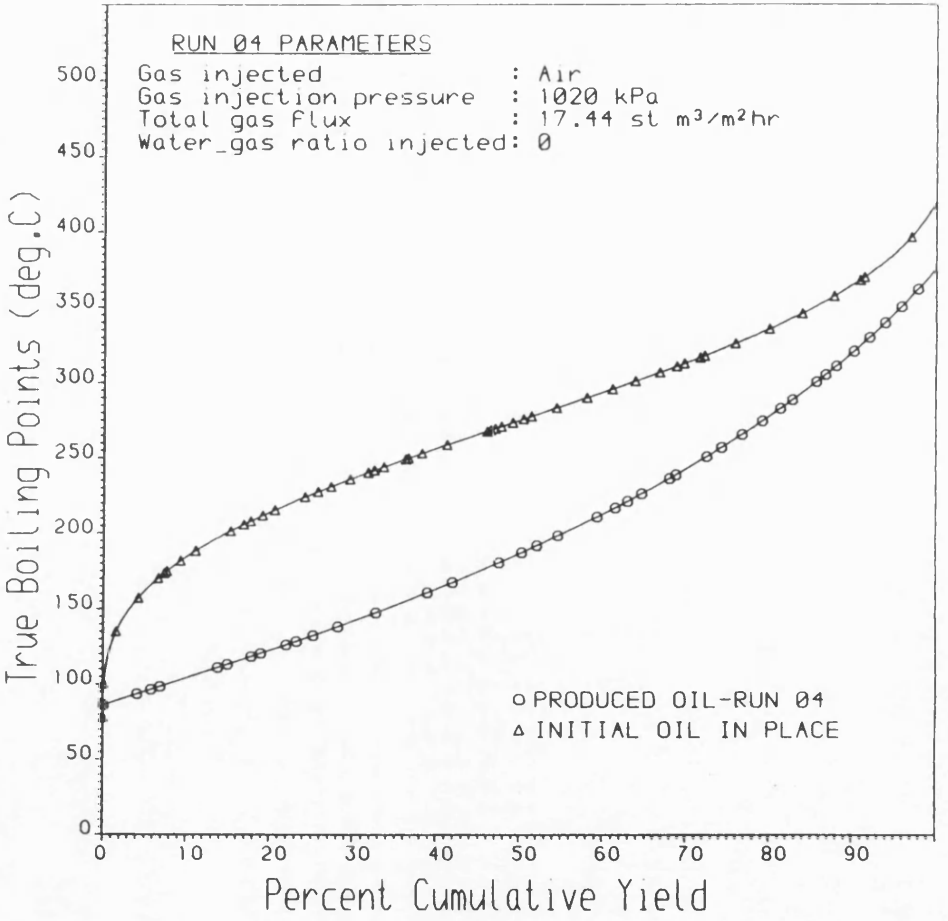

Fig. 7.21 SIMULATED BOILING POINT DISTRIBUTION CURVE OF MAYA CRUDE

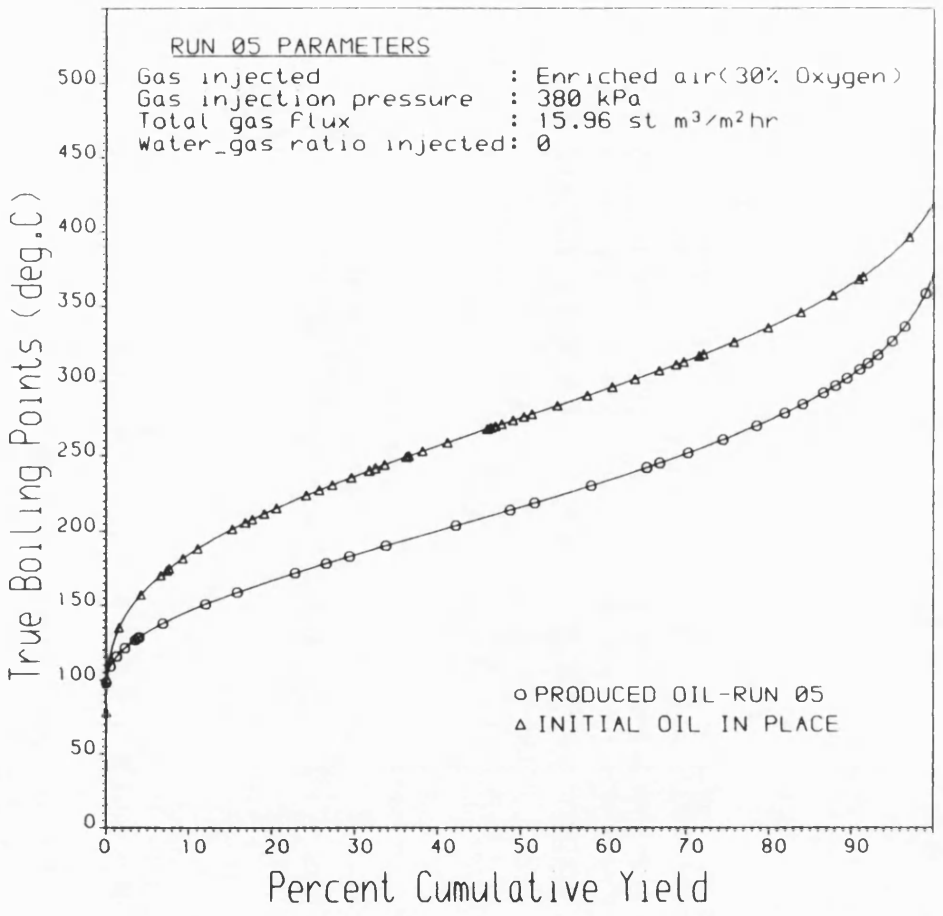

Fig. 7.22 SIMULATED BOILING POINT DISTRIBUTION CURVE OF MAYA CRUDE

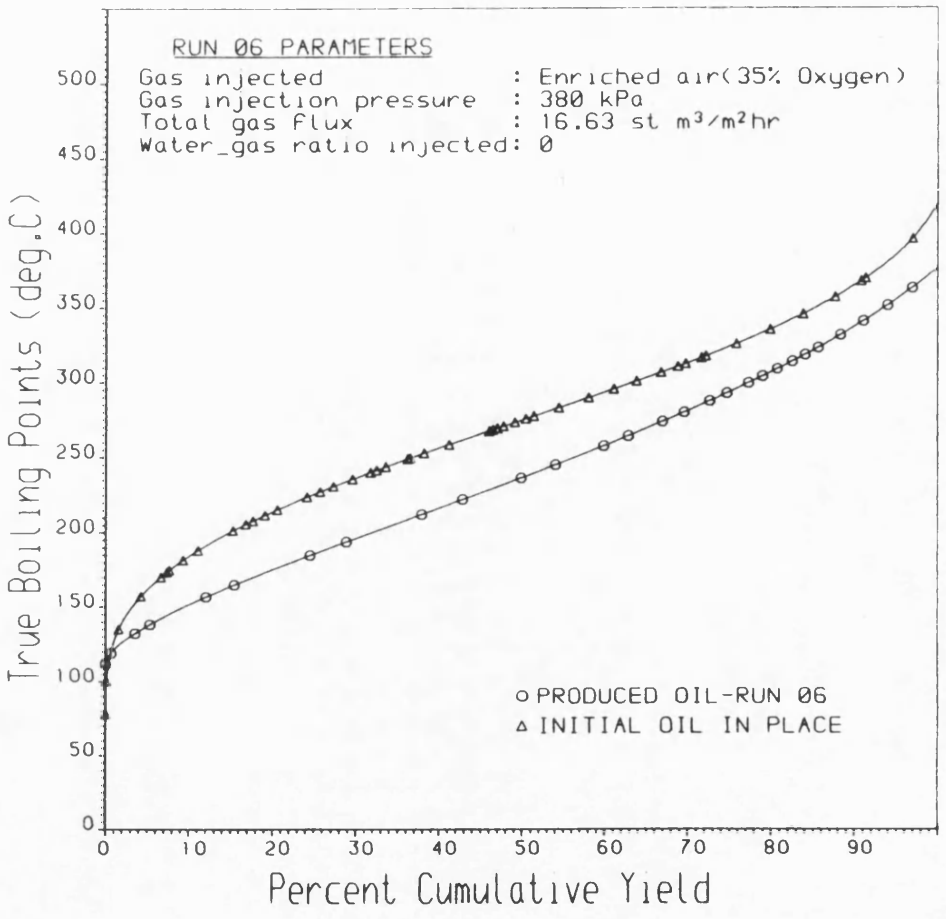

Fig. 7.23 SIMULATED BOILING POINT DISTRIBUTION CURVE OF MAYA CRUDE

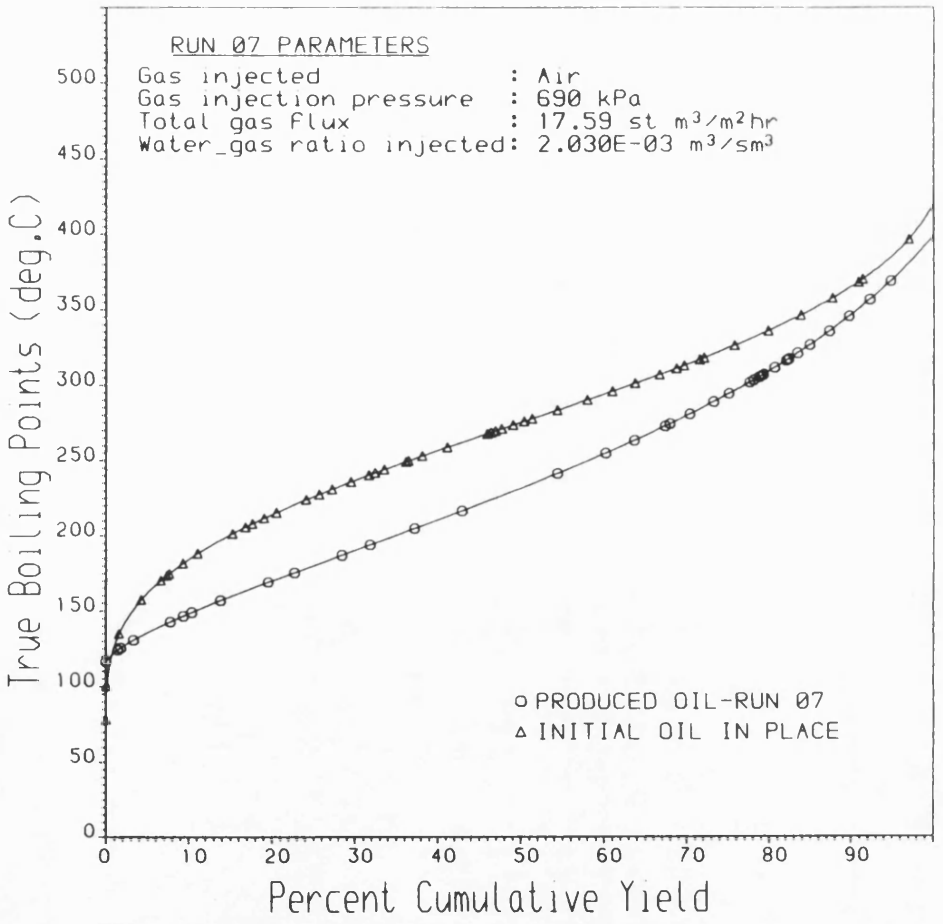

Fig. 7.24 SIMULATED BOILING POINT DISTRIBUTION CURVE OF MAYA CRUDE

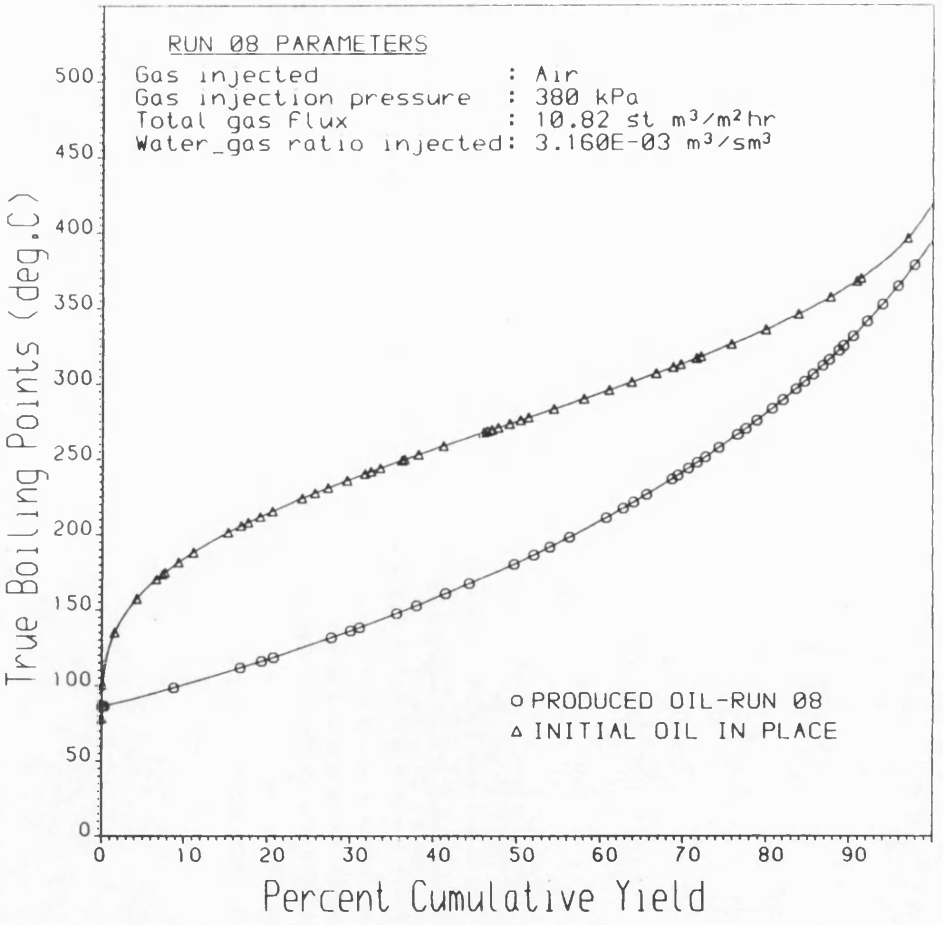

Fig. 7.25 SIMULATED BOILING POINT DISTRIBUTION CURVE OF MAYA CRUDE

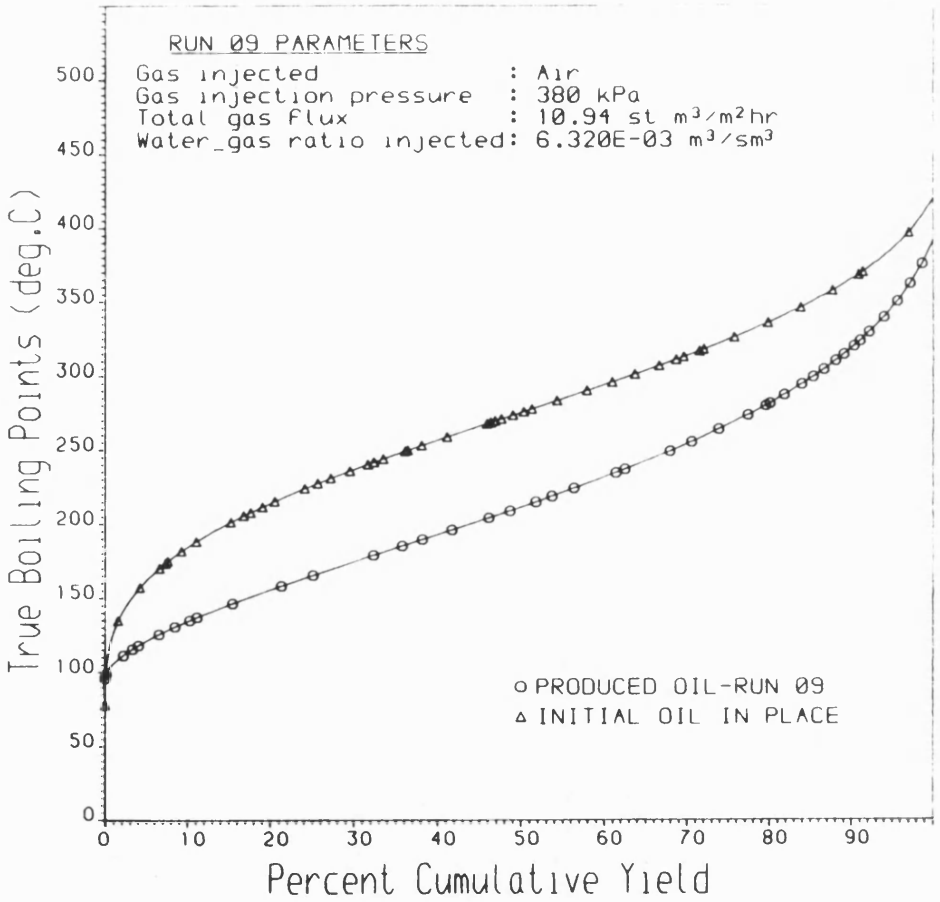

Fig. 7.26 SIMULATED BOILING POINT DISTRIBUTION CURVE OF MAYA CRUDE

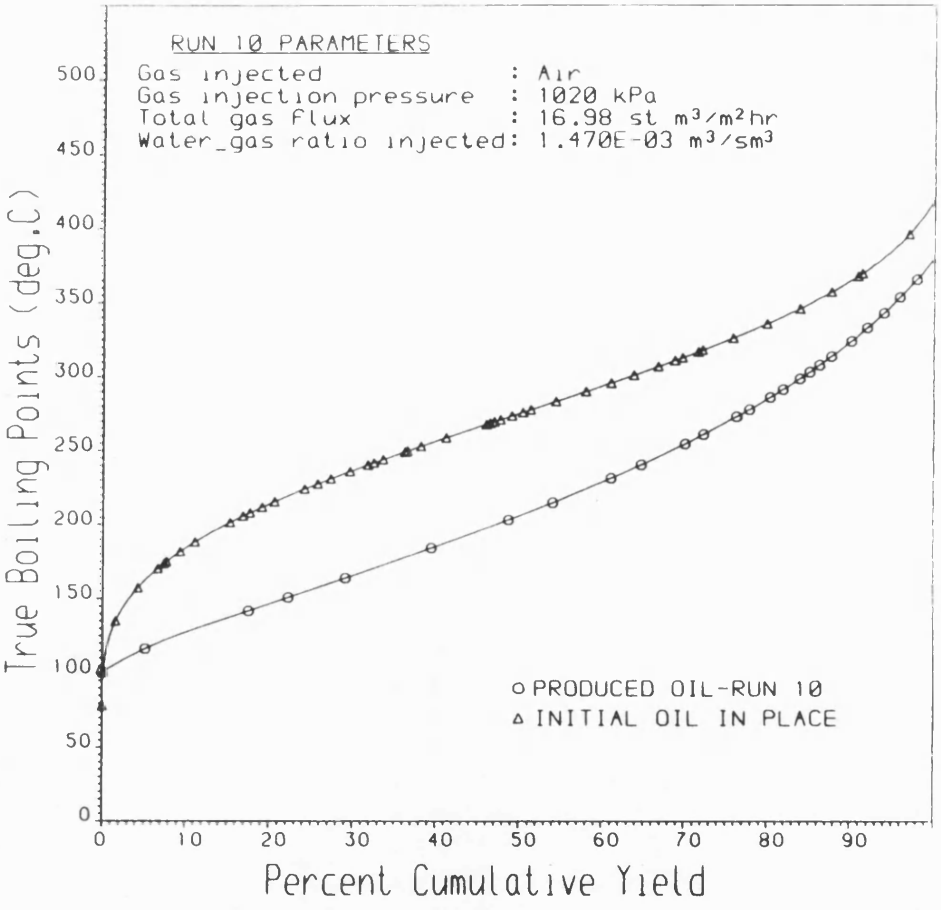

Fig. 7.27 SIMULATED BOILING POINT DISTRIBUTION CURVE OF MAYA CRUDE

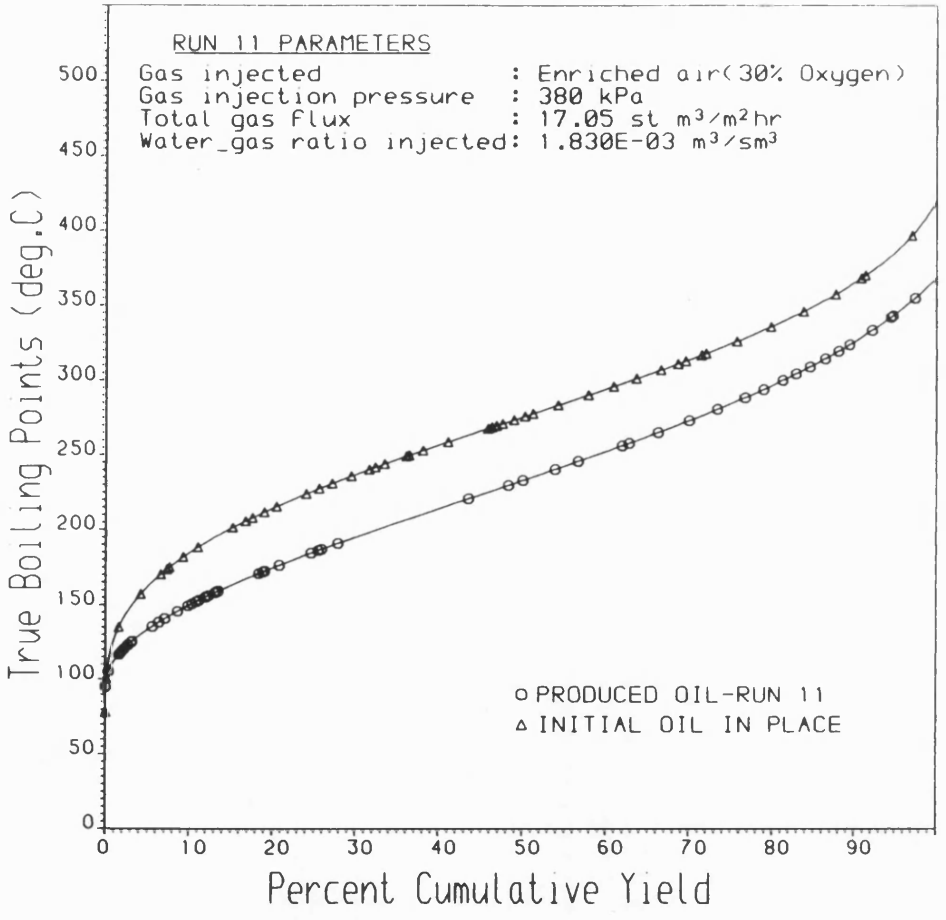

Fig.7.28 SIMULATED BOILING POINT DISTRIBUTION CURVE OF MAYA CRUDE

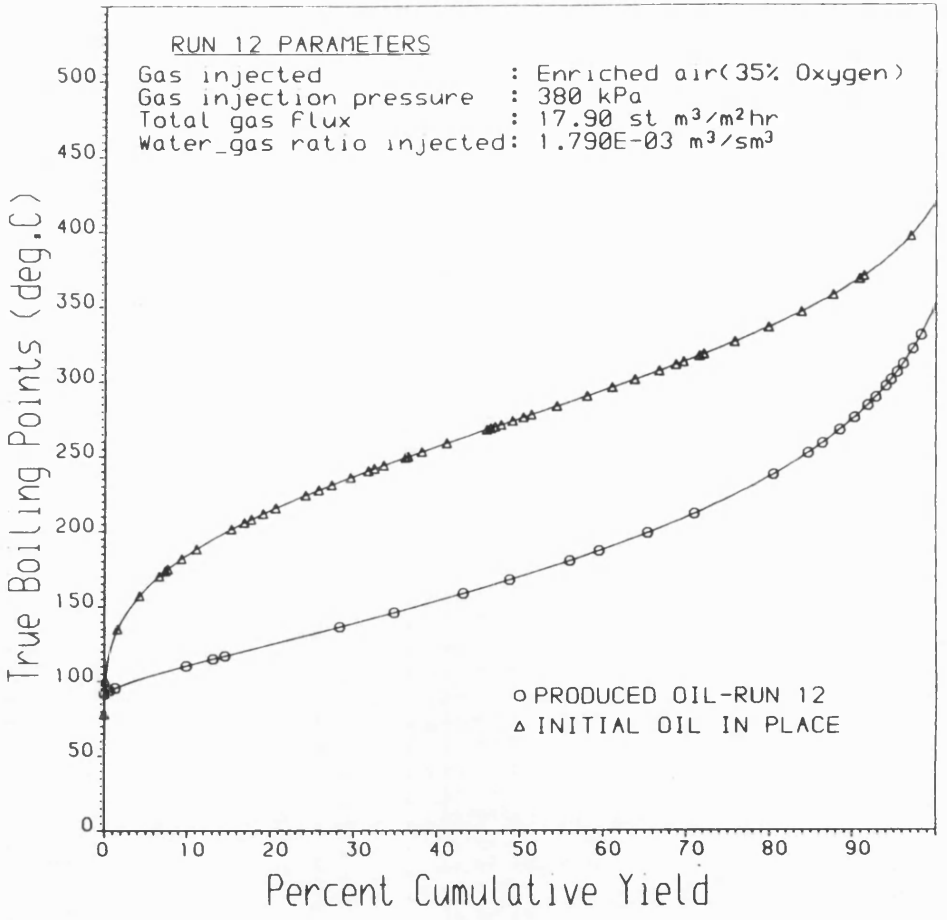

Fig. 7.29 SIMULATED BOILING POINT DISTRIBUTION CURVE OF MAYA CRUDE

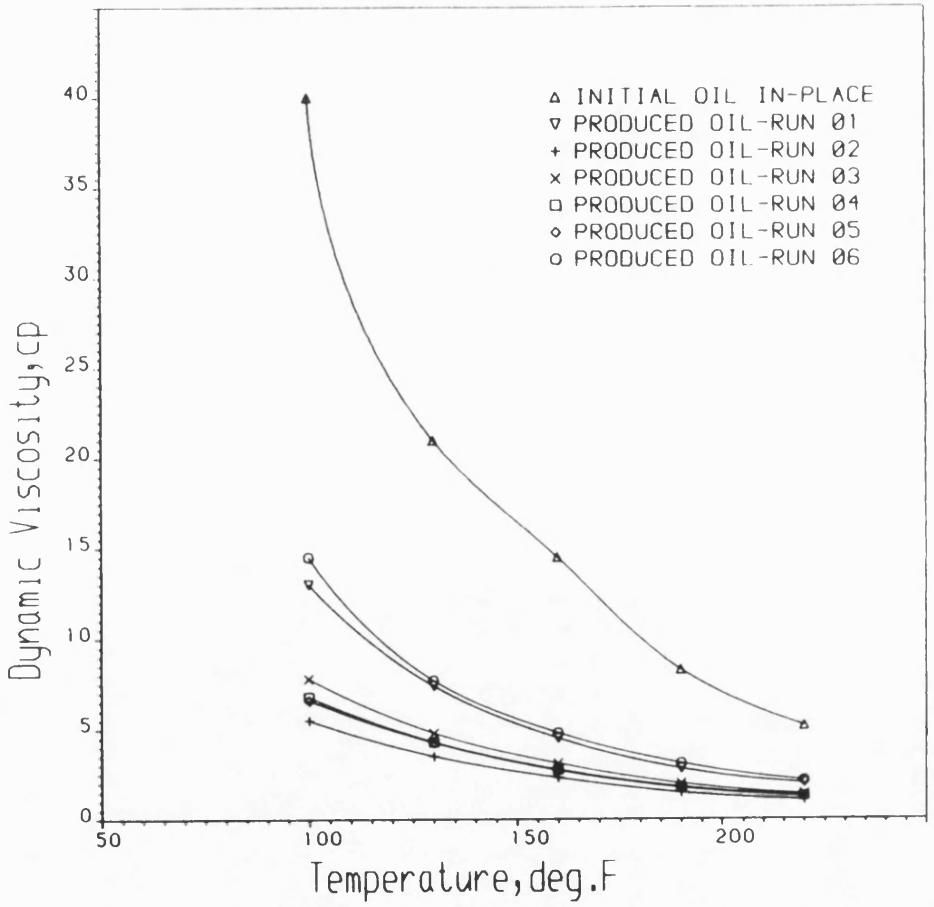

Fig. 7.30 VISCOSITY OF MAYA CRUDE Vs. TEMPERATURE

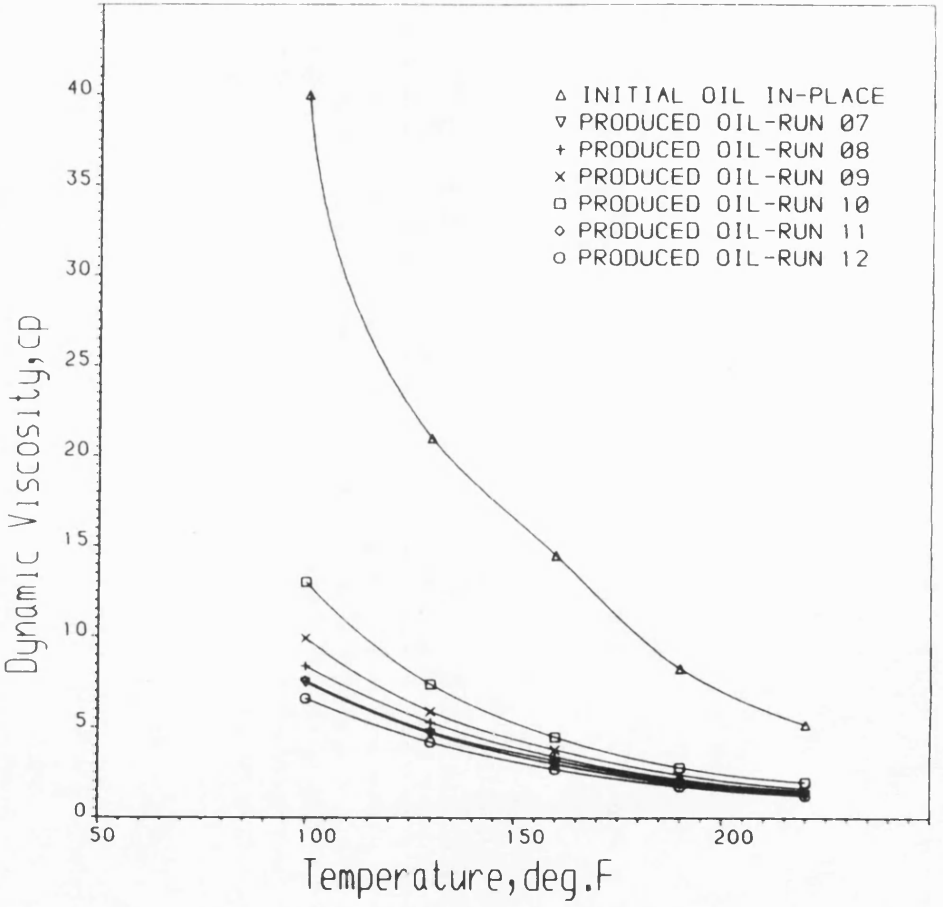

Fig. 7.31 VISCOSITY OF MAYA CRUDE Vs. TEMPERATURE

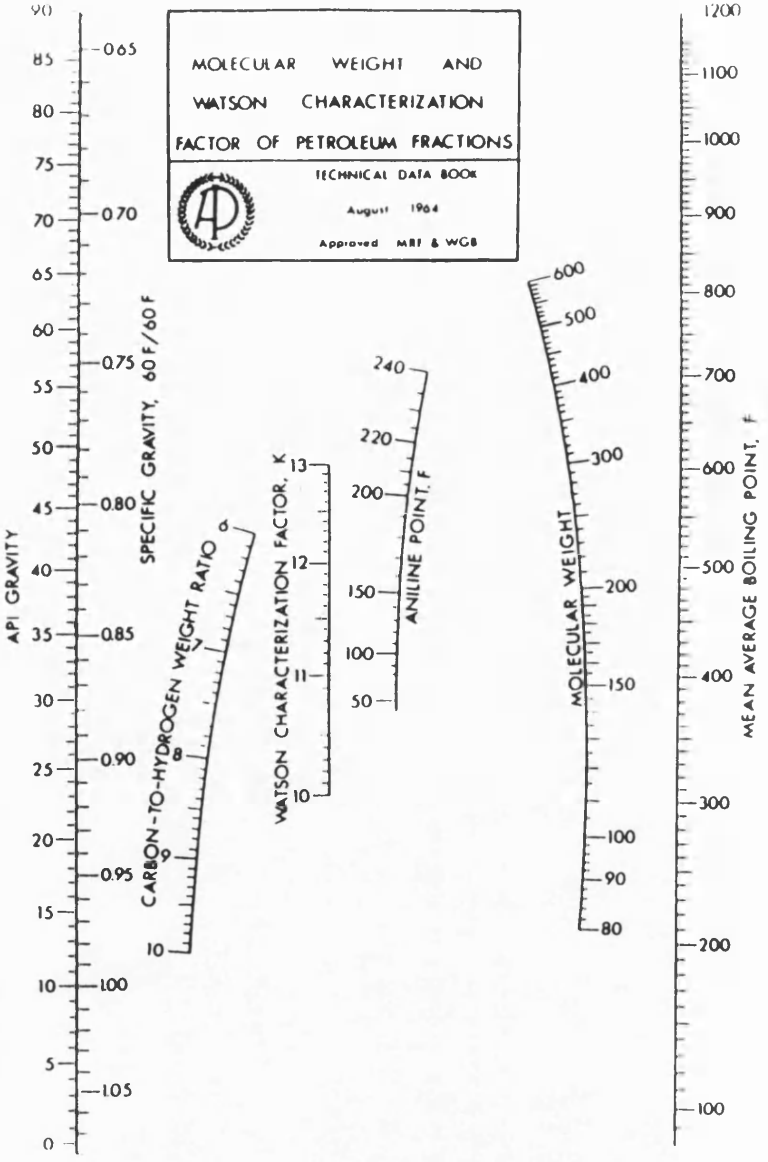

Figure 7.32 PROPERTIES OF PETROLEUM FRACTIONS

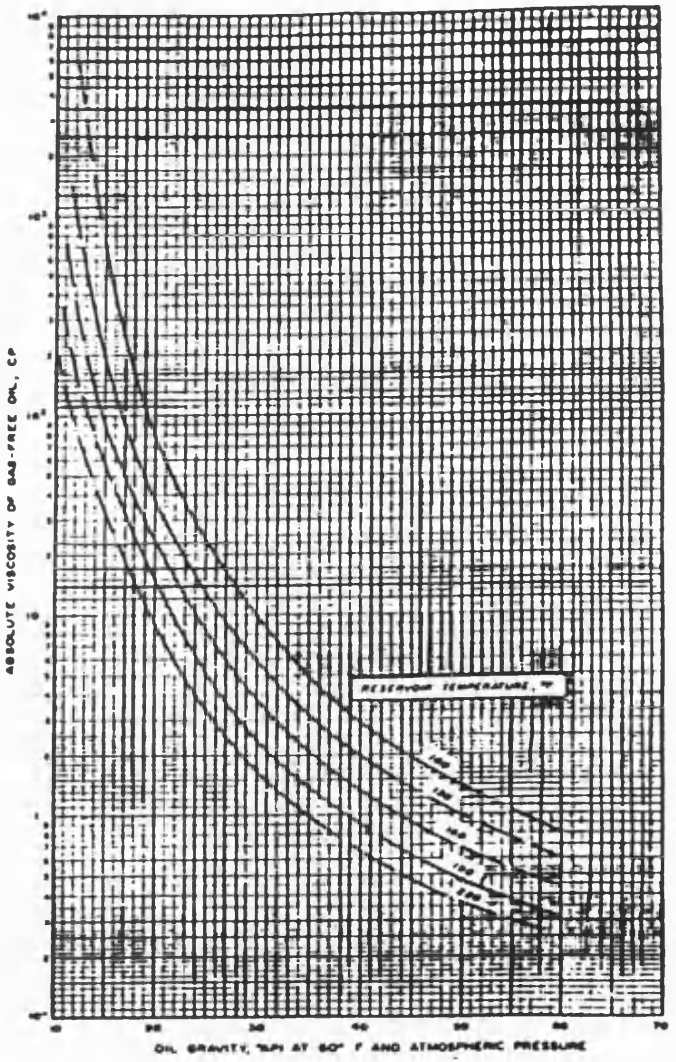

AFTER BEAL(1946)

Figure 7.33 DEAD OIL VISCOSITY AT RESERVOIR TEMPERATURE AND ATMOSPHERIC PRESSURE

Chapter 8

RECOMMENDATIONS

Based on the findings of this study, the following recommendations for future work are made.

1. In-situ combustion is applicable to crude oils with wide range of API gravities, however, the main target is heavy oil. This is because primary and secondary recovery of heavy oils is low due to their low mobility. Hence future work should consider crudes heavier than the one employed in this study. In addition, different porous medium types which are typical of heavy oil reservoirs should be investigated. These include sandstones, limestones, dolomites and poorly consolidated sands with high initial oil saturations (Farouq Ali, 1974). It is also desirable that representative reservoir rock materials be studied, but these may be non-homogeneous.

2. In applying in-situ combustion to recover residual oil from depleted reservoirs, it is essential that the oil saturation be high enough to provide sufficient fuel in order to sustain combustion. An investigation of the lower limit of the initial oil saturation for successful application of in-situ combustion is therefore important.

3. In heavy oil reservoirs, formation thicknesses of 50Ft. or over are very common. The heat loss to the surrounding strata will be small, so that in-situ combustion can therefore be assumed to occur under adiabatic conditions (Farouq Ali, 1974; Vossoughi et al., 1982). In order to achieve a close approach to adiabatic combustion tube operation, more band heaters, distributed over the length of

the combustion tube should be installed. In fact, this should aim for 100% coverage of the tube and computer control of the heating system for optimum efficiency. Notwithstanding this, attention should be directed to some detailed analysis of the energy balance, to quantify any effect of radial heat loss during a combustion experiment.

4. To more closely approach in-situ combustion under reservoir condition, it will be useful to investigate the horizontal mode of combustion tube operation. However, gravity segregation effect will need to be carefully controlled. This can be achieved by rotating the tube while the experiment is in progress. Horizontal combustion tube experiments will enable studies of gas override to be made, and the effect particularly on combustion front stability.

5. Since in-situ combustion experiments vary in length up to 12 hours, or considerably more in some cases, a fully automated operation is desirable. This should be designed to ensure that the experiments are carried out as efficiently and safely as possible, supervising all various operating, control and data logging tasks.

6. The present study has investigated the in-situ combustion characteristics at the selected operating conditions and relatively low pressures. This work should be extended to reservoir conditions at high pressures. High operating pressure will significantly affect the combustion parameters as discussed in chapter 5. Account must also be taken of the increasing amount of the air stored in the burned zone, however operating at high pressures should enable higher WGR's to be used and other beneficial effect may be achieved due to

swelling of the oil resulting from the increased solubility of CO_2. A high pressure combusiton tube facility, with capability to 4000psi is therefore recommended to cover the pressure range of heavy oil reservoirs and watered out light oil reservoirs. Furthermore, based on the considerable advantages of using oxygen enriched air, as found in this study, higher oxygen enrichment than employed in this study should be investigated in future work. Under such high pressure conditions, with high oxygen concentration, the safety aspects will require special attention.

7. A combustion tube behaves like an integral reactor since both carbon concentration and oxygen partial pressure are functions of time and reaction path. Thus the kinetic data obtained will be of integral form. To more closely approach a differential reactor condition, the combustion gases could be sampled at discreet locations along the tube. Thus, a moveable sampling probe could be employed to sample the interior of the sand pack (Thomas et al., 1978). Information provided by measurements taken directly from the combustion zone will enable more precise determinations of reaction conditions, thus eliminating end effects. Data obtained in this way could also enhance the 'real time' energy and material balance computations.

8. In addition to the adverse effects of LTO described in Section 3.1.1, it may also cause spontaneous ignition (Fassihi, 1981). Although steps can be taken to eliminate LTO in laboratory combustion tube experiments, as the case in this study, its occurence in the field is more likely. Therefore, the effects of LTO of the crude on the performance of the in-situ combustion process

needs to be investigated. Also, the conditions under which spontaneous ignition could be caused by the occurence of LTO need to be investigated in more detail.

9. Thermogravimetric analysis (TGA) and a differential scanning calorimetry (DSC) techniques are recommended to supplement in-situ combustion tube runs for the purpose of obtaining kinetic information. In TGA, the derivative of the weight loss-time curve provides information on the process of distillation, cracking and oxidation which take place. These derivative thermograms can then be fitted to the appropriate kinetic model to obtain the relevant kinetic parameters. On the other hand, the area under a DSC thermograms represents the total heat of reaction which includes the energy required for vaporization (Vossoughi et al., 1982). These techniques are particularly suitable for investigating thermal stability, surface area and catalytic effects such as that of clay.

10. In diffusion controlled regime (wet combustion) the sand grain specific surface area and the relative permeabilities of the porous medium to the gaseous reactants may have a significant effect on the overall reaction rate. This can be investigated by varying the particle size of the sand media in the absence of clay additions. In this way, the effects of clay can be excluded. It may, however, be necessary to use a heavy crude oil which will deposit sufficient fuel to sustain the combustion.

11. In order to achieve a more detailed characterization of the produced oil, the analysis needs to be extended to include molecular

weight distribution, elemental determinations and identification of chemical groups such as saturates, aromatics and polar compounds. This further characterisation will contribute significantly to the material and energy balance descriptions and also aid kinetic studies.

On-line analysis of the oil samples would be a valuable means of determining the properties of the oil produced throughout the combustion experiment. In cases where the oil samples collected over a given period of time are too small to be analysed, one remedy apart from increasing the initial oil saturation, is to add carbon disulfide. CS_2 does not affect liquid chromatography using a flame ionization detector.

NOMENCLATURE

Symbol	Definition	Units
A_r	Arrhenius constant	
Ar	Air requirement	sm^3/m^3
Cb	Carbon burned	kg/100kgsand
Cbo	Unburned carbon in the sand pack	kg/100kgsand
Cc	Carbon concentration	kg/100kgsand
Cg	Gas heat capacity	J/kg°K
Cm	Heat capacity of silica sand	J/kg°K
Co	Heat capacity of crude oil	J/kg°K
Cr	Sand pack heat capacity	J/m^3°K
C_{sh}	Superheated steam heat capacity	J/kg°K
Cw	Heat capacity of liquid water	J/kg°K
E	Activation Energy	J/kgmole
F	Exit gas flow rate	sm^3/hr
Fg	Gas fraction (on dry basis)	
Fs	Steam fraction (mole basis)	
GFR	Gas-fuel ratio	sm^3/kg
GOR	Gas-oil ratio	sm^3/kg
H	Heat released by combustion	cal/gmfuel
hs	Steam enthalpy	J/kg
k	Reaction rate constant	
K	Thermal conductivity of sand pack	J/hr m°K
K_f	Thermal conductivity of the saturating phase	J/hr m°K
K_g	Thermal conductivity of nitrogen	J/hr m°K
K_m	Thermal conductivity of silica sand	J/hr m°K
K_o	Thermal conductivity of crude oil	J/hr m°K
K_w	Thermal conductivity of liquid water	J/hr m°K
L	Combustion zone thickness	m
Lc	Heat released by combustion	J/kgfuel
m	Reaction order on carbon concentration	
Mo	Oil produced per unit volume of reservoir swept	kg/m^3
n	Reaction order on oxygen partial pressure	
p	Atomic H/C ratio	
Ph	Radial heat loss, percent	
Po_2	Oxygen partial pressure	kPa
Ps	System pressure	kPa
q	Molar CO_2/CO ratio	
Q	Radial heat loss	J/m^3hr
r	Radius of combustion tube	m
R	Universal gas constant	J/kgmole°K
-Rc	Carbon combustion rate	kg/100kgsandhr
$-R_f$	Coke combustion rate	kg/m^3hr
S	Steam heat (Vaporized Combustion Water)	J/m^3hr
Sg	Fractional gas saturation in the sand pack	
S_l	Sand pack density	kgsand/m
So	Fractional oil saturation in the sand pack	
Sw	Fractional water saturation in the sand pack	
t	Combustion (reaction) time	hr
tt	Stabilized combustion period	hours
T	Temperature	°K

Symbol	Definition	Units
T_1	Peak combustion temperature	°K
Ua	Total air flux	sm^3/m^2hr
Ug	Gas flux	sm^3/m^2hr
Vb	Combustion-front velocity	m/hr
W	Water of combustion	kg/kgfuel
WGR	Water-gas injection ratio	m^3/Msm^3
X	Linear distance	m
Y	Oxygen utilisation, percent	
YCO	Mole fraction of CO in the produced gas	
YCO_2	Mole fraction of CO_2 in the produced gas	
YN_{2_i}	Mole fraction of nitrogen in the injected gas	
YO_{2_i}	Mole fraction of oxygen in the injected gas	
YO_2	Mole fraction of oxygen in the produced gas	
Z	Fuel consumption	kg/m^3
Θ	Axial temperature gradient within the combustion zone	°K/m
Φ	Fractional porosity of sand pack	
ρ_g	Gas density	kg/m^3
ρ_m	Density of silica sand	kg/m^3
ρ_o	Density of crude oil	kg/m^3
ρ_s	Density of steam	kg/m^3
ρ_w	Density of liquid water	kg/m^3
α	Convective-Conductive term (Equaton 3.17)	
β	Heat term (Equation 3.18)	
δ	Partial derivative (Equations 3.9 - 3.19)	

REFERENCES

1. Alderman, J.H., and Osoba, J.S.: "A Study of Oil Recovery by In-Situ Combustion with the Addition of Water," SPE -3684 presented at the 42nd Annual Regional Meeting of the Society of Petroleum Engineers of AIME, Los Angeles, California (November 4-5, 1971)

2. Allag, O.: "Experimental Investigation of the Kinetics of Underground Dry, Forward Combustion," Ph.D. dissertation, University of Tulsa (1978)

3. Archer, J.S.: "Thermal Properties of Heavy Oil Rock and Fluid System," Paper presented at one day seminar on Problems Associated with the Production of Heavy Oil, organised by Oyez Scientific and Technical Services Ltd., London W2 (March 18, 1985)

4. Armento, M.E., and Miller, C.A.: "Stability of Moving Combustion Fronts in Porous Media," Soc. Pet. Eng. J. (December 1977), pp. 423-430

5. Bailey, H.R., and Larkin, B.K.: "Heat Conduction in Underground Combustion," J. Pet. Tech. (May, 1959), pp. 123-129; Trans. AIME (1959), Vol. 216

6. Bailey, H.R., and Larkin, B.K.: "Conduction-Convection in Underground Combustion," Trans. AIME (1960), Vol. 219, pp. 320-331

7. Beal, C.: "Viscosity of Air, Water, Natural Gas, Crude Oil and its Associated Gases at Oil-Field Temperatures and Pressures," Trans. AIME (1946) 165, pp. 94-115

8. Beckers, H.L., and Harmsen, G.J.: "The Effect of Water Injection on Sustained Combustion in a Porous Media," Soc. Pet. Eng. J. (June, 1970), pp. 145-163

9. Benham, A.L., and Poettman, F.H.: "The Thermal Recovery Process - An Analysis of Laboratory Combustion Data," Trans. AIME (1958), Vol. 213, pp. 406-408

10. Bousaid, I.S.: "Oxidation of Crude Oil in Porous Media," Ph.D. Dissertation, Texas A & M University (May, 1967)

11. Bousaid, I.S., and Ramey, H.J., Jr.: "Oxidation of Crude Oil in Porous Media," Soc. Pet. Eng. J. (June, 1968), pp. 137-148; Trans. AIME, Vol. 243

12. Burger, J.G., and Sahuquet, B.C.: "Chemical Aspects of In-Situ Combustion - Heat of Combustion and Kinetics," Soc. Pet. Eng. J. (October, 1972), pp. 410-422

13. Burger, J.G., and Sahuqet, B.C.: "Laboratory Research on Wet Combustion," J. Pet. Tech. (October, 1973), pp. 1137-1146

14. Burger, J., and Sahuquet, B.: "In-Situ Combustion - Principles and Laboratory Studies," Rev. Inst. Fr. Pet. (1977), Vol. 32, No. 2, pp. 141-188

15. Buxton, T.S.: "Wet In-Situ Combustion Aids Recovery of Oil, AIChE Told," Oil and Gas J. (April, 1972), pp. 50-53

16. Buxton, T.S., and Cragi, F.F., Jr.: "Effect of Injected Air-Water Ratio and Reservoir Oil Saturation on the Performance of a Combination of Forward Combustion and Waterflooding," Paper presented at AIChE 71st National Meeting, Dallas (February 20-23, 1972), pp. 27-30

17. Campbell, G.G., Burwell, E.L., Sterner, T.E., and Core, L.L., "Underground Combustion Oil-Recovery Experiments in the Venango Second Sand, Reno Pool, Venango County, Pa.," Report of Investigations, R.I. 6942, U.S. Bureau of Mines (April, 1967)

18. Chu, C.: "Two-Dimensional Analysis of a Radial Heat Wave," J. Pet. Tech. (October, 1963), pp. 1137-1144

19. Chu, C.: "The Vaporization - Conduction Phenomena in a Linear Heat Wave," Soc. Pet. Eng. J. (June, 1964) pp. 85-89

20. Chu, C.: "A Study of Fireflood Field Projects," J. Pet. Tech. (February, 1977), pp. 111-119

21. Chu, C.: "State-of-the-Art Review of Fireflood Field Projects," J. Pet. Tech. (January, 1982), pp. 19-36

22. Clair, J.H., and Simister, W.F.: "Process to Recover CO_2 from Flue Gas Gets First Large-Scale Try-Out in Texas," Oil and Gas J. (February, 1983)

23. Clark, G.A., Jones, R.G. Kinney, W.L., Schilson, R.E., Surkalo, H., and Wilson, R-S.: "The Fry In-Situ Combustion Test - Performance," J. Pet. Tech. (March, 1965), pp. 348-353

24. Coats, K.H.: "In-Situ Combustion Model" Soc. Pet. Eng. J. (December, 1980), pp. 533-554

25. Cooperman, P.: "Some Criteria for In-Situ Combustion of Crude Oil," Journal of Applied Physics (September, 1959), Vol. 30, No. 9, pp. 1370-1380

26. Crawford, P.B.: "Water Technology - Underground Combustion of Hydrocarbons," Producers' Monthly (June, 1968), p. 15

27. Crookston, R.B., Culham, W.E., and Chen, W.H.: "A Numerical Simulation Model for Thermal Recovery Processes," Soc. Pet. Eng. J. (February, 1979) pp. 37-58

28. Dabbous, M.K.: "In-Situ Oxidation of Crude Oils in Porous Media," Ph.D. Dissertation, University of Pittsburgh (1971)

29. Dabbous, M.K., and Fulton, P.K.,: "Low Temperature Oxidation Reaction Kinetics and Effects on the In-Situ Combustion Process," Soc. Pet. Eng. J. (June, 1974), pp. 253-262

30. Dew, J.N., and Martin, W.L.: "Air Requirements for Forward Combustion," Petroleum Engineer (December, 1964) Vol. 36, p. 82; (January, 1965), Vol. 37, p. 82

31. Dietz, D.N.: "Wet Underground Combustion, State of The Art," J. Pet. Tech. (May, 1970), pp. 605-617

32. Dietz, D.N., and Weijdema, J.: "Wet and Partially Quenched Combustion," SPE-1899 presented at the 24nd Annual Fall Meeting of the Society of Petroleum Engineers of AIME, Houston, Tex. (October 1-4, 1967)

33. Ejiogu, G.J. Bennion, D.W., Moore, R.G., Donnelly, J.K.: "Wet Combustion - A Tertiary Recovery Process for the Pembina Cardium Reservoir," J. Can. Pet. Tech. (July-September, 1979), pp. 58-66

34. Farouq, Ali, S.M.: "A Current Appraisal of In-Situ Combustion Field Tests," J. Pet. Tech. (April, 1972), pp. 477-486

35. Farouz, Ali, S.M.: "Heavy Oil Recovery - Principles, Practicality, Potential and Problems," SPE-4935 presented at the Regional Meeting of the Society of Petroleum Engineers of AIME, Billings, Mont. (May 15-16, 1974)

36. Farouq, Ali, S.M.: "Multiphase, Multidimensional Simulation of In-Situ Combustion," Paper 6896, presented at the 52nd Annual Fall Meeting of SPE, Denver, Colorado (October, 9-12, 1977)

37. Fassihi, M.R.: "Analysis of Fuel Oxidation in In-Situ Combustion Oil Recovery," Ph.D. Dissertation, Stanford University (1981)

38. Fassihi, M.R., Ramey, H.J., Jr., Brigham, W.E.: "The Frontal Behaviour of In-Situ Combustion," SPE-8907 presented at the 50th Annual California Regional Meeting of the Society of Petroleum Engineers of AIME, Los Angeles, California (April, 9-10, 1980)

39. Fassihi, M.R., Ramey, H.J., Jr., Brigham, W.E.: "The Reaction Kinetics of In-Situ Combustion," SPE-9454 presented at the 55th Annual Fall Technical Conference and Exhibition of the Society of Petroleum Engineers of AIME, Dallas, Texas (September 21-24, 1980)

40. Fassihi, M.R., Brigham, W.E., and Ramey, H.J., Jr.: "Reaction Kinetics of In-Situ Combustion: Part 1 - Observations" Soc. Pet. Eng. J. (August, 1984), pp. 399-407

41. Flock, D.L., and Dranchuk, P.M.: "A Current Review of Forward Combustion," J. Can. Pet. Tech. (April-June, 1971), pp. 33-39

42. Garon, A.M., and Wygal, R.L.: "A Laboratory Investigation of Fire-Water Flooding," Soc. Pet. Eng. J. (December, 1974), Vol. 14, No. 6, pp. 537-544

43. Gates, C.F., and Ramey, HLJ., Jr.: "Field Results of South Belridge Thermal Recovery Experiment," Trans. AIME (1958), Vol, 213, pp. 236-244

44. Gottfried, B.S.,: "A Mathematical Model of Thermal Oil Recovery in Linear Systems," Trans. AIME (1965), Vol. 234, pp. 196-210

45. Gottfried, B.S., "Some Theoretical Aspects of Underground Combustion in Segregated Oil Reservoirs," Soc. Pet. Eng. J. (September, 1966), pp. 281-290; Trans. AIME Vol. 237

46. Grabowski, J.W., Vinsome, P.K., Lin, R.C., Behie, A., and Rubin, G.: "Fully Implicit General Model in In-Situ Combustion," SPE-8396 presented at the 54th Annual Fall Technical Conference and Exhibition of the Society of Petroleum Engineers of AIME, Las Vegas, Nevada (September 23-26, 1979)

47. Grant, B.F., and Szasz, S.E.: "Development of an Underground Heat Wave for Oil Recovery," Trans. AIME (1954), Vol. 201, pp. 108-118

48. Hansel, J.G., Benning, M.A., Fernbacher, J.M.: "Oxygen In-Situ Combustion for Oil Recovery: Combustion Tube Tests," SPE 11253 presented at the Eastern Regional Meeting of the Society of Petroleum Engineers of AIME, Washington D.C., (November 3-5, 1982), pp. 15-27

49. Hardy, W.C.: "Deep-Reservoir Fire-Flooding for Independents," Oil and Gas J. (January 18, 1971) pp. 60-68

50. Hardy, W.C., Fletcher, P.B., Shepard, J.C., Dittman, E.W., and Zodow, D.W.: "In-Situ Combustion in a Thin Reservoir Containing High-Gravity Oil," J. Pet. Eng. (February, 1972), Vol. 24, No. 2, pp. 199-208

51. Heinemann, Z.: "Study of the Application of Underground Combustion followed by Water Injection," Banyasz Lapok (1967) vol. 100, No. 3, pp. 198-203

52. Herbeck, E.F., Heintz, R.C., and Hastings, J.R.: "Fundamentals of Tertiary Oil Recovery," Petroleum Engineer (February, 1977), pp. 46-56

53. Hester, D.V., and Menzie, D.E.: "Development of Sub-Surface Combustion Drive," Petroleum Engineer (November, 1954), Vol. 26, No. 12, pp. B-82 - B-92

54. Howard, F.A.: "Process for Distilling Crude Oil Underground," U.S. Patent No. 1,473,348 (November 6, 1923)

55. Hughes, D.S.: "A Numerical Assessment of Oxygen-Supported In-Situ Combustion as an EOR in a Waterflooded North Sea Reservoir," 3rd European Meeting on Improved Oil Recovery, Rome (April 16-18, 1985)

56. Hzivdos, L.J., Howard, J.V., and Roberts, G.W.: "Enhanced Oil Recovery Through Oxygen-Enriched In-Situ Combustion: Test Results from the Forest Hill Field in Texas," J. Pet. Tech. (June, 1983), pp. 1061-1070

57. Kaye, S.E., Ting, V.C., and Fair, J.C.: "Development of a System that Utilizes Flue Gas from Enhanced-Oil Recovery Combustion Projects," J. Pet. Tech. (January, 1982), pp. 181-188

58. Khelil, C.: "A Study of In-Situ Combustion in a Segregated System," SPE 2519, presented at 44th Annual Fall Meeting of Society of Petroleum Engineers, Denver, Colorado (September 28 - October 1, 1969)

59. Kuhn, C.S., and Koch, R.L.: "In-Situ Combustion - Newest Method of Increasing Oil Recovery," Oil and Gas J. (August 10, 1953), Vol. 52, No. 14, pp. 92-96

60. Langnes, G.L., and Besson, C.M.: "In-Situ Combustion Combined with Water Flooding," Petroleum Engineer (July, 1965), pp. 92-101

61. Lewis, J.O.: U.S. Bur. Mines Bull (1917), Vol. 148, No. 128

62. Lewis, W.K., Gilliland, E.R., and Paxton, R.R.: "Low-Temperature Oxidation of Carbon," Ind. & Eng. Chem. (June, 1954), Vol. 46, No. 6, pp. 1326-1331

63. Lin, C.Y., Chen, W.H., Lee, S.T., Culham, W.E.: "Numerical Simulation of Combustion Tube Experiments and the Associated Kinetics of In-Situ Combustion Processes," Soc. Pet. Eng. J. (December, 1984), pp. 657-667

64. Martin, W.L., Alexander, J.D., and Dew, J.N.: "Process Variables of In-Situ Combustion," J. Pet. Tech. (February, 1958), Vol. 10, No. 2, pp. 28-35

65. Martin, W.L., Alexander, J.D., and Dew, J.N.: "Factors Affecting Fuel Availability and Composition During In-Situ Combustion," Tans. AIME (1962), Vol. 225, pp. 1154-1164

66. McNeil, J.S. Jr., Moss, J.T.: "Recent Progress in Oil Recovery by In-Situ Combustion," Petroleum Enginner (July, 1958), Vol. 30, No. 7, pp. B-29 - B-42

67. Meyer, R.F., Kuuskraa, V.A., and Hammershaimb, E.: "World Resources of Heavy Oil," Hydrocarbon Processing (May, 1984), pp. 162-B - 162-o

68. Moll, A.J. and Dickenson, R.L.: "Synthesis Gas: An Exciting Future is Expected," Oil and Gas J. (March 12, 1984), pp. 68-73

69. Moss, J.T.: "Laboratory Investigation of the Oxygen Combustion Process for Heavy Oil Recovery," SPE 10706 presented at the California Regional Meeting of the Society of Petroleum Engineers, San Francisco, CA (March 24-26, 1982)

70. Moss, J.R., White, P.D., and McNeil, J.S., Jr.: "In-Situ Combustion Process-Results of a Five Well Field Experiment in Southern Oklahoma," Trans. AIME (1958), Vol. 216, pp. 28-35

71. Nelson, W.L.: Petroleum Refinery Engineering McGraw-Hill Book Company, New York, 4th edition (1969)

72. Nelson, T.W., and McNeil, J.S., Jr.: "Oil Recovery by Thermal Methods," Producers' Monthly (February, 1959), Vol. 23, No. 3, pp. 14-27

73. Nelson, T.W., and McNeil, J.S., Jr.: "How to Engineer an In-Situ Combustion Project," Oil and Gas J. (1961), Vol. 59, No. 23, pp. 58-65

74. Okandan, E., Baggi, S., Demiral, B., Parlaktuna, M., Topkaya, I., And Gurpinar, O.: "Laboratory Dry Combustion Tests for Limestone Containing Light Crude Oil," 2nd European Symposium, Paris, (November, 1982) pp. 489-494

75. Parrish, D.R., and Craig, F.F.: "Method of Forward In-Situ Combustion Utilizing Air-Water Injection Mixtures," U.S. Patent No. 3,171,479 (March 2, 1965)

76. Parrish, D.R., and Craig, F.F., Jr.: "Laboratory Study of a Combination of Forward Combustion and Waterflooding- the COFCAW Process," J. Pet. Tech. (June, 1969), pp. 753-761

77. Parrish, D.R., Pollock, C.B., and Craig, F.F., Jr.: "Evaluation of COFCAW as a Tertiary Recovery Method, Sloss Field, Nebraska," J. Pet. Tech, (June, 1974), pp. 676-686

78. Penberthy, W.L., Jr.: "The Design and Operation of a Combustion Tube for Investigation of Combustion Oil Recovery," M.Sc. Thesis, Texas A & M University (May 1965)

79. Penberthy, W.L., Jr.: "An Investigation of the Fundamentals of Combustion Oil Recovery," Ph.D. Dissertation, Texas, A & M University (May, 1967)

80. Penberthy, W.L., and Ramey, H.J., Jr.: "The Design and Operation of Laboratory Combustion Tubes," Soc. Pet. Eng. J. (June, 1966), pp. 183-198

81. Perry, J.H.: Chemical Engineers Handbook, McGraw-Hill Book Company, Inc., New York, 4th edition (1963)

82. Poettmann, F.H.: "In-Situ Combustion: A Current Appraisal," World Oil (April, 1964), Vol. 158, No. 5, pp. 124-128; (May, 1964), Vol. 148, No. 6. pp. 95-98

83. Poettmann, F.H., Schilson, R.E., and Surkalo, H.: "Philosophy and Technology of In-Situ Combustion in Light Oil Reservoirs," World Oil (1967), Vol. 165, pp. 487-497

84. Poollen, H.K. Van, and Associates, Inc.: Fundamentals of Enhanced Oil Recovery, PennWell Books, Division of PennWell Publishing Company, Tulsa, Oklahoma (1980), pp. 41-50

85. Pratts, M.: Thermal Recovery, Monograph published by Society of Petroleum Engineers of AIME, Dallas, Vol. 7 (1982)

86. Pusch, G.: "A Simplified Method of Determining Kinetic Data of a Wet In-Situ Combustion in an Oil Field," Erdoel-Erdgas Z (1976), Vol. 92, No. 1, pp. 5-10

87. Rall, C.G., and Tallafero, D.B.: "A Method for Determining Simultaneously the Oil and Water Saturations of Oil Sand," Report of Investigation, No. R-I. 4004, U.S. Bureau of Mines (December, 1946)

88. Ramey, H.J., Jr.: "Transient Heat Conduction During Radial Movement of Cylindrical Source - Application to Thermal Recovery Processes," Trans. AIME (1959), vol. 216, pp. 115-122

89. Reed, R.L., Weber, L., and Gottfried, B.S.: "Differential Thermal Analysis and Reaction Kinetics," Paper presented at the Spring Meeting of American Chemical Society, Los Angeles, California (March 31-April 5, 1963)

90. Rubin, B., Buchanan, W.L.: "A General Purpose Thermal Model," Soc. Pet. Eng. J. (April, 1985), pp. 202-214

91. Schumacher, M.M.: Enhanced Recovery of Residual and Heavy Oils, Noyes Data Coroporation, New Jersey, USA, 2nd edition (1980)

92. Sheinman, A.B., Dubrovai, K.K., Sorokin, N.A., Charvigin, M.M., Zaka, S.L., and Zinchenko, K.F.: "Gasification of Crude Oil in Reservoir Sands - Part I," Petroleum Engineer (December, 1938), Vol. 10, pp. 27-30; part II, ibid (February, 1938), Vol. 10, pp. 91-100

93. Showalter, W.E.: "Combustion-Drive Tests," Soc. Pet. Eng. J. (March, 1963), Vol. 3, No. 1, pp. 53-58

94. Skirrow, G., and Tipper, C.F.: "Some Processes in Gaseous Slow Combustion, Formation of Carbon Monoxide and Carbon Dioxide, 7th Symposium (International) on Combustion, London Butterworths Scientific Publications (1959), pp. 134-141

95. Smith, J.M.: Chemical Engineering Kinetics, McGraw-Hill Book Company, Inc., New York (1956)

96. Smith J.T.: "Numerical Simulation of In-Situ Combustion in a Two-Dimensional System," Ph.D. Dissertation, The Pennsylvania State University (1971)

97. Smith, J.T., and Farouq Ali, S.M.,: "Simulation of In-Situ Combustion in a Two-Dimensional System," SPE-3594 presented at the 46th Annual Fall Meeting of the Society of Petroleum Engineers of AIME, New Orleans, La (October 3-6, 1971)

98. Smith, F.W., and Perkins, T.K.: "Experimental and Numerical Simulation Studies of the Wet Combustion Recovery Process," J. Can. Pet. Tech. (July-September, 1973), pp. 44-54

99. Stinson, D.L., Carpenter, H.C., and Cegielski, J.M., Jr.: "Power Recovery from In-Situ Combustion Exhaust Gases," SPE Paper no. 5332, presented in Denver, Colorado (April, 1975)

100. Szasz, S.E.: Proc. of First Adv. Petro. Engr. Seminar, University of Okla, (February, 9-10, 1960)

101. Szasz, S.E.: "Evaluating the Heat Wave Process," World Oil (August, 1961), Vol. 153, No. 2, pp. 89-93

102. Tadema, H.J.: "Mechanism of Oil Production by Underground Combustion," Proceedings of the 5th World Petroleum Congress (1959), Section II, paper 22, pp. 279-287

103. Thomas, G.W.: "A Theoretical Analysis of Forward Combustion in Petroleum Reservoirs," Ph.D. Dissertation, Stanford University, Stanford, California (February, 1963)

104. Thomas, G.W.: "A Study of Forward Combustion in a Radial System Bounded by Permeable Media," J. Pet. Tech. (October, 1963), pp. 1137-1144

105. Thomas, G.W., Buthod, A.P., and Allag, O.: "An Experimental Study of the Kinetics of Dry Forward Combustion - Final Report," Report No. BETC-1820-1, distributed by Department of Energy (February, 1979)

106. Thomas, F.B., Bennion, D.W., and Moore, R.G.: "Using Combustion Tube Data To Tune a Numerical Simulation," Paper No. 83.33.44 presented at the 34th Annual Technical Meeting of the Petroleum Society of CIM in Banff (May 10-13, 1983)

107. Verma, B.V.: "A Theoretical Investigation of Forward Combustion in a One Dimensional System," Ph.D. Dissertation, University of Tulsa (1978)

108. Vossoughi, S., Willhile, G.P., Kritikos, W.P., Guvenir, I.M., and Shoubang, Y.E.: "Automation of an In-Situ Combustion Tube and Study of the Effects of Clay on the In-Situ Combustion Process," Soc. Pet. Eng. J. (August, 1982), pp. 493-502

109. Williams, R.L., Ramey, H.J., Jr., Brown, S.C., and Sanyal, S.K.: "An Engineering Economic Model for Thermal Recovery Methods," SPE-8906 presented at the 50th Annual California Region Meeting of the Society of Petroleum Engineers of AIME, Los Angeles, California (April 9-11, 1980)

110. Wilson, L.A., Wygal, R.J., Reed, D.W., Gergins, R.L., and Henderson, J.H.: "Fluid Dynamicas During an Underground Combustion Process," Trans. AIME (1958), Vol. 213, pp. 146-154

111. Wilson, L.A., Reed, R.L., Reed, D.W., Clay, R.R., and Harrison, N.H.: "Some Effects of Pressure on Forward and Reverse Combustion," Soc. Pet. Eng. J. (June 1963) pp. 127-137

112. Youngren, G.K.: "Development and Application of an In-Situ Combustion Reservoir Simulator," Soc. Pet. Eng. J. (February, 1980), pp. 39-51

APPENDIX A

SOLUTION OF HEAT TRANSFER MODEL

Heat Transfer Model

$$\frac{d^2T}{dx^2} - \alpha \frac{dT}{dx} = \beta \qquad \text{(A1)}$$

I.C. and B.C.

(1) $T(0) = T_1$

(2) $T(x) = Tx$

(3) $\frac{dT}{dx}(x) = \Theta, \quad 0 < x \leq L$

Solution

$$\text{Let } p = \frac{dT}{dx} \qquad \text{(A2)}$$

Introducing Equation (A2) into (A1) we have,

$$\frac{dP}{dx} - \alpha p = \beta$$

On rearringing we obtain,

$$\frac{dp}{\beta + \alpha p} = dx$$

$$\frac{1}{\alpha}\log_e(\alpha p + \beta) = x + c_1$$

where C_1 = constant of integration

$$\log_e(\alpha p + \beta) = \alpha x + \alpha c_1$$

$$\alpha p + \beta = e^{\alpha x} e^{\alpha c_1}$$

$$= c_2 e$$

where c_2 is a constant replacing e^{xc_1}

$$\alpha p = C_2 e^{\alpha x} - \beta$$

$$p = (C_2/\alpha)e^{\alpha x} - \beta/\alpha \qquad \text{(A3)}$$

replacing p by $\frac{dT}{dx}$ in Equation (A3), we have

$$\frac{dT}{dx} = (c_2/\alpha)e^{\alpha x} - \beta/\alpha \qquad (A4)$$

On integrating, we obtain

$$Tx = (C_2/\alpha^2)e^{\alpha x} - (\beta/\alpha)x + C_3$$

using B.C. (3) in Equation (A4), we obtain

$$\theta = (C_2/\alpha)e^{\alpha L} - \beta/\alpha$$

$$\alpha\theta = C_2\, e^{\alpha L} - \beta$$

$$C_2 = \frac{\alpha\theta + \beta}{e^{\alpha L}} \qquad (A6)$$

Applying 1.C (1) in Equation (A5) we have,

$$T_1 = C_2/\alpha + C_3$$

$$C_3 = T_1 - C_2/\alpha$$

$$= T_1 - (\theta\alpha + \beta)\alpha e^{\alpha L} \qquad (A7)$$

Substituting Equations (A6), (A7) into Equation (A5), we obtain, after further simplification,

$$Tx = \beta \left(\frac{e^{\alpha x} - 1 - xe^{\alpha L}}{\alpha e^{\alpha L}} \right) + \frac{T_1 e^{\alpha L} + \theta e^{\alpha x} - \theta}{e^{\alpha L}} \qquad (A8)$$

Making β, the subject of equation, Equation (A8) becomes

$$\beta = \frac{\alpha e^{\alpha L}(Tx - T_1) - \alpha\theta(e^{\alpha x} - 1)}{e^{\alpha x} - 1 - xe^{\alpha L}} \qquad (A9)$$

Recall:

$$\beta = - R_f(Lc - Wh_s - Q)/K \qquad (A10)$$

using Equation (A10) in Equation (A9) we have,

$$- \frac{R_f(Lc - Whs) - Q}{K} = \frac{\alpha e^{\alpha L}(Tx-T_1) - \alpha\theta(e^{\alpha x} - 1)}{e^{\alpha x} - 1 - xe^{\alpha L}} \qquad (A11)$$

making Q the subject of equation, we obtain

$$Q = \frac{K\alpha\left(e^{\alpha L}(Tx - T_1) - \theta(e^{\alpha x} - 1)\right)}{e^{\alpha x} - 1 - xe^{\alpha L}} + R_f(Lc - Whs) \qquad (A12)$$

APPENDIX B

HEAT FLOW PROFILE IN COMBUSTION ZONE
PART B1

Thermal and Physical Properties of Reservoir and its Contained Fluids

Porosity, Φ, percent	29.00
Initial Oil Saturation, So_i, percent	23.00
Initial Water Saturation, Sw_i, percent	17.00
Initial gas (N_2) Saturation, Sg_i, percent	60.00
Thermal Conductivity of oil at 0°C, Ko, J/hr m°K	428.36
Thermal Conductivity of water at 0°C, Kw, J/hr m°K	2160.00
Thermal Conductivity of gas (N_2) at 0°C, Kg, J/hr m °K	93.38
Thermal Conductivity of Silica sand at 0°C, Km, J/hr m°K	4679.00
Heat capacity of oil at 0°C, Co, J/kg °K	1691.55
Heat capacity of water at 0°C, Cw, J/kg °K	4190.00
Heat capacity of gas (N_2) at 0°C, Cg, J/kg °K	1040.00
Heat capacity of silica sand at 0°C, Cm, J/kg °K	743.00
Density of oil at 0°C, ρo, kg/m^3	92.00
Density of water at 0°C, ρw, kg/m^3	1000.00
Density of gas (N_2) at 0°C, ρg, kg/m^3	1.16
Density of silica sand at 0°C, ρm, kg/m^3	1600.00

Heat Capacity of Combustion Gases

Reference temperature = 0°C

Molal Heat Capacity at Opsig:

T°C	CO	CO_2	N_2	steam	CH_4	Units
0	1.042×10^3	0.846×10^3	1.041×10^3	1.867×10^3	2.238×10^3	J/kg°K

Mean Molal Heat Capacity at Opsig (0°C to T°C):

T°C	CO	CO_2	N_2	Steam	CH_4	Units
300	1.057×10^3	0.962×10^3	1.052×10^3	1.911×10^3	2.693×10^3	J/kg °K
400	1.067×10^3	0.996×10^3	1.060×10^3	1.956×10^3	2.871×10^3	J/kg °K
500	1.078×10^3	1.025×10^3	1.071×10^3	1.986×10^3	3.049×10^3	J/kg °K

Densities of Combustion Gases (0°C, opsig)

CO	CO_2	N_2	steam	CH_4	Unit
1.2501	1.9768	1.2507	0.794	0.7167	kg/m^3

Total gas flux 10.53sm^3/m^2hr

Combustion gas composition:

CO	:	3.388	vol.%
CO_2	:	13.182	vol.%
N_2	:	83.419	vol.%

Combustion zone thickness L = 0.0508 m

Combustion front velocity = 0.068 m/hr

Combustion tube radius = 0.03175 m

TABLE B1 RADIAL HEAT LOSS CALCULATION DATA (Run 1)

Combustion time Hours	CO produced kmoles	CO_2 produced kmoles	N_2 in exit gas kmoles	CO_2/CO mol./mol	Water of combustion kg	H/C ratio mol/mol	Fuel burned kg	Combustion peak temp. °C	Temperature downstream* °C	Total gas produced kmoles
1.18	8.9E-07	35.5E-07	20.33E-06	4.00	1.6E-05	0.400	5.5E-05	406	354	2.477E-05
2.67	8.9E-07	34.5E-07	20.45E-06	3.88	2.0E-05	0.514	5.4E-05	404	342	2.479E-05
3.27	8.8E-07	33.2E-07	20.11E-06	3.76	2.2E-05	0.590	5.3E-05	420	352	2.432E-05
3.85	8.8E-07	33.5E-07	20.59E-06	3.83	2.5E-05	0.659	5.4E-05	391	327	2.482E-05
4.85	8.6E-07	35.3E-07	20.65E-06	4.10	2.0E-05	0.499	5.5E-05	402	352	2.504E-05
5.60	8.4E-07	34.5E-07	20.50E-06	4.10	2.1E-05	0.553	5.4E-05	397	334	2.479E-05
6.42	8.5E-07	34.5E-07	20.50E-06	4.08	2.2E-05	0.556	5.4E-05	408	349	2.479E-05
7.02	8.3E-07	33.8E-07	20.60E-06	4.10	2.5E-05	0.658	5.3E-05	388	327	2.481E-05
7.93	8.8E-07	35.1E-07	20.39E-06	4.00	1.8E-05	0.457	5.5E-05	394	344	2.478E-05
8.68	8.8E-07	33.6E-07	21.12E-06	3.81	2.9E-05	0.762	5.4E-05	388	331	2.535E-05
9.35	9.0E-07	35.7E-07	20.29E-06	3.95	1.4E-05	0.357	5.5E-05	407	350	2.476E-05

* Temperature at a distance 0.0508m from combustion front location

APPENDIX B contd.
Part B2

Heat Flow Sample Calculation For Run 1

Using the expressions in section 3.2 and the data in Part B1 and Table B1; for time 1.18 hours (after ignition), to determine:

(1) Gross Calorific value (GCV)

$$GCV = \frac{265,700 + 197,850(1/q)}{(1 + 1/q)(12 + p)} + \frac{31,175p - 171,700}{12 + p}$$

where p = H/C ratio, q = CO_2/CO ratio.

Substituting values of p and q, we have

$$GCV = \frac{265,700 + 197,850(1/4.0)}{(1 + 1/4)(12 + 0.40)} + \frac{31,175(0.4) - 171,700}{12 + 0.40}$$

$$= 7,492 \text{ cal/gfuel}$$

$$= \underline{31.367 \times 10^6} \text{ J/kgfuel}$$

(2) Sand pack heat capacity at initial saturations, Cr.

$$Cr = \Phi(SwCwpw + SoCopo + SgCgpg) + (1 - \Phi)Cmpm$$

$$= 0.29\ ((0.17x4.19x10^6)+(0.23x1.692x10^3x92)+(0.60x1.04x10^3x1.16)) + (1-0.29)(0.743x10^3x1600)$$

$$= \underline{1.061x10^6} \text{ J/m}^3\text{°K}$$

(3) Sand pack thermal conductivity at initial saturations, K

$$K = \Phi K_f + (1 - \Phi)Km$$

$$= 0.29(2.160x10^3+0.428x10^3+0.093x10^3) + (0.71x4.679x10^3)$$

$$= \underline{4.100 \times 10^3} \text{ J/m hr°K}$$

(4) Vaporized formation water, VFW

$$VFW = \pi r^2 L \Phi S_w \rho_w$$

$$= \pi(0.03175)^2 \times 0.0508 \times 0.29 \times 0.17 \times 10^3$$

$$= \underline{0.00793\text{kg}}$$

(5) Average Reaction Rate, $-R_f$

Average combustion rate = 0.0032 kgfuel/hr

Volumetric sweeping rate = 0.0002 m^3/hr

Stabilised Run period = 1.18 to 9.35 = 8.17 hours

Bed porosity, Φ = 29%

(Φ is assumed constant as a first approximation)

$$\text{Avg. Reaction Rate, } -Rf = \frac{0.0032}{0.0002 \times 0.71 \times 8.17}$$

$$= \underline{2.759} \text{ kg fuel/m}^3\text{hr.}$$

(6) By definition

$$W = \frac{1.6 \times 10^{-5} \text{ kgsteam}}{5.5 \times 10^{-5} \text{ kgfuel}}$$

$$= \underline{0.291} \text{ kgsteam/kg fuel}$$

(7) Convective term (J/m^2hr^oK)

$(UgpgFgCg)CO = 10.53(1.250)(0.03388)(1.042\times10^3) = 0.372 \times 10^3$

$(UgpgFgCg)CO_2 = 10.53(1.9768)(0.13182)(0.846\times10^3) = 2.321 \times 10^3$

$(UgpgFgCg)N_2 = 10.53(1.2507)(0.83419)(1.041\times10^3) = 11.437 \times 10^3$

$$(UgpsFsCsh)\text{steam} = 10.53(0.794)\frac{(1.6 + 793) \times 10^{-5}/18}{((1.6 + 793)/18 + 2.477)\times10^{-5}}(1.867\times10^3) = 14.780\times10^3$$

Total $\underline{28.910 \times 10^3}$

$$\alpha = -\frac{(Cr+\Phi SwpwCw)Vb - Ug(pgFgCg+psFsCsh)}{K}$$

$$= -\frac{0.068(1.061\times10^6+0.29\times0.17\times10^3\times4.190\times10^3)-28.910\times10^3}{4.100 \times 10^3}$$

$$= \underline{-13.972}$$

(8) Temperature gradient in combustion zone

$$= \frac{\Delta T}{x} = \frac{354 - 406}{0.0508}$$

$$= \underline{-1023.6°C/m}$$

(9) Steam enthalpy (h_s)

hs = steam enthalpy

At vaporisation,

Hs = Cw(Ts - Tref)+ hfg

Where Hs = steam enthalpy at vaporisation

Cw = heat capacity of water at Tref.

hfg = Enthalpy of vaporisation or latent heat of steam

From steam tables:

at Opsig, Ts = 100°C, hfg = 2.2567×10^6 J/kg

Therefore, Hs = $4.19 \times 10^3(373 - 273) + 2.2567 \times 10^6$

$$= \underline{2.676 \times 10^6 J/kg}$$

Alternatively, Hs = hg

$$= 2.6758 \times 10^6 \text{ J/kg from steam tables}$$

But the steam is superheated.

Hence hs = Hs + Csh(Tc - Ts)

$$= 2.676 \times 10^6 + 1.956 \times 10^3(679 - 373)$$

$$= \underline{3.275 \times 10^6 J/kg}$$

(10) Radial heat loss in combustion, Q

$$Q = K\alpha\left(\frac{(Tx-Tc)\exp(\alpha L)-\Theta(\exp(\alpha x)-1)}{\exp(\alpha x)-1-x(\exp(\alpha L))}\right) + R_f(Lc - Whs)$$

$$= 4.10\times10^{3}(-13.972)\left(\frac{(354-406)\exp(-13.972\times0.0508)+1023.6(\exp(-13.972\times0.0508)-1}{\exp(-13.972\times0.0508)-1-0.0508\exp(-13.972\times0.0508)}\right)$$

$$+ 2.759(31.367 \times 10^{6} - 0.291 \times 3.275 \times 10^{6})$$

$$= -5.864\times10^{7} + 2.759(30.414 \times 10^{6})$$

$$= \underline{2.536 \times 10^{7}}\ J/m^{3}hr$$

(11) Percent radial heat loss Ph

$$Ph = \frac{100Q}{R_f Lc}$$

$$= \frac{100 \times 2.536 \times 10^{7}}{2.759(31.367\times10^{6})}$$

$$= \underline{29}\ \text{percent.}$$

The analysis was repeated in a similar manner for all of the combustion front locations, using a computer program written in fortran IV (see Appendix D). The results are given in Table B2 overleaf.

TABLE B2 HEAT FLOW PROFILE IN COMBUSTION ZONE (Run 1)

Combustion Time	Combustion Front Location*	Heat Liberated	Heat Liberation Rate	Rate of Radial Heat Loss	Inst. Radial Heat Loss	Cum. Radial Heat Loss
Hours	Metre	J/kgfuel	J/m^3hr	J/m^3hr	Percent	Percent
1.18	0.130	31.369E+06	86.546E+06	25.362E+06	29	29
2.67	0.180	32.160E+06	88.731E+06	15.571E+06	18	23
3.27	0.230	32.638E+06	90.047E+06	9.711E+06	11	21
3.85	0.280	33.240E+06	91.708E+06	15.492E+06	17	19
4.85	0.330	32.243E+06	88.959E+06	29.369E+06	33	21
5.60	0.380	32.661E+06	90.126E+06	15.687E+06	17	22
6.42	0.430	32.672E+06	90.142E+06	20.018E+06	22	21
7.02	0.480	33.478E+06	92.365E+06	19.458E+06	21	21
7.93	0.530	31.822E+06	87.798E+06	28.558E+06	33	22
8.68	0.580	34.006E+06	93.822E+06	24.816E+06	26	23
9.35	0.640	30.977E+06	85.466E+06	18.737E+06	22	22

NOTE: 1 $J/m^3hr = 2.775 \times 10^{-7} kW - hr/m^3hr$

* From top of sand pack

APPENDIX C

LIQUID MASS BALANCES

Sample Calculation for Run 10

Gas Phase

Injected gas analysis:

N_2	79.0 vol.%
O_2	21.0 vol.%

Produced gas:

Total volume	0.37256 sm^3
Pressure	18.7 psi

Analysis (Dry basis)

CO_2	13.703 vol.%
CO	2.591 vol.%
O_2	0.007 vol.%
N_2	83.677 vol.%
CH_4	0.022 vol.%

Liquid Phase

Initial oil in sand pack, g	127.97
Produced Oil, g	88.98
Residual H-C in sand pack, g	1.02
Initial water in sand pack, g	107.73
Water injected, g	558.60
Produced water, g	597.51
Residual water in sand pack, g	25.29

Basis: 0.37256 sm^3 of produced gas

Estimate of the water vapour in the produced gas is based on the assumption that produced gas is saturated with water at 0°C.

Assuming ideal gas behaviour, volume of water vapour in the produced

gas mixture is given by

$$Vwv = Pwv\ V_T/P_T$$

where Vwv = Volume of water vapour in produced gas, sm^3
Pwv = Saturated vapour pressure at 0°C, psi
P_T = Total pressure of produced gas, psi
V_T = Volume of the produced gas, sm^3

Also, Mwv = Vwv/Vg

where Mwv = Mass of water vapour, kg
Vg = Specific volume of water vapour at 0°C, m^3/kg

Now, at 0°C, Pwv = 0.0886 psi,
Vg = 206.3 m^3/kg

$$\text{Therefore, } Vwv = \frac{0.0886 \times 0.37256}{18.7}$$
$$= \underline{0.00176 sm^3}$$
$$Mwv = 0.00176/206.3$$
$$= \underline{8.5 \times 10^{-6}\ kg}$$

Comment: The water vapour in the produced gas is too small to be detected by the gas chromatograph.

The volume of Bone-dry gas produced
= 0.37256 - 0.00176
= $\underline{0.3708 sm^3}$

Assuming that all oxygen not reported in the produced gas analysis reacted with hydrogen in the fuel (coke) to form water, the relevant reactions are:

$$C + O_2 \rightarrow CO_2$$
$$C + \tfrac{1}{2}O_2 \rightarrow CO$$
$$H_2 + \tfrac{1}{2}O_2 \rightarrow H_2O$$

Furthermore, since nitrogen passes through the system unreacted, it is selected as the tie component. Thus, the amount of nitrogen injected equals the amount produced, provided there is no nitrogen accumulation. Other components of the system can therefore, be referred to nitrogen as a basis (See end of Appendix C).

Nitrogen Balance

N_2 produced	= 0.83677 (0.3708)	= 0.31027 sm^3
	= 0.31027 (1.2507)	= 0.38806 kg
N_2 injected		= 0.31027 sm^3
		= 0.38806 kg

Carbon Balance

CO_2 produced	= 0.13703 (0.3708)	= 0.05081 sm^3
	= 0.05081 (1.9768)	= 0.10044 kg
CO produced	= 0.02591 (0.3708)	= 0.00961 sm^3
	= 0.00961 (1.2501)	= 0.01201 kg
C burned	$= 12\left(\frac{0.10044}{44} + \frac{0.01201}{28}\right)$	= 0.03254 kg
CH_4 produced	= 0.00022 (0.3708)	= 0.00008 sm^3
	= 0.00008 (0.7167)	= 0.00006 kg

Oxygen Balance

O_2 injected	= (0.21/0.79) x 0.31027	= 0.08248 sm^3
	= 0.08248 (1.4289)	= 0.11785 kg
Unreacted O_2	= 0.00007 (0.3708)	= 0.00003 sm^3
	= 0.00003 (1.4289)	= 0.00004 kg

H_2 burned $= \frac{4}{22.4}\left(0.08248 - 0.00003 - 0.05081 - \frac{0.00961}{2}\right)$ = 0.00479 kg

Water generated by combustion $= \frac{18}{2}(0.00479)$ = 0.04313 kg

Fuel (Coke) Balance

Coke burned = C burned + H_2 burned = 0.03733 kg

Oil Balance

Initial oil in sand pack, g	127.97
Oil produced as liquid, g	88.98
Oil consumed as fuel, g	37.33
Oil produced as gas, g	0.06
Residual H-C in sand pack, g	1.02
Total, g	127.39
Difference, g	0.58
Percent error in balance	0.45

Water Balance

Initial water in sand pack, g	107.73
Water injected, g	558.60
Water generated by combustion, g	43.13
Total, g	709.46
Water produced as liquid, g	597.51
Water produced as gas, g	0.01
Residual water in sand pack, g	25.29
Total, g	622.81
Difference, g	86.65
Percent error in balance	12.21

Overall Liquid Balance

Input:		
	Oil, g	127.97
	Water, g	709.46
	Total, g	837.43
Output:		
	Oil, g	127.39
	Water, g	622.81
	Total, g	750.20
	Difference, g	87.23
	Percent error in balance	10.42

Nitrogen as tie component

Some injected gas is stored in the burned zone. the amount stored increases in proportion to the pressure in the burned zone.

$$\text{Free pore volume of air stored} = \Phi \text{ (Total volume burned)}$$

$$\cong 0.25\ (0.002091)$$

$$\cong \underline{0.0005229} sm^3$$

Assuming a factor of 3 for the effect of maximum injection pressure (1020kPa), we have

$$\text{Air stored} \cong 3\ (0.0005229)$$

$$\cong \underline{0.001569} sm^3$$

$$\%\ \text{Air stored} \cong \frac{\text{Air stored}}{\text{Air injected}} \times 100$$

$$\cong \frac{0.001569}{0.39275} \times 100$$

$$\cong \underline{0.4\%}$$

The error incurred by using nitrogen as the tie component is thus very small. It will however be more significant at much higher pressures.

APPENDIX D

PROGRAM FOR HEAT TRANSFER IN COMBUSTION ZONE

```
00100 * THIS PROGRAM DETERMINES THE RADIAL HEAT LOSS IN
00110 * COMBUSTION ZONE AT DIFFERENT COMBUSTION FRONT LOCATIONS
00120 *
00130 dimension T(40,40),A(40,40),H1(40),H2(40),H3(40),H4(40),H5(40),
00140 & H6(40),W(40),UH20(40),UCn2(40),UCco(40),UCco2(40),UCH20(40),
00150 & UC(40),w(40),DT(40),P1(40),P2(40),a(40),f(40),AQ1(40),AQ2(40),
00160 & AREAA01(40),AREAAQ2(40),01(40),02(40),Q3(40),F(40),ff(40),FF(40)
00170 *
00180 * SAND PACK PARAMETERS DEFINED
00190 * po = Porosity,fraction
00200 * Soi= Initial oil saturation,fraction
00210 * Swi= Initial water saturation,fraction
00220 * Sgi= Initial gas saturation,fraction
00230 *
00240 * Ko   Thermal conductivity of oil at ref. temp.,J/hr.m.degK
00250 * Kw = Thermal conductivity of water at ref. temp.,J/hr.m.degK
00260 * Kg = Thermal conductivity of gas at ref. temp.,J/hr.m.degK
00270 * Km = Thermal conductivity of silica sand at ref. temp.,J/hr.m.degK
00280 *
00290 * Co = Heat capacity of oil at ref. temp.,J/kg.degK
00300 * Cw = Heat capacity of water at ref. temp.,J/kg.degK
00310 * Cg = Heat capacity of gas at ref. temp.,J/kg.degK
00320 * Cm = Heat capacity of silica sand at ref. temp.,J/kg.degK
00330 *
00340 * Do = Density of oil at ref. temp.,kg/cu.m
00350 * Dw = Density of water at ref. temp.,kg/cu.m
00360 * Dg = Density of gas at ref. temp.,kg/cu.m
00370 * Dm = Density of silica sand at ref. temp.,kg/cu.m
00380 *
00390 * L = Combustion front thickness chosen,metre
00400 * x = Linear distance from combustion front location,metre
00410 * r = Combustion tube radius,metre
00420 *
00430 *
00440 real *4 L,K,Ko,Kw,Kg,Km
00450 *
00460 * DATA INPUT
00470 * NOTE: file30 has the same format as Table B1(Appendix B)
00480 *
00490 print,'input the value of po '
00500 read,po
00510 print,'input the values of Soi,Swi,Sgi'
00520 read,Soi,Swi,Sgi
00530 print,'input the values of Ko,Kw,Kg,Km'
00540 read,Ko,Kw,Kg,Km
00550 print,'input the values of Co,Cw,Cg,Cm'
00560 read,Co,Cw,Cg,Cm
00570 print,'input the values of Do,Dw,Dg,Dm'
00580 read,Do,Dw,Dg,Dm
00590 print,'input the values of x ,L and r'
00600 read,x,L,r
00610 print,'input the airflux,AF(st.cu.m/sq.m hr)'
00620 read,AF
00630 print,'input the avg. composition of produced gas(%):N2,CO,CO2'
00640 read,AN2,ACO,ACO2
00650 print,'input the Avg. CFvelocity,Vb'
00660 read,Vb
00670 print,'input the Average Reaction Rate(kg.fuel/cu.m. hr)'
00680 read,Rf
00690 print,'input the no of data in each column of file30'
00700 read,n
00710 do 150 i=1,n
00720 read(30,100) (A(i,J),J=1,11)
00730 100format(v)
00740 T(i,1)=A(i,1)
00750 150continue
00760 *
```

```
00770 * DETERMINE THE SAND PACK THERMAL PROPERTIES
00780 * Heat capacity,CR(cal/cu.m degK)
00790 CR=(po*(Swi*Cw*Dw+Soi*Co*Do+Ssi*Cs*Ds)+(1-po)*Cm*Dm)/4.187
00800 * Thermal conductivity,K(cal/hr.m.degK)
00810 K=(po*(Kw+Ko+Ks)+(1-po)*Km)/4.187
00820 *
00830 * DETERMINE VAPORIZED FORMATION WATER(kg)
00840 VFW=(3.142*r**2)*L*po*Swi*Dw
00850 *
00860 do 250 i=1,n
00870 * DETERMINE THE HEAT OF COMBUSTION(cal./gm.fuel)
00880 H1(i)=(265700+197850*(1/A(i,5)))/((1+(1/A(i,5)))*(12+A(i,7)))
00890 H2(i)=(31175*A(i,7)-171700)/(12+A(i,7))
00900 H3(i)=H1(i)+H2(i)
00910 *
00920 * DETERMINE THE RATE OF HEAT LIBERATION(cal./cu.m. hr)
00930 H4(i)=1000*H3(i)*Rf
00940 *
00950 * DETERMINE THE STEAM ENTHALPY AT THE COMB. PEAK TEMP.(cal./gm)
00960 H5(i)=(2.676E+06+1.956E+03*(A(i,9)-100))/(4.187*1.0E+03)
00970 *
00980 * DETERMINE THE STEAM-FUEL RATIO,W
00990 W(i)=A(i,6)/A(i,8)
01000 *
01010 * DETERMINE THE QUANTITY 'Rf(Lc-Whs)'(cal./cu.m. hr)
01020 H6(i)=H4(i)-(Rf*W(i)*(1.0E+03*H5(i)))
01030 250continue
01040 *
01050 * DETERMINE GAS AND STEAM FLUXES(st.cu.m/sq.m hr)
01060 Un2=(AN2/100)*AF
01070 Uco=(ACO/100)*AF
01080 Uco2=(ACO2/100)*AF
01090 do 300 i=1,n
01100 UH2O(i)=(((A(i,6)+VFW)/18)/(((A(i,6)+VFW)/18)+A(i,11)))*AF
01110 300continue
01120 *
01130 do 400 i=1,n
01140 * DETERMINE THE CONVECTIVE TERMS(cal/cu.m hr deg.K)
01150 UCn2(i)=(Un2*1.2507*1.041E+03)/4.187
01160 UCco(i)=(Uco*1.2500*1.042E+03)/4.187
01170 UCco2(i)=(Uco2*1.9768*0.846E+03)/4.187
01180 UCH2O(i)=(UH2O(i)*0.794*1.867E+03)/4.187
01190 *
01200 * DETERMINE THE HEAT LOSS TERM(cal./cu.m hr)
01210 UC(i)=Vb*(CR+po*Swi*Dw*(Cw/4.187))-UCn2(i)-UCco(i)-UCco2(i)-UCH2O(i)
01220 w(i)=-UC(i)/K
01230 DT(i)=A(i,10)-A(i,9)
01240 G=DT(i)/L
01250 p1(i)=K*w(i)*(DT(i)*exp(w(i)*L)-G*(exp(w(i)*x)-1.0))
01260 p2(i)=p1(i)/(exp(w(i)*x)-1.0-(x*exp(w(i)*L)))
01270 q(i)=p2(i)+H6(i)
01280 *
01290 * DETERMINE THE INSTANTANEOUS
01300 * FRACTIONAL RAADIAL HEAT LOSS
01310 f(i)=q(i)/H4(i)
01320 400continue
01330 *
01340 * DETERMINE THE ABSOLUTE HEAT LIBERATED
01350 * AND RADIAL HEAT LOSS(cal/min)
01360 do 500 i=1,n
01370 AQ1(i)=(H4(i)*0.003167*x)/60.0
01380 AQ2(i)=(q(i)*0.003167*x)/60.0
01390 500continue
01400 *
01410 * DETERMINE THE CUMULATIVE
01420 * FRACTIONAL RADIAL HEAT LOSS
01430 do 550 k=2,n
01440 AREAAQ1(1)=AQ1(1)
01450 AREAAQ2(1)=AQ2(1)
01460 F(1)=AREAAQ2(1)/AREAAQ1(1)
01470 B1=T(k,1)*60.0
01480 B2=T(k-1,1)*60.0
01490 H=B1-B2
01500 AREAAQ1(k)=AREAAQ1(k-1)+(H*AQ1(k-1))+(0.5*H*(AQ1(k)-AQ1(k-1)))
01510 AREAAQ2(k)=AREAAQ2(k-1)+(H*AQ2(k-1))+(0.5*H*(AQ2(k)-AQ2(k-1)))
01520 F(k)=AREAAQ2(k)/AREAAQ1(k)
01530 550continue
01540 *
```

```
01550 * CONVERT HEAT LIBERATION AND
01560 * HEAT LOSS TERMS INTO S.I Units
01570 do 575 i=1,n
01580 * Heat Liberated(J/kg.fuel)
01590 Q1(i)=4.187E+03*H3(i)
01600 * Heat Liberation Rate(J/cu.m hr)
01610 Q2(i)=4.187*H4(i)
01620 * Radial Heat Loss(J/cu.m hr)
01630 Q3(i)=4.187*q(i)
01640 575 continue
01650 *
01660 * DETERMINE INSTANTANEOUS & CUMULATIVE
01670 * RADIAL HEAT LOSS,percent
01680 do 585 i=1,n
01690 ff(i)=100.0*f(i)
01700 FF(i)=100.0*F(i)
01710 585 continue
01720 *
01730 * OUTPUT DATA
01740 write(12,600)
01750 write(12,601) (Q1(i),Q2(i),Q3(i),T(i,1),i=1,n)
01760 600format(1X,'The Inst. Heat Liberated,Q1(J/kg.fuel),
01770 & Heat Liberation Rate,Q2(J/cu.m hr),Radial Heat Loss,Q3(J/cu.m hr),
01780 & and the combustion time,T(Hrs.) are resply'//,
01790 & 6X,'Q1(i)',6X,'Q2(i)',6X,'Q3(i)',14X,'T(i,1)'/,
01800 & 6X,'------',6X,'------',6X,'-----',15X,'--------')
01810 601format(4(1X,f12.2))
01820 write(12,602)
01830 write(12,603) (ff(i),FF(i),T(i,1),i=1,n)
01840 602 format(1X,'The Inst. Radial Heat Loss,ff(%),
01850 & The Cum. Radial Heat Loss,FF(%),and
01860 & the Combustion time,T(Hrs.) are resply'//,
01870 & 8X,'ff(i)',8X,'FF(i)',8X,'T(i,1)'/,
01880 & 6X,'----------',6X,'---------',6X,'--------')
01890 603format(3(1X,f12.2))
01900 write(12,604)
01910 write(12,605)F(n)
01920 604format(1X,'The net heat loss fraction for the run is'/)
01930 605format(1X,f12.8)
01940 stop
01950 end
```

APPENDIX E

SI METRIC CONVERSION FACTORS

acre	x 4.046 873	E + 03	= m^2
acre-ft	x 1.233 489	E + 03	= m^3
°API	141.5/(131.5 + °API)		= g/cm^3
bbl	x 1.589 873	E-01	= m^3
BtU	x 1.055	E + 03	= J
cal	x 4.187	E + 00	= J
cp	x 1.0	E - 03	= Pa.s
°F	(°F-32)/1.8		= °C
in	x 2.54	E + 00	= cm
lbm	x 4.535 924	E - 01	= kg
psi	x 6.894 757	E + 00	= kPa
scf	x 2.863 640	E - 02	= std m^3
watt	x 1.0	E + 00	= J/S